Fall 2015

Analysis of effects of surface roughness and local surface imperfections on measured pressure

Laurin Ashley Bookout

ANALYSIS OF EFFECTS OF SURFACE ROUGHNESS AND LOCAL SURFACE IMPERFECTIONS ON MEASURED PRESSURE

by

LAURIN ASHLEY BOOKOUT

A DISSERTATION

Presented to the Faculty of the Graduate School of the

MISSOURI UNIVERSITY OF SCIENCE AND TECHNOLOGY

In Partial Fulfillment of the Requirements for the Degree

DOCTOR OF PHILOSOPHY

in

EXPLOSIVES ENGINEERING

2015

Approved by

Dr. Jason Baird, Advisor
Dr. Paul Worsey
Dr. Kakkattukuzhy Isaac
Dr. Norbert Maerz
Dr. Eric Rinehart

ABSTRACT

When tests using pressure to characterize the performance or effects of an explosive are conducted in laboratory or other small scale, highly controlled settings, it is expected that any gages will be ideally mounted and there will not be any surface imperfections or roughness near the gage location. However, when explosive tests are scaled up, the test beds typically do not have perfect surfaces. Instead there may be rough surfaces with various types of geometry or situations where it is extremely difficult to get the gage flush mounted with a flat surface. In a time where tests with multiple replications are increasingly limited, it is critical to understand the experimental error present in a test.

This document discusses pressure and optical data gathered from shock tube tests for flat and rough surfaces spanning two geometries and three amplitudes as well as three different imperfect mounting configurations.

For each test, pressure data was recorded from gages mounted in the roughness plates and on a wing mount to provide information on how the measured pressure varied due to the location of the gage. In addition to the pressure data, Schlieren video was recorded for each shot on the same timebase as the pressure gages. Both geometry and amplitude of the roughness affected the shock structure and corresponding pressure waveform. The combination of pressure data and Schlieren video allowed particular waveform characteristics to be attributed to specific shock structures.

With the roughness plates in place, the measured pressure varied from 12 to 85% higher than the baseline, while the impulse varied from 6% lower to 49% higher. The gage mounted on the wing at 7-inches above the floor of the shock tube remained unaffected during the test series, with only a 4% variance in peak pressures and impulses.

ACKNOWLEDGMENTS

First and foremost, I would like to thank my husband, Will, for all the support he provided during the writing of this document. Thank you for knowing when to push, when to lay off, for all the things you did so that I could focus on writing, and finally, for your patience with me throughout the process.

Next, I would like to thank my committee for their timely advice and contributions when I needed it. Dr. Baird, I appreciate your thoughtful advice and careful review of my work throughout this process. The combination of your guidance and expectations resulted in a higher quality of work than what I could have created otherwise. Dr. Rinehart, without you, this project would never have been completed. I sincerely appreciate your support during the planning phase and for being willing to discuss the direction of the paper with me during the writing process. Dr. Worsey, thank you for all of your efforts getting the Explosives program in place so that this education was available to me, and for your thoughtful suggestions for this paper. Dr. Isaac, conversations with you during the planning phase were extremely helpful; thank you for your insights. Dr. Maerz, your extensive knowledge about surface roughness was eye-opening, and useful.

Also, I would like to acknowledge the contributions of my friends Mark Schmidt and Will Karst for their help during testing, and Ryan Pahl for his help with LaTeX formatting issues and discussions throughout the construction of this document.

A heartfelt thank you goes out to Gillian Worsey, DeWayne Phelps, Jimmie Taylor, Shirley Hall, Barb Robertson, and Judy Russell for their support during my time in the department. Whether it was checking in on my progress, reminding me of deadlines, tracking down signatures, or providing suggestions, it all helped get me through the process.

I also appreciate the support and encouragement I received from my family to date; I couldn't have made it this far without you.

TABLE OF CONTENTS

Page

LIST OF ILLUSTRATIONS

LIST OF TABLES

1. INTRODUCTION

1.1. BACKGROUND AND JUSTIFICATION

Pressure measurements are widely used in explosive research that covers a wide range of topics such as structural response under explosive loading, testing of new explosive formulations, and characterization of explosive effects. Pressure measurements are one of the few types of data that can be reliably collected during an explosive event. Other types of instrumentation fielded during an explosive event may include accelerometers, thermal diagnostics, or optics; however, all instrumentation has limitations, especially where the magnitude and rate of loading are very high.

One reason for the popularity of measuring pressure during explosive tests is that pressure measurements can be used to directly validate calculations. Other parameters required in high fidelity hydrocode calculations are density, internal energy, and particle velocity, none of which can be measured real-time during a dynamic event. Photo and video can be rendered ineffective due to the cloud of detonation products or dust, if testing in an outside environment. Temperature data can be obtained in some situations, but the response times of thermocouples are slow compared to the duration of the detonation and subsequent shock wave positive phase. Given the limitations on the type of instrumentation that can be used during explosive tests, it is prudent to understand the effect that the testing environment has on the recorded data.

Despite the extensive use of pressure transducers in explosive research, the effects of the environment immediately adjacent to the transducer have not been thoroughly investigated and documented.

1.2. MOTIVATION

For many industry applications related to explosives testing, there is neither enough time or funding to complete a full test matrix that would satisfy design of experiments criteria. Instead, engineers and scientists plan a series of experiments to meet as many test objectives as possible within time and budgetary limitations. Due to these limitations, replications are typically very few or even singular. Without sufficient replications to conduct statistical analyses, the person(s) who analyzes the data often need to make engineering judgments based on experience or other similar tests. One such engineering judgment, or rule of thumb, is that the variance in pressure data gathered from field tests can be more than twice the actual value.

The large assumed variance in the rule of thumb is largely a result of the complicated environment that is involved in field testing. Lab scale testing is often at a fairly small scale, and can be highly controlled. Unfortunately, the application of explosives and explosive systems is usually most relevant outside of lab conditions. Therefore, the repeatability and standard deviations gathered from lab testing can not always be reliably extrapolated to field conditions.

The combination of very few replications combined with an assumed large variance leads to difficulties in confidently determining whether the configuration tested performed better or worse relative to the baseline. In a field where a 5% or 10% increase is hard to achieve, a 2x assumed variance makes it impossible to determine if the results were due to the configuration tested or are an artifact of the diagnostics.

A controlled, highly repeatable set of data that represents possible field pressure transducer mounts would be valuable to researchers who conduct or analyze data from explosive testing. If the effects of surface roughness or poorly mounted gages are quantified, researchers can use a more realistic standard deviation value for their data sets. The use of better assumptions for analysis of limited data sets will allow researchers to have a higher confidence in conclusions drawn regarding certain systems or configurations. The testing

series presented and analyzed in this document investigate the effects of uniform surface roughnesses and imperfectly mounted gages on measured pressure.

1.3. PROJECT OBJECTIVES AND SCOPE OF WORK

This research effort intends to address the following three main objectives:

1. Quantify the effect surface topography around the transducer has on pressure measurements, to include surface roughness, recessed and protruding transducer mounts, and local surface imperfections around the transducer.

2. Determine the flow structure of the shock as it moves across selected rough surfaces.

3. Provide recommendations for placing transducers when measuring incident pressures in environments with rough surfaces.

The scope of work was as follows: First, a baseline was established using a flat surface with flush mounted transducers. Subsequently, four additional roughness plates with flush mounted transducers were tested to determine the effect of surface roughness on measured pressure. Additionally, a flat surface with improperly mounted transducers allowed the researcher to quantify the effect that a non-ideal mount has on measured pressure.

The shock tube driver fluid was standard compressed air, and remained constant throughout the course of testing. Two separate shock strengths, created using readily available diaphragm thicknesses, provided a variance in pressure to see how the pressure differential affected the shock characteristics.

The tests conducted were all at the same scale, multiple shock tube diameters were not used, so no comparisons of how the data scales are made in this document.

1.4. ORGANIZATION OF THIS DISSERTATION

The first section of this dissertation provides a background on the measurement of different pressure types, how pressure transducers work, and information on shock wave travel through air. Previous studies related to this area of knowledge are summarized, along with the importance of this research topic.

Section 2 covers the motivation for the research, touching on both academic and industry need. Then, the project objectives and scope of work are discussed. Section 3 details the experimental setup and design of the various components required. The results are presented in Section 4, and the discussion and analysis of the data are given in Section 5 along with the comparison of accepted data correction methods to the experimental data. Finally, conclusions drawn from this work are given in Section 6.

2. LITERATURE REVIEW

2.1. PRESSURE MEASUREMENTS DURING EXPLOSIVE EVENTS

There are several types of pressure that can be measured during an explosive test. Each type provides different information about the environment, so depending on the objectives of the test and geometry of the test bed, one or more types of pressure may be measured. While the four types of pressure covered below are defined differently, the units are all the same; pounds per square inch (psi) or multiple units of Pascals (kPa, MPa). A brief description of each pressure type is provided in the paragraphs below.

2.1.1. Incident Pressure. The first type of pressure is commonly measured, and is known by several names; incident, free-field, side-on, or overpressure. Throughout this document, the term "incident" will be used. Incident pressure is a measurement of the pressure at a given time and location relative to ambient (atmospheric) pressure. [1] In order to measure incident pressure, the transducer must be oriented perpendicular to the direction of the moving shock so that the shock passes across the measurement surface of the transducer. Incident pressures can typically be directly compared between tests, after any necessary charge weight scaling factors have been applied. The ability to do test-to-test comparisons is extremely useful when evaluating multiple explosive configurations.

2.1.2. Reflected Pressure. Another type of pressure frequently measured is reflected pressure, which is easily obtained from gages mounted in rigid surfaces oriented parallel to the shock front. Reflected pressure is defined as the pressure caused by a reflection of a shock wave from a non-responding surface. [1] Reflected pressure measurements are very useful for evaluating blast barriers, walls, and other structural elements that would be in the path of a shock front as it is the actual load experienced by the structure.

The maximum reflected pressure is obtained when the shock front is parallel to the surface, but any inclination of the surface will result in a reflected pressure component. The material off which the shock wave reflects, the incident overpressure (related to the Mach number), and specific heat ratio, γ, also contribute to the reflection factor, which can range from 2 to nearly 15. In the tests covered in this document, γ is assumed to be constant at 1.4, since the temperatures during testing do not vary enough to cause an appreciable change in γ.

As a general rule of thumb, the reflected pressure is roughly approximated as twice the incident pressure. Figures 2.1 and 2.2, originally published in Reference [1], provide the reader with an understanding of reflection factors for both normal and oblique shock waves.

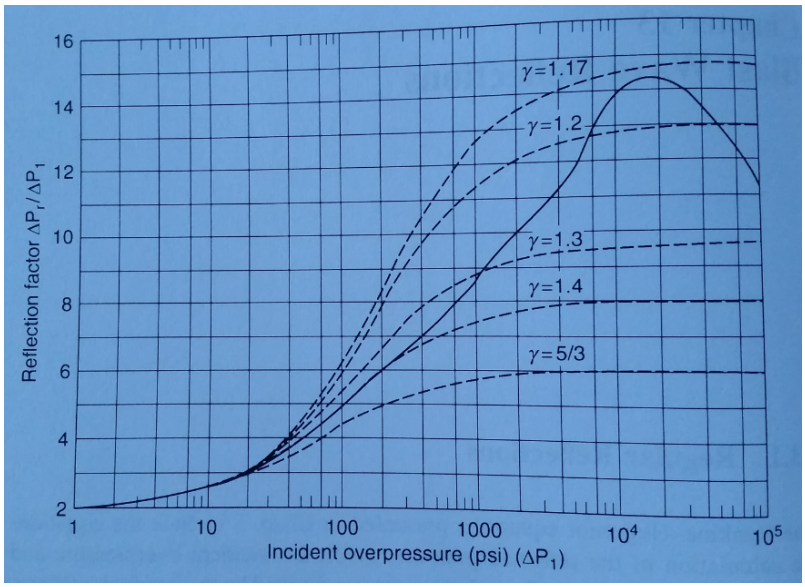

Figure 2.1. Normal reflection factors for adiabatic shocks in sea level air, Reference [1].

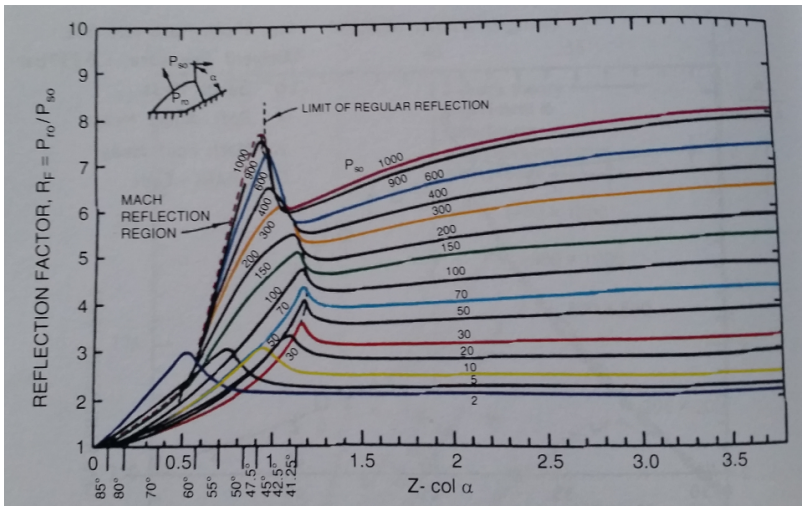

Figure 2.2. Reflection factors as a function of the cotangent of the incident angle, Reference [1].

However, solving the P-u Hugoniot for a shock traveling through one material and interacting with a second material at a perpendicular interface show that the particle velocity (of the shock), u_0, is doubled at the interface. [10] A doubling of the particle velocity does not necessarily equate with a doubling of the pressure. Understanding reflection factors is relevant to instrumentation that is not mounted parallel to the direction of travel of the shock front or when the objective is to study a loading profile on an object from which the shock reflects.

The P-u Hugoniot solution for a reflected shock is only applicable to a shock striking a surface parallel to the shock front. There are many potential cases where a shock may strike a rigid boundary at an oblique angle. Figures 2.1 and 2.2 are useful for determining the reflection factor for reflections off oblique surfaces, or in high temperature environments.

2.1.3. Stagnation Pressure. Stagnation pressure, also known as total pressure, is the pressure that occurs when the fluid velocity is zero. [2] When a fluid flows around either side of an object, there is a streamline that has a point which the fluid does not move.

This stationary point is known as the stagnation point. Figure 2.3 shows example velocity contours and the stagnation point for a sample configuration. Placing a pressure gage at the stagnation point allows for the measurement of stagnation pressure. However, the detached shock in front of the probe separates the supersonic and subsonic flow. To obtain the true shock parameters from a stagnation pressure measurement, correction factors need to be applied to the measured pressures.

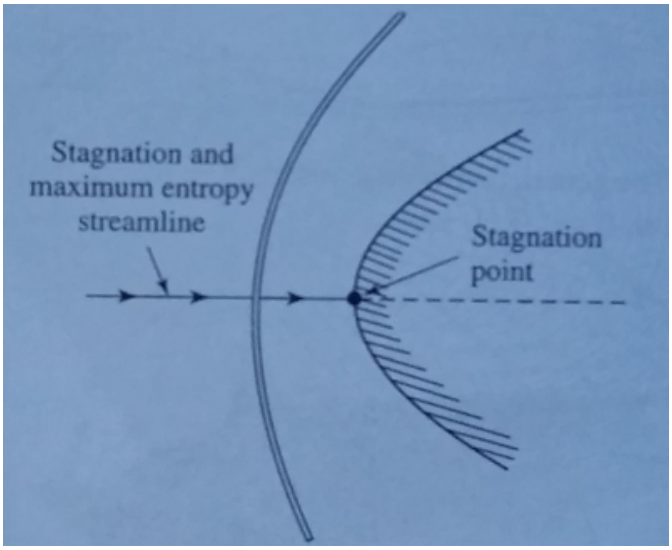

Figure 2.3. Stagnation streamline and point, Reference [2].

2.1.4. Dynamic Pressure. Dynamic pressure is the force per unit area that is caused by the motion of the gas, and is typically defined as Equation 2.1, from Reference [1], where ρ is the material density, and U is the shock velocity. In other words, the dynamic pressure is the kinetic energy of the gas. At the time of this writing, there exists no method to directly measure the dynamic pressure during an explosive event. However, the dynamic pressure can be calculated if both incident and stagnation measurements are made. Incident (static), stagnation and dynamic pressure are related by Equation 2.2. [3] Special gage mounts are required if stagnation pressure measurements are desired, and not all test environments can

accommodate that type of gage mount. Due to these limitations and difficulties fielding special gage mounts, stagnation pressure is not as commonly measured during explosive test events as incident and reflected pressures.

$$DynamicPressure = \frac{1}{2}\rho\,|U|\,U \tag{2.1}$$

$$DynamicPressure = StaticPressure - StagnationPressure \tag{2.2}$$

2.2. SHOCK WAVE CHARACTERISTICS AND BEHAVIOR

The study of compressive flow and shock waves is a complicated subject, even with simplifying assumptions such as stationary shocks, adiabatic shocks, and the medium represented as a perfect, non-reacting gas. Data gathered from explosive testing does not satisfy the aforementioned simplifying assumptions and complicates the analysis of an already complex problem. Compressible flow textbooks, such as Reference [2], cover many aspects of compressible supersonic flow, including normal and oblique shocks, reflected shocks, three-dimensional flow, and high-temperature flow.

2.2.1. Hugoniot Equations. In the simplest of terms, a shock wave, or shock front represents a discontinuity between the "unshocked" and "shocked" material. There is not a smooth transition between the unshocked and shocked material. Rather, the pressure (P), density (ρ), internal energy (e), shock velocity (U), and particle velocity (u) differ between the shocked and unshocked states. [10] The Rankine-Hugoniot jump equations provide a method of calculating the previously mentioned variables on both sides of the shock, derived from the principle that mass, momentum, and energy must be conserved across the shock front. Equations 2.3 (conservation of mass), 2.4 (conservation of momentum), and 2.5 (conservation of energy) give the three Rankine-Hugoniot jump equations.

$$\frac{\rho_1}{\rho_0} = \frac{U - u_0}{U - u_1} = \frac{\upsilon_0}{\upsilon_1} \tag{2.3}$$

$$P_1 - P_0 = \rho_0(u_1 - u_0)(U - u_0) \tag{2.4}$$

$$e_1 - e_0 = \frac{P_1 u_1 - P_0 u_0}{\rho_0(U - u_0)} - \frac{1}{2}(u_1^2 - u_0^2) \tag{2.5}$$

The Rankine-Hugoniot equations result in five variables and three equations, which is why Equations of State (EOS) are required to solve for all the variables. Equations of State are derived from experimental data, therefore the Rankine-Hugoniot jump equations cannot be solved with theory alone. In addition to Equations 2.3, 2.4, and 2.5, additional relationships are required to solve for the five variables present in a simple shock wave problem. Three Hugoniot planes are defined below, which allow all five variables (P, ρ, *E, U, and u*) to be solved for. These required equations represent three planes of the Hugoniot, the *U-u* plane, *P-v* plane, and the *P-u* plane, and are shown in Equations 2.6, 2.7, and 2.8. Additional variables required for the Hugoniot planes are C_0, which is the bulk sound speed of the material; s, which is the slope of the line relating shock velocity and particle velocity for the *U-u* plane; and υ, the specific volume of the material.

The *U-u* plane relates the particle velocity to the shock velocity of a material, and the equation for this plane is given in 2.6. The variable s is dimensionless and represents the slope of the line through the *U-u* data. The y-intercept is referred to as the bulk sound speed, C_0, and has units of km/s or mm/μs.

$$U = C_0 + su \tag{2.6}$$

The *P-v* plane, given by Equation 2.7 is obtained by combining the *U-u* Hugoniot equation with the momentum and mass equations. The EOS represents all the states in

which a particular material can exist. The shock loading of a material is not represented by the line described by Equation 2.7. Instead the shocked and un-shocked states are joined by a straight line, called the Rayleigh line. However, the path the material states take during unloading of the material are closely represented by Equation 2.7.

$$P = C_0^2(\upsilon_0 - \upsilon)[\upsilon_0 - s(\upsilon_0 - \upsilon)]^{-2} \tag{2.7}$$

The third commonly used Hugoniot plane, the *P-u* plane, is represented by Equation 2.8. Unlike the *P-v* plane, the *P-u* plane uses Eulerian coordinates. The use of Eulerian instead of Lagrangian coordinates allows for differentiation and analysis of left-going and right-going shocks in a given material.

Additional in-depth discussions of the Rankine-Hugoniot jump equations and the Hugoniot planes can be found in Reference [10].

$$P_1 = \rho_0 u_1(C_0 + s u_1) \tag{2.8}$$

2.2.2. Attenuation of Shocks. Once a shock is formed, it decays, or attenuates, as it moves through the material in which it formed. The rear of the shock wave, also known as the rarefaction or relief wave, is traveling through a denser (shocked) medium than the front of the shock wave, and so it moves more quickly. The rarefaction overtakes the front of the shock wave and begins to knock down the peak pressure until the shock decays to a sound wave and then attenuates completely.

One driving factor for the attenuation rate of the shock is the volume through which the shock expands. This concept of the attenuation rate stems from the initial energy present in the explosive charge relative to the volume available for the expansion of energy that occurs when the explosive detonates.

For a free air burst, the attenuation of pressure can be roughly approximated by the spherical volume that the shock wave encompasses at a given point in time. Pressure decay

in environments other than a free air burst will attenuate at a different rate that is based on the confining geometry relative to the explosive charge and the volume available for expansion.

Shock flow and attenuation in a shock tube is different than in free air, since the shock has only one dimension of travel, instead of three. As a result, the pressure decay versus distance in a shock tube is nearly linear. In a shock tube, prior to rupture of the diagram, there is a high pressure region in the driver section and an ambient or low pressure region in the driven section. When the diaphragm ruptures, a shock moves into the low pressure region and a rarefaction moves into the high pressure region. When the rarefaction reaches the closed end of the driver section, it reverses direction and heads towards the driven section. If the initial shock passes across the gage location before the rarefaction overtakes it, the resulting pressure profile will resemble a square wave, or flat-top wave. However, if the rarefaction overtakes the initial shock prior to passing across the gage location, a more traditional Friedlander shaped waveform will be produced. By varying the length of the driver and the length of the driven section, the waveform can be tailored to a certain profile and positive phase duration. Extensive information on flows in shock tubes can be found in Reference [18].

Simple free air or hemispherical bursts and their relative shock wave decay rates have been extensively documented previously. The data set covering shock attenuation rate due to the presence of rough surfaces is extremely small, although some limited distribution work has been performed in both free air and confined environments.

2.2.3. Mach Stem Formation and Mach Reflections. In addition to incident, oblique, and reflected shock waves, another commonly seen shock characteristic is the Mach stem. The Mach stem forms when the reflected shock catches the incident shock. The illustration in Figure 2.4 demonstrates the principle of Mach stem formation. Figure 2.4 shows a detonation location at some point above a rigid surface. The incident shock reflects off the surface, resulting in a reflected shock. After some time and distance, the

reflected shock overtakes the incident shock and a Mach stem forms below the point of intersection of the two shocks, known as the triple point. Typically, the Mach stem travels in a direction perpendicular, or nearly perpendicular to the surface.

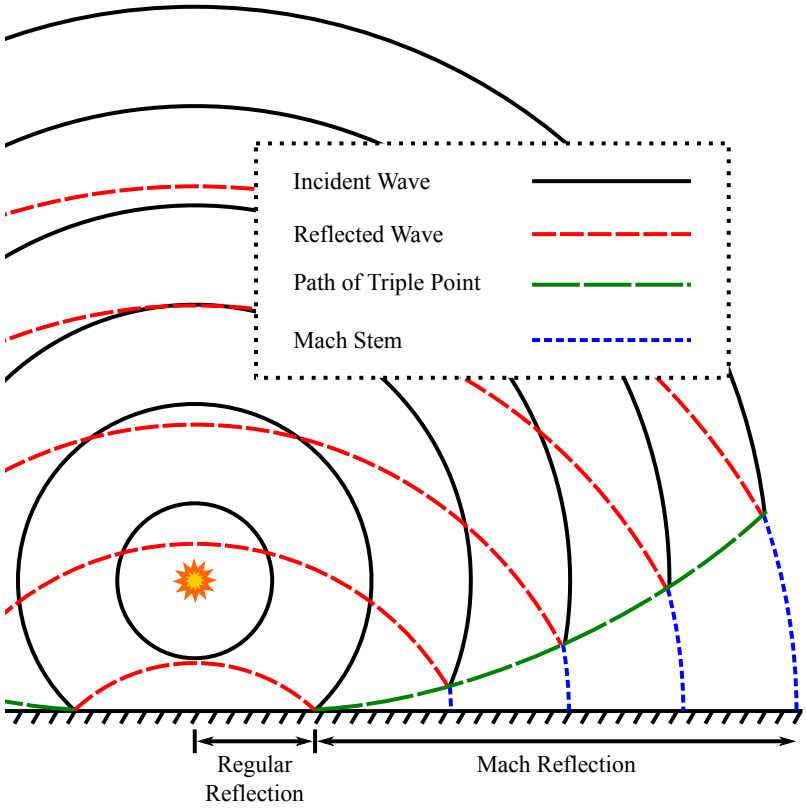

Figure 2.4. Mach stem formation from a free-air burst.

When a shock encounters a wedge with a fixed angle, multiple types of reflection can occur, including regular reflections (RR), single Mach reflections (SMR), transitional Mach reflections (TMR), or double Mach reflections (DMR). One criteria suggested for the RR-SMR transition point, the sonic criterion initiated by J. von Neumann, says that SMR cannot occur when the velocity of the reflected shock is less than the velocity of the incident shock because the perturbations induced by the wedge cannot catch up to the reflection point. [1] [18]

A line drawing of a SMR, from Reference [1] is shown in Figure 2.5. The shock is moving from left to right and reflecting from a plane placed at an angle relative to the incident shock. The ambient region is denoted by I, the region of gas that has been shocked once is denoted by II, while the gas in region III is just behind the Mach stem and is at a higher pressure than region II. The curved reflection is indicated by *R* and the gas within region IV has been affected by both the incident and reflected shocks. The triple point (TP) of the system is at the intersection of the incident, Mach, and reflected shocks.

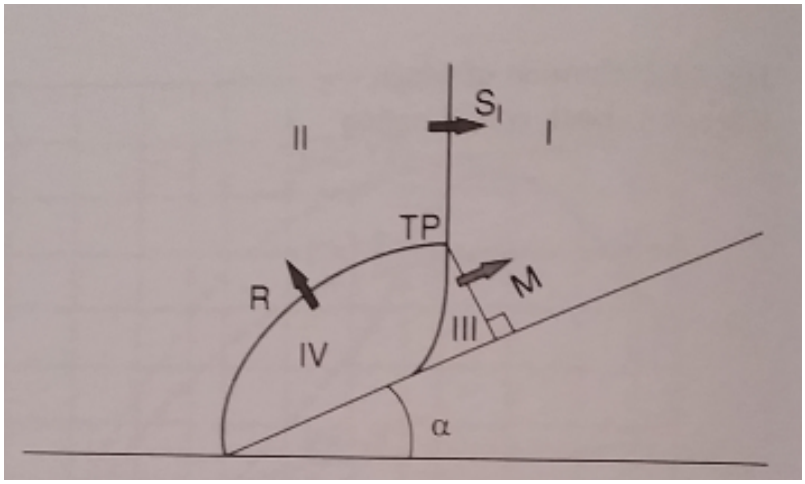

Figure 2.5. Line drawing of a single Mach reflection, from Reference [1].

2.2.4. Description of Surface Roughness. ANSI B46.1 (Reference [6]) covers definitions of surface roughness, waviness, and lay, as well as methods for measuring surface texture. Lay is the direction of the predominant surface pattern. Waviness is the more widely spaced component of surface texture, while roughness consists of the finer irregularities. Roughness can be considered as superimposed on a wavy surface, as shown in Figure 2.6 from Reference [6]. By the ANSI definitions, "Peak" refers to a point of maximum height, and "valley" refers to a point of maximum depth. The peak to valley distance corresponds to *d* in the term *d/D* that describes the surface texture height relative to the

height of the pipe in which it is contained. Spacing is determined by the average spacing between adjacent peaks.

In the tests covered in this document, the geometric spacing was held constant at 4-inches in both directions, while the *d/D* ratios were 0.015, 0.029, and 0.059.

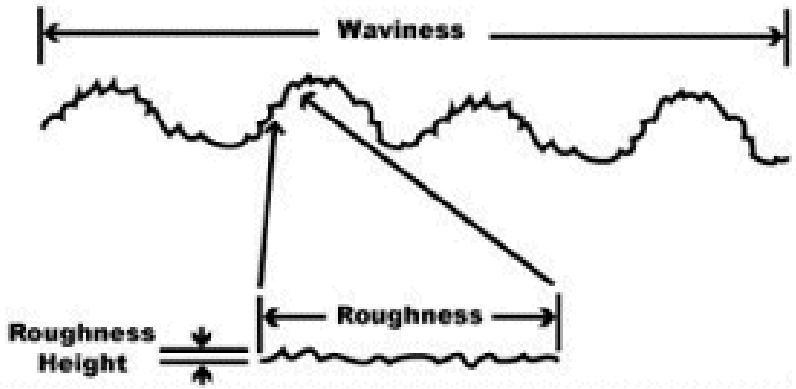

Figure 2.6. Illustration of Roughness and Waviness, Reference [6].

2.2.5. Previous Studies on the Effect of Macro Scale Surface Roughness. The Norwegian Defence Construction Service performed studies comparing airblast attenuation in smooth walled steel tubes to attenuation rates in rough walled tunnels in underground magazines. [7] [8] The results from the steel tube were compared with rough walled tunnels with diameters of 2.7 and 6.0 meters with average wall roughness heights of 0.12 and 0.15 meters, respectively.

Several shots with charge weights of 100-1000 kg TNT were conducted, and pressure measurements were taken at various distances from the charge. Instrumentation was located along the centerline of the tunnel, which allowed the researchers to focus on the attenuation rate of the shock without complicating the pressure measurements with wall-shock interactions.

After scaling the results to account for the different tunnel diameters, the researchers determined that the rough tunnel surfaces could reduce the pressure by a factor of two or more. The authors attributed a large portion of the pressure losses to the tunnel roughness, but did not provide in depth discussion on the topic.

2.3. BACKGROUND ON PRESSURE TRANSDUCER FUNCTION AND USE

2.3.1. Piezoelectric and Piezoresistive Materials. The two main types of pressure transducers are piezoelectric and piezoresistive, which are named for the materials of which they are made.

The piezoelectric effect is present in both natural quartz crystals or man-made polycrystalline ceramics. When a piezoelectric material is strained, positive and negative ions accumulate on opposite sides of the crystal. The applied force is directly proportional to the charge produced, allowing the transducer to be calibrated. [9]

Piezoresistive materials include piezoresistive silicon, which undergoes a change in resistance when strained or bent. Piezoresistive transducers typically consist of a Wheatstone bridge circuit that measures the change in resistance over time of the piezoresistive material. The change in resistance is proportional to the strain applied to the transducer.

Piezo materials and the instrumentation made with them are susceptible to various factors that can affect the intended measurement. Some of these factors include: live electrical cabling near the instrumentation cabling, photoflash response, thermal drift, and acceleration and vibration sensitivity. Several of these factors can be partially or entirely mitigated by the researcher by careful experimental design, while others cannot.

Thermal drift is often present in the late time data gathered by pressure transducers during explosive testing. Piezoresistive gages are less affected by temperature shifts than piezoelectric gages.

2.3.2. Transducer Placement in Test-Bed. Placement and orientation of the pressure transducers in the test bed affects the type and quality of measurement made. Figure

2.7 shows a general diagram of pressure types measured at various locations around a charge detonated at some height above the surface. Incident pressures are measured by gages oriented such that the shock passes cleanly across the gage surface, with no oblique component. Incident gages are usually mounted either flush with a surface or on pencil gages in open space. Reflected pressures are seen by gages placed such that the shock reflects off of the surface in which they are mounted. Stagnation and incident pressure gages are typically located on the same mount, with the stagnation gage at the front of the mount facing the shock front, and the incident gage located flush with the side of the mount. A basic understanding of shock propagation, along with careful planning for gage placement is required to obtain useful data.

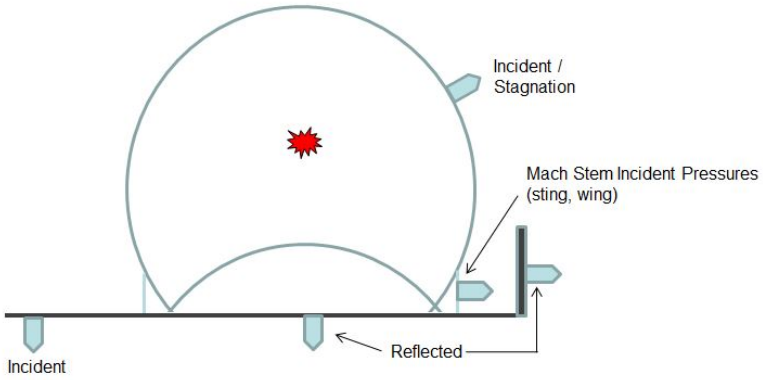

Figure 2.7. Pressure measurement types based on gage location and orientation.

2.3.3. Transducer Misalignment. Several types of mounting errors can occur when mounting pressure transducers, such as, a gage that is misaligned with respect to the shock, or misaligned with respect to the surface in which it is mounted. Several previous works cover some aspects of the consequences of mounting errors and are discussed below.

For free field pressure measurements, using a pencil mount, wing mount, pie plate, or similar mount, gage misalignment can easily occur. Any misalignment of the gage relative to the shock front will result in some reflected pressure measured at the gage location.

Reference [13] investigated the effect of misalignment of pencil probes, skimmer plates, and blunt cylinders on measured pressure. Pencil probes had a small amount of error if the alignment was +/- 5 degrees. Pressure measurements made using skimmer plate mounts were penalized a larger amount for a given misalignment angle.

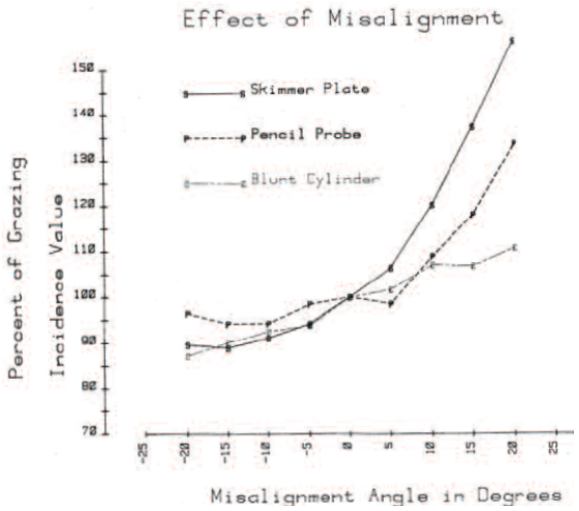

Figure 2.8. Effect of gage mount misalignment, Reference [13].

Difficulties encountered in deploying pressure transducers in non-laboratory conditions may result in a gage that is recessed to some degree from an otherwise flat surface. Reference [14] provides one example comparing the pressure measurements obtained from a flush-mounted gage (ideal condition) vs. a recessed gage, and the calculated response from a flush-mounted gage. The results shown below in Figure 2.9, originally published in Reference [14], show that the pressure recorded by the recessed gage is approximately 30% higher than the pressure measured by the flush mounted gage. This work states that

the cavity created by a recessed gage can act as a resonator, resulting in an erroneously portrayed pressure-time history. For affected pressure records, the standard assumption is that only the initial peak pressures and early time data are affected by an imperfect mounting condition.

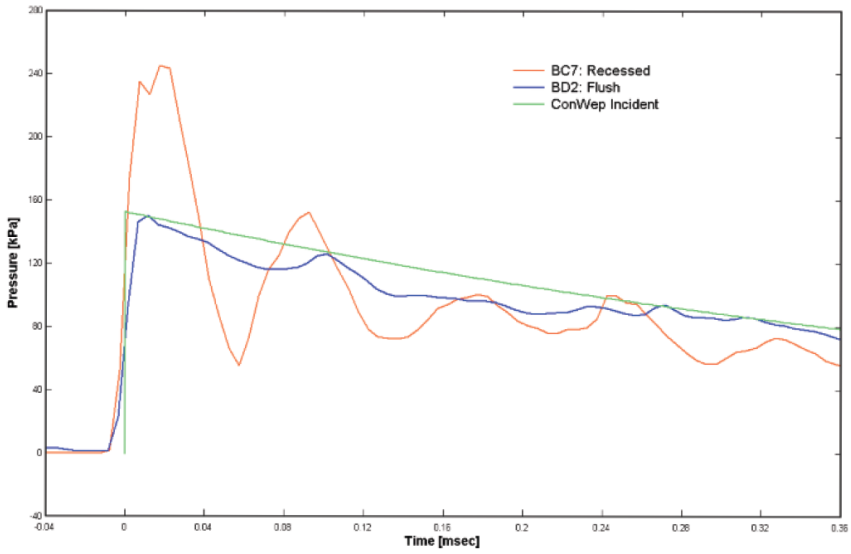

Figure 2.9. Pressures measured by flush mounted and recessed gages, Reference [14].

Recommendations for mounting of transducers are available from a variety of sources. These recommendations and best practices assume that the transducer will be mounted in a flat, smooth surface, such as the wall of a shock tube or a specialized pencil/sting mount, stagnation probe, pie plate, or wing mount. The type of mount used, and the orientation of the mount with respect to the shock wave affect the type and magnitude of pressure measured.

2.4. VISUAL TECHNIQUES FOR STUDY OF SHOCK WAVES

2.4.1. Brief History of Schlieren and Shadowgraph Techniques. Schlieren and shadowgraph techniques are two distinct methods that allow density differences in transparent media to be visualized and captured on film. Schlieren techniques have been used since as early as the 17^{th} century, when Robert Hooke devised a system to observe the plume of a candle using two candles and a concave lens. By the 20^{th} century, Schlieren imaging was being used at various laboratories in the US to study shock wave motion in air.

Schlieren imaging is based on the deflection of light by a refractive index gradient, which is directly related to the flow density gradient. Schlieren imaging techniques allow for visualization of density differences that would otherwise be invisible to the human eye.

An extensive history of Schlieren and shadowgraphs, theory, and practical discussion can be found in Reference [15], and will not be restated in great detail here.

A sample image of shock waves obtained using Schlieren techniques is given in Figure 2.10.

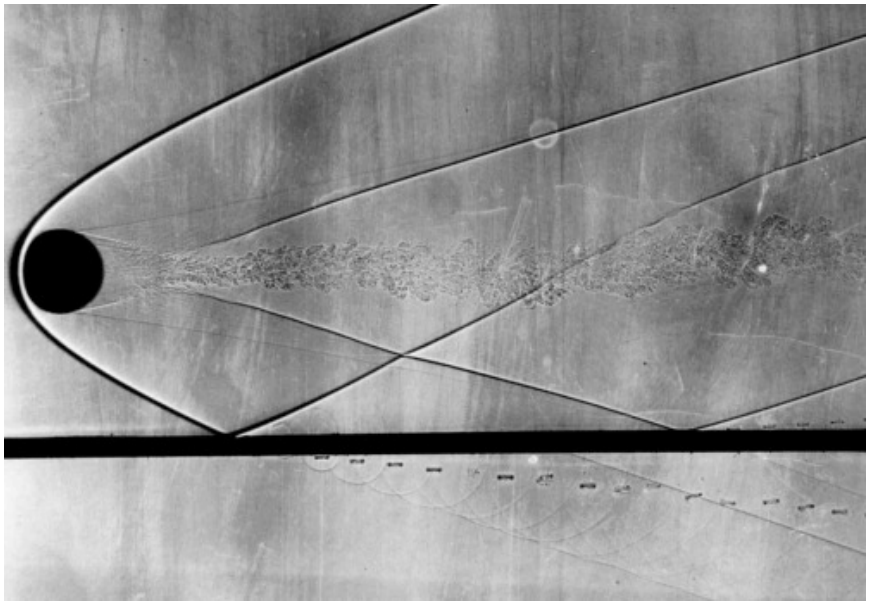

Figure 2.10. Schlieren Image, Army Ballistic Research Lab.

2.5. SHOCK INTERACTION STUDIES

2.5.1. Calculation of Shock Interaction in Smooth Walled Tubes. A study conducted by Damazo, et. al., 2010 has both experimental and calculation components investigating the effect of turbulence on measured pressure. [17] The study measured and calculated incident and reflected pressures in a smooth walled shock tube. The article reported differences in measured and calculated pressures for reflected shock waves, despite closely matching the calculated shock speed with the experimental shock speed. In the calculations, when the shock speed matches the experimental data, the calculated pressures are approximately 20% below the data, and if the reflected pressures are matched, the shock speeds differ. The authors of this study suggest that the differences are due to a flow that is not one-dimensional and viscous boundary effects at the tube wall.

A calculation from Reference [17] of the reflected shock in the shock tube clearly shows a bifurcated shock wave with a series of vortices near the surface of the tube. Figure 2.11 has two parts, one showing pressure contours from the calculation, and one of the

pressure-time histories from tracer points at various heights above the shock tube surface. The pressure-time histories, plotted for tracers at 0, l, 10, and 20 mm above the surface, along with a 1-D solution, do not all agree with each other. The waveform is noticeably different than the 1-D solution at 0 and 1 mm above the surface. However, the waveforms at 10 and 30 mm above the surface agree very well with the 1-D solution, indicating that the turbulent effects are only seen close to the surface.

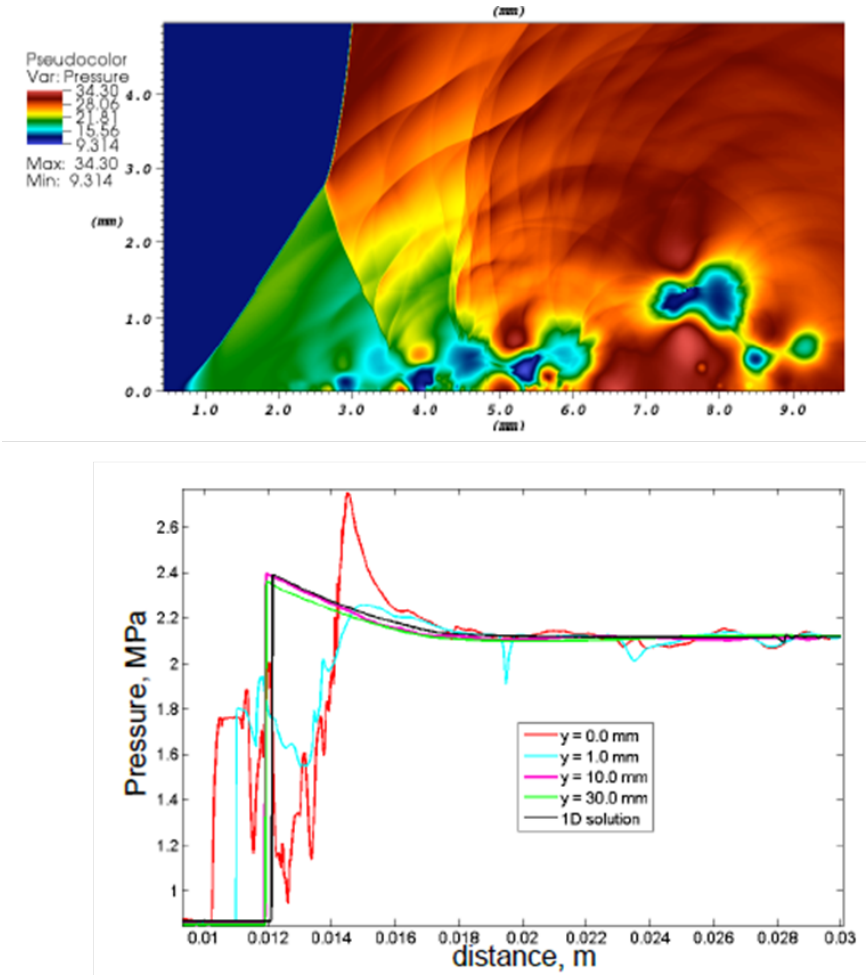

Figure 2.11. Calculation of pressures at varying heights from tube wall, Damazo, 2010.

3. EXPERIMENTAL SETUP

3.1. SHOCK TUBE DESIGN AND CONFIGURATION

The existing shock tube driver and driven sections available for use both had a 17 in. interior diameter, circular cross section. The existing tube sections were 7.5 ft. in length and could be added or removed as needed. The driver section length was adjustable in 0.5 in. increments. However, the circular cross section was not ideal for accommodating the roughness plates which were used to vary the surface geometry. Detailed discussion of the roughness plates is provided in Section 3.1.2.

To simplify the manufacture of the roughness plates and to provide the best possible conditions for Schlieren imaging in a shock tube environment, a 17 in. square cross section extension was fabricated and added on to the end of the existing shock tube. While the abrupt change in cross section shape caused some disturbance in the shock front, previous researchers have used circular driver sections into square driven sections with good results. [12] [16]

A general rule of thumb is that between 3-10 diameters downstream from a disturbance, the shock front will have reformed and will not display any evidence of having been disturbed. Before finalizing the shock tube extension dimensions, a 3D calculation was completed using CTH, a code developed by Sandia National Laboratories. CTH is an Eulerian code that is capable of modeling strong shocks and large deformations using second-order numerical methods. [19]

The quarter-symmetry 3D calculation was completed for the case of a circular tube mated directly to a square tube. The initial conditions for the driver pressure were obtained from previous tests in the shock tube which used the 0.032-in. T-6061 aluminum membranes. The initial conditions at time-zero consisted of the elevated driver pressure in the

driver section and ambient atmospheric conditions throughout the rest of the tube geometry. Several tracer points were located along the length of the tube to see how the pressure-time histories varied along the length of the tube before and after the round-to-square transition. At a distance of 5.6 diameters downstream from the transition, the simulation showed a clean, planar shock profile free of any perturbations caused from the transition from the round to square section.

Both the rule of thumb and the calculation results were both considered as guidelines while finalizing the length of the square tube section. The square extension had final dimensions of a 17-in. square interior with an overall length of 12-ft. The instrumentation section was 7.0 diameters from the transition, well past the calculated distance required for the shock to become planar again after the transition. The placement of the instrumentation section left 2-ft. from the rear of the instrumentation area to the end of the tube. The instrumentation section was encompassed by a 17-in. by 24-in. by 1.5-in. tray on the bottom of the tube which created a recess for mounting the smooth and rough plates. Also, 6-in. square windows present on each side of the shock tube allowed for line of sight through the shock tube, which was a necessity for the Schlieren setup.

3.1.1. Driver Specifications and Shock Characteristics. The existing driver section consisted of a 17-in. I.D. pipe that allowed 0.5-in. increment adjustments to driver length. A 12.5-in. driver section filled with compressed air was selected to provide the initial pressure condition for each test.

The desired upper pressure for the tests was roughly 30 psi, which was near the upper limit of allowable pressures for the structure housing the shock tube. A second shock strength of roughly 20 psi provided data for comparison of effects based on shock speed and strength. In order to obtain two shock strengths for comparison, the test series used two thicknesses of 6061-T6 Aluminum; 0.032 in. and 0.025-in. The diaphragms were made from rolled aluminum sheet, so care was taken to align the grain orientation the same way

on every test to prevent any diaphragm performance differences due to the directionality of the metal micro-structure.

To minimize the number of shots to "zero" in on the desired pressure and profile, 2D calculations were performed prior to the test. The calculations used an estimated driver pressure of 225 psi to represent the 0.032-in. diaphragm burst pressure.

Two driver lengths were tried during the shots set aside to finalize the test conditions. The first two tests using an 18-in. long driver generated a shock profile that would be very difficult to analyze. An additional test shot using the 12.5-in. driver length produced an acceptable pressure profile that was more similar to the Friedlander profile than the pressure-time history generated with the 18-in. long driver. The 12.5-in. driver was then selected for use on all subsequent shots.

3.2. ROUGHNESS PLATES

The effect of two magnitudes and two geometric types of roughness were examined in this testing series. Both a smooth, wavy surface and a sharply pointed surface were used to represent conditions that may be found in non-laboratory test-beds. The peak-to-peak spacing was consistent across all of the perturbation plates, at 4-in. Two amplitudes of each geometry were tested, a 1/4-in. and 1/2-in. amplitude of the sine wave plates and 1/2-in. and 1-in. amplitudes for the pyramid plates. In order to maximize the range of amplitudes used in the study, only one amplitude (1/2-in.) was used for both geometries. The amplitude and spacing dimensions fell within the realm of real-world conditions of interest.

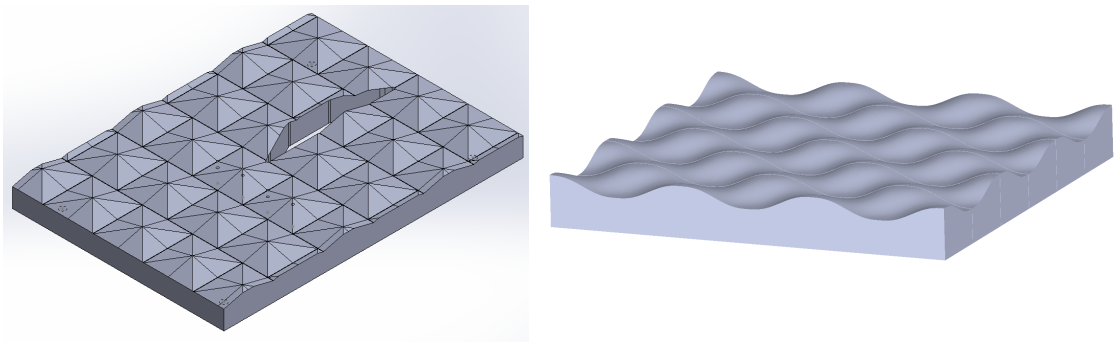

Figure 3.1. Drawings of the two types of roughness plate geometry.

Before settling on the configurations shown in Figure 3.1, other types of roughnesses were considered. One option considered was a random roughness pattern. This option was discarded due to the difficulty of determining what characteristics of the random roughness affected the measured pressure. A second option considered using a pattern that consisted of waves along only one axis of the plate. This second option was discarded due to the concern that the results would not be representative of real-world situations.

The roughness patterns chosen had consistent amplitudes and spacing across each plate, which helps to simplify the data analysis. The construction of the plates allows both a "peak" and a "valley" measurement at the same distance from the diaphragm. The consistent distance from the diaphragm allowed the data collected from the peak and valley gages to be compared directly without attenuation corrections that would be necessary if the gages were not equidistant from the diaphragm.

Three of the four perturbation plates were machined out of high-density polyethylene (HDPE), and the fourth was from medium-density fiberboard (MDF).

The 1-inch peaked plate was machined from MDF for expediency since it was last minute addition when the testing series was ahead of schedule. The wing mount and associated gages were not included on the 1-inch peaked plate shots. Due to the expedited nature of manufacturing the fourth plate, the wing mount could not be accommodated.

3.3. INSTRUMENTATION

In order to meet the objectives stated previously, pressure time histories from all incident gages and Schlieren video were required for all shots. The stagnation pressure data was desired, but not required. When successfully collected, the combination of stagnation and incident pressures enabled the calculation of dynamic pressure.

The data from twelve pressure gages was recorded using a 16-channel MeDAQ Data Acquisition System (DAS), recording at a minimum sample rate of 1 MS/sec. Additional information regarding the MeDAQ DAS can be found in the operating manual.

A high speed Phantom v7.3 camera was used to capture the shock as it passed over the roughness plates and pressure transducers mounted in the plate. The Phantom v7.3 is a monochrome camera that can record up to 500,000 frames per second with a 1 microsecond intra-frame time.

The data acquisition system and Phantom camera used the same trigger, ensuring that the timestamps were consistent between pressure and optical data. By utilizing the same trigger, the optical data was easily compared to the pressure data for each frame of video acquired.

3.3.1. Pressure Transducers. The testing series used Endevco 8350A-100 and 8350A-200 piezoresistive pressure transducers. The only 8350A-200 transducer was mounted in the stagnation pressure probe. Ten 8350A-100 gages located throughout the tube provided shock speed, baseline pressure, pressure across the perturbation plates, measurements within the boundary layer, and incident pressure to complement the stagnation pressure measurement.

All gages were calibrated using a static pressure setup. While a dynamic calibration is preferred when gages will be used to measure rapidly changing conditions, it requires more specialized equipment than was available. In some cases, a gage will pass a static calibration, and fail in a dynamic environment. However, this behavior is relatively rare,

and there were enough planned replications in the test series that a single failure would not compromise the entire data set.

Figure 3.2 shows a cutaway view of the tube and the gage locations for the tests. The placement of the top- and wing-mounted transducers remained constant throughout the test series and Figure 3.3 shows various views of the wing mount and stagnation probe.

The two transducers located on the top of the shock tube, spaced 6-in. apart provided data to calculate shock speed from each shot. A total of five transducers were located within the wing mount. The bottom three transducers on the wing measured incident pressure at distances of 0.5-in., 1-in., and 2-in. above the flat plate. The other two sensors on the wing measured stagnation and incident pressure at a height of 7-in. from the flat plate.

The four remaining transducers, measured pressure as the shock passed over the flat or perturbation plates. For the perturbation plate tests, two transducers measured pressure on the peak and two measured pressure in the valley, to provide redundant data for each test. The four floor transducers were mounted with 2-inch spacing for all tests. Figure 3.4 shows the spacing of Gages 1-4 and their peak and valley positions on one of the perturbation plates. When a roughness plate was in place, Gages 1 and 3 were mounted on peaks, while Gages 2 and 4 were mounted in valleys.

During certain the tests with the flat plate, the transducers were mounted flush with the surface, recessed, protruding, or had local surface imperfections around the transducer. These mounting configurations were intended to assess the error introduced by imperfectly mounting conditions on an otherwise perfectly smooth surface. See Figure 3.5 for the various mounting configurations. The Delrin insert containing Gage 1 was recessed by 0.1270-in., and the insert containing Gage 4 protruded by 0.1235-in. The insert containing Gage 2 was cut down so that the gage face was level with the plate surface but a circular recession surrounded the gage. The circular recession was 0.1265-in. wide and 0.1210-in. deep. All of the gage faces were kept parallel to the plate, no oblique cases were studied.

For details on the number of tests conducted with each gage mount and plate configuration, refer to the test matrix in Section 3.1.4.

The data sampling rate of 1 MS/sec was selected to give a fine time-resolution of the shock wave, and was sufficient to resolve the rise of the shock front given the anticipated shock speed and gage diameter. The data acquired by the transducers allowed for detailed analysis of the shock flow over the plates and boundary layer extents, as affected by the perturbation plates and shock strength.

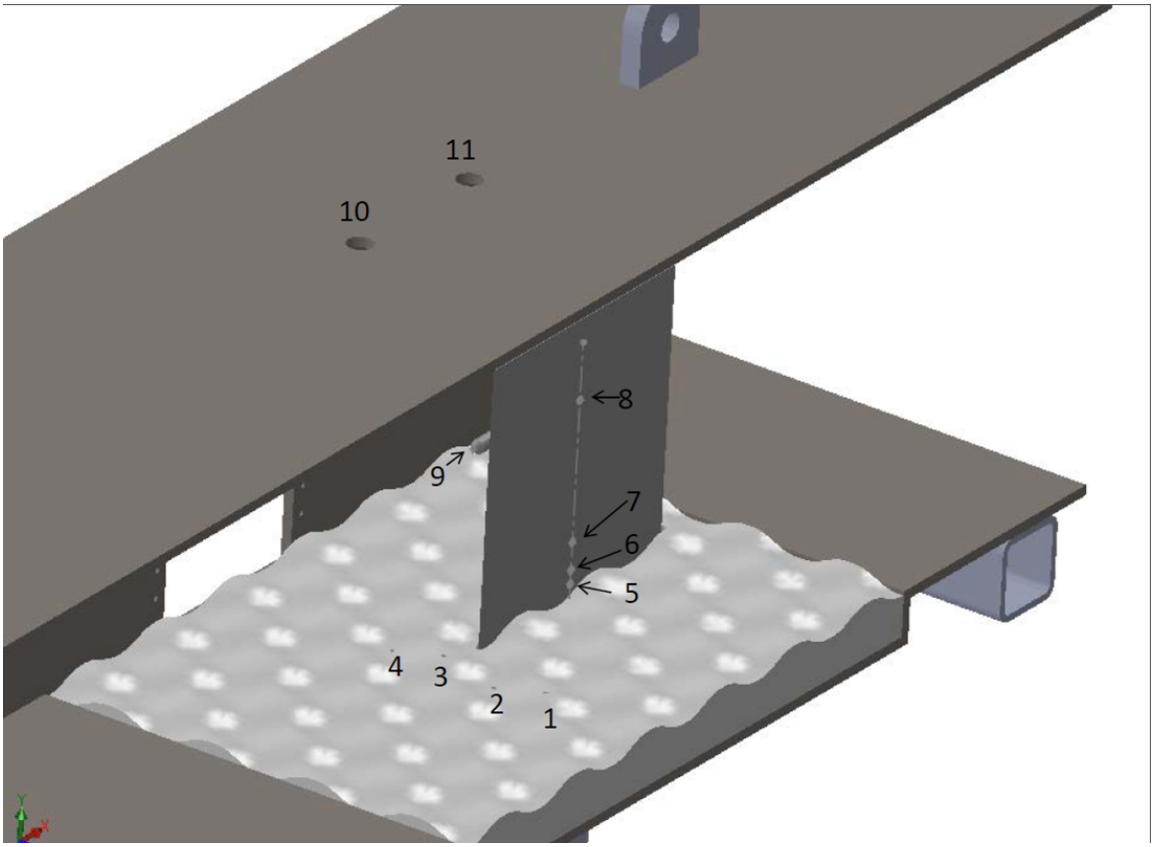

Figure 3.2. Pressure gage locations in the instrumentation section.

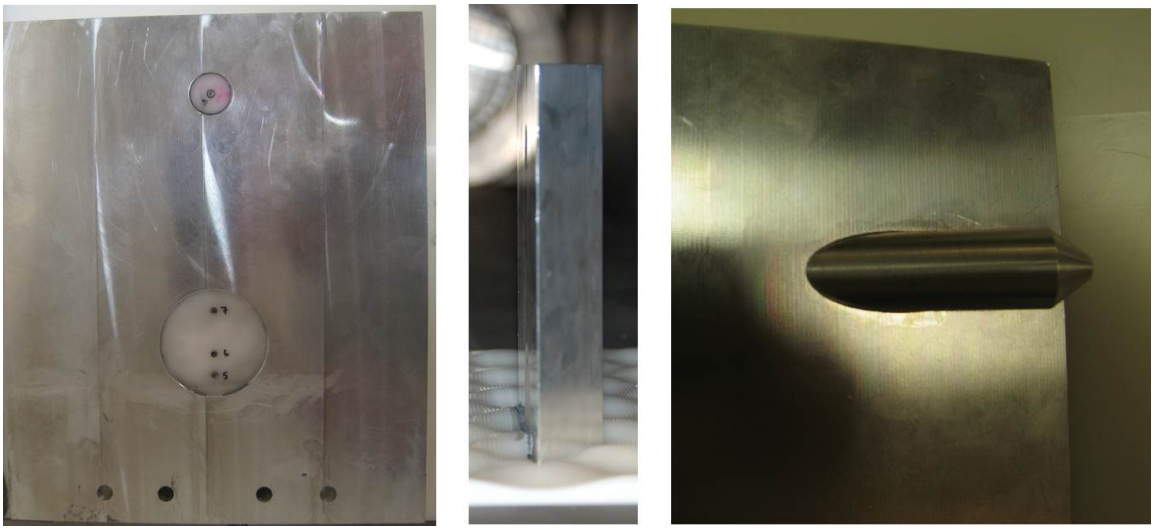

Figure 3.3. Photos of the wing mounted gages, both incident and stagnation.

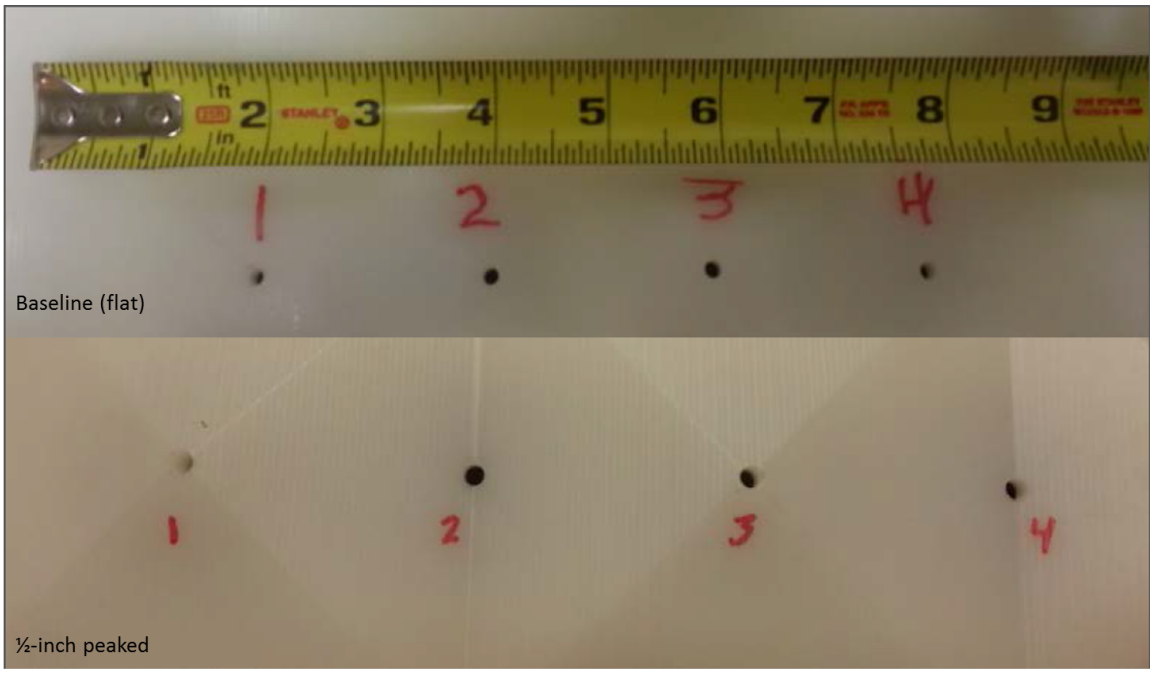

Figure 3.4. Photos of the floor mounted gages for both the baseline and 1/2-inch peaked cases.

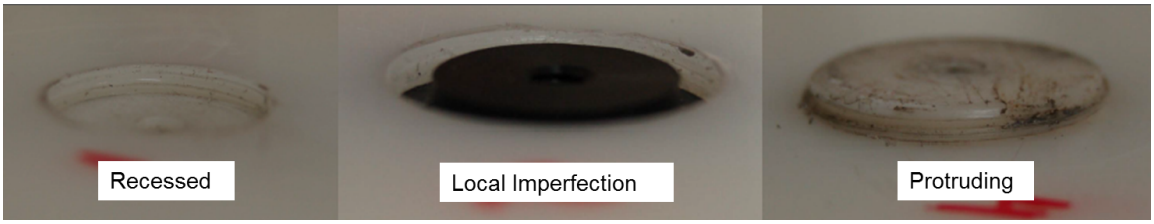

Figure 3.5. Photos of the the imperfect mounting configurations.

3.3.2. Schlieren Video. As covered in Section 2.5.1 Schlieren imaging techniques allow the visualization of density differences that are otherwise invisible to the human eye.

Since there are a large number of factors that can influence shock wave structure and pressure, obtaining pressure measurements for a variety of variables is only part of the solution. Without a secondary method of observing the environment at and behind the shock front, it would be extremely difficult, if not impossible, to determine what causes a pressure-time history to vary from an "ideal" profile. For this test series, the secondary method of characterizing the environment was high speed Schlieren video.

While the Schlieren video did not provide any direct measurements about the shock, the information gathered provides images of the structure of the shock during each test and can help identify the cause of non-standard pressure-time history profiles. The Schlieren setup for this test series provided a visual record of the shock front as it passed over the area where the transducers were mounted in the plates. The qualitative optical recordings complimented the quantitative pressure measurements, providing a better understanding of the relationship between shock structure and measured pressure.

The equipment used to obtain the Schlieren video included a Phantom v7.3 high speed camera, custom circuit and LED flash, and a 4.5-in. diameter concave mirror. The basic setup is shown in Figure 3.6, the camera and light source are visible in the bottom half of the photograph, with the mirror in sight through the shock tube windows. The custom

circuit synced the LED flashes with the camera frame rate using the Transistor-Transistor Logic (TTL) output signal from the Phantom.

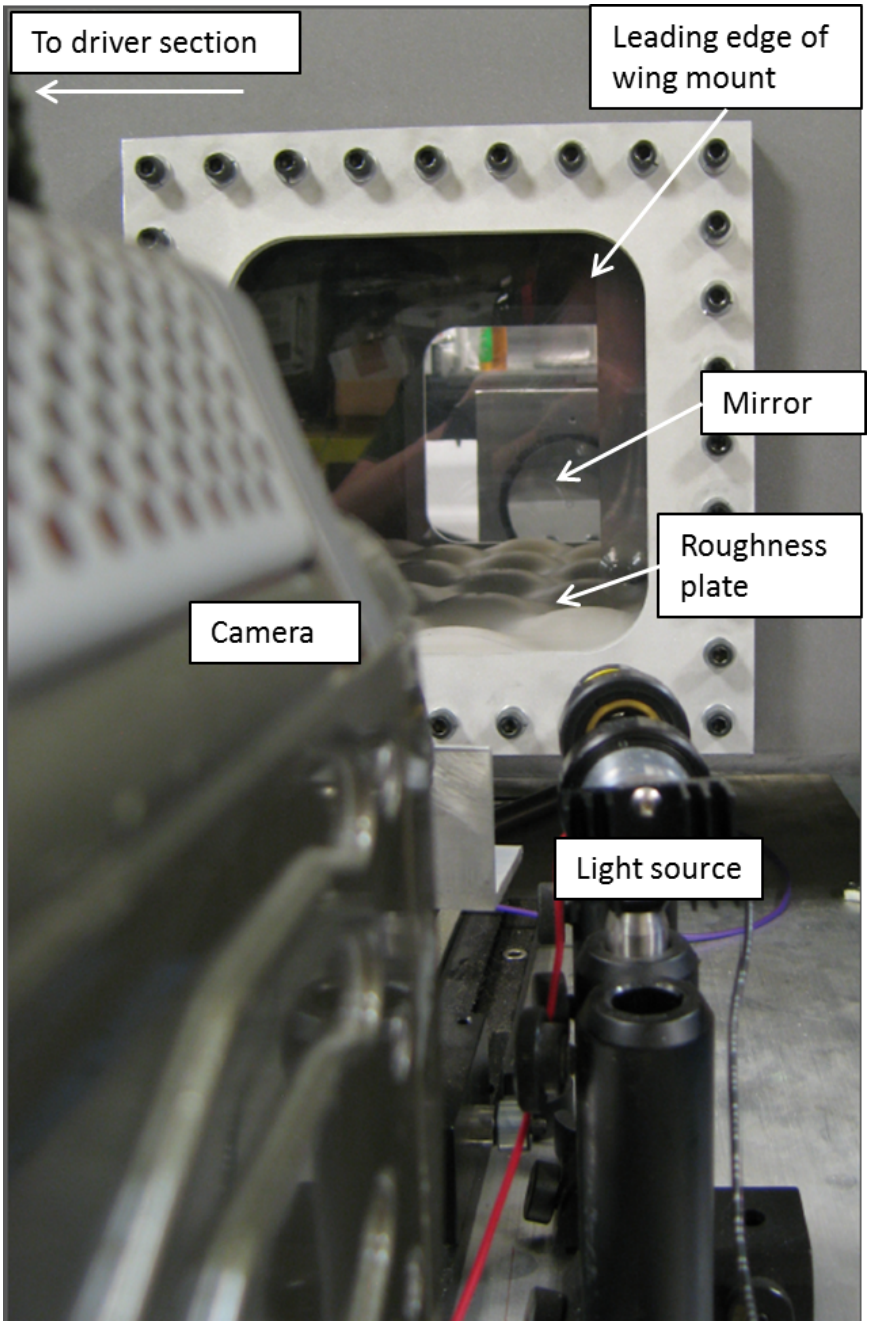

Figure 3.6. Photograph of the Schlieren setup, looking through the shock tube windows.

The size of the viewing area is limited by the size of the mirror, which had a 4.5-inch diameter. The optical board and mirror were positioned such that the field of view encompassed the location of the gages mounted in the plates. The camera Field Of View (FOV) was periodically adjusted throughout the testing series, and the frame rate varied from 64,516-78,431 fps to accommodate the changes in FOV. The frame rate range used during the test series was selected after considering both the resolution and number of frames taken while the shock passed through the 4.5-in. FOV.

Figure 3.7 shows a sample FOV, with scale. The dark circle visible on the center of the mirror served two purposes. The circle allowed the camera to be easily focused and also provided a fixed scale within the field of view. The diameter of the small circle was 0.317-in. The dark lines visible in the sample FOV are from imperfections in the windows, which affected how the light refracted. The leading edge of the wing mount is also visible on the right hand side of the figure.

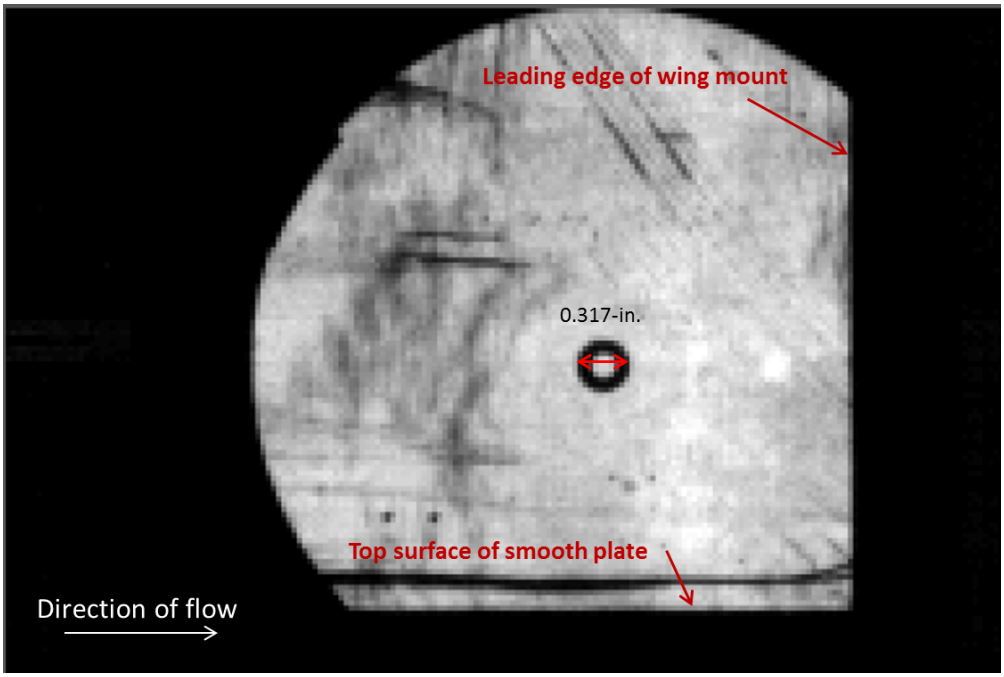

Figure 3.7. Sample FOV of the Schlieren setup. The leading edge of the wing, the top surface of the plate, the mirror, and the center circular scaling/focusing mark are visible.

3.4. TEST MATRIX

The as-completed test matrix is given in Table 3.1. The test matrix denotes the configuration and number of replications for all of the 46 shots in the test series.

Table 3.1. As-completed test matrix.

Number of Shots	**Surface Type**	**Gage Mounting Configurations**			**Diaphragm Thickness (inches)**		**Driver Length (inches)**
		Flush	Wing	Imperfect	0.032-in.	0.025-in.	
3	Smooth	x	x		x		12.5
2	Smooth	x	x			x	12.5
4	1/2" Wavy	x	x		x		12.5
4	1/2" Wavy	x	x			x	12.5
4	1/2" Peaked	x	x		x		12.5
4	1/2" Peaked	x	x			x	12.5
2	Smooth	x			x		12.5
4	1/4" Wavy	x	x		x		12.5
4	1/4" Wavy	x	x			x	12.5
4	Smooth		x	x	x		12.5
4	Smooth		x	x		x	12.5
5	1" Peaked	x			x		12.5
2	1" Peaked	x				x	12.5

4. RESULTS

The order in which the tests are discussed herein does not fit the chronological test order, but is presented in an order that makes the text easy to follow and understand. Throughout the section, figures that include pressure traces from multiple replications of the same set of variables include an average pressure trace in red. The average pressure trace is to allow the reader to quickly distinguish the typical waveform in addition to visualizing the consistency of the data obtained from a certain test configuration.

4.1. SUMMARY OF TESTS CONDUCTED

The test matrix in Section 3 summarizes the variables and gages present on each test, as well as other selected parameters. Two of the gage locations required switching transducers mid-series due to gage failures. Gage 3 recorded pressures that were very different from Gages 1, 2, and 4; all four of these gages had equivalent mounting conditions and distance from the diaphragm during the baseline tests. After verifying the calibration factors for the gages were correct, Gage 3 was swapped partway through the test series, but the measurements did not align with Gages 1, 2, and 4. It is possible that a channel on the MeDAQ acquisition system was not functioning properly, but due to the limited testing time available, the exact cause of the questionable measurements was not determined. Consequently, the Gage 3 data is not presented in this document.

The other transducer that failed during the test was Gage 8, the incident gage located on the wing 7-in. above the bottom of the shock tube. However, instead of an immediate failure, Gage 8 experienced a gradual failure that went undetected until after the test series. Throughout the duration of the test series, Gage 8 passed the autobalance checks conducted prior to each shot using the MeDAQ. One possible mechanism of failure that would cause this gradual decline while allowing the transducer to pass the autobalance checks is a slow

decay of the bond between the piezoresistive material and the Wheatstone bridge circuit. The data for Gage 8 is presented through Shot 21, at which point the data was determined to no longer be of sufficient quality to use for comparisons.

4.1.1. Driver Pressures and Shock Speeds. The burst pressures and diaphragm failure modes were very consistent throughout the test series. The 0.032-inch diaphragms had an average burst pressure of 235.4 psi, and a standard deviation of 4.1 psi. The 0.025-inch diaphragms had an average burst pressure of 171.4 psi, and a standard deviation of 6.2 psi. Adjusted for local atmospheric conditions, the diaphragm thicknesses of 0.032 and 0.025-inches resulted in average shock speeds of Mach 1.81 and 1.72, respectively.

4.2. DATA PROCESSING

The post-test data processing was kept to a minimum; only a 10-point moving average smoothing function was applied to the data traces. The purpose of the smoothing function was to remove any high-frequency spikes from the data recording system that may be mistaken for pressure measurements.

For the comparison plots presented in this section, the trace times-of-arrival (TOAs) were adjusted to the same value. This adjustment provided a visually simple figure to identify similarities and differences in the pressure and impulse time histories.

As mentioned in Section 2.1.3, corrections to the measured stagnation pressure are required to get the actual shock parameters, due to the formation of a detached shock in front of the stagnation probe. However, this author consulted with colleagues who have decades of experience in explosives testing and learned that corrections to stagnation probe data are not commonly applied. Furthermore, no negative effects had been seen with regard to determining the effectiveness of the explosive/target configurations tested. So, corrections to the stagnation probe and wing mounted transducers were not made in an attempt to keep the data as close to the as-measured condition as possible, which corresponds to the treatment of other pressure data gathered on a variety of research topics.

4.3. BASELINE TESTS

Multiple repetitions were conducted with both diaphragm thicknesses to establish baseline pressures and waveform characteristics. Additionally, the wing mount was removed for two tests to verify that it did not affect the pressures measured by the floor gages due to a bow shock or other disturbance of the planar shock front.

The shock front remained planar for all cases using the flat plate. Figure 4.1 shows a frame from the Schlieren video taken during Shot 4 as the shock front passed over the floor gage locations. The shock is traveling from left to right in the image shown, and the shock front is 0.32-inches thick. All of the shots using the flat plate to establish baseline pressure measurements had similar planar shock fronts.

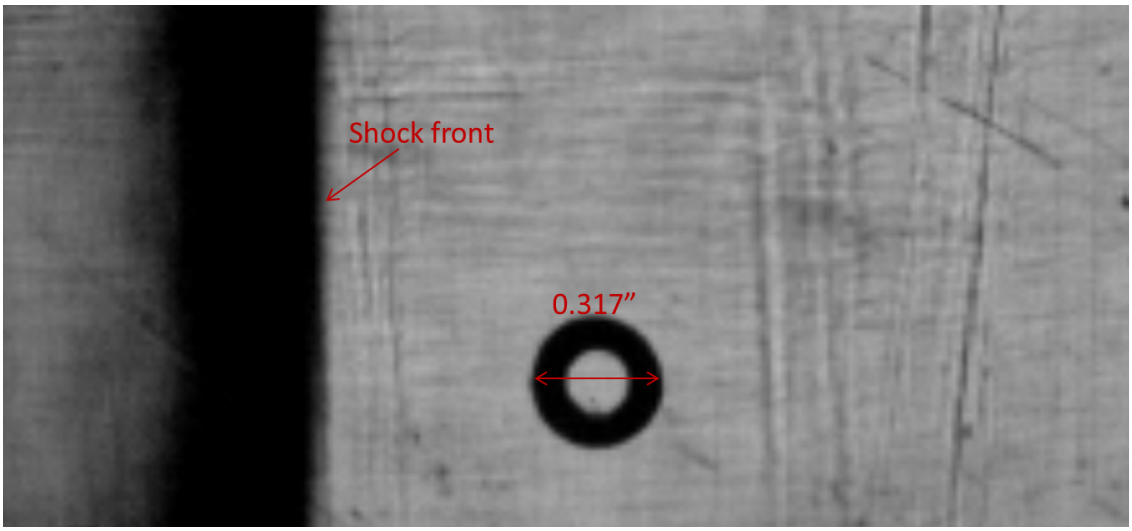

Figure 4.1. Planar shock front from Shot 4, baseline case. Direction of travel is left to right.

Table 4.1 summarizes the pressure data from Shots 3-5, which established the baseline using the 0.032-inch diaphragms. The peak pressures were very consistent, as demonstrated by the small standard deviations at each gage. One item worth noting is that while

Channels 1-4 (floor mounted) were equidistant from the diaphragm and were all mounted in the flat plate, the peak pressures were not consistent across all four gage locations. This phenomenon means that pressure and impulse data across the test series should only be compared at the same gage location.

Table 4.1. Shots 3-5 max pressures, averages, and std. deviation. (0.032-inch diaphragm) Gages 1, 2, and 4 were all flush mounted with the floor of the shock tube. Gages 5, 6, 7, and 8 were mounted on the wing at 0.5, 1.0, 2.0, and 7.0-inches above the surface, respectively.

Gage	CH1	CH2	CH4	CH5	CH6	CH7	CH8
Shot 3	21.70	18.12	22.49	25.56	25.31	23.64	29.54
Shot 4	20.46	18.00	22.46	24.72	25.65	22.98	29.56
Shot 5	21.42	17.49	21.78	24.54	24.56	23.31	28.97
Shot 3-5 Avg	21.19	17.87	22.24	24.94	25.17	23.31	29.35
Shot 3-5 Stdev	0.65	0.34	0.40	0.55	0.56	0.33	0.33

Figure 4.2 shows the pressure traces for Shots 3-5 for Gages 1, 2, and 4 which were all located in the floor. On each graph, an average pressure trace is shown in red. Figure 4.3 shows the pressure traces for Shots 3-5 for the wing mounted gages: 5, 6, 7, and 8.

Figures 4.2 and 4.3 demonstrate the repeatability of the pressure data. Both the shape of the pressure traces and the peak pressures are highly reproducible at each gage location. For shots using a perturbation plate or non-flush gage mounting configuration, differences in peak pressure or trace shape can be attributed to effects of the perturbation plate and not variability of the shock tube environment.

In Figure 4.2 the Gage 4 records do not align as closely with each other as do the records from Gages 1 and 2. The records start to diverge around 12 ms, which is likely due to a minor issue with the gage returning to its baseline value following a dynamic event. Since the Gage 1 and Gage 2 records align closely throughout the entire event, the data set

was not compromised by the late time Gage 4 drift. The Gage 4 impulse curves in Figure 4.2c were truncated at T+15 ms to eliminate falsely high impulse values due to the gage's slow return to baseline.

The impulse values for all of the gage locations on Shots 3-5 had a fairly small spread for the duration of the positive phase. The Gage 4 records were all truncated at T+15 ms, as mentioned previously, at which time the records likely had not been severely affected by the late time gage behavior.

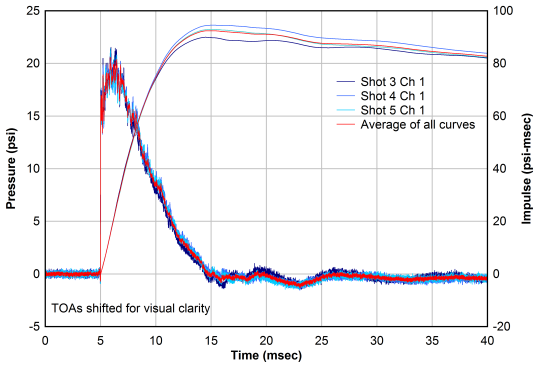

(a) Ch. 1.

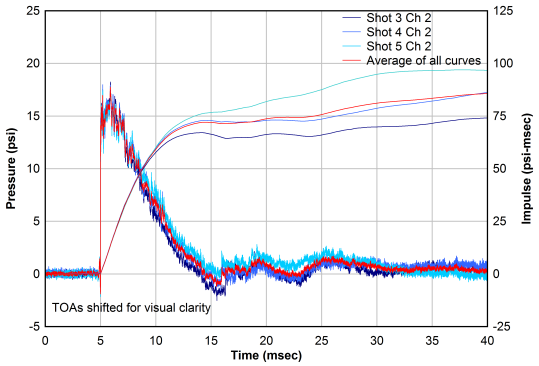

(b) Ch. 2.

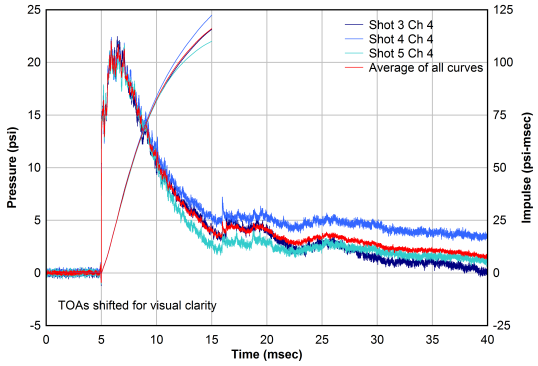

(c) Ch. 4.

Figure 4.2. Flat Plate - Floor Gage Comparisons. All gages flush mounted with the flat plate.

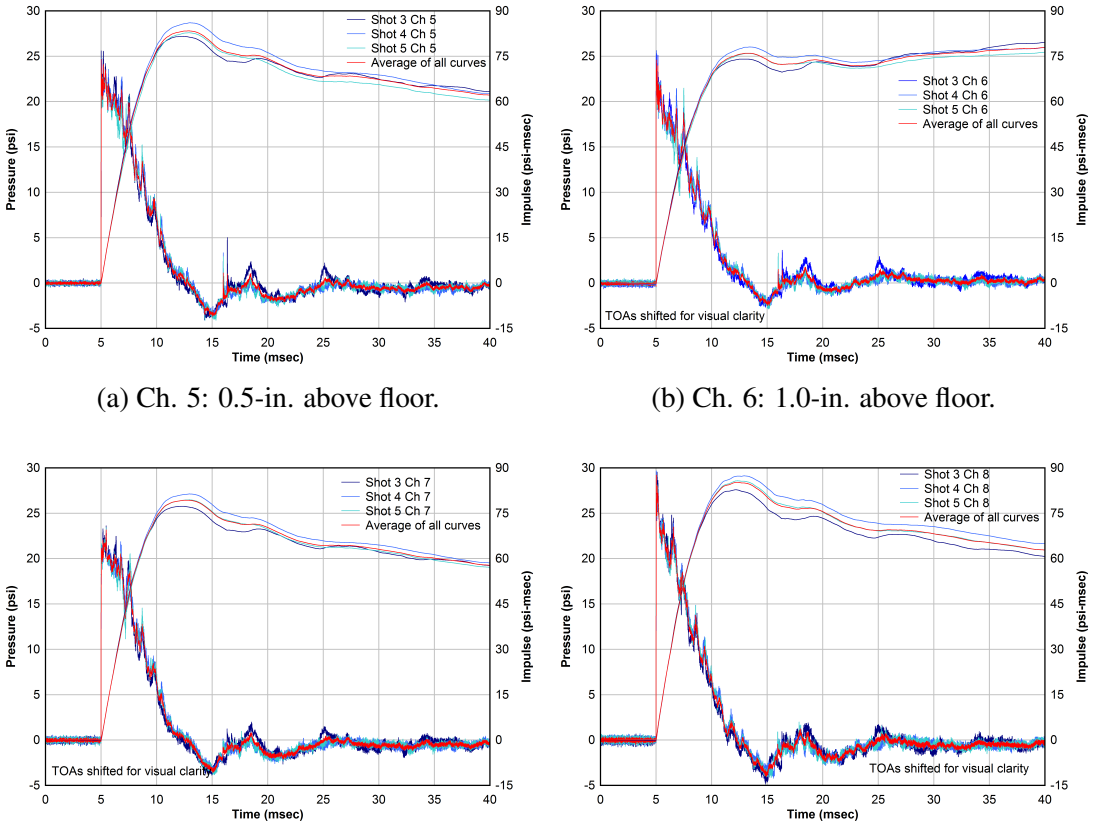

(a) Ch. 5: 0.5-in. above floor.

(b) Ch. 6: 1.0-in. above floor.

(c) Ch. 7: 2.0-in. above floor.

(d) Ch. 8: 7.0-in. above floor.

Figure 4.3. Flat Plate - Wing Mounted Gage Comparisons.

4.3.1. Stagnation Pressure Data. One stagnation pressure gage was fielded on the wing mount, located at 7-inches above the floor of the shock tube. Stagnation pressures are typically measured to allow for the calculation of dynamic pressure, which cannot currently be directly measured. However, over the course of this series of tests, neither of the two different gages used at the stagnation location (Gage 9) survived for the entire series; therefore the stagnation dataset is limited. While extensive characterizations of the environment using the stagnation data will not be provided, one plot is shown in Figure 4.4 to provide an example of the stagnation pressure present. The pressure traces for the stagnation and incident pressure are plotted in Figure 4.4, and the peak pressures are quite similar,

although the later time impulse varies by roughly 9 psi-ms. The dynamic pressure over the course of the test, calculated as stagnation minus incident pressure, was small.

To obtain the true stagnation pressure, the data gathered from Gage 9 would need to be adjusted to account for the detached shock that occurs in front of the stagnation probe. The differences between adjusted versus unadjusted stagnation data are very small compared to the amount of error present due to other factors on non-laboratory tests. Based on these conversations, the decision was made not to alter the stagnation data gathered during this series.

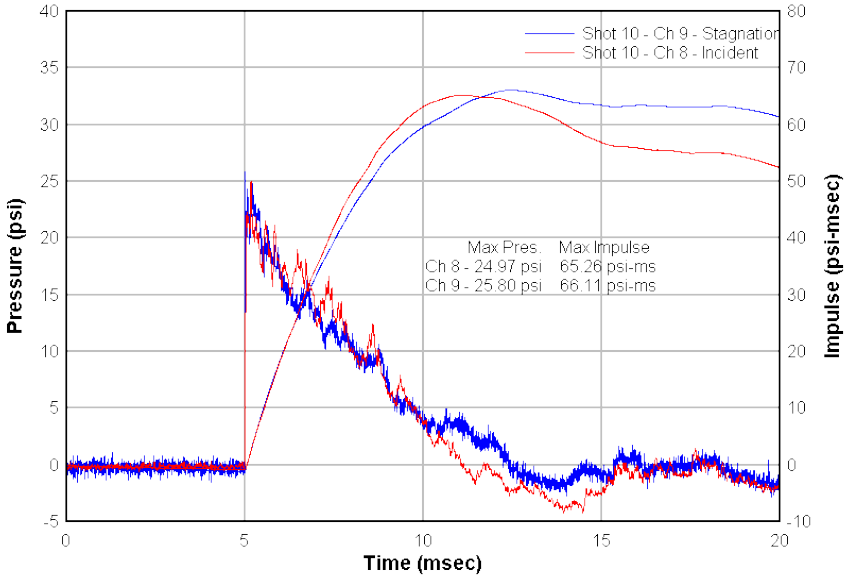

Figure 4.4. Shot 10 - Stagnation and Incident Pressure Traces. Both stagnation and incident pressure gages located at 7.0-in. above the floor of the shock tube.

4.4. WAVY PLATE TESTS

4.4.1. 1/4-inch Amplitude Wavy Plate Tests. With the 1/4-inch sine wave perturbation plate in place, eight shots were conducted, four with the 0.032-inch diaphragm and four with the 0.025-inch diaphragm. Tables 4.2 and 4.3 summarize the peak pressure

data along with the averages and standard deviations for each gage location. As covered previously, the data from Gages 3 and 8 are not included in the summary tables because the quality of the data was suspect at this point in the test series.

The standard deviations for all gage locations for tests conducted with the 1/4-inch wavy perturbation plate are higher than the standard deviations calculated for the baseline cases. The difference in standard deviations indicates that a rough surface increases the variability from shot to shot. For the wing mounted gages, the standard deviation decreases as the distance from the gage to the plate increases. The trend of decreasing variability with height indicates that the presence of a perturbation plate creates effects that are only observed locally.

Table 4.2. Shots 24-27 maximum pressures, averages, and standard deviation (0.032-in. diaphragm). Gage 1: floor mounted, on a peak. Gages 2 and 4, floor mounted, in valleys. Gage 5: 0.5-in. above floor. Gage 6: 1.0-in. above floor. Gage 7: 2.0-in. above floor.

Gage	CH1	CH2	CH4	CH5	CH6	CH7
Shot 24	36.97	31.49	32.45	41.01	30.97	27.21
Shot 25	37.02	33.60	33.73	36.68	30.46	26.04
Shot 26	41.29	30.91	32.48	36.52	27.97	24.96
Shot 27	41.20	33.33	33.24	36.53	27.71	24.47
Shot 24-27 Avg	39.12	32.33	32.97	37.68	29.28	25.67
Shot 24-27 Stdev	2.45	1.33	0.62	2.22	1.67	1.22

Table 4.3. Shots 28-31 max pressures, averages, and std. deviation (0.025-in. diaphragm). Gage 1: floor mounted, on a peak. Gages 2 and 4, floor mounted, in valleys. Gage 5: 0.5-in. above floor. Gage 6: 1.0-in. above floor. Gage 7: 2.0-in. above floor.

Gage	CH1	CH2	CH4	CH5	CH6	CH7
Shot 28	35.03	26.01	27.43	31.83	23.25	21.12
Shot 29	34.00	25.28	27.00	29.78	22.66	22.12
Shot 30	36.85	25.60	27.01	31.48	22.58	20.91
Shot 31	34.64	25.74	26.85	32.10	21.01	20.84
Shot 28-31 Avg	35.13	25.66	27.07	31.30	22.37	21.25
Shot 28-31 Stdev	1.22	0.31	0.25	1.04	0.96	0.59

The standard deviations for most of gage locations for tests conducted with the 1/4-inch wavy plate in place were higher than those for the baseline data. The two exceptions were Gages 2 and 4 (floor mounted, valley) with the 0.025-inch diaphragm in place. For the lower shock strength the shot-to-shot variability was lower with the 1/4-inch roughness plate in place. For most cases, the presence of the 1/4-inch wavy plate data demonstrates that the slight surface roughness increases the scatter in the data.

The gage mounted on a peak (Gage 1) of the wavy plate had more scatter in the data than the gages mounted in valleys in the wavy plate (Gages 2 and 4). The data from these eight tests indicate that measurements from a gage located on a peak are less consistent than from a gage mounted in a valley or on the wing mount.

The standard deviations for the wing mounted gages (Gages 5-7) decrease as the height between the floor of the shock tube and the gage location increases. The data from Gages 5, 6, and 7 show that the Mach reflection and disturbance to the planar shock front near the rough surface affect the measured pressure. The further the gage is from the rough surface, the less the pressure measurement is affected.

Figure 4.5 shows the pressure traces for Shots 24-27 for Gages 1, 2, and 4, which are all located in the floor equidistant from the diaphragm. Gage 1 is mounted on a peak,

while Gages 2 and 4 are mounted in valleys. On each graph, and an average pressure trace is shown in red.

The pressure waveforms for the floor mounted gages in the 1/4-inch wavy perturbation plate are noticeably different from waveforms gathered from the baseline tests with gages flush mounted in a flat plate. The Gage 1 waveform has a tall, narrow spike just after the shock front TOA, a characteristic not present on the Gage 1 baseline waveforms. The Gage 2 and Gage 4 waveforms also have a sharper, taller peak than their baseline counterparts, but the difference is more subtle than seen at the Gage 1 location.

All of the peak pressures measured by Gages 1, 2, and 4 on the 1/4-inch wavy plate shots were higher than their baseline counterparts. The tall, narrow pressure spike present just after TOA on the Gage 1 records did not significantly affect the impulse values, as compared to the baseline. The Gage 1 impulse values between the baseline and 1/4-inch wavy plate shots were very similar through the duration of the positive phase. Due to the larger negative phase that occurred when the 1/4-inch roughness plate was in place, the impulse curves for Gage 1 began to diverge at the end of the positive phase. The Gage 2 impulse curves with the 1/4-inch wavy plate in place were much larger, nearly 50%, than the baseline, due to the higher pressures recorded at this gage location.

While the wing mounted gages had a larger shot-to-shot spread in impulses than floor mounted Gages 1 and 2, the difference relative to the baseline values was less than seen on Gages 1 and 2. In other words, the variance in impulses was larger for the wing mounted pressures, but the roughness plate did not create a large difference in the peak impulse values.

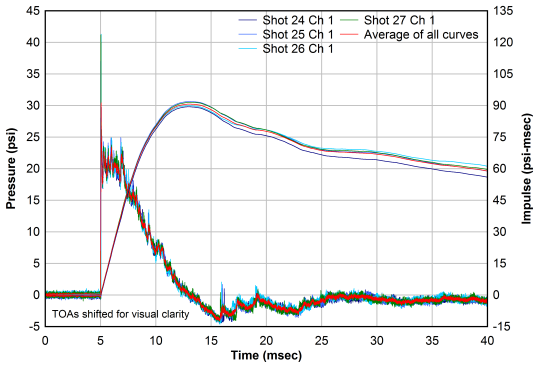

(a) Ch. 1: Floor mounted, peak.

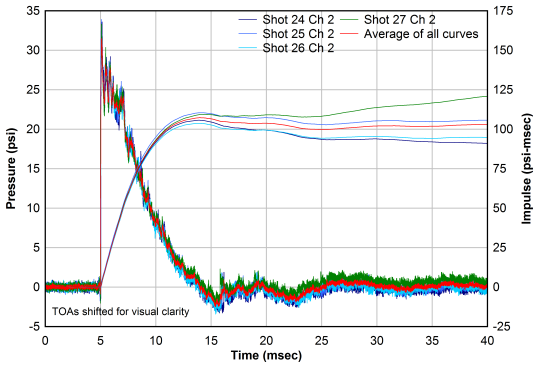

(b) Ch. 2: Floor mounted, valley.

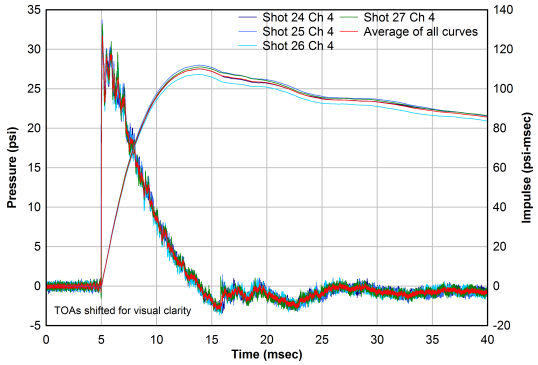

(c) Ch. 4: Floor mounted, valley.

Figure 4.5. 1/4-in. Wavy Perturbation Plate - Floor Gage Comparisons.

Figure 4.6 shows the pressure traces for Shots 24-47 for the wing mounted transducers, Gages 5, 6, and 7. The peak pressure was highest on Gage 5, which was located closest to the perturbation plate. The variance in the pressures measured by the wing mount gages may be due to the gradient of shock strengths within the shock front created as it travels up an inclined surface due to the formation of a single Mach reflection.

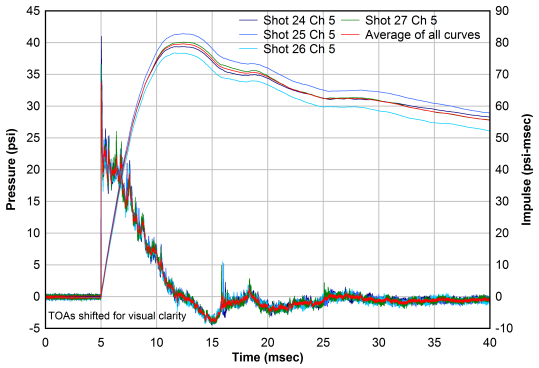

(a) Ch. 5: 0.5-in. above floor.

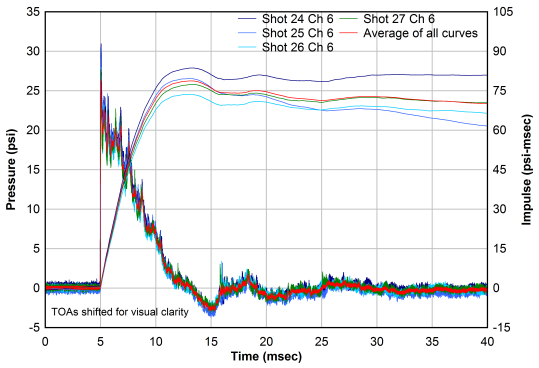

(b) Ch. 6: 1.0-in. above floor.

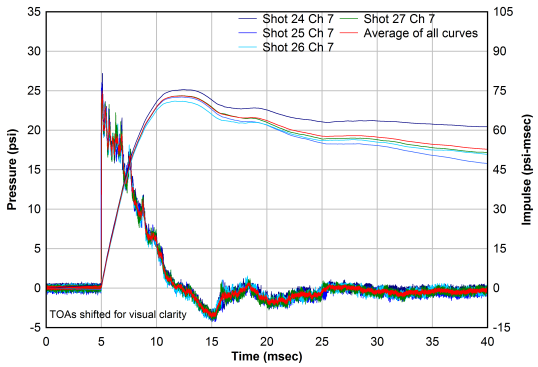

(c) Ch. 7: 2.0-in. above floor.

Figure 4.6. 1/4-in. Wavy Plate - Wing Mounted Gage Comparisons.

Figure 4.7 shows one frame from the high speed video taken on Shot 24. Additional frames and discussion are included in Section 5. In Figure 4.7 multiple shocks are visible as well as a lambda structure in the bottom half of the FOV.

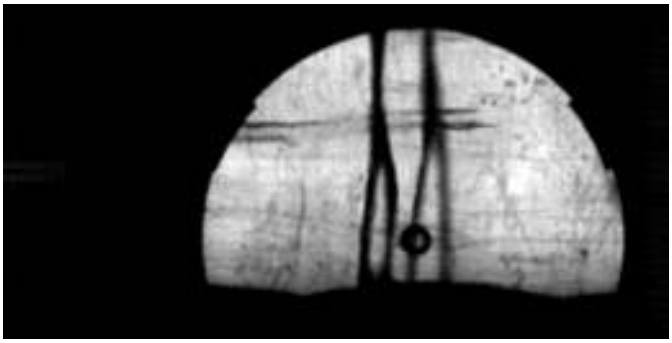

Figure 4.7. Example Schlieren Frame from Shot 24 - 1/4-inch wavy plate. Direction of flow is left to right.

4.4.2. 1/2-inch Amplitude Wavy Plate Tests. With the 1/2-inch sine wave perturbation plate in place, eight shots were conducted, four with the 0.032-inch diaphragm and four with the 0.025-inch diaphragm. Tables 4.4 and 4.5 summarize the Shot 6-13 maximum pressure data along with the averages and standard deviation for each gage location. Gage 1 had the largest standard deviation in the recorded data. The pressures measured by the gages located on the wing mount were higher than the pressures measured by the floor mounted channels.

Table 4.4. Shots 6-9 pressure data summary. (0.032-in. diaphragm) Gage 1: floor mounted, on a peak. Gages 2 and 4, floor mounted, in valleys. Gage 5: 0.5-in. above floor. Gage 6: 1.0-in. above floor. Gage 7: 2.0-in. above floor. Gage 8: 7.0-in. above floor.

Gage	CH1	CH2	CH4	CH5	CH6	CH7	CH8
Shot 6	29.65	22.14	24.51	39.66	34.11	24.42	29.52
Shot 7	25.27	22.22	26.22	37.76	35.10	25.19	29.71
Shot 8	24.83	22.77	26.18	39.48	32.65	24.43	30.00
Shot 9	22.16	22.87	27.53	38.47	31.04	24.62	29.15
Shot 6-9 Avg	25.48	22.50	26.11	38.84	33.23	24.66	29.59
Shot 6-9 Stdev	3.10	0.37	1.24	0.89	1.77	0.36	0.35

Table 4.5. Shots 10-13 pressure data summary. (0.025-in. diaphragm) Gage 1: floor mounted, on a peak. Gages 2 and 4, floor mounted, in valleys. Gage 5: 0.5-in. above floor. Gage 6: 1.0-in. above floor. Gage 7: 2.0-in. above floor. Gage 8: 7.0-in. above floor.

Gage	CH1	CH2	CH4	CH5	CH6	CH7	CH8
Shot 10	19.31	20.48	22.57	30.83	25.18	20.16	24.97
Shot 11	22.91	26.68	23.56	32.45	25.87	20.18	24.93
Shot 12	21.68	21.13	24.24	31.46	25.67	20.36	25.04
Shot 13	21.35	21.36	24.35	33.74	27.84	20.12	24.94
Shot 10-13 Avg	21.31	22.41	23.68	32.12	26.14	20.20	24.97
Shot 10-13 Stdev	1.49	2.87	0.82	1.27	1.17	0.10	0.05

The pressure waveforms for Gage 1 with the 1/2-inch wavy perturbation plate exhibit similar waveforms to those measured with the 1/4-inch wavy perturbation plate in place. The Gage 1 waveform has a very high initial peak with a short time duration that is not seen on Gage 2 and 4. This high, narrow peak may be the result the position of Gage 1, which was located on a peak of the perturbation plate. Unfortunately, Gage 3 did not record good data throughout the series, so comparisons of the two peak mounted gages do not exist.

Gage 2 and 4 waveforms had a slightly different shape than what was seen in Shots 24-27. With the 1/2-inch wavy plate in place, Gages 2 and 4 had roughly 3 ms of oscillation after the arrival of the shock. After this period of oscillation, the pressure attenuated at a rate similar to previous shots.

The peak pressures recorded for Gages 1, 2, and 4, all of which were located in the perturbation plate, were higher than the baseline pressures at the same gage locations. The waveforms for these three gages are shown in Figure 4.8. The data from Gage 2 shows that the attenuation rate changes at roughly T+16 ms. One possible explanation for the later time data scatter on Gage 2 is shock interactions occurring near the center of the floor of the tube due to the geometry of the 1/2-inch wavy roughness plate.

Some scatter was present in the impulse curves for the floor mounted gages (Gages 1, 2, and 4) with the 1/2-inch wavy plate in place. The spread of maximum impulses during

the positive phase was under 10% for both Gages 1 and 4. Gage 2 had more variance in the impulses due to the change in attenuation rates at approximately T+16 ms.

Relative to the baseline impulses, the average Gage 1 impulse was 13% lower than the baseline value despite a higher overall peak pressure. Gage 2 had slower attenuation rates than the baseline and 1/4-inch wavy plate shots, resulting in a larger impulse, while Gage 4 had a lower peak pressure than the 1/4-inch wavy plate shots but nearly the same impulse curve and peak value.

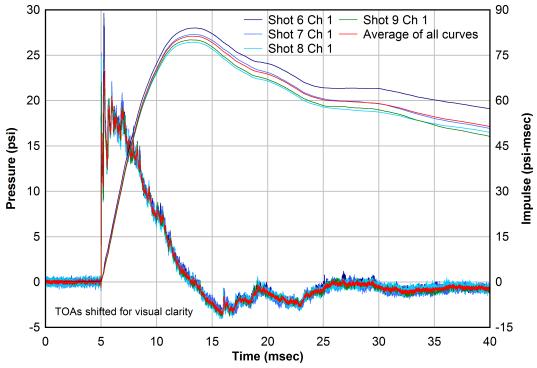

(a) Ch. 1: Floor mounted, peak.

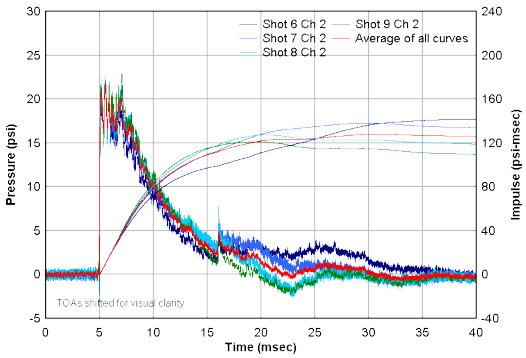

(b) Ch. 2: Floor mounted, valley.

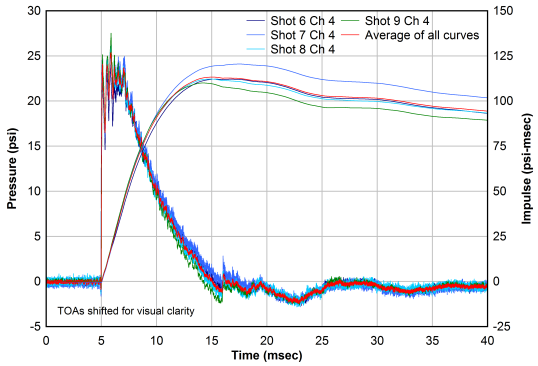

(c) Ch. 4: Floor mounted, valley.

Figure 4.8. 1/2-in. Wavy Perturbation Plate - Floor Gage Comparisons.

Figure 4.9 shows the pressure time histories for the wing mounted gages (5-8) for Shots 6-9. On the wing mount, the average pressure recorded during Shots 6-9 was highest

on Gage 5 (closest to the floor), and got progressively lower at Gages 6 and 7. With the exception of Gage 8, which is located at 7-in. above the floor, a larger distance between the perturbation plate and the gage resulted in a lower measured pressure. In addition to the pressure gradient seen in the Gages 5-7 waveforms, Gages 5 and 6, have a tall, narrow spike just after the arrival of the shock at the gage location. This tall, narrow spike is not seen at Gages 7, and 8, which were mounted further from the plate.

The increased roughness magnitude to shock tube diameter (d/D) resulted in a thicker boundary layer and a stronger reflected shock. The combination of the thicker boundary layer and stronger reflected shock likely produced a very complex environment near the roughness plate, which may explain the lack of a decreasing pressure trend on wing mounted Gages 5-8.

The impulse curves for the wing mounted gages were fairly tightly grouped throughout the duration of the positive phase, as seen in Figure 4.9. Despite having the lowest pressure variance relative to the baseline, the Gage 8 data had the largest spread in impulse values of the wing mounted gages, at roughly 6%. When compared to the baseline data, the average impulses for the Gage 5-8 data had minimal differences, 3% or less. The 3% difference in wing gage impulse values is likely within the experimental error inherent to the shock tube setup.

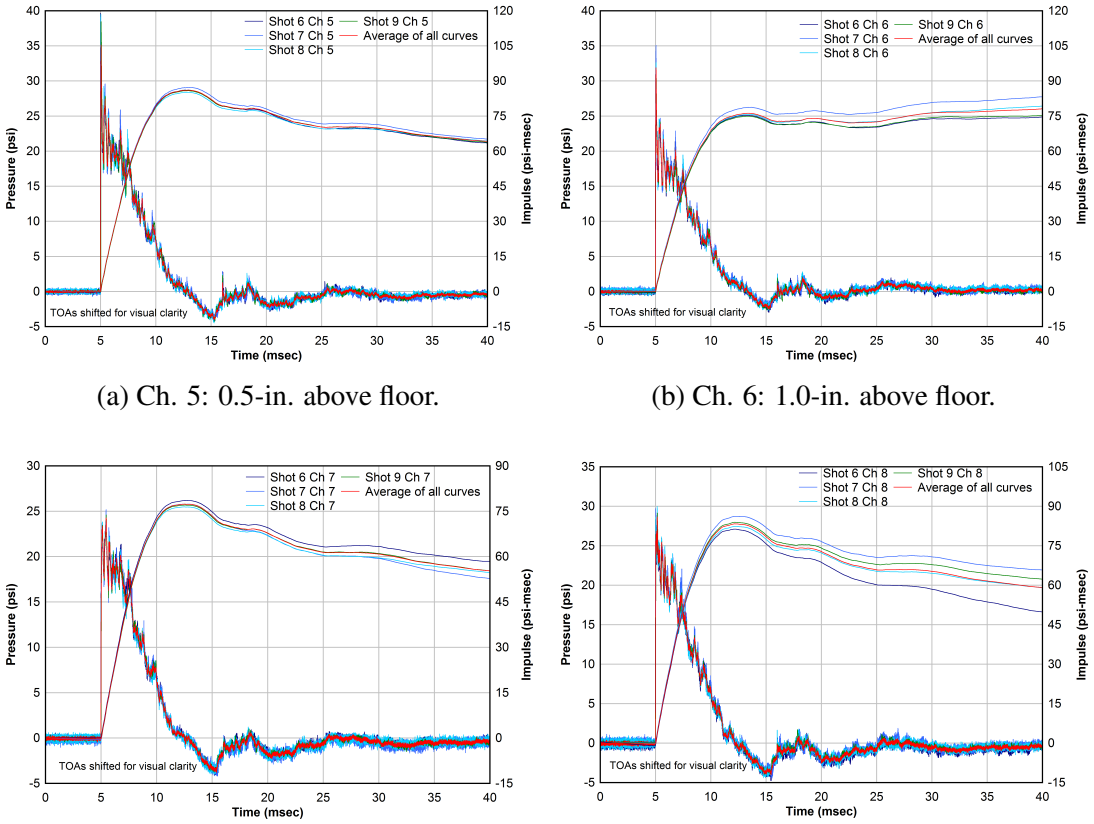

(a) Ch. 5: 0.5-in. above floor.

(b) Ch. 6: 1.0-in. above floor.

(c) Ch. 7: 2.0-in. above floor.

(d) Ch. 8: 7.0-in. above floor.

Figure 4.9. 1/2-in. Wavy Perturbation Plate - Wing Mounted Gage Comparisons.

Figure 4.10 shows one frame from the high speed video taken on Shot 10. Additional frames and discussion are included in Section 5. In Figure 4.10 a reflected shock is visible behind the main shock front. The reflection was caused from the interaction of the shock front and the surface roughness.

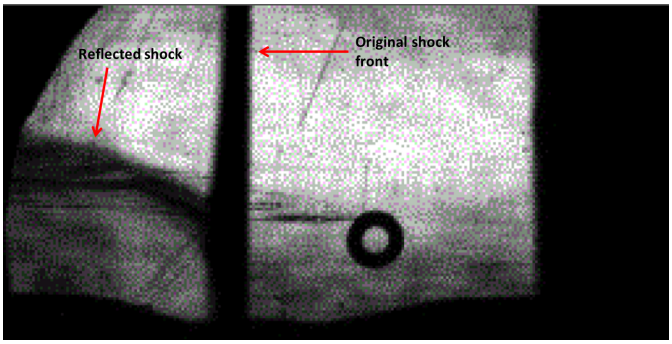

Figure 4.10. Example Schlieren Frame from Shot 10 - 1/2-inch wavy plate. Direction of flow is left to right.

4.4.3. Summary of Wavy Perturbation Plate Tests. During the sixteen shots performed with the two amplitudes of wavy plates in place, several items worth noting were discovered. The pressures measured at all locations except for Gage 8 were noticeably higher than the baseline. With the 1/2-inch wavy plate in place, pressures measured at the Gage 8 location were only 1% higher than the baseline. By the time the shots with the 1/4-inch wavy plate were conducted, Gage 8 had failed so no direct comparisons can be made for those shots.

In addition to the higher pressures measured across all gage locations, pressures on the wing mount also varied. The average pressure at the Gage 5, 6, and 7 locations showed a trend of increasing pressure with decreased distance between the roughness plate and the gage.

The shape of the waveform also differed from the baseline locations for several of the gage locations. The Gage 1, 5, and 6 records had a tall, narrow pressure spike just after the TOA, which was not present in the baseline data nor was it present on the Gage 2, 4, 7, or 8 locations. The spike is likely an the result of certain gage location and geometry combinations.

The peak impulses recorded on the floor mounted gages were different than those recorded on the baseline shots, regardless of which amplitude of wavy plate was in place

during the shot. However, the impulses recorded at the wing gage locations on the wavy plate tests were not significantly different than the baseline data.

4.5. PEAKED PLATE TESTS

4.5.1. 1/2-inch Peaked Plate Tests. With the 1/2-in. peaked perturbation plates in place, eight shots were conducted, four with the 0.032-in. diaphragm, and four with the 0.025-in. diaphragm in place. Tables 4.6 and 4.7 summarize the maximum pressures, along with the averages and standard deviations for each gage location during Shots 14-21. The data from Gages 3 and 9 are not present in Tables 4.6 and 4.7 due to the failures of these gages, as discussed previously.

For Shots 14-17, Gages 1, 2, and 4, all of which were mounted in the perturbation plate, had standard deviations that were approximately 3x higher than their baseline counterparts. In addition to a larger variance at each gage location, the majority of the gages recorded pressures higher than the baseline. The average peak pressure recorded on Gages 7 and 8 were similar to those of the baseline, with only a 6% and 3% difference, respectively.

Table 4.6. Shots 14-17 pressure data summary. Gage 1: floor mounted, on a peak. Gages 2 and 4, floor mounted, in valleys. Gage 5: 0.5-in. above floor. Gage 6: 1.0-in. above floor. Gage 7: 2.0-in. above floor. Gage 8: 7.0-in. above floor.

Gage	CH1	CH2	CH4	CH5	CH6	CH7	CH8
Shot 14	20.95	22.95	23.26	29.96	26.11	23.53	29.63
Shot 15	23.82	24.24	25.27	30.36	26.57	23.70	28.62
Shot 16	24.74	25.24	26.19	28.80	27.22	24.03	30.40
Shot 17	24.72	23.93	24.91	29.88	-	24.45	28.54
Shot 14-17 Avg	23.56	24.09	24.91	29.75	26.63	23.93	29.30
Shot 14-17 Stdev	1.79	0.95	1.22	0.67	0.56	0.40	0.88

Table 4.7. Shots 18-21 pressure data summary. (0.025-in. diaphragm) Gage 1: floor mounted, on a peak. Gages 2 and 4, floor mounted, in valleys. Gage 5: 0.5-in. above floor. Gage 6: 1.0-in. above floor. Gage 7: 2.0-in. above floor. Gage 8: 7.0-in. above floor.

Gage	CH1	CH2	CH4	CH5	CH6	CH7	CH8
Shot 18	21.96	19.03	19.63	25.81	23.65	19.61	24.48
Shot 19	22.50	20.60	20.53	26.02	22.75	20.26	25.81
Shot 20	22.19	20.40	19.91	25.96	23.21	19.87	25.11
Shot 21	21.85	19.84	19.75	24.96	21.82	19.20	25.09
Shot 18-21 Avg	22.12	19.97	19.95	25.69	22.86	19.74	25.12
Shot 18-21 Stdev	0.29	0.70	0.40	0.49	0.78	0.45	0.54

Figure 4.11 shows the pressure traces for Shots 14-17 recorded on Gages 1, 2, and 4, all of which were mounted in the perturbation plate. As on previous shots, Gage 1 was mounted on a peak, while Gages 2 and 4 were mounted in valleys. Gages 1, 2, and 4 were equidistant from the diaphragm, consistent with the other shots in the series.

In Figure 4.11, note that the pressure waveforms for Gages 1, 2, and 4 exhibit a "double peak" waveform that was not present on the data from the wavy plate tests. The double peak for this test configuration is characterized by an initial peak pressure followed by 0.50-0.75 ms of attenuation and a second, larger peak pressure. After the second peak pressure, the pressure attenuates in a manner similar to previously discussed tests.

Despite the "double peak" waveforms present on the floor gages with the 1/2-inch peaked plate in place, the maximum impulses for Gages 1, 2, and 4 were fairly consistent. The spreads on the data gathered from Gages 1, 2, and 4 were under 10% for the duration of the positive phase, although the impulse curves diverged later in the record. All of the average maximum impulses for Gages 1, 2, and 4 with the 1/2-inch peaked place in place were lower than the baseline pressures. Gage 1, located on a peak, had an impulse value 40% lower than the baseline value, while the Gage 2 and 4 impulse values were only 8% and 13% lower than the baseline, respectively.

Figure 4.12 shows the pressure traces for the wing mounted gages (5-8) recorded on Shots 14-17. The overall maximum pressure was highest on Gage 5, which was also

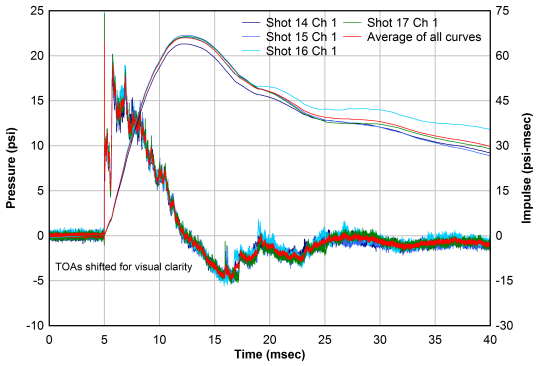

(a) Ch. 1: Floor mounted, peak.

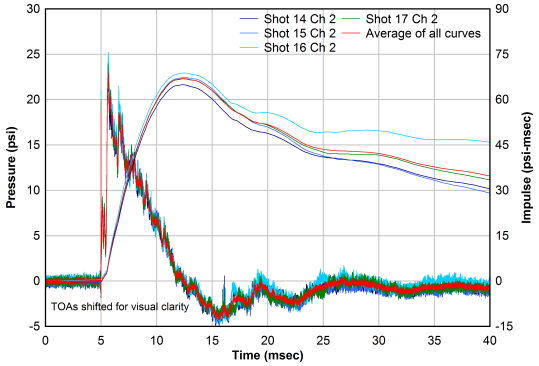

(b) Ch. 2: Floor mounted, valley.

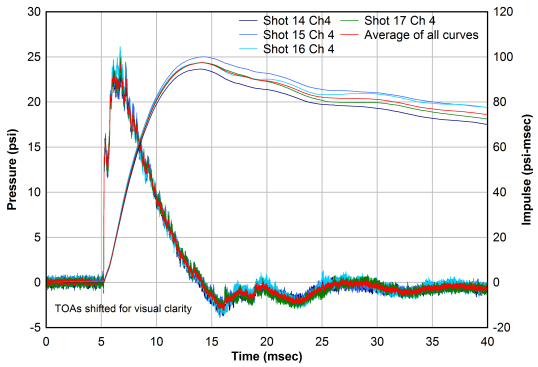

(c) Ch. 4: Floor mounted, valley.

Figure 4.11. 1/2-in. Peaked Perturbation Plate - Floor Gage Comparisons.

closest to the perturbation plate. The peak pressures from Gages 5, 6, and 7 show that as distance between the perturbation plate and the gage increases, the pressure decreases.

Again, the impulse curves with the 1/2-inch peaked plate in place were fairly consistent during the positive phase, although they diverged somewhat later in time. The average impulses for Gages 5-8 were only slightly different from the baseline values, the maximum values from all four gages were within 4%.

The double peak seen on the gages mounted in the perturbation plate (Figure 4.11) is not present on the wing mounted gage pressure traces for the 1/2-in. peaked plate shots. The fact that the double peak is only present on the Gages 1, 2, and 4 lends support to the

idea that the surface geometry in which the gage is mounted influences the magnitude of the peak pressure along with the shape of the pressure time history.

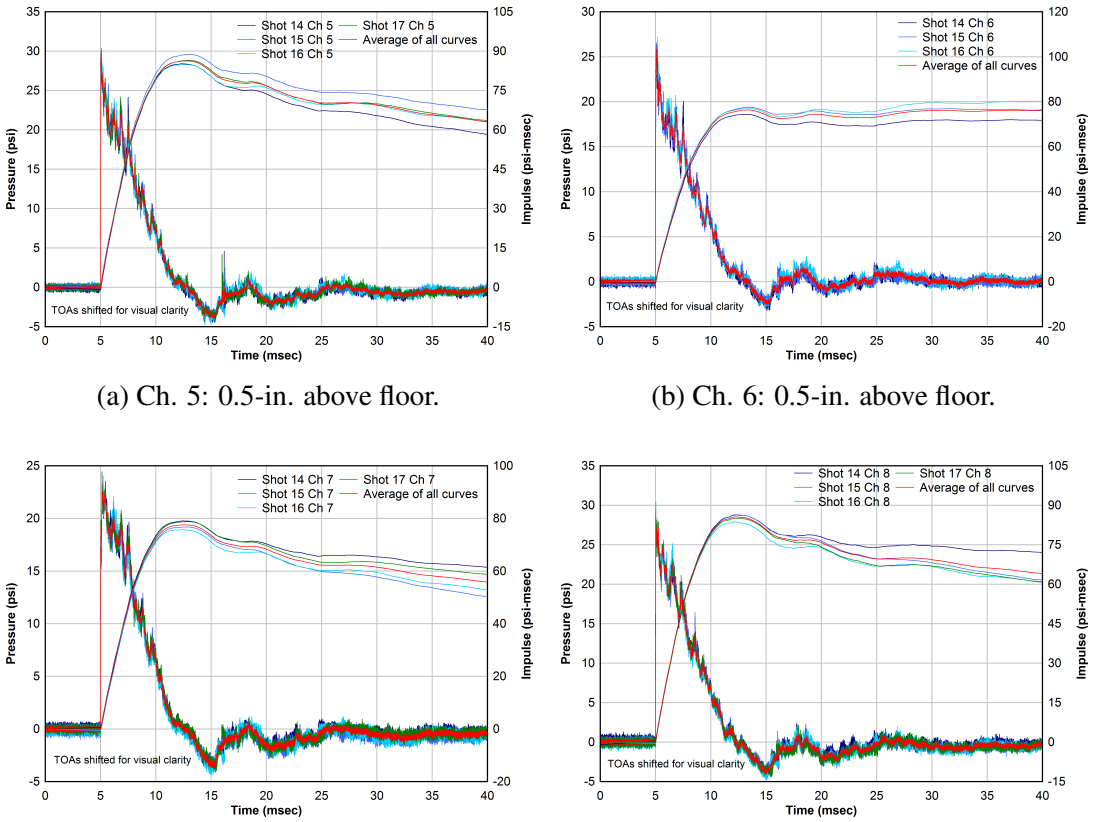

(a) Ch. 5: 0.5-in. above floor.

(b) Ch. 6: 0.5-in. above floor.

(c) Ch. 7: 2.0-in. above floor.

(d) Ch. 8: 7.0-in. above floor.

Figure 4.12. 1/2-in. Peaked Perturbation Plate - Wing Mounted Gage Comparisons.

One frame from the Shot 21 Schlieren video is given in Figure 4.13. Additional frames from the Schlieren sequence are presented and discussed in Section 5. Unlike previously presented Schlieren sequences, the frame in Figure 4.13 has a FOV that does not include the wing mount. The change in FOV allowed more of the upward travel of the reflected shock to be captured. Two interesting characteristics are visible in the selected frame from Shot 21. The shock front is not a single, planar entity as it was during the base-

line shots. Instead, the shock front has split into multiple, thinner shocks. Additionally, the reflection off of the peak in the FOV is visible.

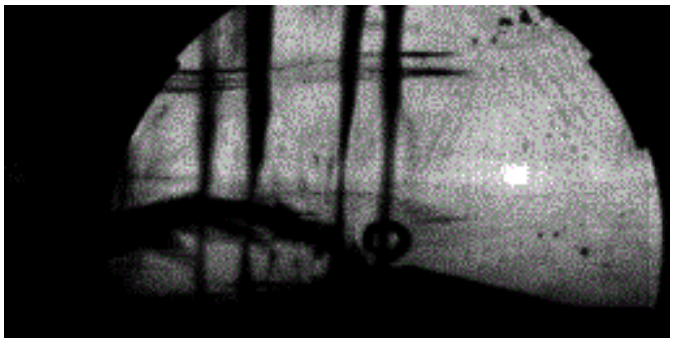

Figure 4.13. Example Schlieren Frame from Shot 21 - 1/2-inch peaked plate. Direction of flow is left to right.

4.5.2. 1-inch Peaked Plate Tests. With the 1-inch peaked perturbation plate in place, seven shots were conducted, five with the 0.032-inch diaphragm and two with the 0.025-inch diaphragm. Tables 4.8 and 4.9 summarize the maximum pressure data plus the averages and standard deviations for each gage location recorded during Shots 46-52.

During the tests with the 1-inch peaked perturbation plate, data for Gage locations 5-9 was not collected since the wing was not in place. However, the data gathered from Shots 46-52 is still valuable for investigating the effect of a larger roughness amplitude on measured pressure.

The standard deviations were higher, on average, with the 1-inch peaked plate versus other perturbation plates. The increased variance may be due to the larger roughness height relative to the tunnel diameter, also known as the d/D ratio.

Figure 4.14 shows the pressure traces for Shots 46-68 & 51-52 for Gages 1, 2, and 4, which are all located in the perturbation plate. Gage 1 is located on a peak, while Gages 2 and 4 are located in valleys. Again, these three gages are equidistant from the diaphragm. On each graph in Figure 4.14 an average pressure trace is shown in red.

Table 4.8. Shots 46-48 & 51-52 pressure data summary. (0.032-in. diaphragm) Gage 1: floor mounted, on a peak. Gages 2 and 4, floor mounted, in valleys.

Gage	CH1	CH2	CH4
Shot 46	34.27	25.80	27.23
Shot 47	30.71	28.84	33.95
Shot 48	28.58	26.47	33.45
Shot 51	29.03	27.42	31.21
Shot 52	29.54	27.31	31.80
Shot 46-52 Avg	30.43	27.17	31.53
Shot 46-52 Stdev	2.29	1.14	2.65

Table 4.9. Shots 49-50 pressure data summary. (0.025-in. diaphragm) Gage 1: floor mounted, on a peak. Gages 2 and 4, floor mounted, in valleys.

Gage	CH1	CH2	CH4
Shot 49	25.17	22.46	26.99
Shot 50	25.82	22.70	26.68
Shot 49-50 Avg	25.49	22.58	26.84

Only one of the floor gages, Gage 1, exhibits the "double" peak shape seen on the shots with the wavy plates in place. The second peak is the result of the reflected shock from the adjacent peak traveling over the gage location. Pressure time histories for Gages 2 and 4 have the initial peak pressure followed by some large oscillations where the pressure may be close to, or exceed the initial peak pressure. Oscillatory behavior of this magnitude was not seen on the 1/2-inch peaked plate tests nor on the wavy plate tests. The pressure traces shown in Figure 4.14 appear to have more shot-to-shot variation than seen with other perturbation plates in place; this observation is confirmed by the standard deviations for Gages 1, 2, and 4 listed in Table 4.8.

The impulse curves from Gages 1, 2, and 4 with the 1-inch peaked plate in place showed some slight differences during the positive phase. No gage had a maximum impulse variance of more than 7% during Shots 46-48. Compared to the baseline impulses, Gage 1

had a lower impulse when the 1-inch peaked plate was present while Gage 2 had a higher maximum impulse.

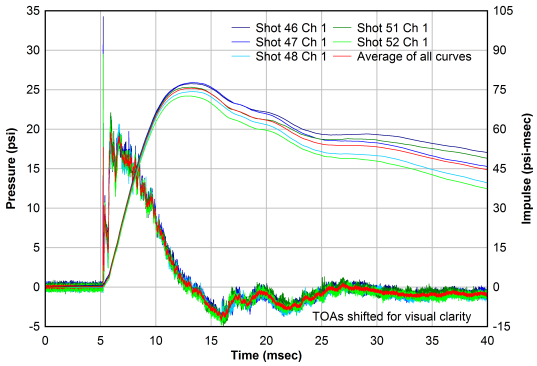

(a) Ch. 1: Floor mounted, peak.

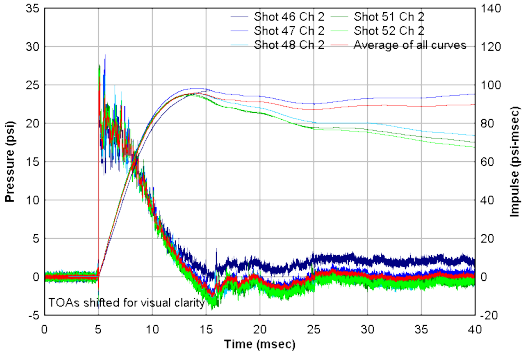

(b) Ch. 2: Floor mounted, valley.

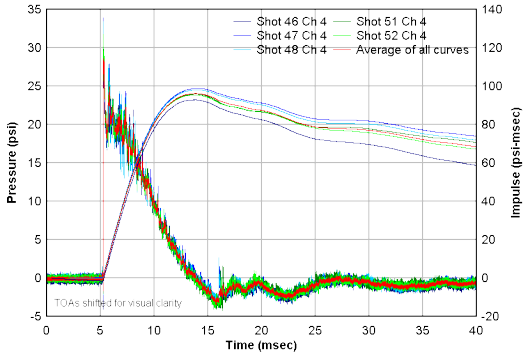

(c) Ch. 4: Floor mounted, valley.

Figure 4.14. 1-in. Peaked Perturbation Plate - Floor Gage Comparisons.

One frame from the Shot 51 Schlieren video is given in Figure 4.15. Additional frames from the Schlieren sequence are presented and discussed in Section 5. Figure 4.15 shows that the shock front has split while traveling down the back side of the peak and expansion fans are seen near the bottom of the shock front. At this point the reflection is still visible and moving upward. The shock structure seen with the 1-inch peaked plate in place is similar to the structure seen on tests that used the 1/2-inch peaked plate.

Figure 4.15. Example Schlieren Frame from Shot 51 - 1-inch peaked plate. Direction of flow is left to right.

4.5.3. Summary of Peaked Perturbation Plate Tests. With the two amplitudes of the peaked plate geometry, higher pressures were measured across all gage locations as compared to the baseline values. The shot-to-shot variance was larger when the 1-inch plate was in place, indicating that the d/D ratio has some effect on the consistency of the data obtained.

The wing mount was not in place when the shots using the 1-inch plate were conducted due to the manufacturing limitations that arose during the last-minute addition to the test matrix. However, data from the wing mounted gages were gathered for all shots using the 1/2-inch peaked plate. The pressure measurements recorded at the Gage 5-7 locations with the 1/2-inch peaked plate in place showed a trend of increasing peak pressure as the distance between the plate and gage decreased.

A "double peak" shape was visible on all floor gage pressure-time histories for data collected with the 1/2-inch peaked plate in place, but this shape was not present in data gathered from the wing gages. For 1-inch plate, the double peak shape was only visible on Gage 1, which was mounted on a peak. The Schlieren video shows that the reflected shock increases in strength as it moves up the compression ramp created by the peaked

geometry, creating the second peak seen in the pressure time history waveform. The lack of a second peak on Gages 2 and 4 on the 1-inch peaked plate tests is due to the weakness of the reflected shock traveling across the downward slope of the peaked geometry.

Impulse curves for each shot with the 1/2-inch and 1-inch peaked plates in place were calculated from the pressure traces. In addition to the individual impulse curves, the average impulse curve for each test was generated from the shot data gathered with the two amplitudes of peaked plates in place. With the 1/2-inch peaked plate in place, all of the average impulse curves for the floor mounted gages were lower than the baseline. Gage 1, peak mounted, was 40% lower than the baseline while Gages 2 and 4, valley mounted, were 8% and 13% lower, respectively. For the 1/2-inch peaked plate geometry, the pressure measurements in the valley mounted surface gages were affected less than the peak mounted gage.

For the tests using the 1-inch peaked plate, the peak pressures and impulses were higher than tests conducted with the 1/2-inch peaked plate in place. The difference in pressures and impulses between the two amplitudes of peaked geometry show that there is a noticeable effect on the data from the height of the roughness.

4.6. GAGE MISALIGNMENT AND LOCAL IMPERFECTION TESTS

Eight shots were conducted using the flat plate with the recessed (Gage 1), protruding (Gage 4), and local imperfection (Gage 2) alignment cases. Four shots used the 0.032-in. diaphragm, and four used the 0.025-in. diaphragm. Tables 4.10 and 4.11 summarize the maximum pressure data plus the averages and standard deviations for each gage location recorded during Shots 32-39.

Figure 4.16 shows the data recorded on Shots 32-35 for the floor gages. Again, the average of all the waveforms is given in red on each plot. The Gage 1 and Gage 2 pressure time histories look similar to the “typical” waveforms obtained during explosive testing. However, the Gage 1 waveform has an initial spike near the TOA that nearly

Table 4.10. Shots 32-35 pressure data summary. (0.032-in. diaphragm) Gage 1: recessed. Gage 2: local imperfection. Gage 4: protruding.

Gage	CH1	CH2	CH4
Shot 32	45.36	29.38	23.04
Shot 33	45.79	28.65	23.13
Shot 34	46.73	29.95	23.93
Shot 35	47.71	28.65	24.33
Shot 32-35 Avg	46.40	29.16	23.60
Shot 32-35 Stdev	1.04	0.63	0.63

Table 4.11. Shots 36-39 pressure data summary. (0.025-in. diaphragm) Gage 1: recessed. Gage 2: local imperfection. Gage 4: protruding.

Gage	CH1	CH2	CH4
Shot 36	37.13	23.70	21.20
Shot 37	38.44	23.55	21.86
Shot 38	37.03	23.29	21.06
Shot 39	36.78	22.92	22.64
Shot 36-39 Avg	37.34	23.37	21.69
Shot 36-39 Stdev	0.74	0.34	0.72

doubles the measured pressure. The pressure spike is likely a result of a reflected pressure component being measured at the gage location due to the recession around the gage. As the shock wave reaches the recessed gage location, the expansion of the shock wave into the recess results in a velocity vector that is traveling perpendicular to the gage face. This perpendicular velocity component results in some reflected pressure being recorded by the gage.

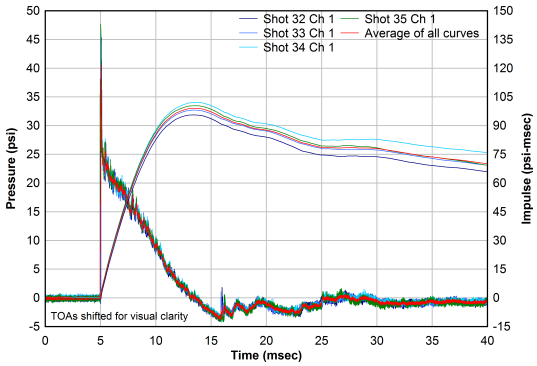

(a) Ch. 1: recessed.

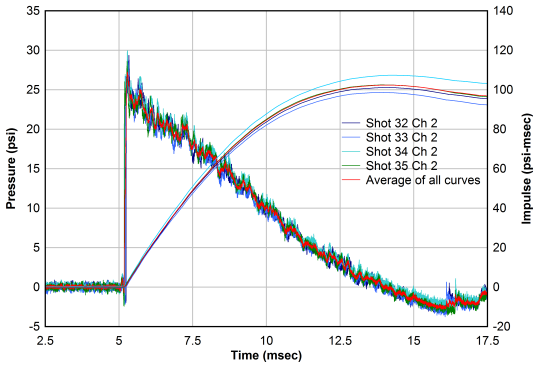

(b) Ch. 2: local imperfection.

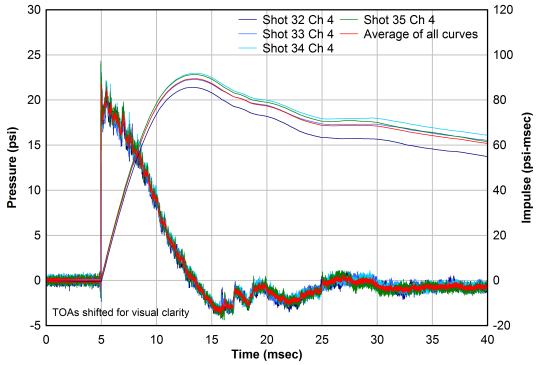

(c) Ch. 4: protruding.

Figure 4.16. Floor Gage Comparisons for Imperfectly Mounted Transducers.

5. ANALYSIS AND DISCUSSION

5.1. EFFECT OF SURFACE ROUGHNESS AT GAGE LOCATIONS

5.1.1. Experimental Scatter of Data. As covered in Section 4.6, three baseline shots with the 0.032-inch diaphragm and 12.5-inch long driver section were conducted. The peak pressures summarized in Table 4.1 also included the average and standard deviations of the measured pressures. While the sample set was small, the very low standard deviations indicate high repeatability of the experimental setup. Experimental data scatter in the baseline data varied from 1-3% across all eight gage locations.

With the roughness plates in place, the shot-to-shot variance for each set of variables was higher than the baseline case, with the exception of the Gage 8 data. Data recorded by Gage 8 was extremely consistent until the gage began to fail, typically within 1% of the baseline pressure values and 1% scatter from shot-to-shot.

For the shots with roughness present, the largest shot-to-shot variance occurred on the floor gages with the scatter ranging from 6% to 12% for the different geometries. The wing mounted gage pressure data was more consistent, with a maximum of 6% variance, with more typical values of 1-3% throughout the series. If testbed conditions mean that a perfectly smooth surface is not present for gage mounting, more consistent data will be gathered if the gage(s) are placed in a wing type mount with some distance between the gage location and the rough plate.

5.1.2. Comparisons at Floor Gage Locations. To provide a simple visualization of the differences in measured pressure and impulse when surface roughness is present, Figure 5.1 shows the average curves for the baseline case and each roughness plate for Gage 1 and 2. Gage 1 was mounted on a peak, while Gage 2 was mounted in a valley.

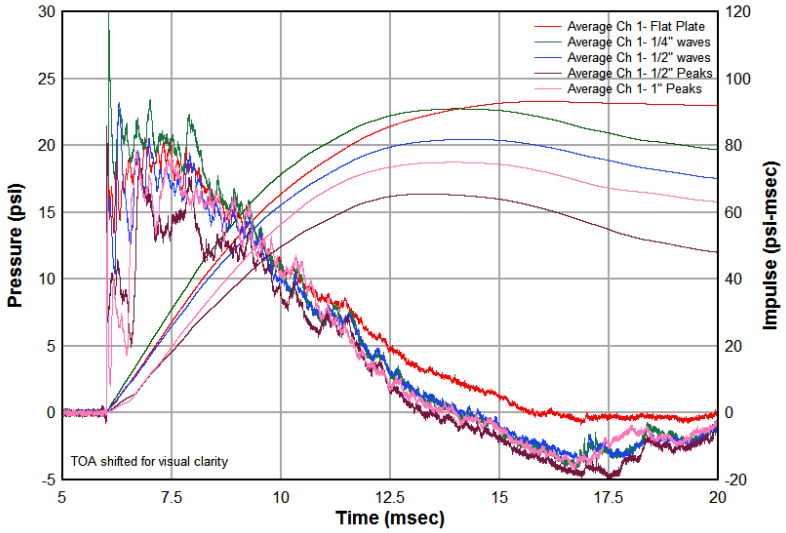

(a) Ch. 1: Floor mounted, peak.

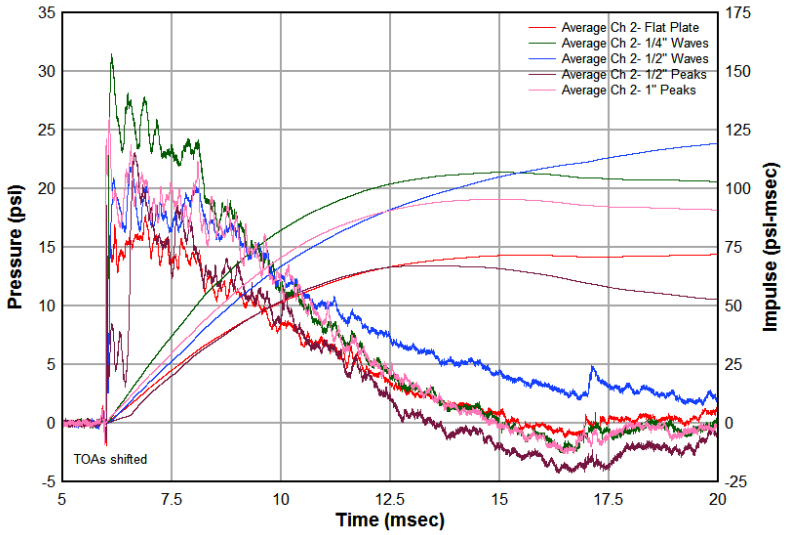

(b) Ch. 2: Floor mounted, valley.

Figure 5.1. Pressure and Impulse Comparisons- All Cases - Floor Gages.

At the Gage 1 location (Figure 5.1a) the overall peak pressure for the baseline case was lower than when any roughness plate was present. However, the impulse for the baseline case was the highest of any case, indicating that a higher peak pressure does not always accompany a larger amount of total energy imparted to the gage, which is commonly known

as impulse. Instead, the presence of surface roughness affects the peak pressure, waveform shape, duration of the positive phase, and impulse. For all of the configurations studied, the peak impulse measured at Gage 1 varied from 66.0 to 92.8 psi-ms. The impulses measured at the Gage 1 location with the roughness plates in place were all less than the baseline case. The difference in peak impulse was due to the occurrence of a shorter positive phase for the tests conducted with surface roughness.

In Figure 5.1b, the average curves for the Gage 2 location are plotted for the baseline case and each roughness plate. Again, the baseline peak pressure is the lowest, however the relationship of the peak impulses is different than what was recorded at the Gage 1 location. The baseline impulse was the second lowest value, only higher than the average curve for the 1/2-inch peaked plate. The average pressure curve for the 1/4-inch wavy plate in Figure 5.1b did not return to its baseline value in a timely manner, so the later time impulse should be ignored.

At the Gage 2 location, the average impulses varied from 67.3-106.9 psi-ms, excluding the late time impulse from the 1/4-inch wavy plate shots. The double peak shape was only present on Gage 2 when the 1/2-inch peaked plate was in place. The 1/4-inch wavy plate pressure trace once again had the highest overall peak pressure, but the shape of the waveform at the Gage 2 location differed from the Gage 1 waveform. At Gage 1, the 1/4-inch wavy plate trace had a very tall, narrow spike followed by some oscillation and then attenuation of pressure. At Gage 2, the average pressure trace for the 1/4-inch wavy plate shots still had the highest overall peak pressure, but the waveform did not have the tall, very narrow pressure spike just after the shock TOA.

The difference in impulses at the Gage 1 and Gage 2 locations are significant because the total amount of energy imparted into the system was nearly constant, as indicated by the constant driver volume and very similar burst pressures, but the total energy measured by the gage (impulse), was quite different. If a peak pressure measurement is obscured or untrusted for some reason, common guidance is to compare the impulses since

they should not be affected as much as the pressure measurements. However, the data presented in Figure 5.1 show that the presence of surface roughness does significantly affect the impulse measurements as well as the peak pressures. The location of the gage on the roughness plate influences the relative difference from the baseline impulse. When the pressure measurement is taken on a peak, the pressures are typically higher than the baseline, while the impulses trend lower. When the gage is located in a valley, both the pressures and impulses are higher than the baseline case.

In addition to the variance in peak pressure and impulse, the shape of the waveforms differed, with the peaked plate cases resulting in the most unusual pressure waveform shape, described previously as a "double peak" shape. At the Gage 1 location, the double peak waveform shape occurred with both the 1/2-inch and 1-inch peaked plates in place. At the Gage 2 location, only the 1-inch peaked plate resulted in a double peak in the pressure waveform. On the 1-inch peaked plate shots, the amplitude of the roughness was large enough that the Mach reflection effects seen by Gage 2, mounted in the valley, were lessened. Regions of low pressure on the pressure waveforms from the peaked geometry shots correspond to regions of low pressure near the surface recorded in interferograms from other sources, such as the one presented in Figure 5.2 from Reference [18].

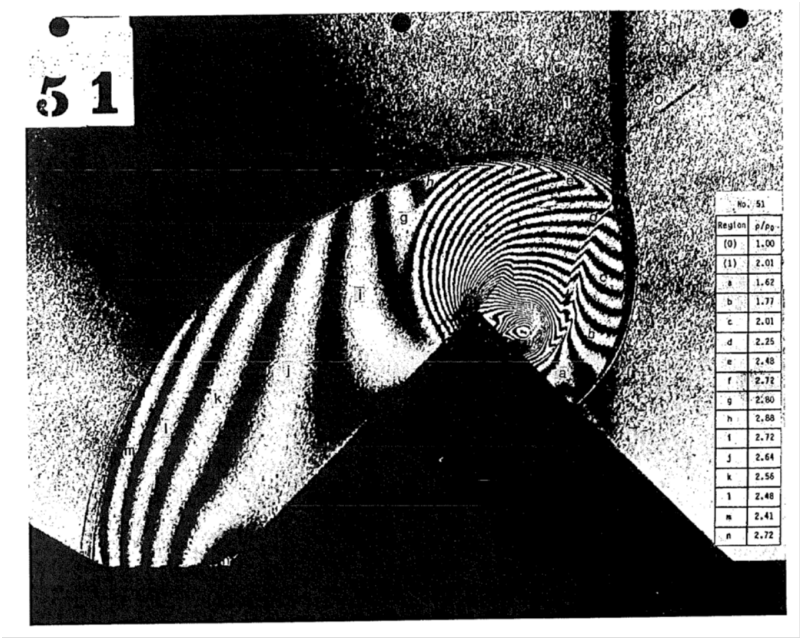

Figure 5.2. Interferogram of a single Mach reflection, Reference [18].

Subtracting the pressure time history obtained during the baseline tests from the pressure time history obtained with the roughness plates in place highlights the differences in pressure versus time. Figures 5.3, 5.4, 5.5, and 5.6 show curve subtractions for Gages 1 and 2 for each type of roughness plate over the positive phase. The difference between the baseline and roughness plate data is given in red on each plot. The differences in the measured pressure and impulse are clearly influenced by both the magnitude and geometry of the surface roughness as well as the gage location on the plate.

With the roughness plates in place, the differences in the Gage 1 records occurred shortly after the shock TOA, and the later time attenuation rate was largely unaffected. However, the Gage 2 location was affected throughout the duration of the record for three of the four surface roughness cases. The pressures measured in the valleys of the plate by Gage 2 had different attenuation rates than the baseline case, which led to a larger disparity in impulse over the positive phase compared to the Gage 1 records. In general, the Gage

1 records had slightly lower experimental errors than the Gage 2 records, relative to the baseline.

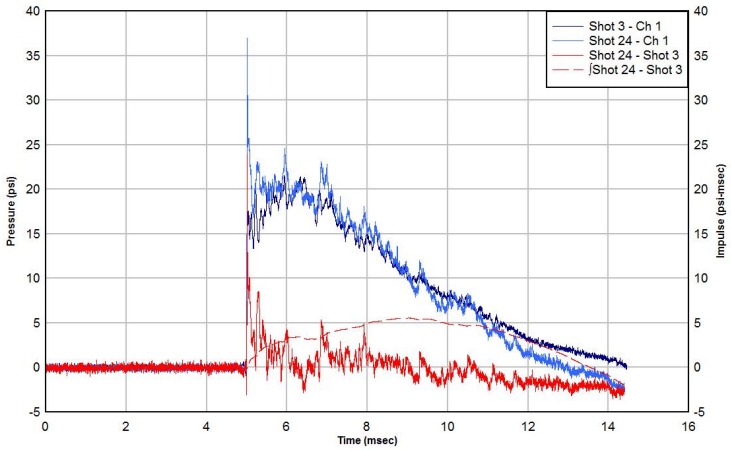

(a) Ch. 1: Floor mounted, peak.

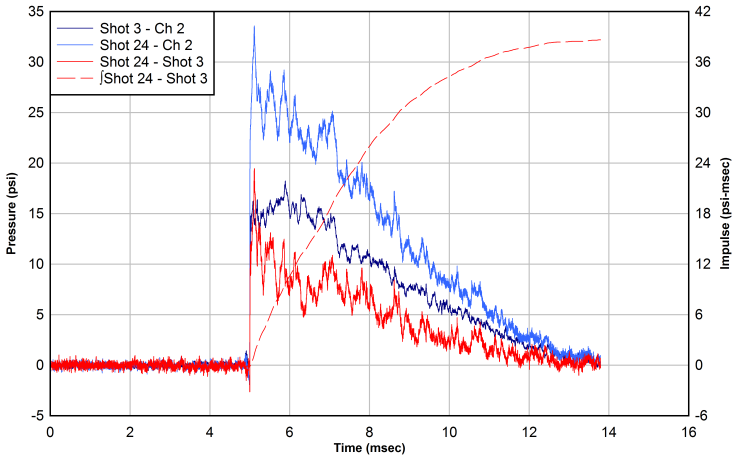

(b) Ch. 2: Floor mounted, valley.

Figure 5.3. Curve subtractions with 1/4-inch wavy plate versus baseline - Floor Gages.

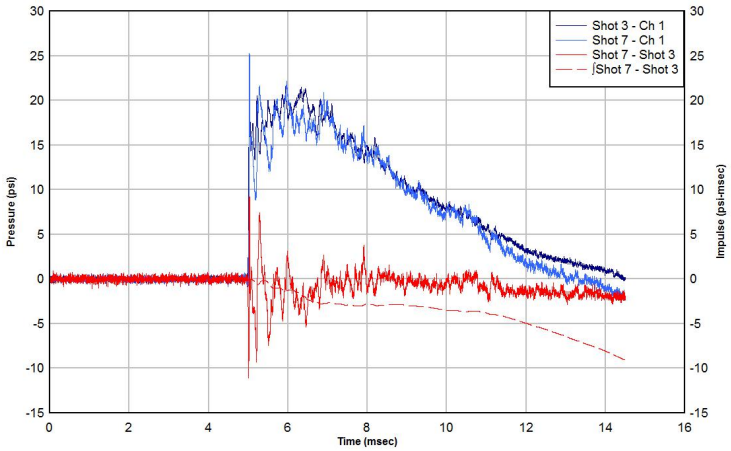

(a) Ch. 1: Floor mounted, peak.

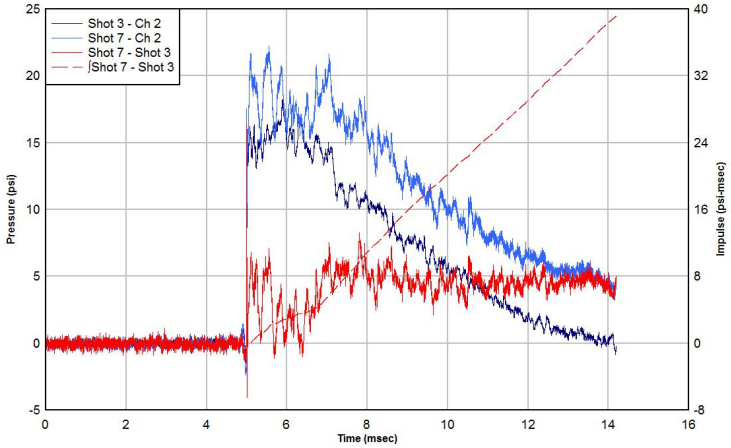

(b) Ch. 2: Floor mounted, valley.

Figure 5.4. Curve subtractions with 1/2-inch wavy plate versus baseline - Floor Gages.

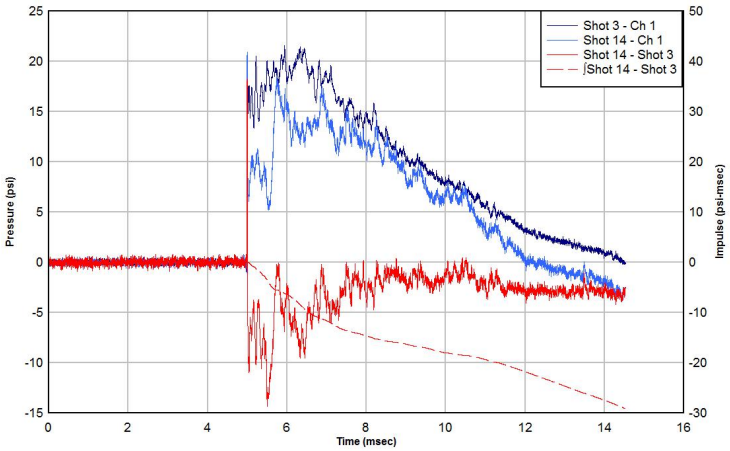

(a) Ch. 1: Floor mounted, peak.

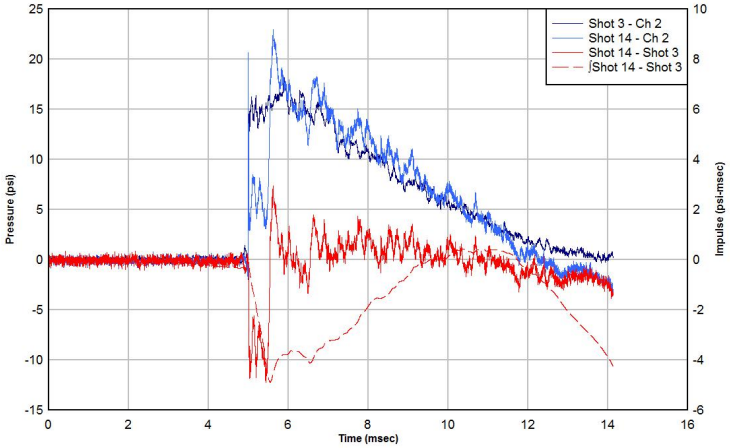

(b) Ch. 2 Floor mounted, peak.

Figure 5.5. Curve subtractions with 1/2-inch peaked plate versus baseline - Floor Gages.

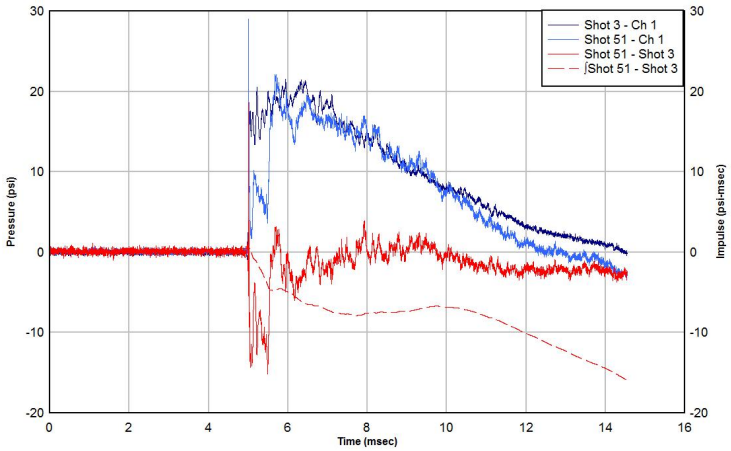

(a) Ch. 1: Floor mounted, peak.

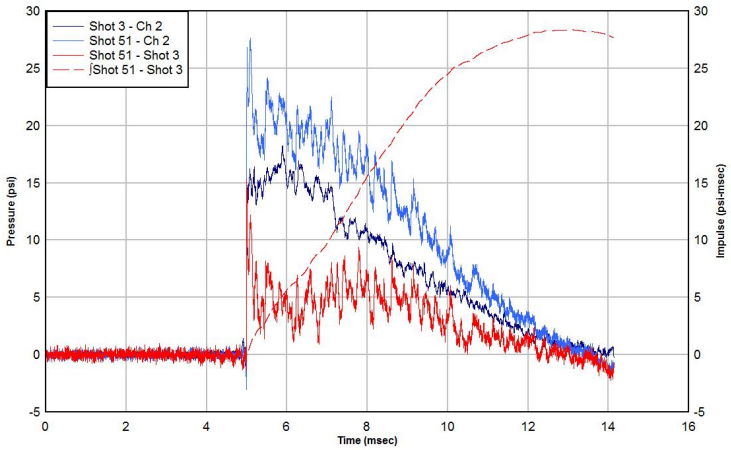

(b) Ch. 2: Floor mounted, valley.

Figure 5.6. Curve subtractions with 1-inch peaked plate versus baseline - Floor Gages.

Table 5.1 summarizes the data obtained from Gages 1 and 2 along with how the pressure and impulse for each roughness plate compared to the baseline shots. Shots with the 1/4-inch wavy plate in place had the largest difference in peak pressure relative to the baseline for both Gages 1 and 2. However, the impulse at the Gage 1 location was only 2% lower than the baseline impulse, while the Gage 2 impulse was nearly 50% larger than the baseline value.

For shots with any roughness plate in place, the peak pressure was always higher than the baseline data. Typically the pressures varied more than the impulses did for their

respective baseline values. At both the Gage 1 and Gage 2 locations, the peak pressure variance from the baseline case was greatest during the tests with the 1/4-inch wavy plate in place.

Table 5.1. Comparisons of Peak Pressure and Impulse for Each Roughness Plate.

Gage 1	Avg. Peak Pressure	% Difference from Baseline	Avg. Impulse	% Difference from Baseline
Flat	21.1	-	93.1	-
1/4-inch waves	39.1	85%	91.0	-2%
1/2-inch waves	25.5	21%	81.8	-12%
1/2-inch peaks	23.6	12%	65.5	-30%
1-inch peaks	30.4	44%	75.0	-19%
Gage 2	Avg. Peak Pressure	% Difference from Baseline	Avg. Impulse	% Difference from Baseline
Flat	17.9	-	71.7	-
1/4-inch waves	32.3	80%	107.0	49%
1/2-inch waves	22.5	26%	-	-
1/2-inch peaks	24.1	35%	67.3	-6%
1-inch peaks	27.2	52%	95.6	33%

5.1.3. Comparisons at Wing Gage Locations. In addition to creating variance in peak pressures and impulses for gages mounted in the floor, the roughness plate affects the measured pressures at some of the wing gage locations. Figures 5.7 and 5.8 show the average curves for the four wing mounted gages aligned to measure incident pressure. Gage

5 was closest to the bottom of the shock tube at 0.5-inches from the surface and Gage 8 was the furthest at 7-inches from the surface.

As seen in the Gage 1 and 2 comparisons, the Gage 5 baseline (flat plate) case recorded the lowest peak pressure. However, at the Gage 5 location, the waveforms are much more similar, and all attenuate at roughly the same rate by approximately 1.5 ms after TOA. Despite having up to 56% difference in peak pressure from the baseline case, the variance in average peak impulse at the Gage 5 location was only 8%. While the perturbation plates introduce some error into the early time pressure measurements, the impulse comparisons from the wing mounted gages yield similar results that are well within the accepted margin of error for most real-world tests.

For the gages located on the wing mount (Gages 5, 6, 7, and 8), the percent difference in peak pressure from the base case decreases as the height from the plate increases. At the Gage 8 location, the pressure and impulse remained very constant throughout the test series, indicating that at 7-inches above the surface, the shock is not affected by the presence of the roughness plates. Instead, the disturbance to the shock is limited to the area local to the rough surface where the Mach reflection occurs. Within a Mach reflection, a pressure gradient is present, and this gradient is captured by Gages 5, 6, and 7 on each test with surface roughness. An interferogram of a single Mach reflection, taken from Reference [18], is shown in Figure 5.2 and provides a visualization of the pressure differences that occur within the Mach reflection.

The trend for the average impulses at the wing mounted gages was not as clear as was the pressure trend. The average impulse curves for each case had the most variance at Gages 5 and 7, while the Gage 6 impulses were very similar. The Gage 8 average impulse curves are very nearly overlaid on one another and had the least case-to-case deviation of any gage location.

At the Gage 8 location, 7-inches above the bottom of the tube, the largest percent difference from the baseline case was only 4%. Unfortunately, Gage 8 began to experience

failure mid-way through the test series, so data is not available for this location for all of the perturbation plates. No observable differences in the pressure, impulse, or waveform shape were present in the Gage 8 data. Also, the data obtained from Gage 8 was extremely consistent, and it is highly likely that the remainder of the shots would have continued to yield consistent data if the gage had not experienced a gradual failure.

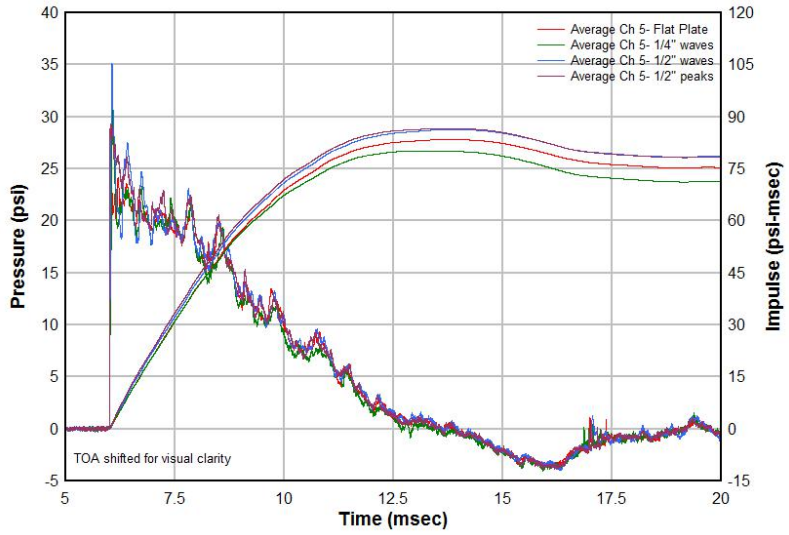

(a) Ch. 5 - located 0.5-inches above floor.

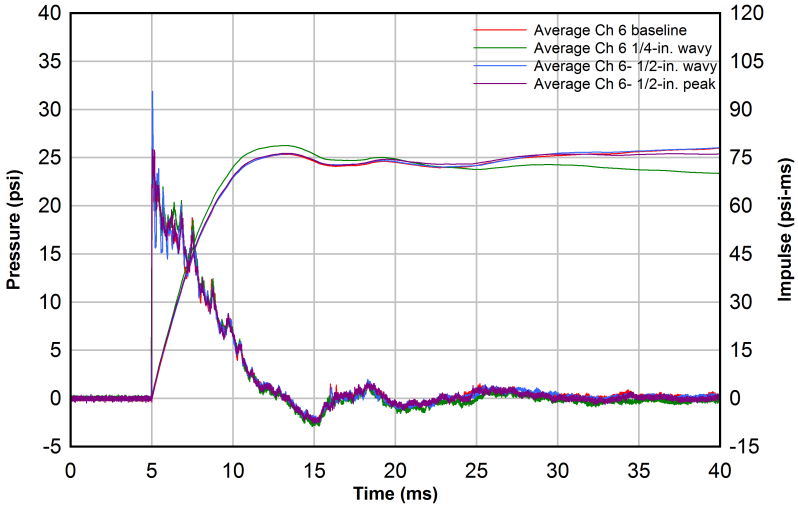

(b) Ch. 6 - located 1.0-inches above floor.

Figure 5.7. Wing gage pressure comparisons, Part 1.

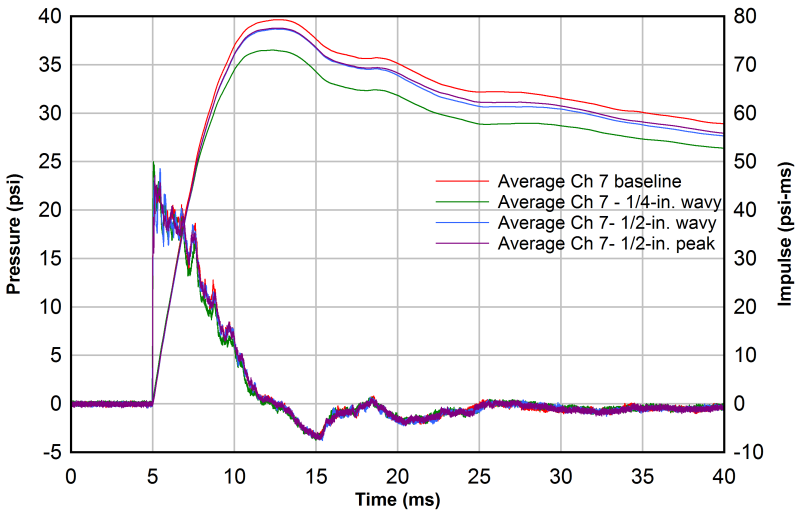

(a) Ch. 7 - located 2.0-inches above floor.

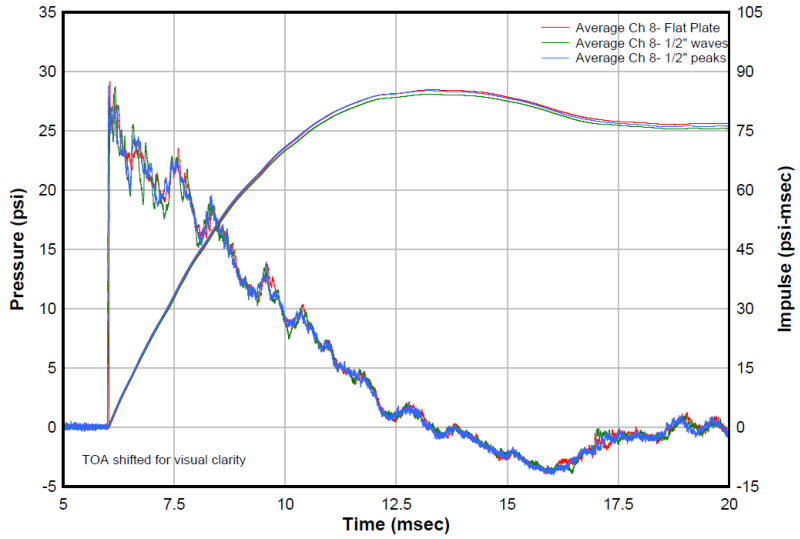

(b) Ch. 8 - located 7.0-inches above floor.

Figure 5.8. Wing gage pressure comparisons, Part 2.

5.2. SCHLIEREN COMPARISONS OF SHOCK STRUCTURE

The images captured by the Schlieren setup throughout the test series and presented in this section show differences in the main shock front and the environment behind it with the various roughness plates in place. The baseline cases, which used a flat plate and flush

mounted gages had a shock front that was planar and fairly uniform in thickness throughout the entire FOV (see Figure 4.1, Section 4). However, with the roughness plates in place, the shock front and environment behind the shock was more complicated than the baseline cases.

5.2.1. 1/4-inch Wavy Plate Schlieren Analysis. Figure 5.9 shows three frames from the high speed video taken on Shot 24, one of the shots conducted with the 1/4-inch wavy plate. In the first four frames of the sequence, the shock is traveling from left to right. Figure 5.9a, shows the FOV just prior to the shock entering the frame. In Figure 5.9b, the shock front has entered the FOV, and some additional shock structures are visible behind the main shock front. The shock is passing over the gage location in Figure 5.9c and the cohesive shock seen in the previous frame has now split into multiple shocks with lambda shape characteristics. The shocks are exiting the FOV in Figure 5.9d and while the lambda structure is still present, the height of the formation is slightly lower. Finally, in Figure 5.9e, a weak reflected shock travels from right to left across the FOV. The reflection is very weak near the floor of the tube and the reflected shock is also much thinner than the original shock front. The reflection likely occurred from the interaction between the shock and the wing mount, downstream. The Schlieren frames did not capture any reflections due to the 1/4-inch plate, so the reflection seen in Figure 5.9e was not due to the inclusion of surface roughness.

Additional discussion regarding how the environment behind the shock front affects the pressure waveform is included later in this document.

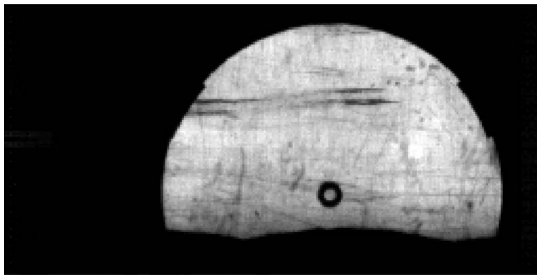

(a) Shot 24, Frame 333.

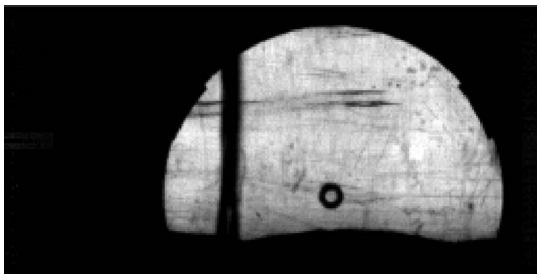

(b) Shot 24, Frame 335.

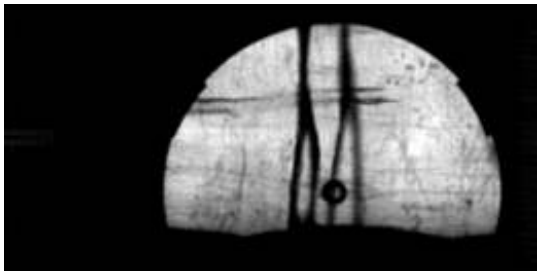

(c) Shot 24, Frame 337.

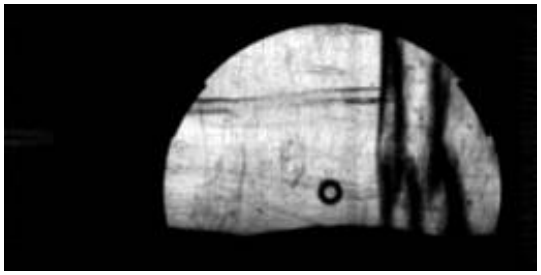

(d) Shot 24, Frame 340.

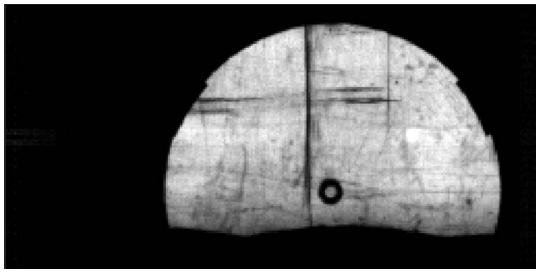

(e) Shot 24, Frame 375.

Figure 5.9. Schlieren Sequence for Shot 24 - 1/4-inch wavy plate. Direction of travel in (b), (c), and (d) is left to right, and is right to left in (e).

Comparisons between the shock structure, as captured by the Schlieren video, and the pressure-time history are made for the roughness plates with the intent of attributing certain characteristics of the waveform to the shock environment.

The Schlieren sequence for Shot 24, which used the 1/4-inch wavy plate, is presented in Figure 5.9. The pressure waveforms for Shot 24, Channels 1 and 2, are shown in Figure 5.10. One point in time is identified with vertical dashed lines.

The multiple shocks seen traversing the gage location were close enough together in time that the data does not show one spike in pressure per visible shock. Line 1 on the zoomed in view in Figure 5.10 corresponds with the arrival of the reflection at the gage location seen in Figure 5.9e. The time resolution of the Schlieren video for Shot 24 (17.0 μs), coupled with the thickness of the reflected shock results in a time-stamp that is approximate, not exact. The weak reflected shock corresponds with an oscillatory peak in the Gage 2 record, but the Gage 1 record did not see any bump in pressure at that time.

The roughly 5 psi increase in pressure around 7 ms does not correspond to a significant shock structure on the Schlieren video. However, a very faint oblique reflection was visible. The reflection is likely off the surfaces of the shock tube and is not related to the presence of the surface roughness.

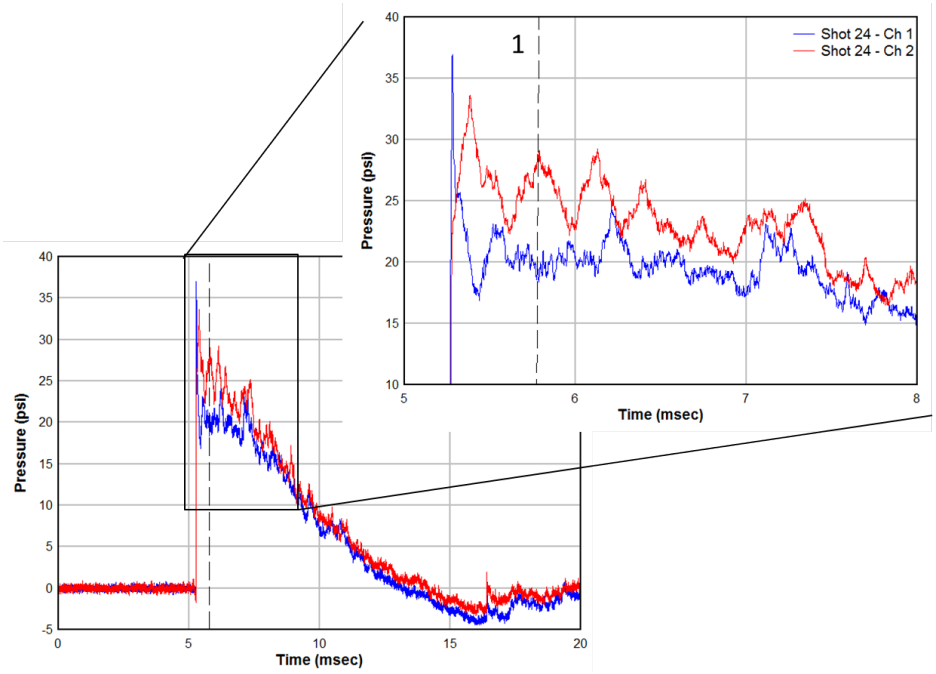

Figure 5.10. Shot 24 - Channel 1 and 2 waveforms, with Schlieren timestamps.

5.2.2. 1/2-inch Wavy Plate Schlieren Analysis. Figure 5.11 shows four frames from the high speed video taken on Shot 10, one of the shots conducted with the 1/2-inch wavy plate. The time duration between the first three frames shown is 3.1 μs. In the first three frames, the shock is traveling from left to right, and the direction is reversed in the fourth frame. In Figure 5.11a, a weak reflected shock is visible behind the main shock front, and the shock front is still quite planar. In Figure 5.11b the reflected shock has overtaken the original shock front. In Figure 5.11c, the reflected shocks created as the shock front traveled across the wavy plate are interacting and the environment around the gage location is quite complex.

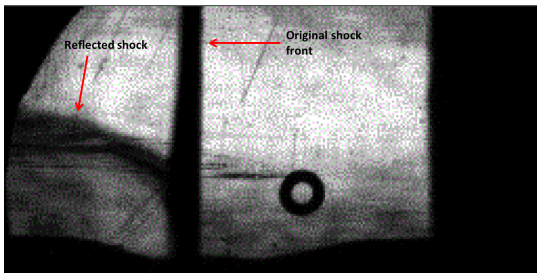

(a) Shot 10, Frame 615.

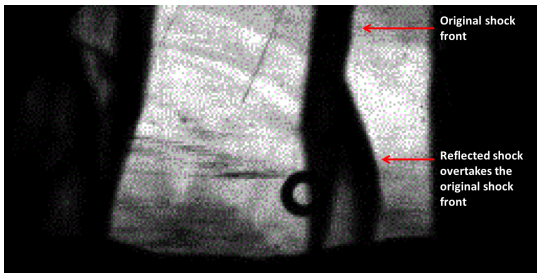

(b) Shot 10, Frame 617.

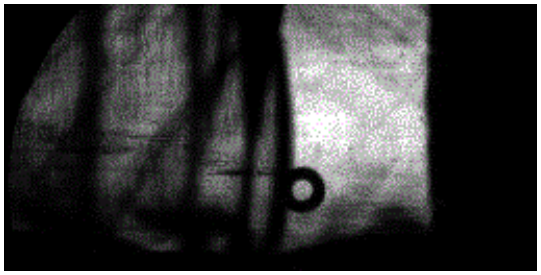

(c) Shot 10, Frame 619.

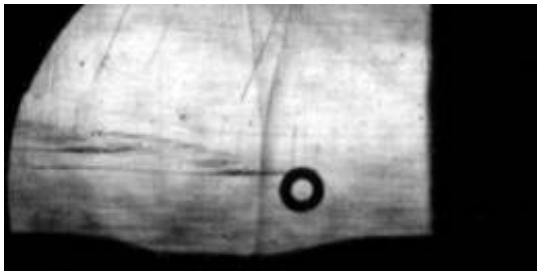

(d) Shot 10, Frame 644.

Figure 5.11. Schlieren Sequence for Shot 10 - 1/2-inch wavy plate. Direction of travel is left to right in (a), (b), and (c), and right to left in (d).

Comparisons between the shock structure, as captured by the Schlieren video, and the pressure-time history are made for the roughness plates with the intent of attributing certain characteristics of the waveform to the shock environment.

The Schlieren sequence for Shot 10, which used the 1/2-inch wavy plate, was presented in Figure 5.11. The pressure waveforms for Shot 10, Channels 1 and 2, are shown in Figure 5.12. Two points in time are identified with vertical dashed lines. While the frames presented in Figure 5.11 were taken at TOA and just after, there are interesting waveform characteristics that occur later in time.

Line 1 on the zoomed in view in Figure 5.12 corresponds with the arrival of a weak reflection at the gage location captured in Figure 5.11d. The time resolution of the Schlieren video for Shot 10 (15.5 μs), coupled with the thickness of the reflected shock results in a time-stamp that is approximate, not exact. The Channel 1 and 2 waveforms appear to oscillate at approximately equal and opposite periods for the first 1.5 ms after TOA. The difference in period is likely due to the differences in local shock speed that occur on the uphill and downhill sides of the geometry; also known as effects due to the compression ramp and expansion fan. The shock speed increases locally as it travels up the compression ramp and decreases as the expansion fan forms on the downhill side of the geometry.

Line 2 indicates the TOA of an additional reflected shock across the floor gage locations. There is a slight bump in pressure which alters the attenuation rate, and therefore the resultant impulse. Reflections occurring and traveling across the gage locations are unavoidable if the gages are surface mounted and the surface is rough. However, even a slight reflection will alter the pressure and attenuation rate, which affects the impulse.

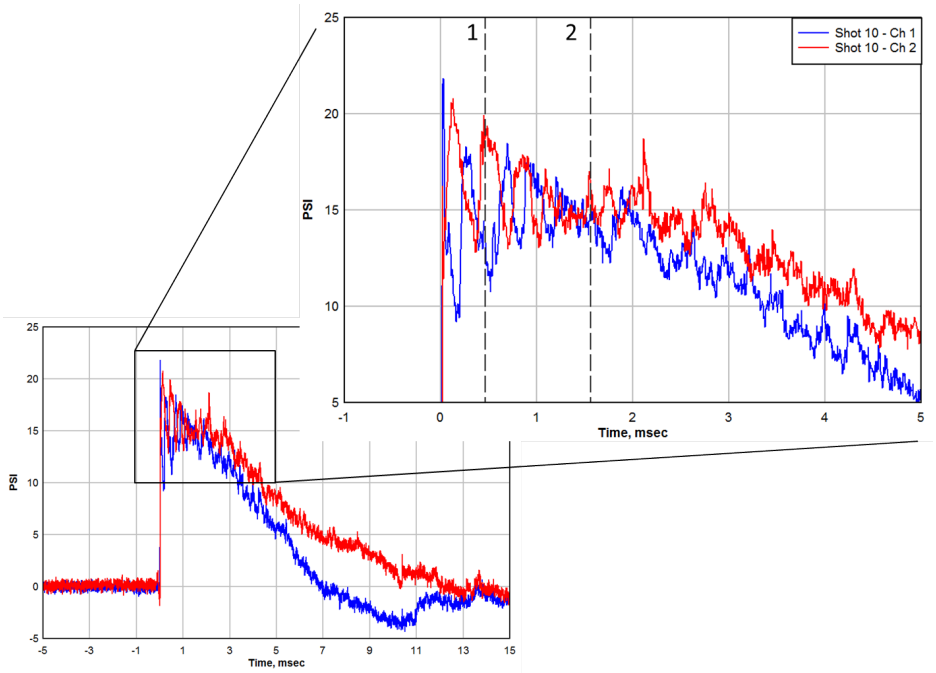

Figure 5.12. Shot 10 - Channel 1 and 2 waveforms with Schlieren timestamps.

5.2.3. 1/2-inch Peaked Plate Schlieren Analysis. A sequence of five frames from the Shot 21 Schlieren video is given in Figure 5.13. Unlike previously presented Schlieren sequences, the five frames in Figure 5.13 have a FOV that does not include the wing mount. The change in FOV allowed more of the upward travel of the reflected shock to be captured. The Schlieren frame sequence for Shot 21, with the 1/2-inch peaked plate, displays some similarities to the 1/2-inch wavy frame sequence, but there are also some notable differences. The main similarity between the two 1/2-inch roughness plates is that a reflection is visible in the frames and that reflection moves upward during the frame sequence.

Although they had the same amplitude, the two plate geometries did not have the same effect on the shock front. The 1/2-inch peaked plate created a shock front that had split into four thinner shocks as it traveled across the plate while the 1/2-inch wavy plate shot had a single, thicker shock front. The thickness of the shocks appears to vary with time with both 1/2-inch roughness geometries.

In Figure 5.13a, the shock front has just entered the FOV. In Figure 5.13b two interesting characteristics are visible. The shock front is not a single, planar entity as it was during the baseline shots. Instead, the shock front has split into multiple, thinner shocks. The reflection to the left of the peak in the FOV is also visible. In the third frame in the series (Figure 5.13c) the reflection is still visible, and has moved upward during the interval between the two frames (3.1 μs). Another observation made from the Shot 21 Schlieren frame sequence is the change in shock speed between travel across upward and downward inclined planes. In Figure 5.13b, the spacing between the shocks is smaller than the spacing seen in Figure 5.13c. The change in distance between the shocks in the two frames shows that the local shock speed is not constant across the roughness geometry.

Figure 5.13 presented the Schlieren sequence for Shot 21, which used the 1/2-inch peaked plate. The primary distinction between the pressure waveforms from the wavy geometry versus the peaked geometry was the strong reflection seen in the waveform at approximately TOA + 0.5 ms, which is shown in Figure 5.13d. With the 1/2-inch peaked plate in place, the strong reflection was present in both the Gage 1 and 2 records. Figure 5.14 provides the pressure waveforms from Shot 21 for Gages 1 and 2, and identifies the arrival of the reflection. Even though multiple shocks were visible in the Schlieren video, the shocks were spaced closely enough in time that multiple peak pressures were not recorded early on in the Shot 21 pressure record. The period of low pressure immediately following the initial pressure spike is a result of the areas of low pressure present near the surface inside the Mach reflection.

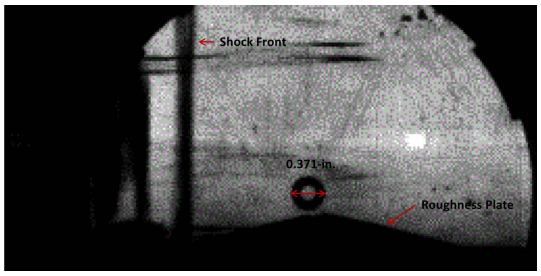

(a) Shot 21, Frame 351.

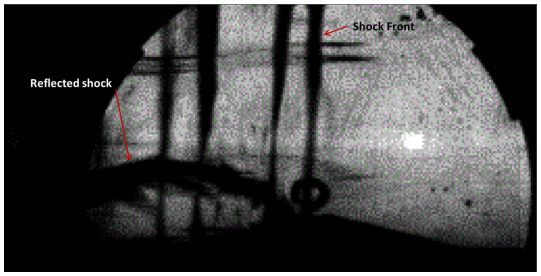

(b) Shot 21, Frame 353.

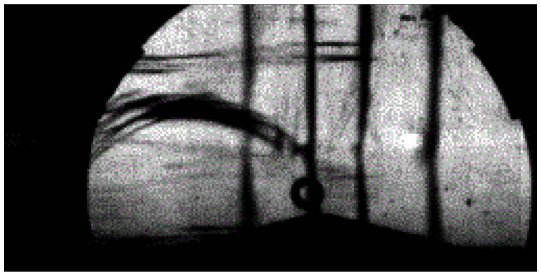

(c) Shot 21, Frame 355

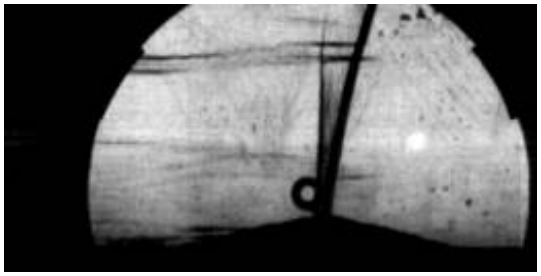

(d) Shot 21, Frame 385

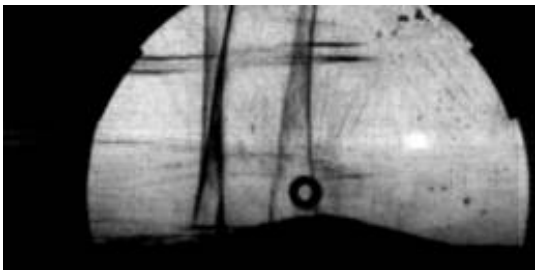

(e) Shot 21, Frame 400

Figure 5.13. Schlieren Sequence for Shot 21 - 1/2-inch peaked plate. Direction of travel is from left to right in (a), (b), and (c) and from right to left in (d) and (e).

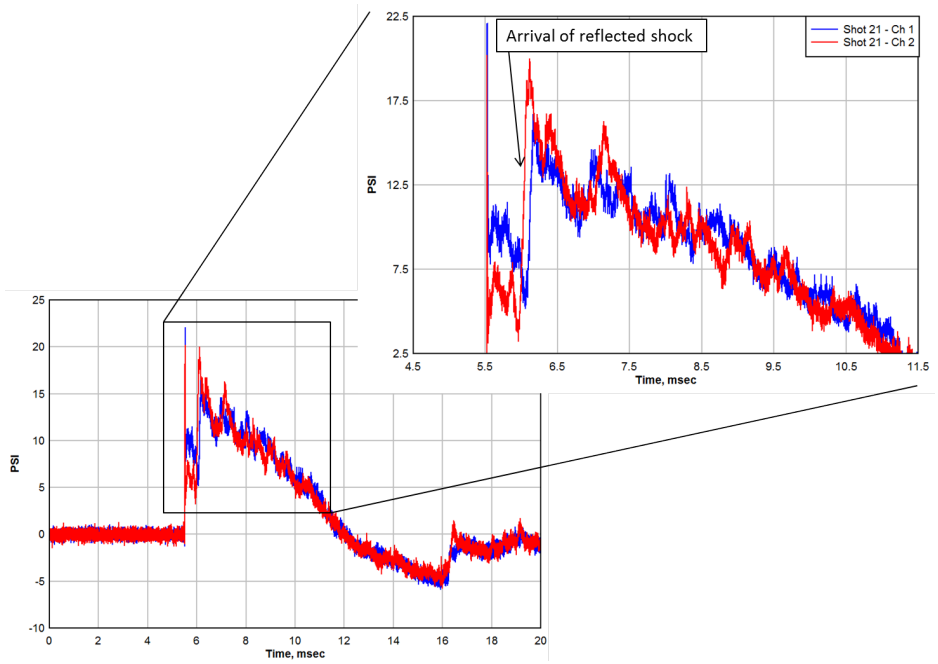

Figure 5.14. Shot 21 - Channel 1 and 2 waveforms with Schlieren timestamps.

5.2.4. 1-inch Peaked Plate Schlieren Analysis. In order to visualize what effect the 1-inch perturbation plate had on the shock front, several frames from the Shot 51 video are shown in Figure 5.15. Figure 5.15a shows the FOV prior to the shock front entering the frame. In Figure 5.15b, the shock front is passing over the peak and a reflection is visible behind the shock. The shock is also visibly thicker near the roughness plate due to the formation of a Mach reflection. Figure 5.15c shows that the shock front has clearly split into multiple shocks while traveling down the back side of the peak and expansions fans are seen near the bottom of the shock front. At this point the reflection is still visible and moving upward. Then, in Figure 5.15d, the shock front has exited the FOV and the reflection from the shock front interaction with the next peak is moving back towards the gage locations. Figure 5.15e, multiple weak reflections are seen moving to the left of the frame and passing over the gages. The environment near the pressure gages is very complex at this point in time. However, only the strong reflected shock seen in Figure 5.15d was strong enough to have a notable effect on the pressure waveform.

The pressure time histories from Shot 51 for Gages 1 and 2 with points marked in time are presented in Figure 5.16. The TOA on the pressure records corresponds to the shock front passing over the peak in Figure 5.15b. Line 1 corresponds to the arrival of the rear shock at the gage location just prior to the frame shown in Figure 5.15c. At the Line 1 location, a bump in pressure occurs at both gage locations, followed by an attenuation in pressure which continued until the reflected shock arrived. The arrival of the reflected shock is noted by the Line 2 location in Figure 5.16. The reflected shock, pictured in Figure 5.15d, increased in strength as it traveled up the peaked geometry, determined from the change in density as viewed from the Schlieren. The reflected shock in Figure 5.15f has strengthened and coalesced as it traveled up the inclined surface of the peaked geometry. The strong reflection was recorded by Gage 1.

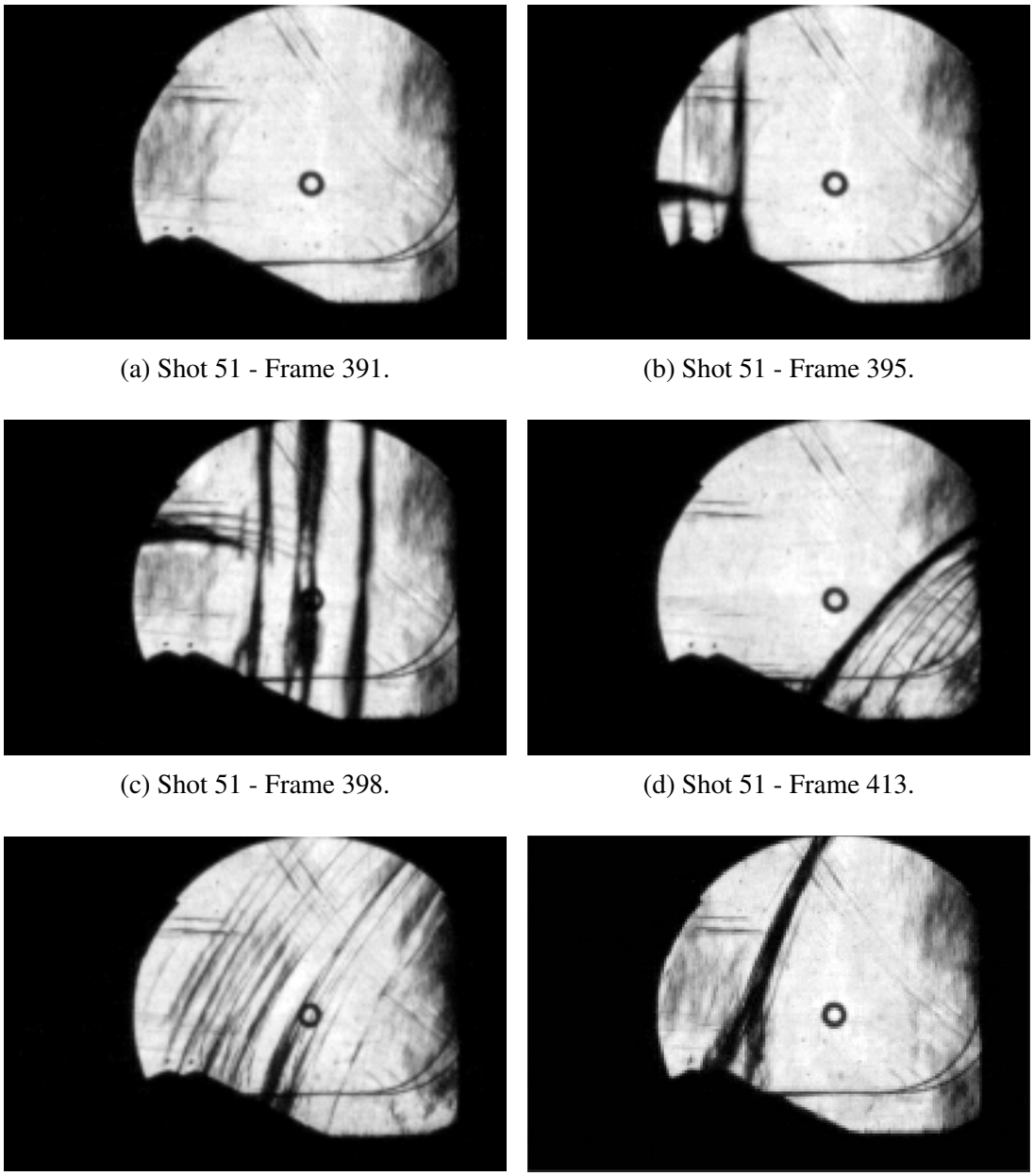

(a) Shot 51 - Frame 391.

(b) Shot 51 - Frame 395.

(c) Shot 51 - Frame 398.

(d) Shot 51 - Frame 413.

(e) Shot 51 - Frame 424.

(f) Shot 51 - Frame 435.

Figure 5.15. Schlieren sequence from Shot 51 - 1-inch peaked plate. Direction of travel is left to right in frames (b) and (c), and is right to left in (d), (e), and (f).

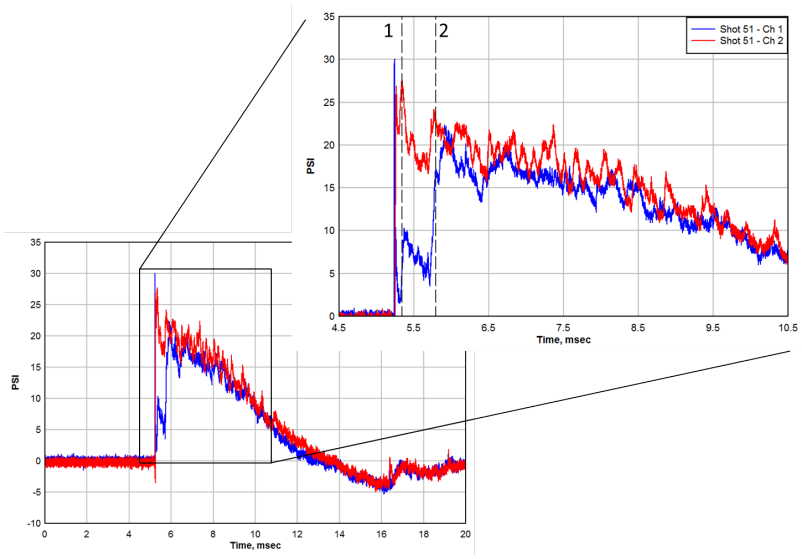

Figure 5.16. Shot 51 - Channel 1 and 2 waveforms with Schlieren timestamps.

5.3. SUMMARY OF ROUGHNESS EFFECTS ON SHOCK STRUCTURE AND MEASUREMENTS

The inclusion of roughness plates can result in a non-planar shock front, cause the shock front to split as it crosses the plate, alter the shock thickness, or cause reflections that can significantly alter the pressure and impulse. The deviations from a single, planar shock front and reflections caused by the surface roughness can also create oscillations in the pressure, which affect the pressure waveform shape and overall impulse value. The measured pressure is also dependent upon the location of the gage relative to the rough surface.

The majority of the differences in measured pressure and impulse occurred shortly after the shock TOA at the Gage 1 locations. However, the pressure time histories recorded at the Gage 2 location with the roughness plates in place were affected over the duration of the positive phase. In three of the four roughness plate cases, the attenuation rate at the Gage 2 location differed from the baseline case. The difference in attenuation rate resulted in an impulse that was much larger than the baseline case. Not only did the roughness plates

affect the pressure and impulse measurements, they increased the shot-to-shot scatter over the baseline tests. At the Gage 1 and 2 locations, mounted in the roughness plate, the pressure measurements were more significantly affected than the impulse, with differences of up to 85% and 49% difference from the baseline, respectively.

Geometry of the roughness also impacted the pressure time histories recorded by the floor mounted gages. The peaked plates resulted in a "double peak" waveform shape, where a region of low pressure followed the initial peak. The pressure at the gage location remained low until the reflection from the next peak traveled back across the gage location, causing the second peak.

The measurements made by the wing mounted gages were also affected by the presence of surface roughness, although to a lesser degree than the gages mounted in the plate. The general trend seen in the data from the wing mounted gages was that the peak pressure decreased with increasing distance from the rough surface. At the Gage 8 location, 7-inches above the bottom surface of the shock tube, the data was extremely consistent, with a variance of only 4% across all the tests for which it acquired data. The affect of the surface roughness appears to be limited to the height of the Mach reflection.

The path of the triple point moves upward with increasing distance from the source of the reflection. It is possible that the height of a gage relative to the axial distance from the height of the roughness must also be considered due to the triple point trajectory. Two gages placed at the same height above the surface, but at different distances downstream may be affected differently. Tests that provide visual data from further downstream in the shock tube would be useful for verifying the reflection trajectory relative to a gage location.

In addition to the pressure measurements, Schlieren video was taken during each shot. The images from the Schlieren video provided a second method of understanding the environment around the gage location. During the baseline tests with the flat plate in place, the shock front was planar and no reflections or other disturbances to the front were visible. However, on tests using the roughness plates, reflections were visible just behind the front,

and the shock front split into multiple fronts in 3 of 4 cases. Later in time, the reflections from downstream traveled back through the FOV and lined up with bumps in pressure in the gage data.

When analyzing data obtained from gages mounted in or near rough surfaces, the geometry and amplitude of the roughness as well as the gage location must be considered. The peak pressure will be higher with roughness in place, but the impulse may be up to 49% higher or 30% lower than with a flat surface despite a very constant input energy to the system. Measurements taken during this series at 7-inches above the floor of the shock tube yielded extremely consistent data, with only a 4% variance. This series maintained a consistent axial distance between the gage and the leading edge of the roughness. However, the axial distance, and the trajectory of the Mach reflection may also be another set of factors to consider during gage placement.

5.4. EFFECT OF IMPROPERLY MOUNTED GAGES ON PRESSURE MEASUREMENTS

As described in previous sections, even if surface roughness is not present, there is the possibility that a gage will be imperfectly mounted in an otherwise flat surface. In other words, the gage may not be perfectly flush with the surface in which it is mounted at the time of the test.

The results for Shots 32 and 39 were covered in detail in Section 4.6. Figure 5.17 compiles the average curves for the baseline cases, and imperfect mounts for the Gage 1, 2, and 4 locations.

With the 0.032-inch diaphragm, the recessed gage had the largest difference from the baseline case, with 119% higher peak pressures than the baseline. The high pressure at the beginning of the record is the result of a partial reflected pressure being recorded by the gage due to the recessed configuration. However, the impulse values for Gage 1 during the baseline and recessed cases were fairly similar, with only a 7% higher impulse for the

recessed gage. While the peak pressure was very high for the recessed gage, the duration of the high pressure was quite short. So, the impulse remained largely unaffected by the high peak pressure that occurred at the beginning of the record.

The local imperfection case, which consisted of a circular void at the edge of the Delrin insert, had the second largest difference from the baseline case with a peak pressure that was 63% higher. Also, the impulse at the gage with the local imperfection was 46% higher than the baseline case. The large deviations from the baseline case show that a gage that is surrounded by a void, but is level with an otherwise flat surface will provide erroneous measurements that cannot be reliably compared to a perfectly mounted gage.

The imperfect configuration that had the lowest pressure deviation from the baseline case was the protruding gage, at only 6% higher. Gage 4 had a delayed return to zero during the baseline shots, so the overall peak impulses can not be directly compared. However, until the time that the attenuation of the baseline pressure waveform deviated from the typical attenuation rate, the waveforms and resultant impulses were quite similar. It is reasonable to conclude that the impulse from the protruding gage would be comparable to the baseline case if the gage had functioned properly late time during all tests.

If the conditions of the test bed do not allow for, or significantly hinder the probability of a perfectly flush gage mount, it is better to err towards a protruding gage mount instead of a recessed one. Of the three imperfect mounting configurations tested, the protruding mount had the lowest difference from the baseline and peak pressure impulse.

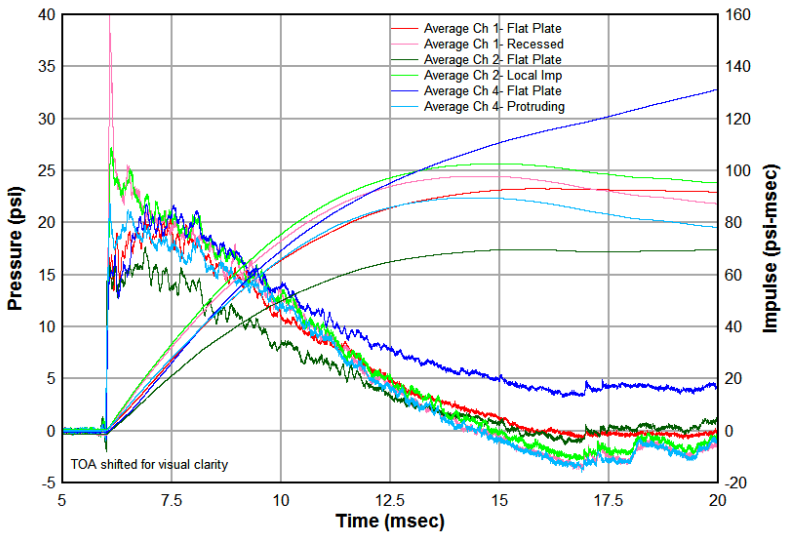

Figure 5.17. View of imperfectly mounted gage configurations.

5.5. EFFECTIVENESS OF VARIOUS DATA CORRECTION METHODS

The difficulties of accurately measuring peak pressure have long been known, and many professionals who study shock waves or explosive effects have methods of altering the data to obtain a more realistic peak pressure. One such technique, described in Reference [3] relies on plotting the data on a linear X, logarithmic Y scale coupled with extrapolation of the data. First, the pressure-time history is plotted so that time is on a linear scale and pressure is on a logarithmic scale. For a Friedlander type waveform, this plot format will result in a portion of the curve that is roughly linear. Then, a straight line is drawn through the linear portion to the shock TOA. The corrected overpressure is the value of the straight line at the TOA. Figure 5.18, from Reference [3] provides a visual example of this correction method.

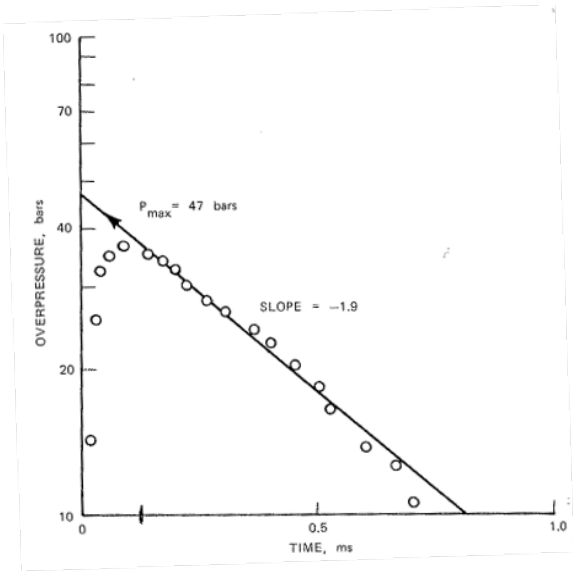

Figure 5.18. Example of logarithmic pressure correction, Reference [3].

The Friedlander curve fit is tuned to fit the decay rate of a free air burst, and was not expected to approximate the pressure profile in a shock tube environment. When a Friedlander approximation was fitted to the data, it did not match the entire pressure-time history very well. The differences near the shock TOA could not be replicated with a simple curve fit. However, if the curve fit is applied from the time of peak pressure through the end of the positive phase, the Friedlander approximation matches the attenuation rate of the data quite well (5.19). This observation is notable because the pressure attenuation rate in the shock tube can be reasonably approximated via an algorithm tuned to free air bursts. Also, it further supports the previous statements that the surface roughness primarily alters the early time data, and the later time attenuation rates typically remain unaffected.

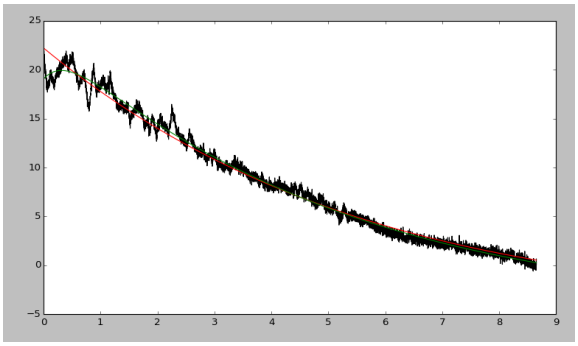

Figure 5.19. Example of Friedlander curve fit from time of peak through end of positive phase.

If pressure data is known to be affected by local surface roughness, the linear X, logarithmic Y correction method would remove a lot of the true structure from the shape of the pressure waveforms. However, the portion of the waveform from the time of peak through the end of the positive phase can be reasonably approximated by the Friedlander curve fit.

5.6. RECOMMENDATIONS FOR GAGE PLACEMENT

Given the spread of experimental error with the different roughness plates and mounting configurations, it is necessary to have a thorough understanding of the environment around the gage location. For consistency of measurement between tests, the best option is to mount gages in a wing-type mount at a height that they are unaffected by the Mach reflection or other shock characteristics that occur due to surface roughness. If the gage is mounted in a wing type mount at a sufficient distance from the surface, the data will be very consistent test to test, within 4% data measurement scatter. Both the Mach reflections and the path of the triple point should be considered when determining the height above surface for the gage placement for a given test. For situations where the environment

does not allow for a wing or sting type mount, the next best option is to mount the gage on a high point or protrusion on the surface.

If the surface can be easily modified with standard heavy equipment, the path between the explosive charge and the gage should be graded to remove any surface aberrations. An additional surface preparation step that may be feasible for some tests is to ensure that the distance between the gage and explosive is covered with a flat concrete pad.

Even for cases where it is not possible to mount the gage at some height above the surface, it should be possible to improve the quality of data obtained by preparing the surface around the gage. Preparations to the surface may include artificially creating a flat area around the gage mount with a large gage canister or small concrete pad. When the shock wave reaches the flat, smooth surround, the shock will begin to "heal", losing the characteristics induced by the surface roughness.

6. CONCLUSIONS

The shock tube testing series covered in this document was designed to quantify the effect surface conditions near the pressure transducer have on the pressure measurements, and to determine the structure of the shock as it moved across gages mounted in selected rough surfaces. The data gathered would then be used to provide recommendations for mounting gages in environments with surface roughness and quantify the amount of error associated with making pressure measurements with four different surfaces roughnesses.

Table 5.1, in Section 5.1.2, listed the average peak pressure and impulse for each roughness plate and mounting configuration. The measured pressure and impulse were not consistent across the series despite a nearly constant amount of energy input to the system via the compressed air driver section. For Gages 1 and 2, which were mounted flush with the surface of the perturbation plates, the measured peak pressure ranged from 12% to 85% higher than the baseline case. The impulses for Gages 1 and 2 were also significantly affected. Gage 1, mounted on a peak tended to have a lower impulse than the baseline (-2 to -30%). Conversely, the impulses from Gage 2, mounted in a valley generally trended higher than the baseline values (-6 to 49%). The impulse was not as highly affected as the peak pressure measurements, but the deviation from the baseline was significant. Additionally, increased amplitudes of roughness appear to correlate with increased standard deviations of pressure and impulse within the sample set.

When gages were mounted in a wing mount at varying heights above the perturbation plate, some trends were observable. The largest percent differences in pressure from the baseline case occurred at the gage location closest to the plate. As the distance between the gage location and the perturbation plate increased, the percent difference from the baseline case decreased. At the Gage 8 location, 7-inches above the plate, the pressures and impulses were essentially the same as the baseline case with only a 4% variance

throughout the series. The effects on pressure measurements were limited to the areas inside the Mach reflection that occurred due to the surface roughness geometry.

Significant differences in pressure and impulse were also present for two of the three imperfectly mounted gage configurations. The recessed transducer measured more than double the baseline pressure, while the transducer with the local imperfections recorded a 63% higher peak pressure. The protruding transducer case had only a 6% difference from the baseline case. For surface mounted gages, if a perfect alignment cannot be achieved, it is better for the transducer to protrude than be recessed.

Despite the spread of pressures and impulses measured, all but one configuration tested (recessed gage in an otherwise flat surface) resulted in experimental error less than the +/-2x rule of thumb. The +/- 2x rule of thumb for complicated testbed geometries makes it difficult to confidently attribute favorable performance to the explosive configuration tested, rather than an inaccurate measurement. The data presented here provides definitive estimations of experimental error associated with multiple types of surface roughness and gage locations that can be used to estimate error bars for small data sets obtained under similar conditions. While none of the measurements taken with the roughness plates in place were more than twice the baseline values, the differences from the baseline case were significant for all perturbation plate and gage location combinations except for the Gage 8 location.

Post-test analysis of data gathered from multiple environments requires an understanding of the gage location and the conditions local to the gage. For consistency of measurement between tests, the best option is to mount gages in a wing-type mount at a height that they are unaffected by the Mach reflection or other shock characteristics which occur due to surface roughness. The height at which the gage will be unaffected by the Mach reflection is likely influenced by the axial (downstream) distance from the surface roughness in addition to the height above the surface. If the environment does not allow

for a wing or sting type mount, the next best option is to mount the gage on a high point or protrusion on the surface.

In some cases, it may be necessary to mount a gage flush with the surface. For these cases, the surface should be prepared as much as feasible to create a flat surface around the gage location. Ideally, the entire distance between the explosive charge and the gage should be smoothed to remove as much of the surface aberrations as possible.

If future work collects additional data from configurations that study the effects of additional roughness amplitudes, spacing, and how axial distance vs height from the roughness affects measured pressure, a function could be created that would serve as a guideline for gage placement. Even without additional data, the results from this series can serve as benchmark validation for calculations performed to understand the effects on local pressure for similar scenarios.

With the more complete understanding of how surface conditions local to the pressure gage affect measurements presented here, researchers can make informed choices when selecting instrumentation locations and analyzing data for situations where surface roughness cannot be avoided.

APPENDIX A

DATA TRACES

APPENDIX A

This appendix contains all of the data traces for the tests conducted in the series. The parameters for each shot are listed in the section header. Figure caption nomenclature: (Shot Number), (Channel Number)-(Gage Serial Number).

SHOT 3 - FLAT PLATE - 0.032-INCH DIAPHRAGM

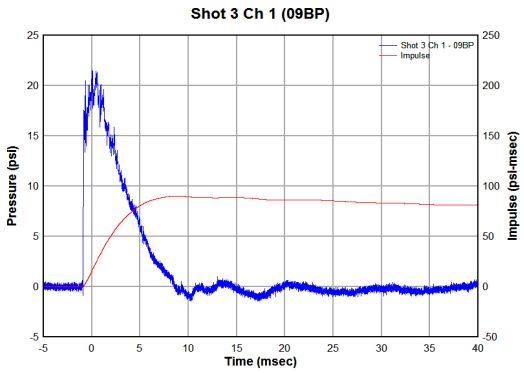

(a) Shot 3, ch1-09bp

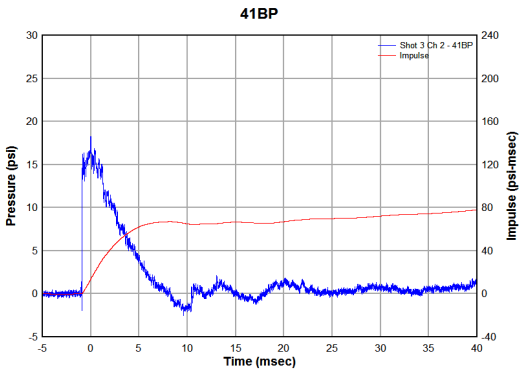

(b) Shot 3, ch2-41bp

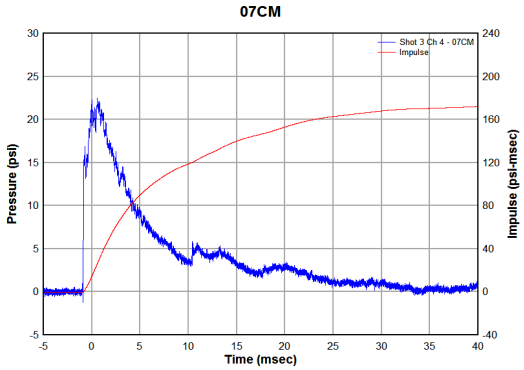

(c) Shot 3, ch4-07cm

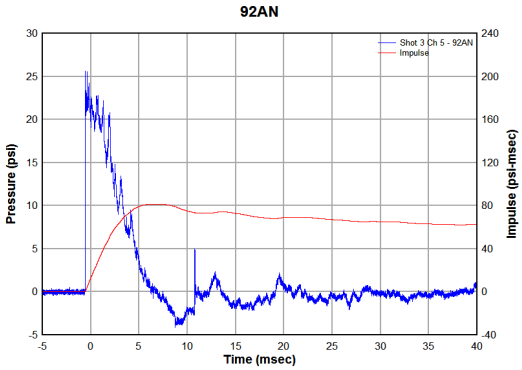

(d) Shot 3, ch5-92an

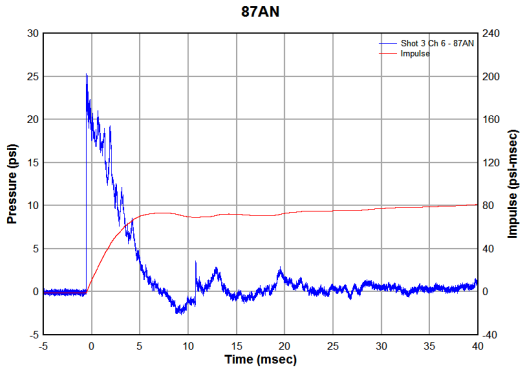

(e) Shot 3, ch6-87an

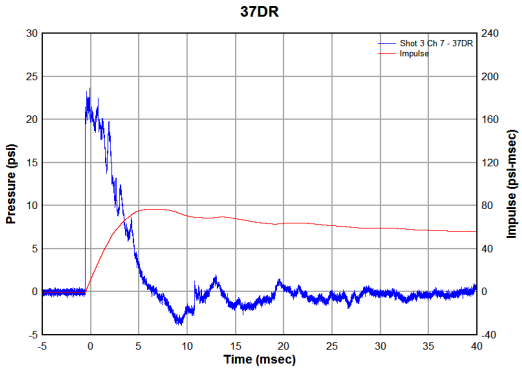

(f) Shot 3, ch7-37dr

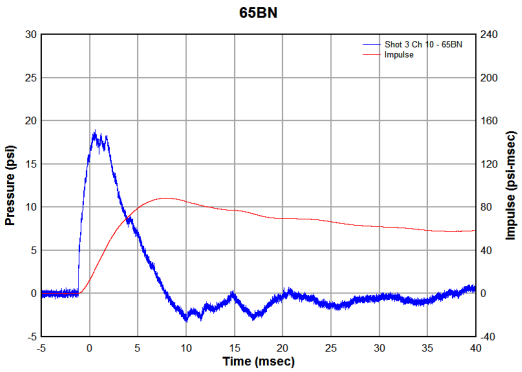

(a) Shot 3, ch10-65bn

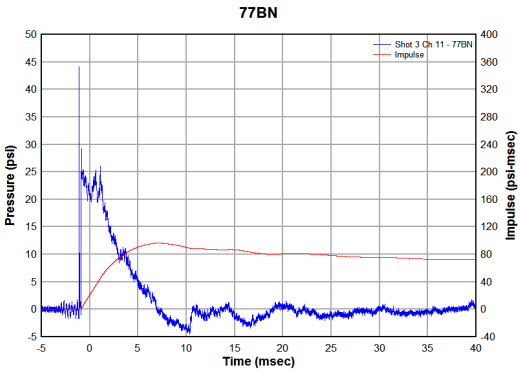

(b) Shot 3, ch11-77bn

SHOT 4 - FLAT PLATE - 0.032-INCH DIAPHRAGM

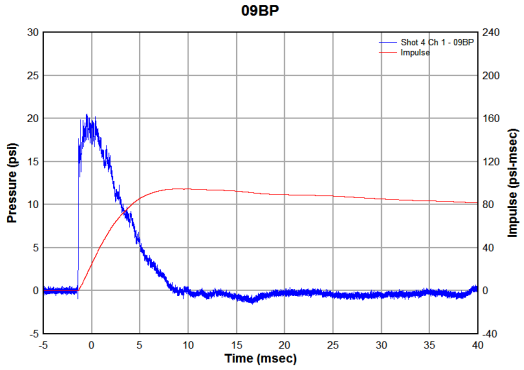

(a) Shot 4, ch1-09bp

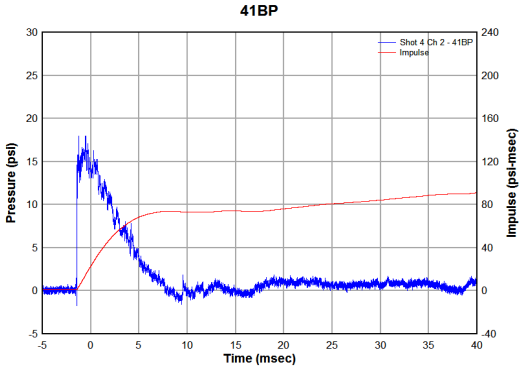

(b) Shot 4, ch2-41bp

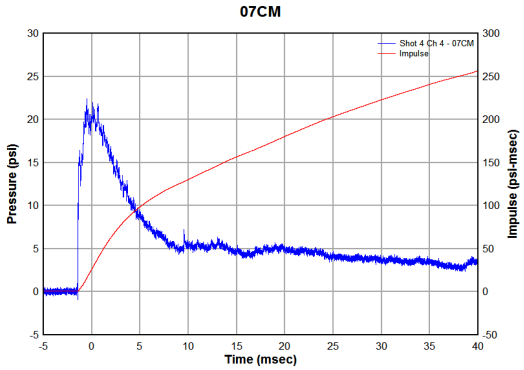

(c) Shot 4, ch4-07cm

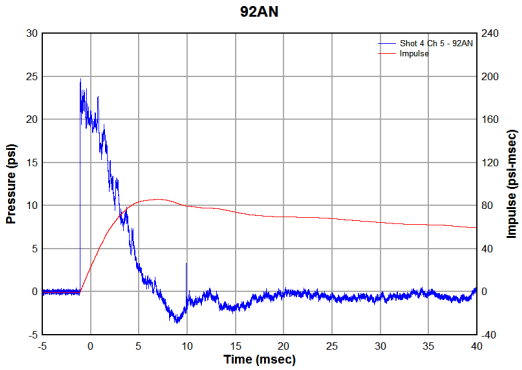

(d) Shot 4, ch5-92an

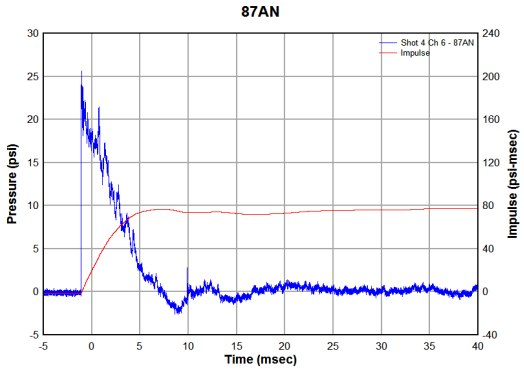

(e) Shot 4, ch6-87an

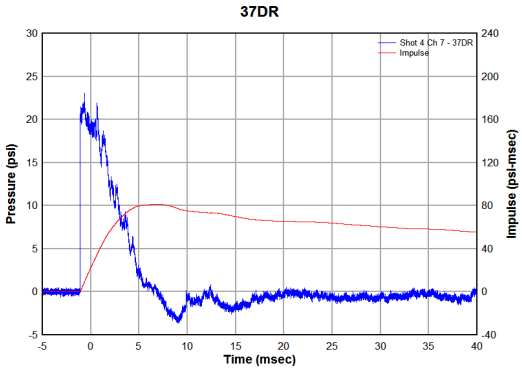

(f) Shot 4, ch7-37dr

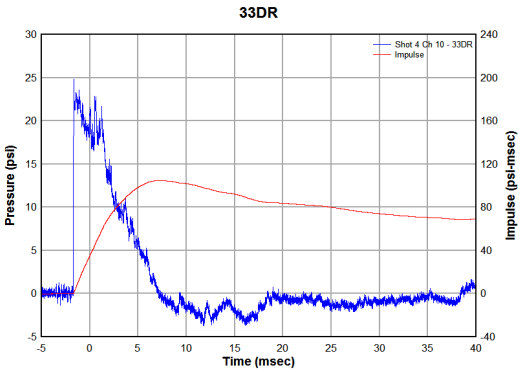

(a) Shot 4, ch10-33dr

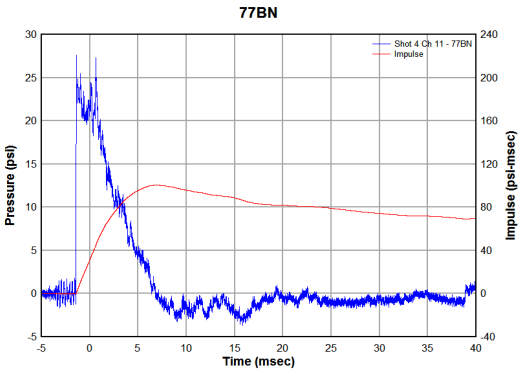

(b) Shot 4, ch11-77bn

SHOT 5 - FLAT PLATE - 0.032-INCH DIAPHRAGM

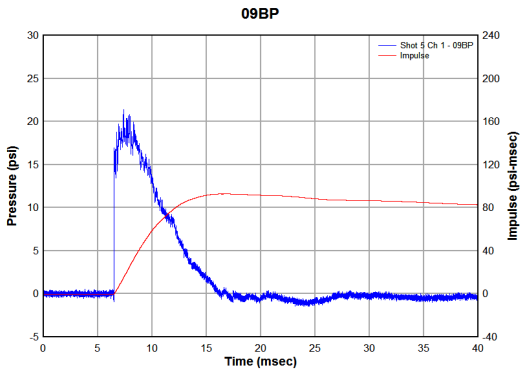

(a) Shot 5, ch1-09bp

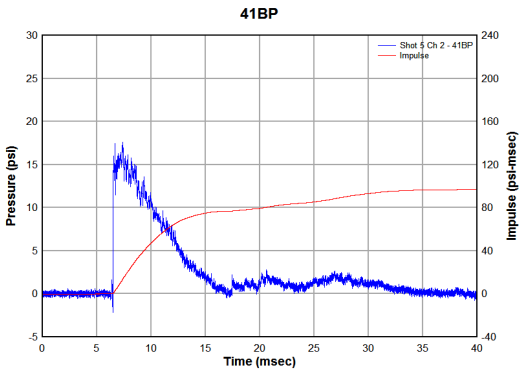

(b) Shot 5, ch2-41bp

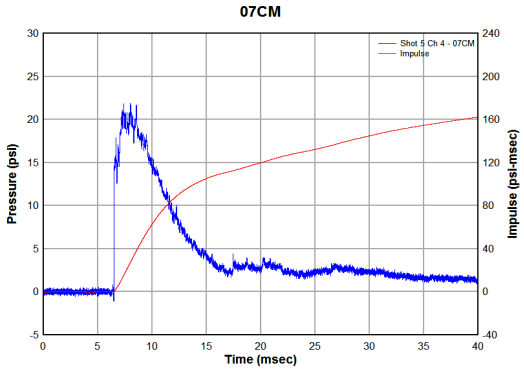

(c) Shot 5, ch4-07cm

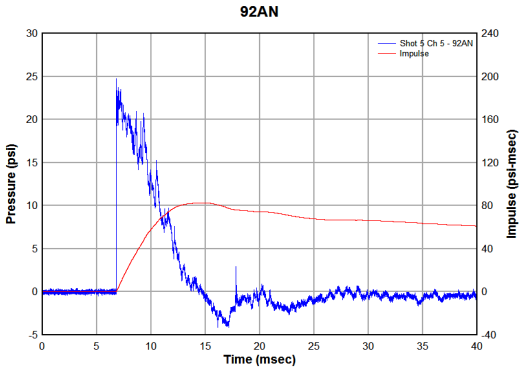

(d) Shot 5, ch5-92an

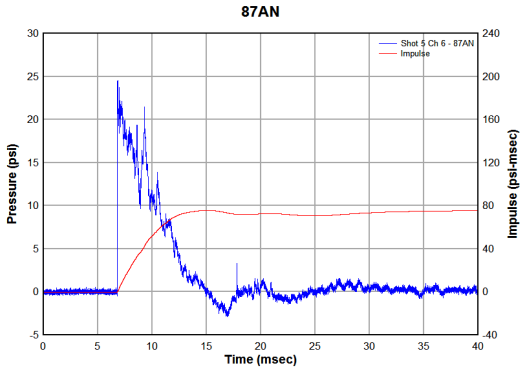

(e) Shot 5, ch6-87an

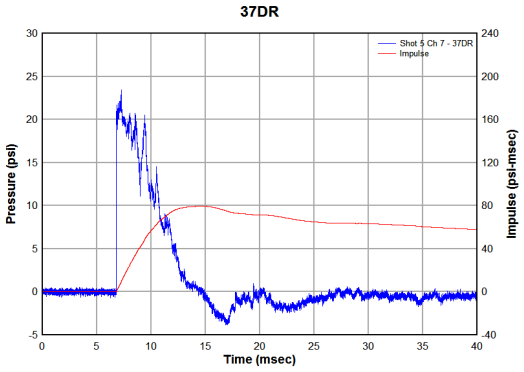

(f) Shot 5, ch7-37dr

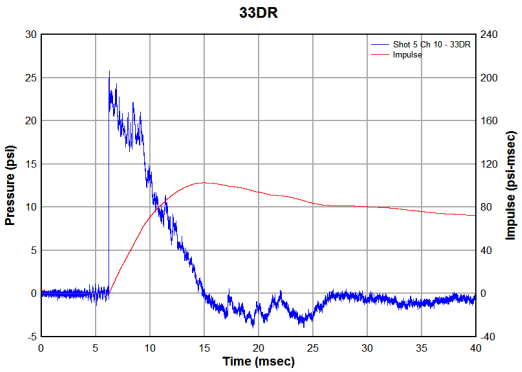

(a) Shot 5, ch10-33dr

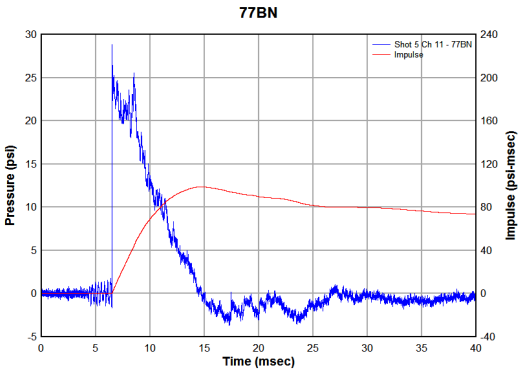

(b) Shot 5, ch11-77bn

SHOT 6 - 1/2-INCH WAVY PLATE - 0.032-INCH DIAPHRAGM

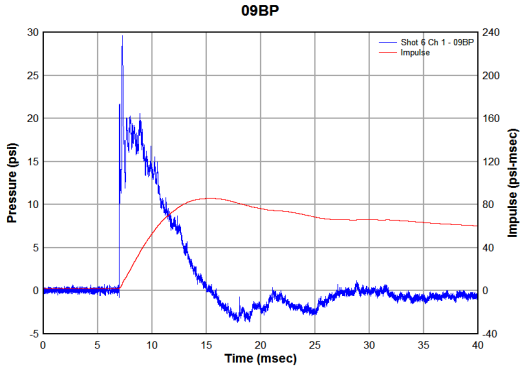

(a) Shot 6, ch1-09bp

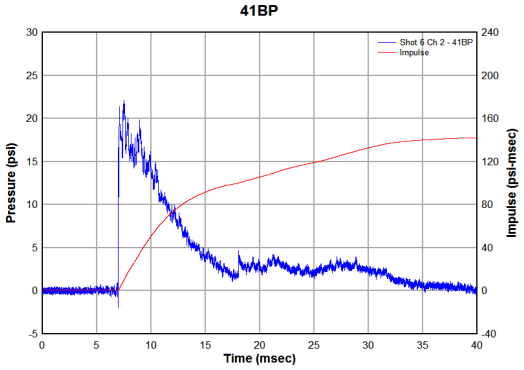

(b) Shot 6, ch2-41bp

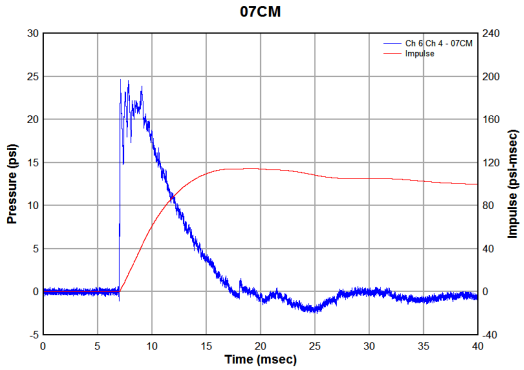

(c) Shot 6, ch4-07cm

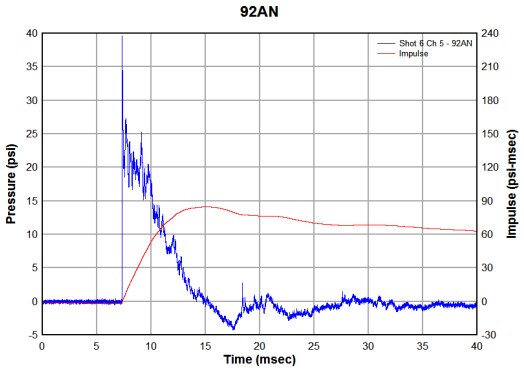

(d) Shot 6, ch5-92an

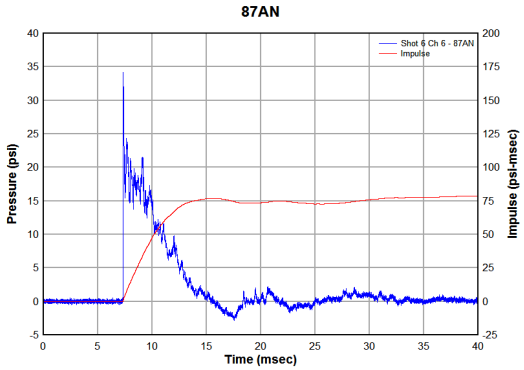

(e) Shot 6, ch6-87an

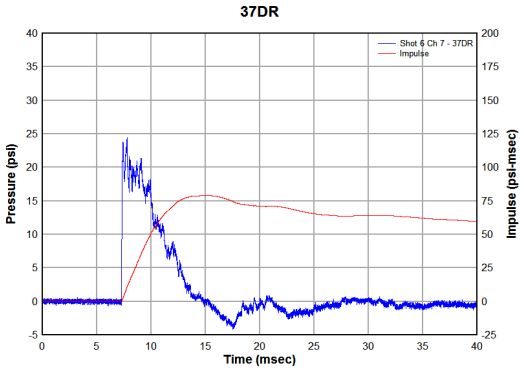

(f) Shot 6, ch7-37dr

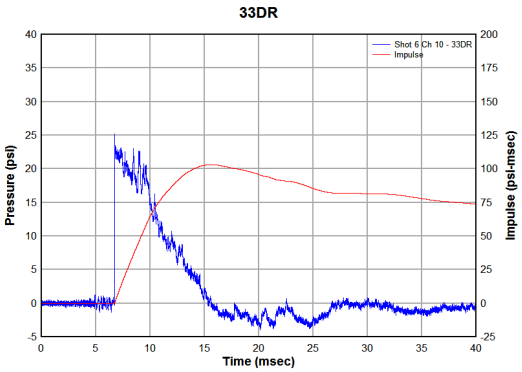

(a) Shot 6, ch10-33dr

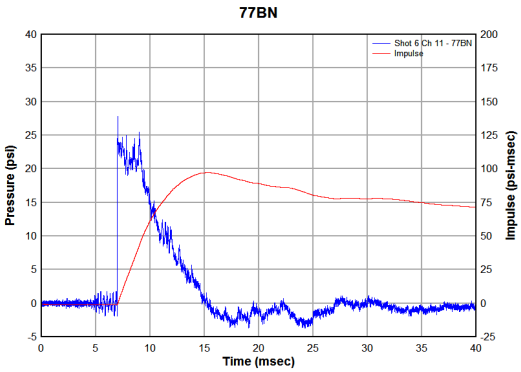

(b) Shot 6, ch11-77bn

SHOT 7 - 1/2-INCH WAVY PLATE - 0.032-INCH DIAPHRAGM

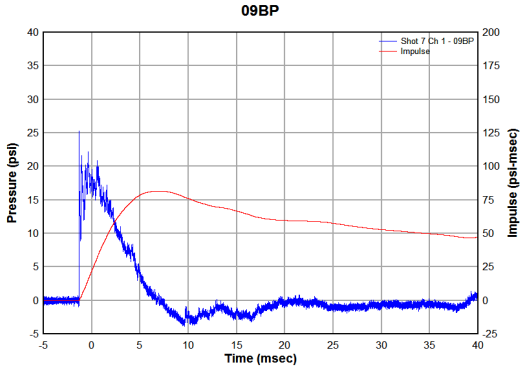

(a) Shot 7, ch1-09bp

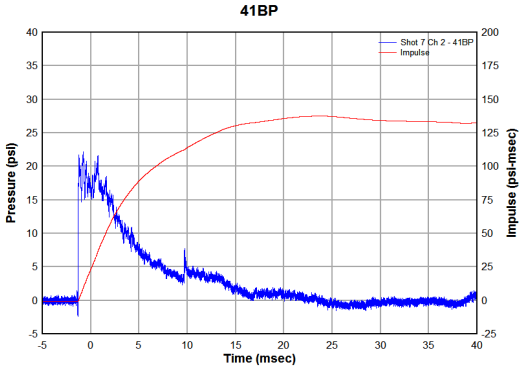

(b) Shot 7, ch2-41bp

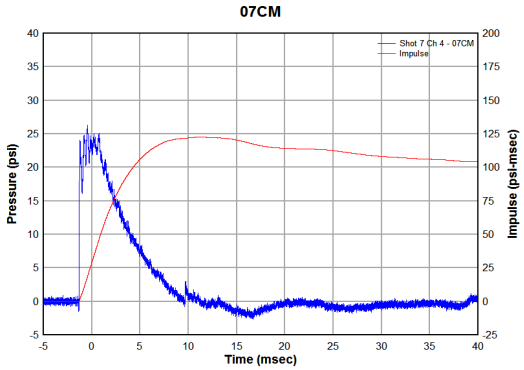

(c) Shot 7, ch4-07cm

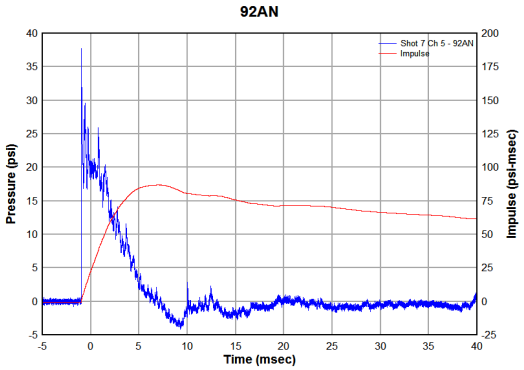

(d) Shot 7, ch5-92an

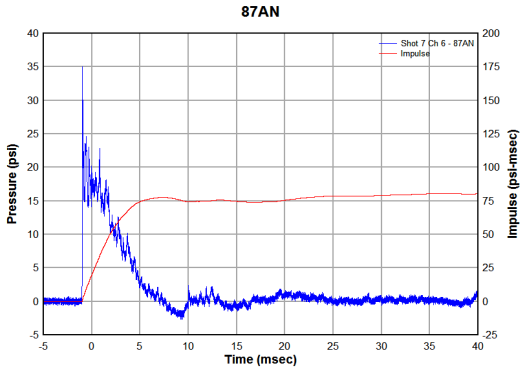

(e) Shot 7, ch6-87an

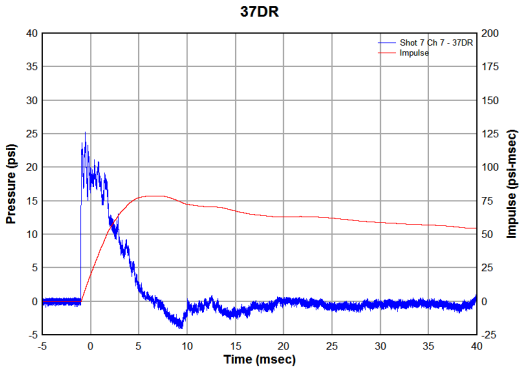

(f) Shot 7, ch7-37dr

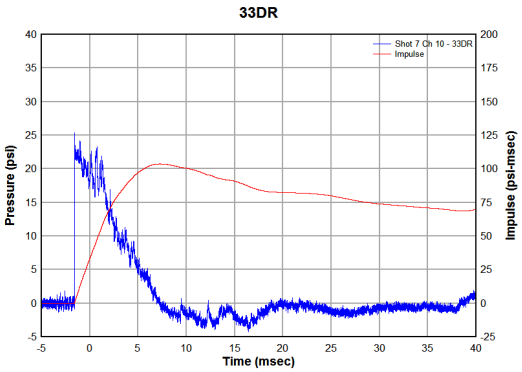

(a) Shot 7, ch10-33dr

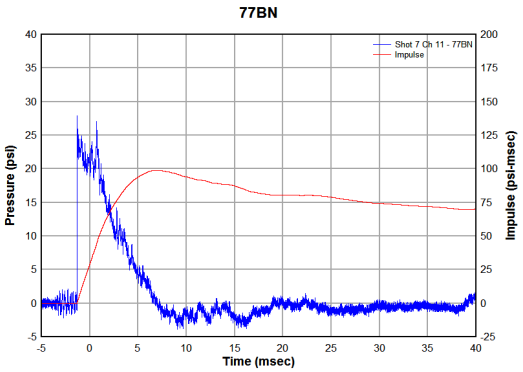

(b) Shot 7, ch11-77bn

SHOT 8 - 1/2-INCH WAVY PLATE - 0.032-INCH DIAPHRAGM

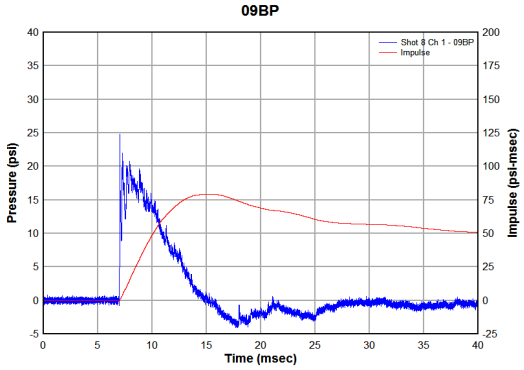

(a) Shot 8, ch1-09bp

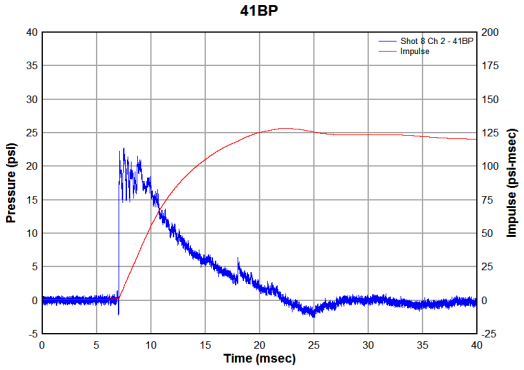

(b) Shot 8, ch2-41bp

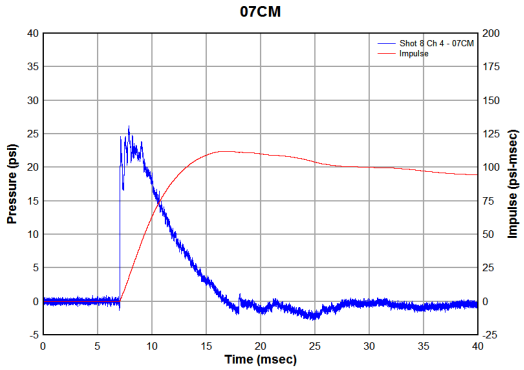

(c) Shot 8, ch4-07cm

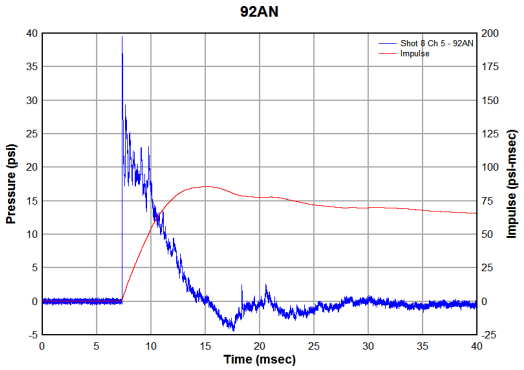

(d) Shot 8, ch5-92an

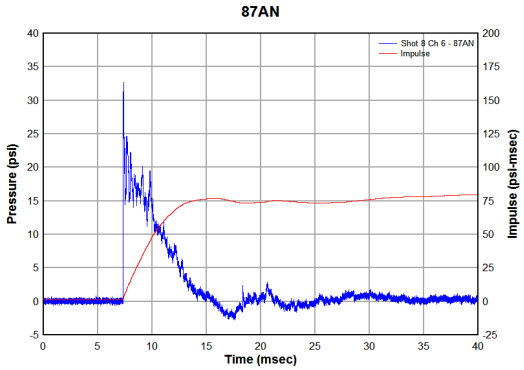

(e) Shot 8, ch6-87an

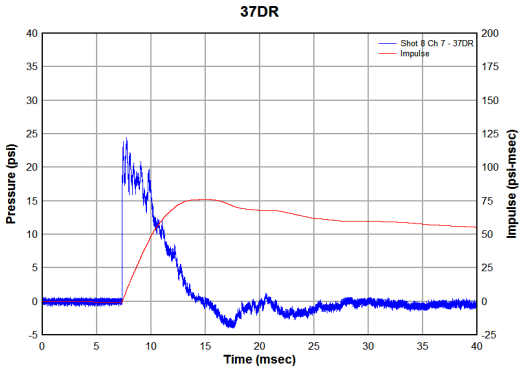

(f) Shot 8, ch7-37dr

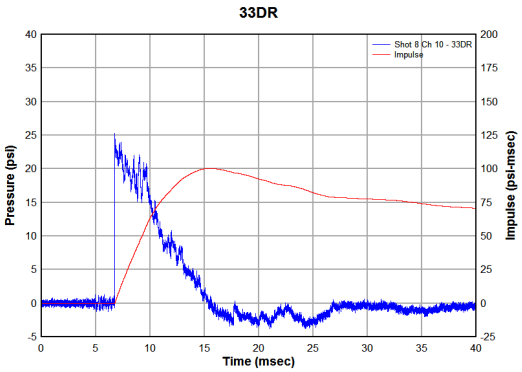

(a) Shot 8, ch10-33dr

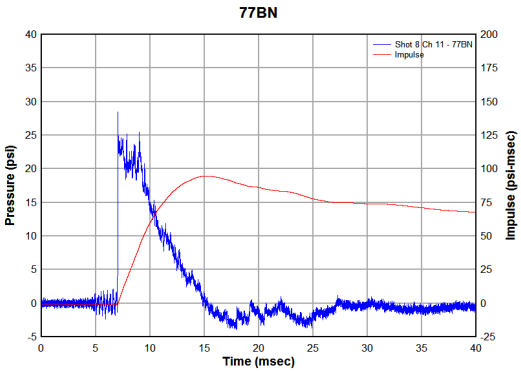

(b) Shot 8, ch11-77bn

SHOT 9 - 1/2-INCH WAVY PLATE - 0.032-INCH DIAPHRAGM

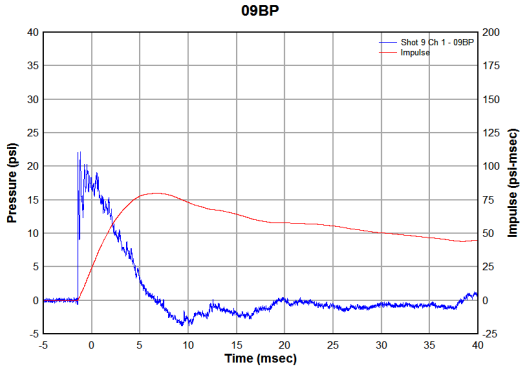

(a) Shot 9, ch1-09bp

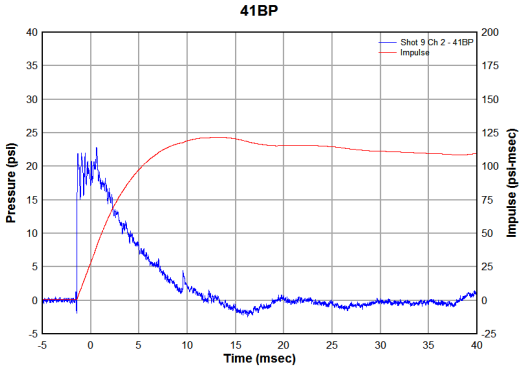

(b) Shot 9, ch2-41bp

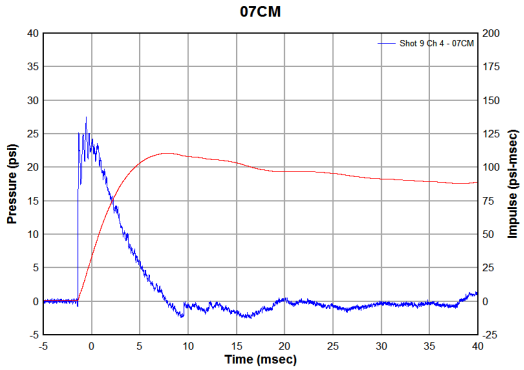

(c) Shot 9, ch4-07cm

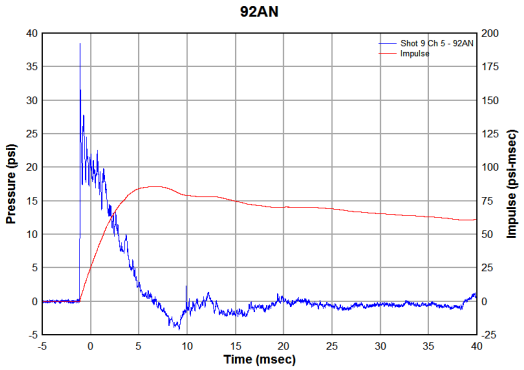

(d) Shot 9, ch5-92an

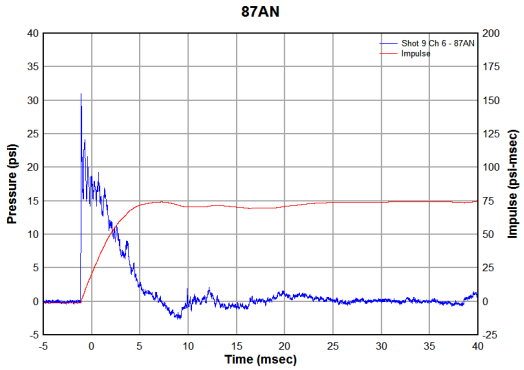

(e) Shot 9, ch6-87an

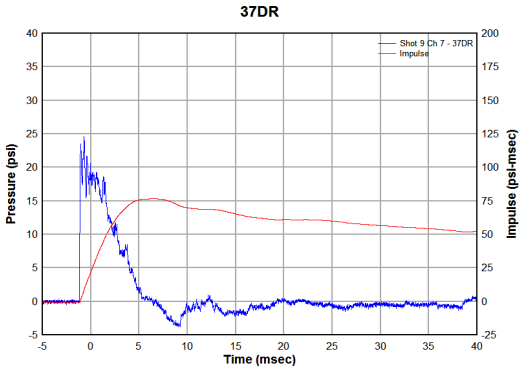

(f) Shot 9, ch7-37dr

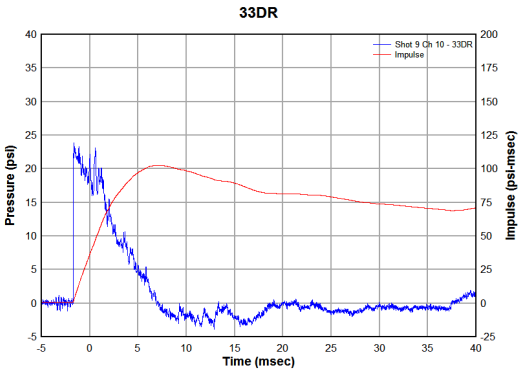

(a) Shot 9, ch10-33dr

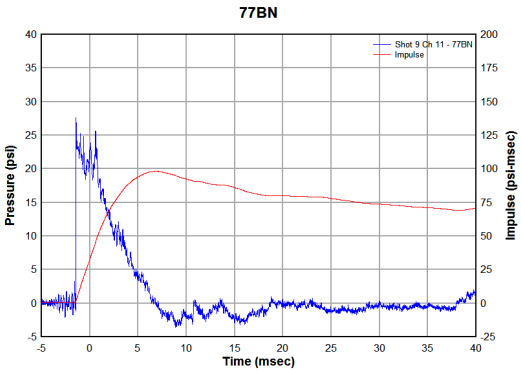

(b) Shot 9, ch11-77bn

SHOT 10 - 1/2-INCH WAVY PLATE - 0.025-INCH DIAPHRAGM

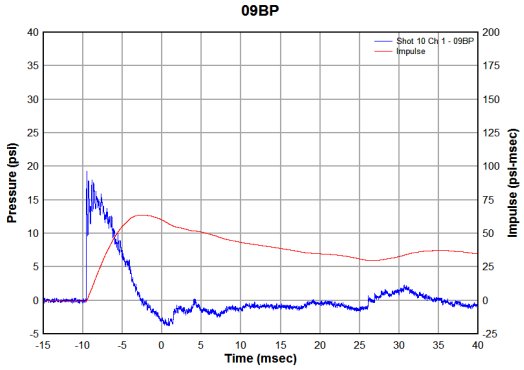

(a) Shot 10, ch1-09bp

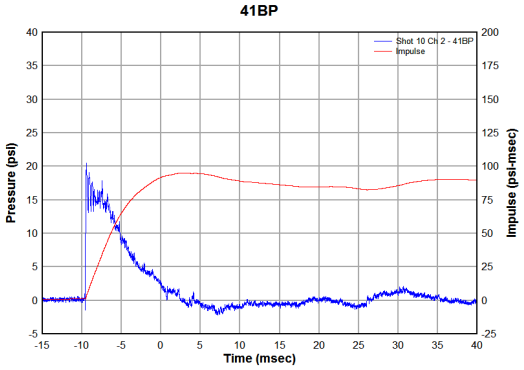

(b) Shot 10, ch2-41bp

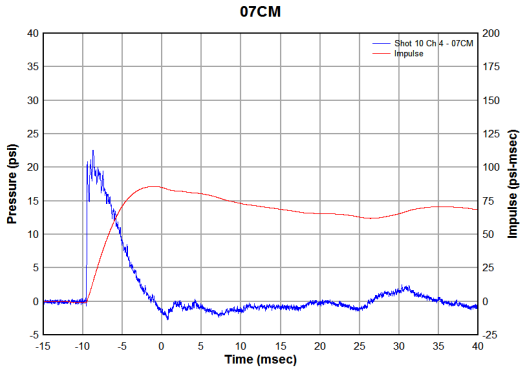

(c) Shot 10, ch4-07cm

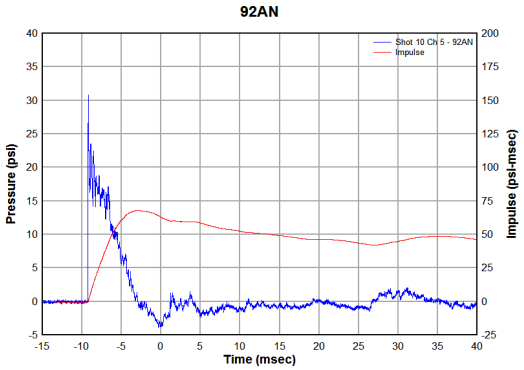

(d) Shot 10, ch5-92an

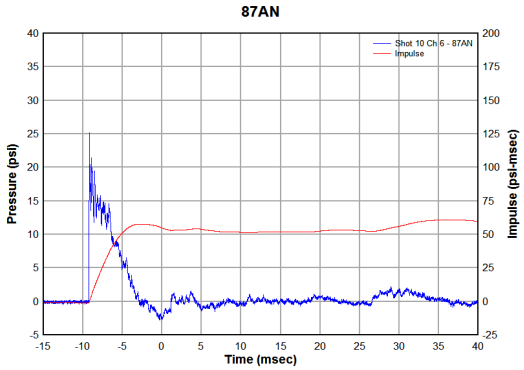

(e) Shot 10, ch6-87an

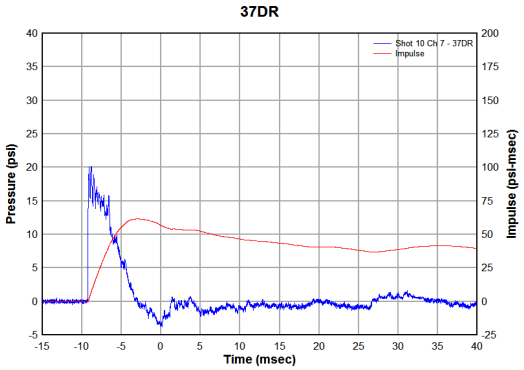

(f) Shot 10, ch7-37dr

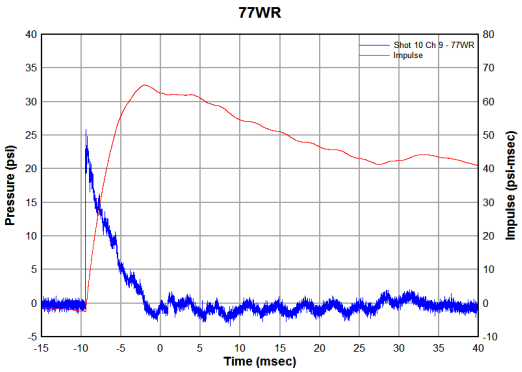

(a) Shot 10, ch9-77wr

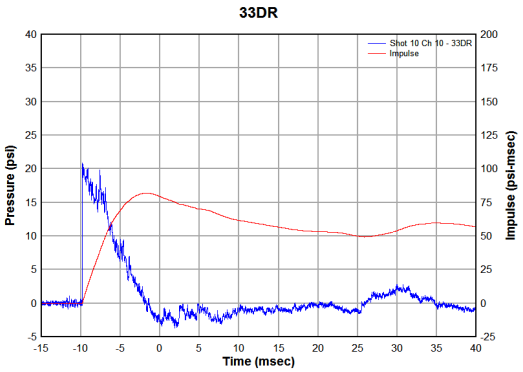

(b) Shot 10, ch10-33dr

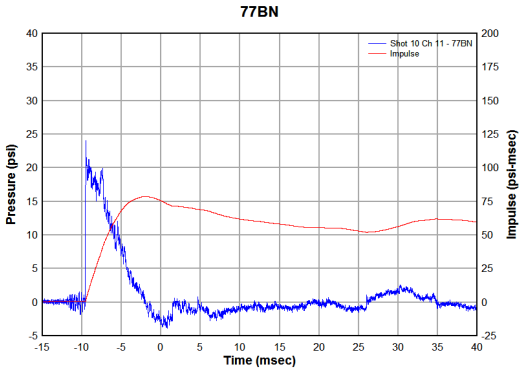

(c) Shot 10, ch11-77bn

SHOT 11 - 1/2-INCH WAVY PLATE - 0.025-INCH DIAPHRAGM

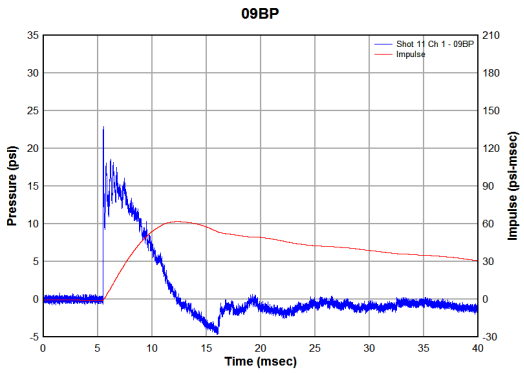

(a) Shot 11, ch1-09bp

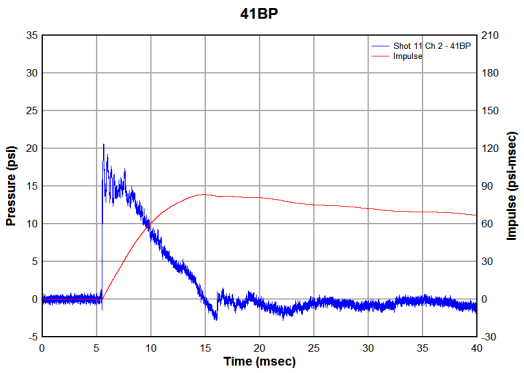

(b) Shot 11, ch2-41bp

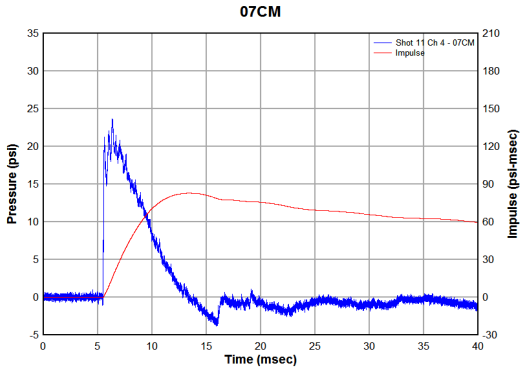

(c) Shot 11, ch4-07cm

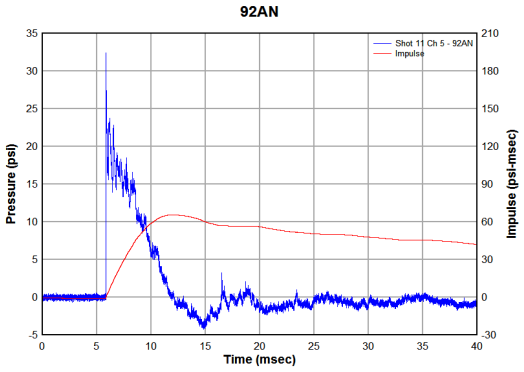

(d) Shot 11, ch5-92an

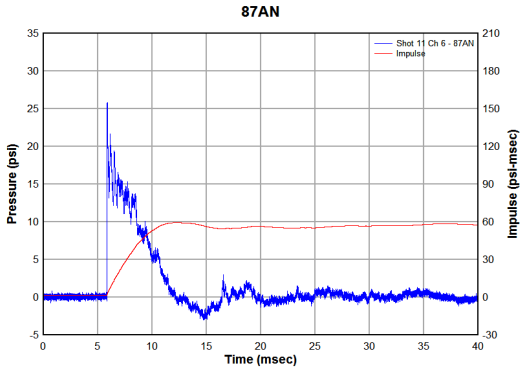

(e) Shot 11, ch6-87an

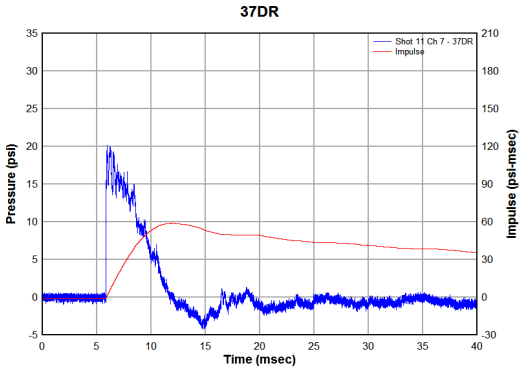

(f) Shot 11, ch7-37dr

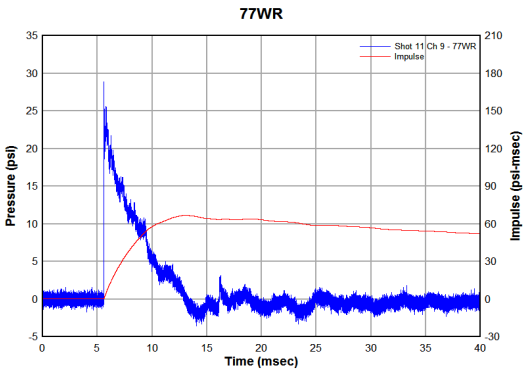

(a) Shot 11, ch9-77wr

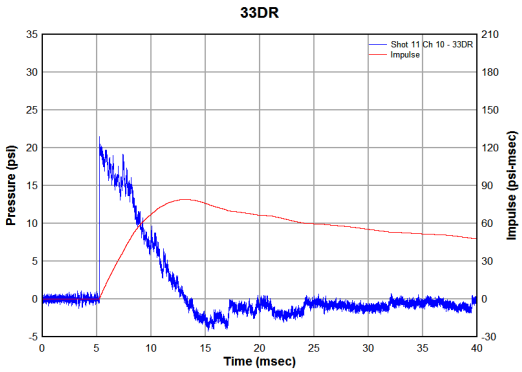

(b) Shot 11, ch10-33dr

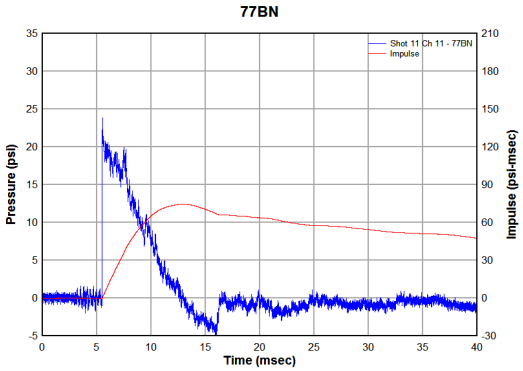

(c) Shot 11, ch11-77bn

SHOT 12 - 1/2-INCH WAVY PLATE - 0.025-INCH DIAPHRAGM

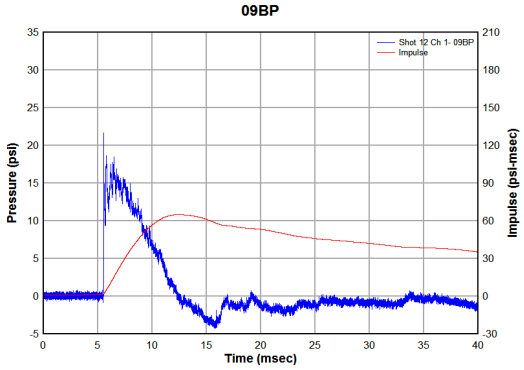

(a) Shot 12, ch1-09bp

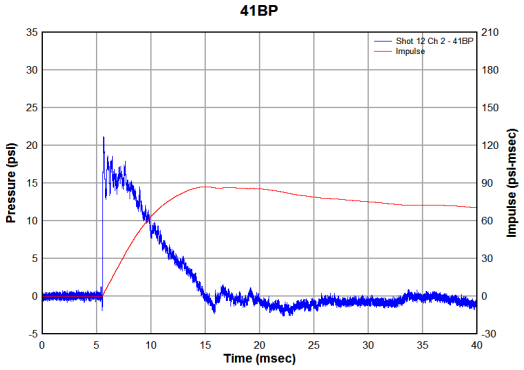

(b) Shot 12, ch2-41bp

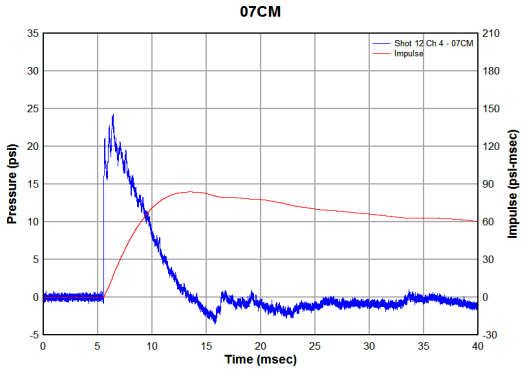

(c) Shot 12, ch4-07cm

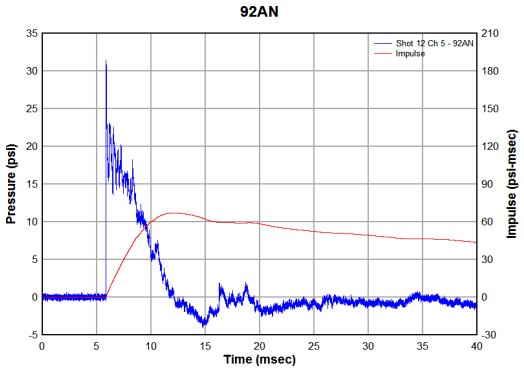

(d) Shot 12, ch5-92an

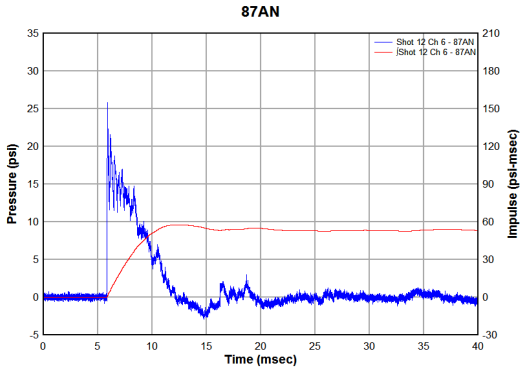

(e) Shot 12, ch6-87an

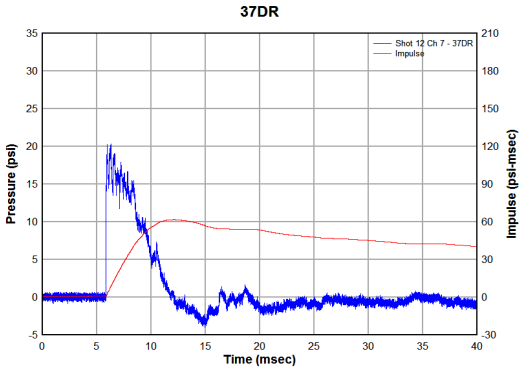

(f) Shot 12, ch7-37dr

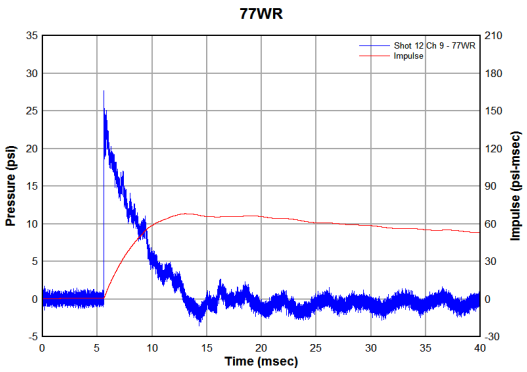

(a) Shot 12, ch9-77wr

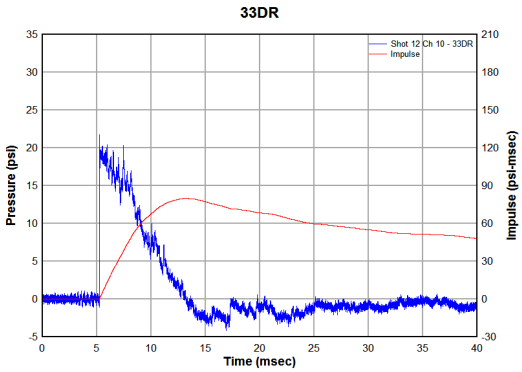

(b) Shot 12, ch10-33dr

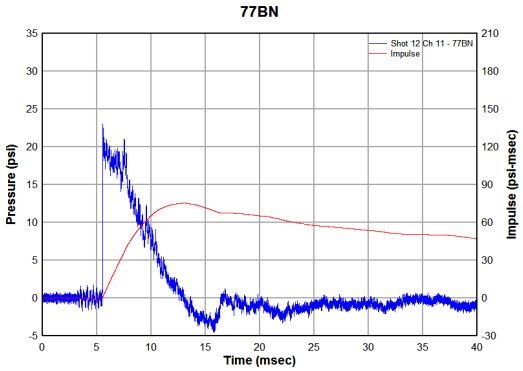

(c) Shot 12, ch11-77bn

SHOT 13 - 1/2-INCH WAVY PLATE - 0.025-INCH DIAPHRAGM

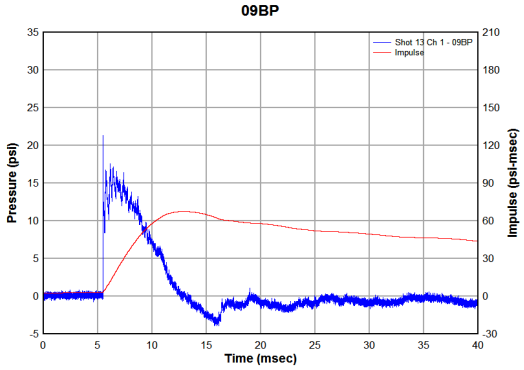

(a) Shot 13, ch1-09bp

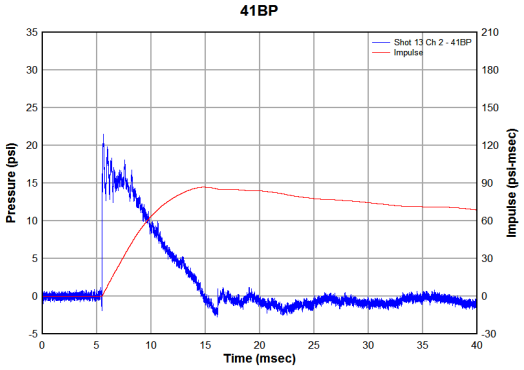

(b) Shot 13, ch2-41bp

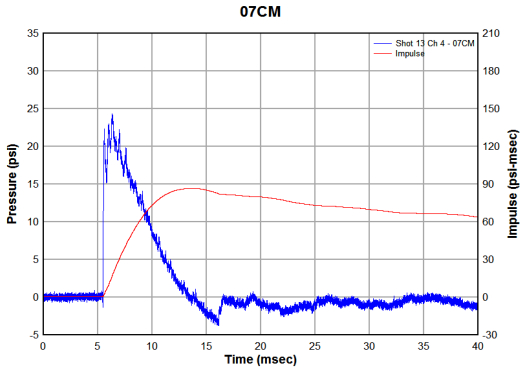

(c) Shot 13, ch4-07cm

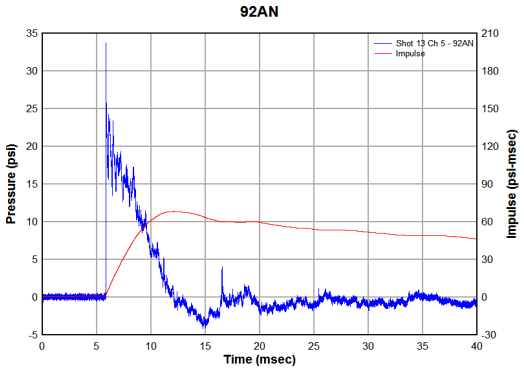

(d) Shot 13, ch5-92an

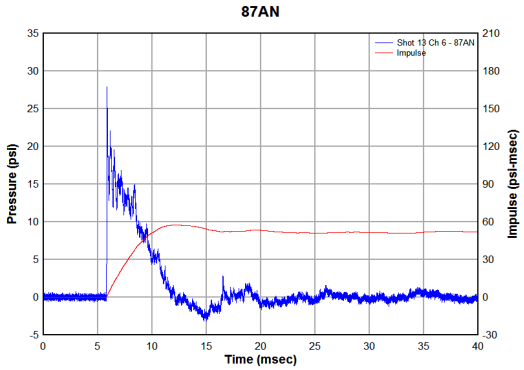

(e) Shot 13, ch6-87an

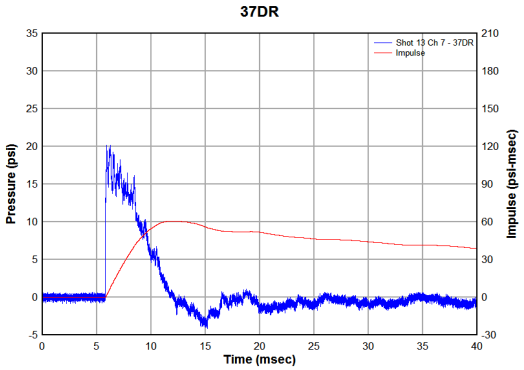

(f) Shot 13, ch7-37dr

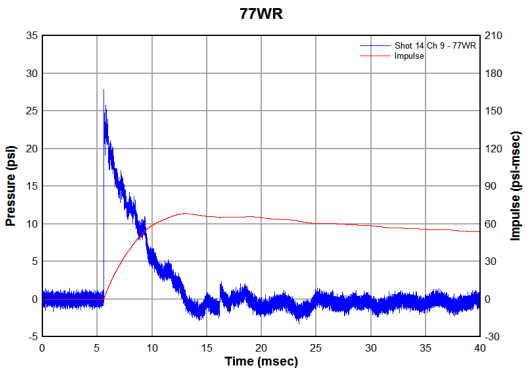

(a) Shot 13, ch9-77wr

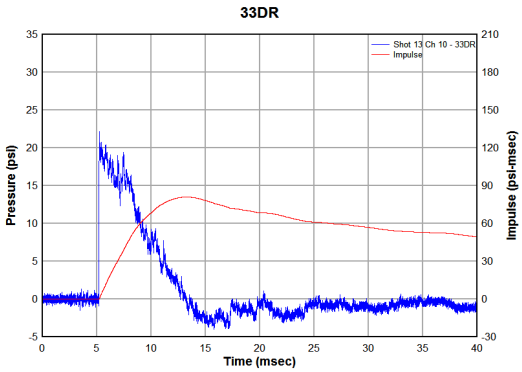

(b) Shot 13, ch10-33dr

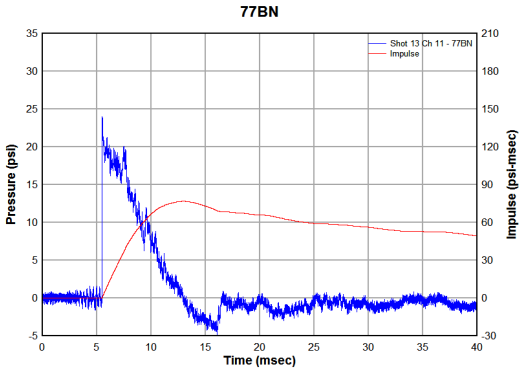

(c) Shot 13, ch11-77bn

SHOT 14 - 1/2-INCH PEAKED PLATE - 0.032-INCH DIAPHRAGM

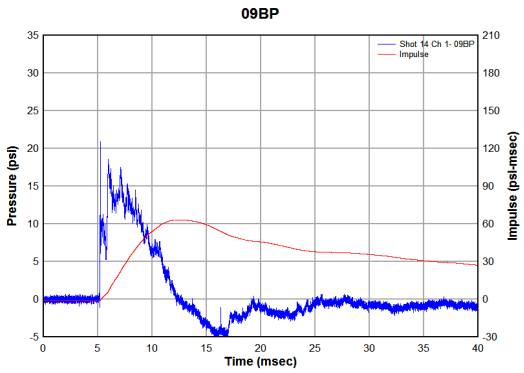

(a) Shot 14, ch1-09bp

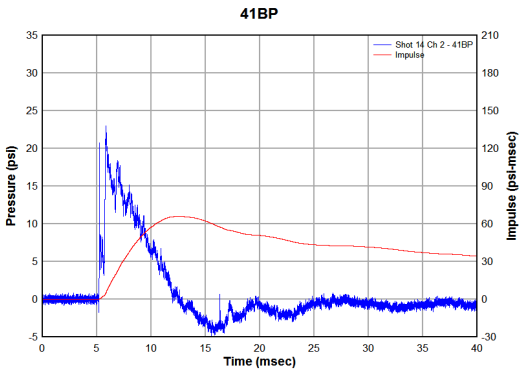

(b) Shot 14, ch2-41bp

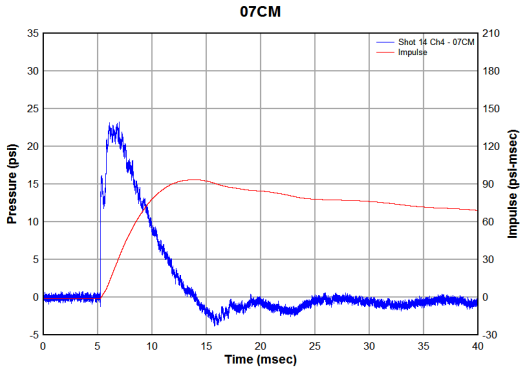

(c) Shot 14, ch4-07cm

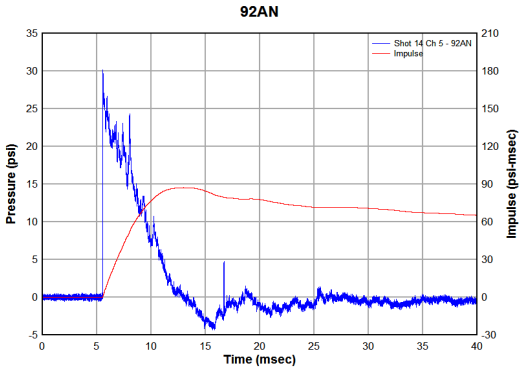

(d) Shot 14, ch5-92an

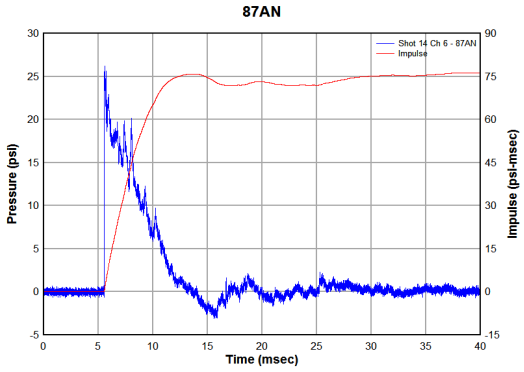

(e) Shot 14, ch6-87an

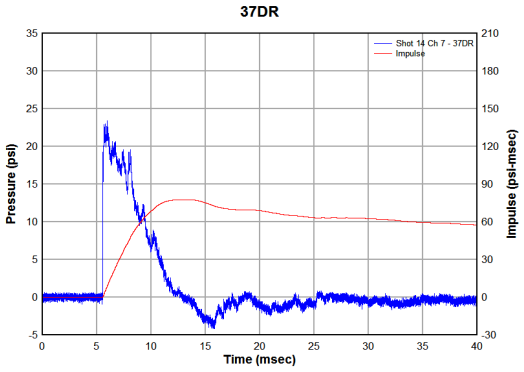

(f) Shot 14, ch7-37dr

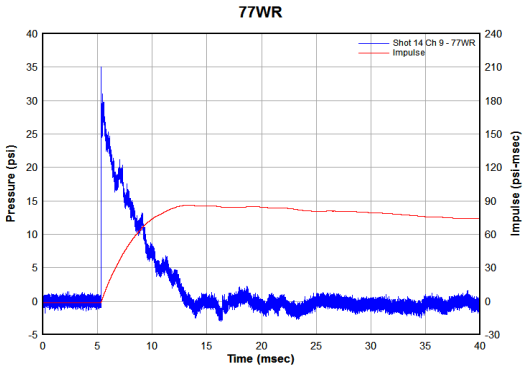

(a) Shot 14, ch9-77wr

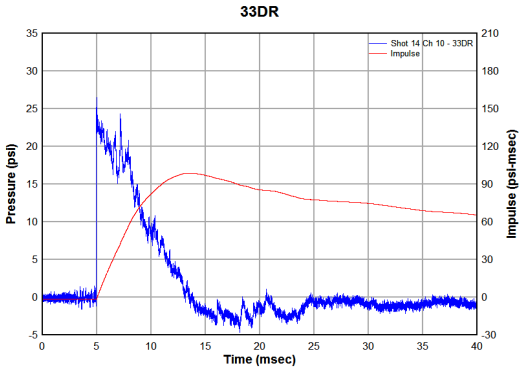

(b) Shot 14, ch10-33dr

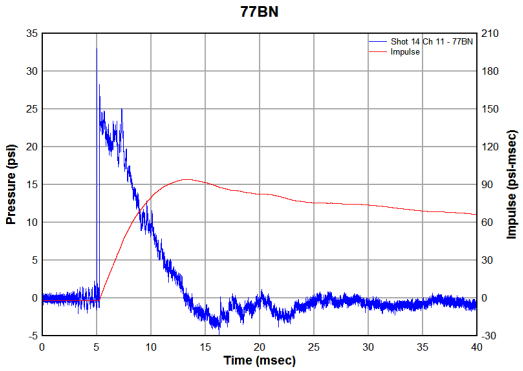

(c) Shot 14, ch11-77bn

SHOT 15 - 1/2-INCH PEAKED PLATE - 0.032-INCH DIAPHRAGM

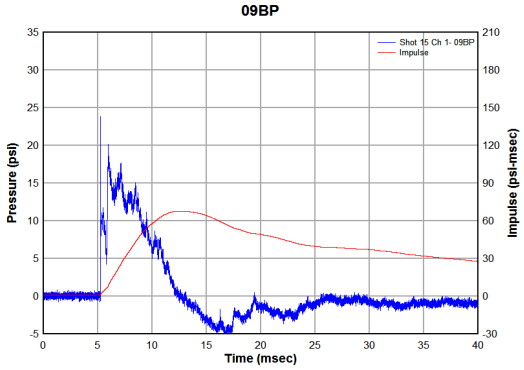

(a) Shot 15, ch1-09bp

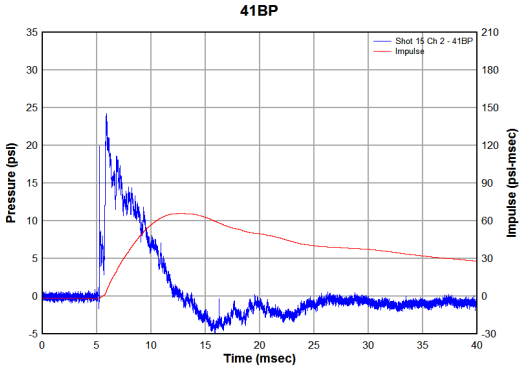

(b) Shot 15, ch2-41bp

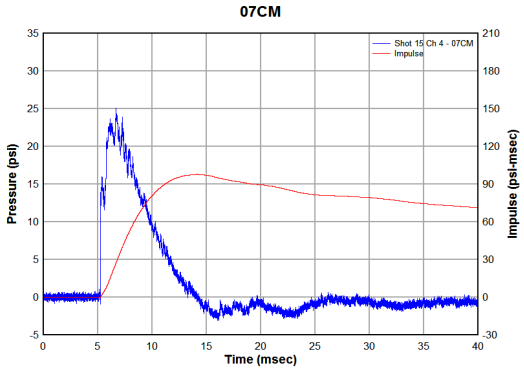

(c) Shot 15, ch4-07cm

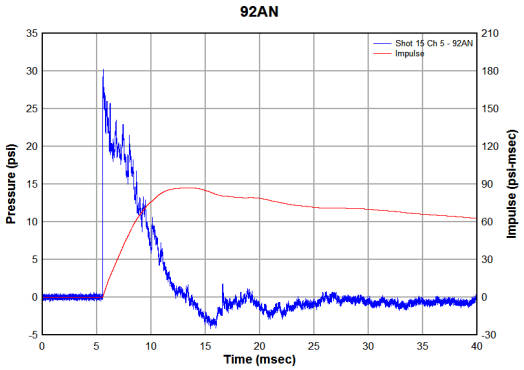

(d) Shot 15, ch5-92an

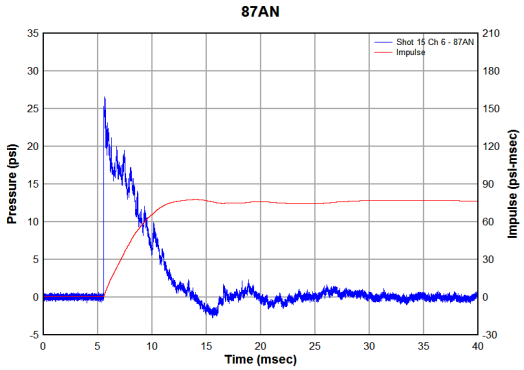

(e) Shot 15, ch6-87an

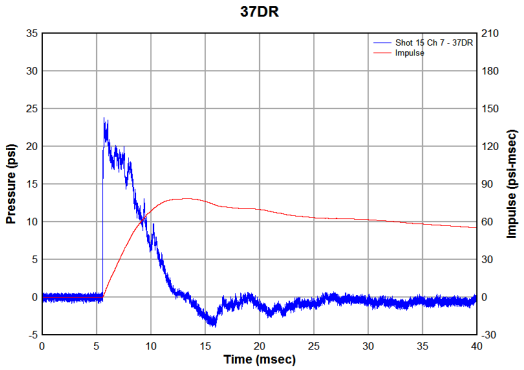

(f) Shot 15, ch7-37dr

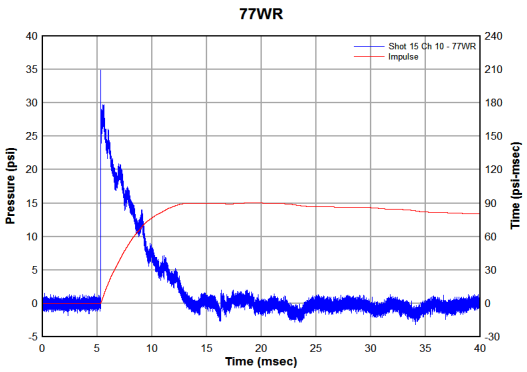

(a) Shot 15, ch9-77wr

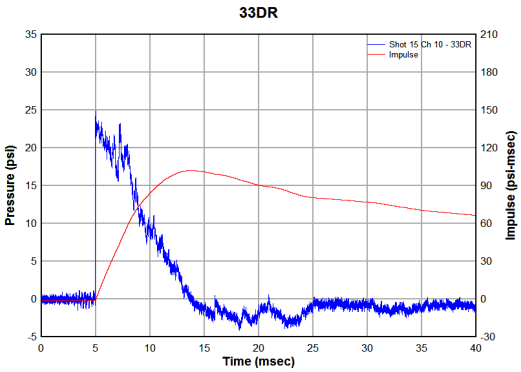

(b) Shot 15, ch10-33dr

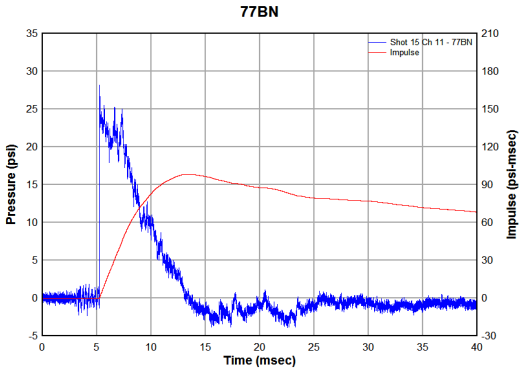

(c) Shot 15, ch11-77bn

SHOT 16 - 1/2-INCH PEAKED PLATE - 0.032-INCH DIAPHRAGM

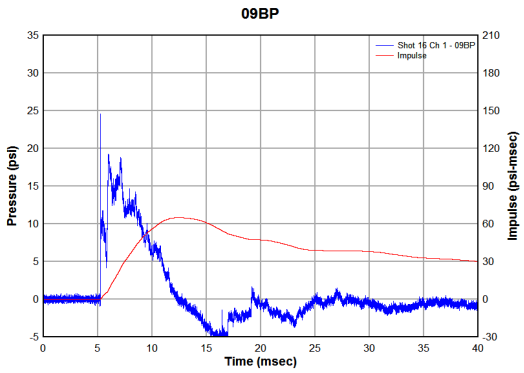

(a) Shot 16, ch1-09bp

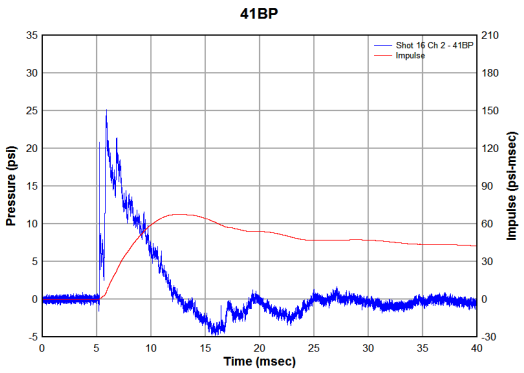

(b) Shot 16, ch2-41bp

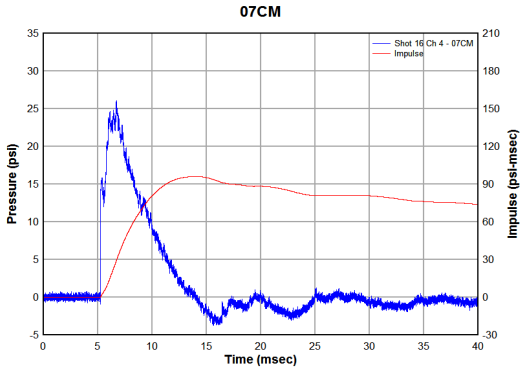

(c) Shot 16, ch4-07cm

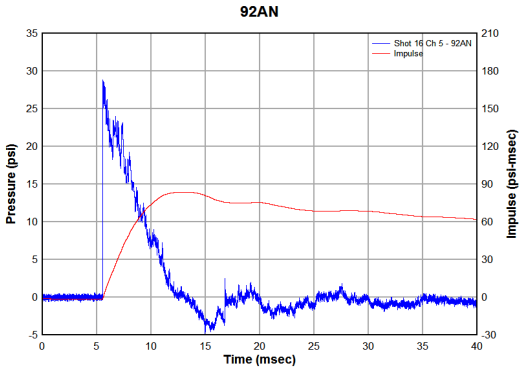

(d) Shot 16, ch5-92an

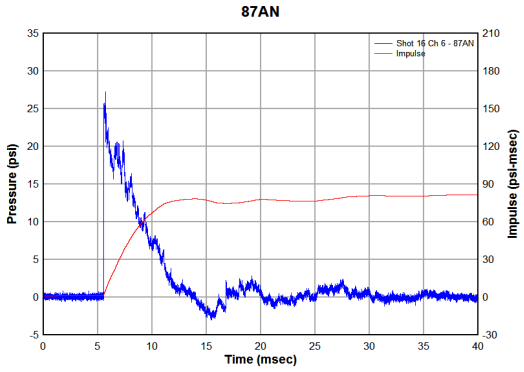

(e) Shot 16, ch6-87an

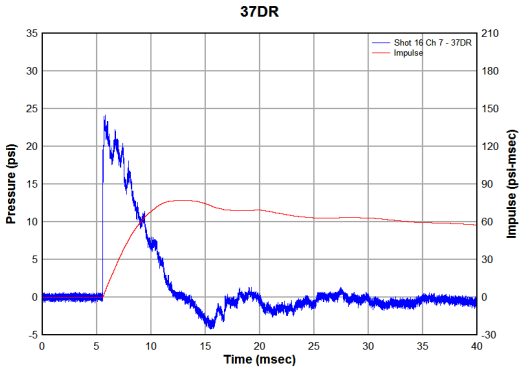

(f) Shot 16, ch7-37dr

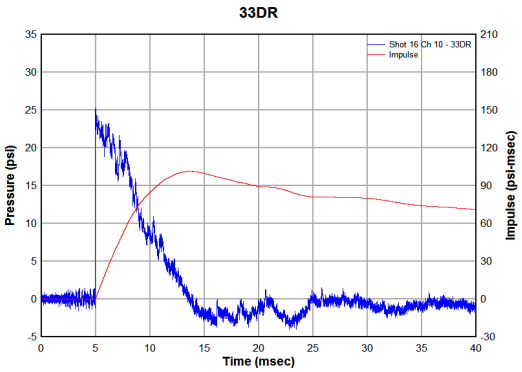

(a) Shot 16, ch10-33dr

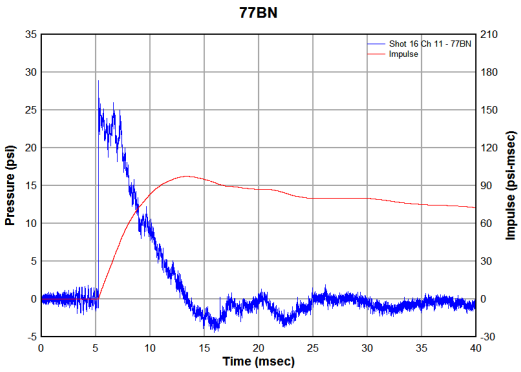

(b) Shot 16, ch11-77bn

SHOT 17 - 1/2-INCH PEAKED PLATE - 0.032-INCH DIAPHRAGM

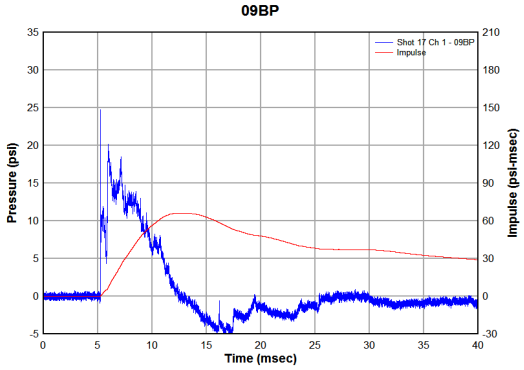

(a) Shot 17, ch1-09bp

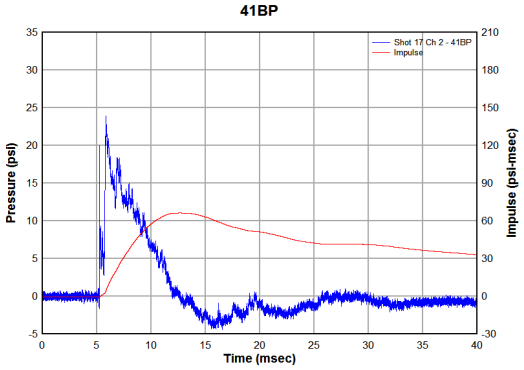

(b) Shot 17, ch2-41bp

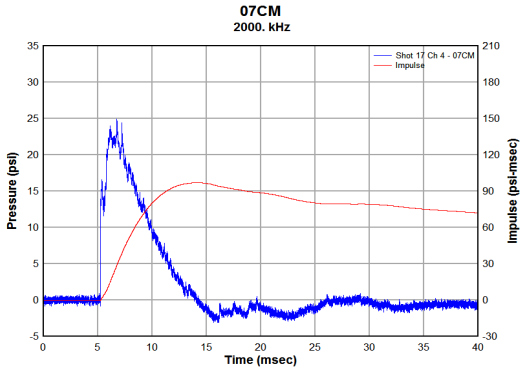

(c) Shot 17, ch4-07cm

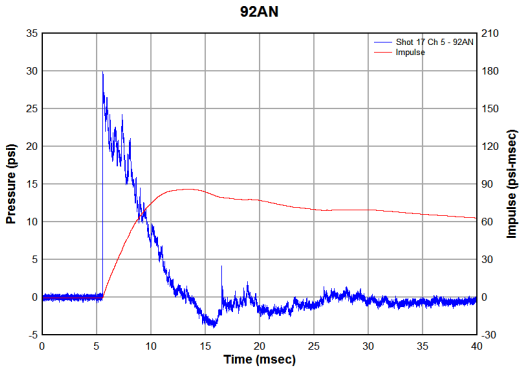

(d) Shot 17, ch5-92an

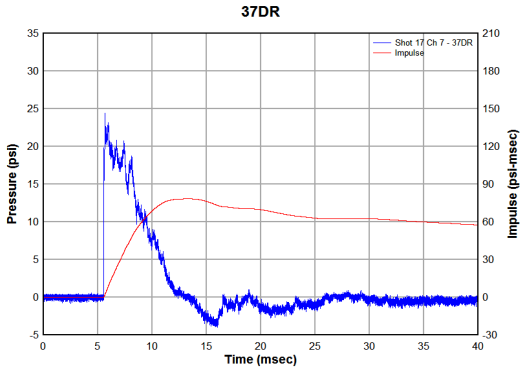

(e) Shot 17, ch7-37dr

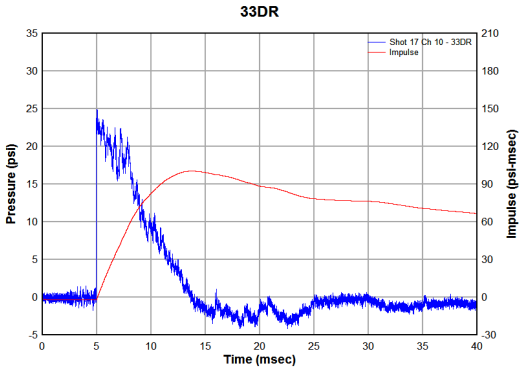

(f) Shot 17, ch10-33dr

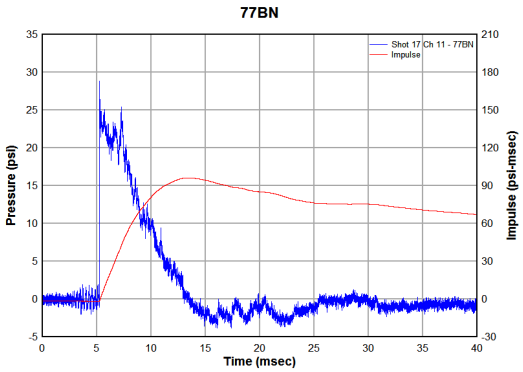

(a) Shot 17, ch11-77bn

SHOT 18 - 1/2-INCH PEAKED PLATE - 0.025-INCH DIAPHRAGM

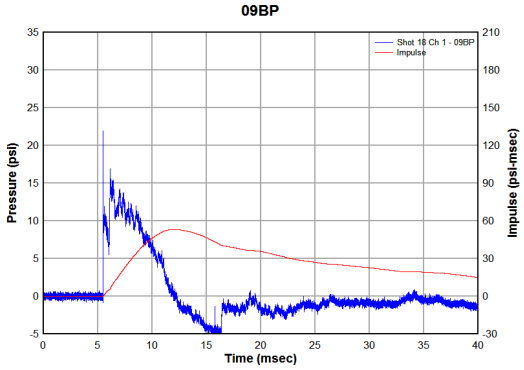

(a) Shot 18, ch1-09bp

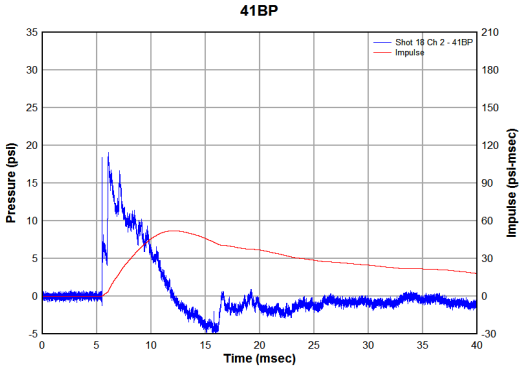

(b) Shot 18, ch2-41bp

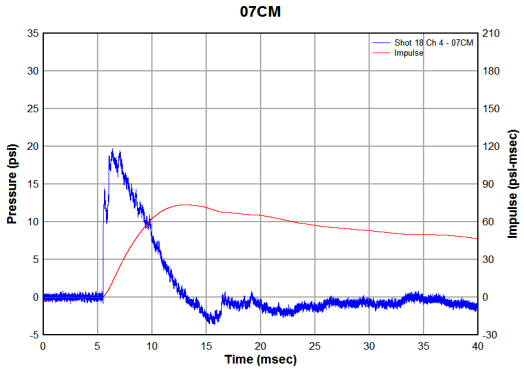

(c) Shot 18, ch4-07cm

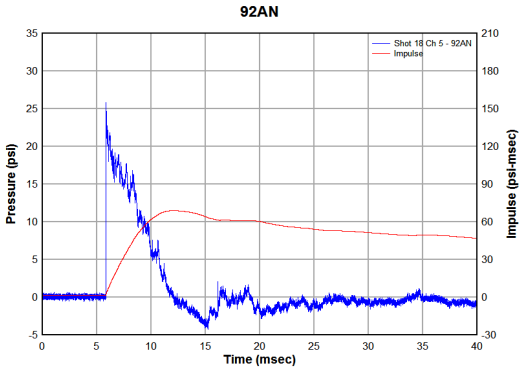

(d) Shot 18, ch5-92an

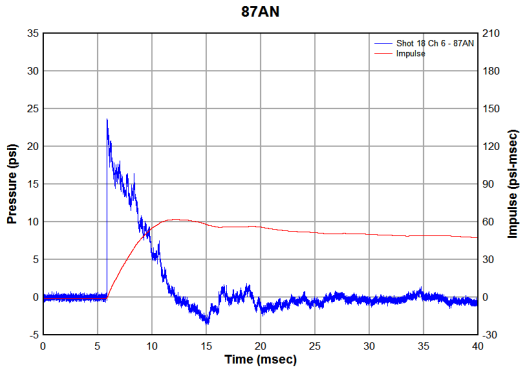

(e) Shot 18, ch6-87an

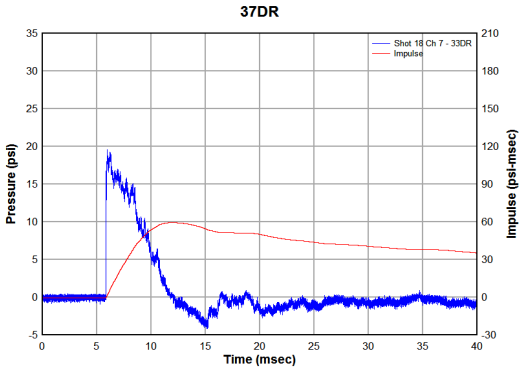

(f) Shot 18, ch7-37dr

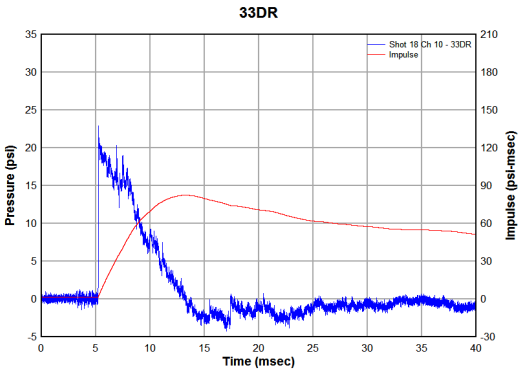

(a) Shot 18, ch10-33dr

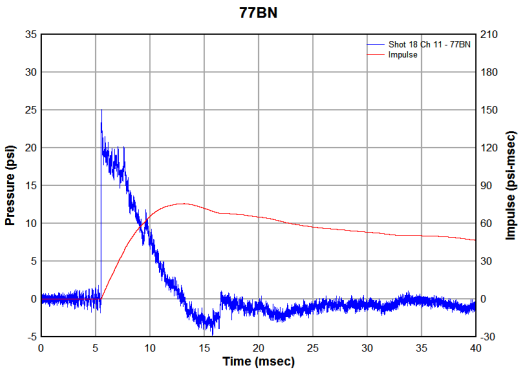

(b) Shot 18, ch11-77bn

SHOT 19 - 1/2-INCH PEAKED PLATE - 0.025-INCH DIAPHRAGM

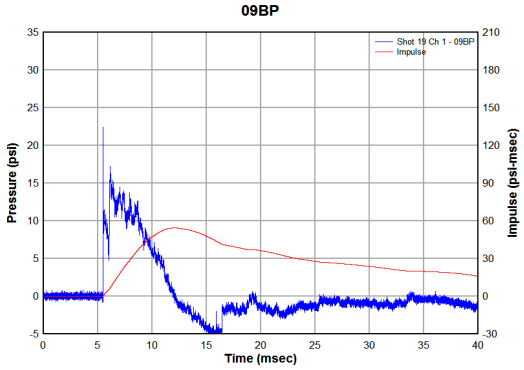

(a) Shot 19, ch1-09bp

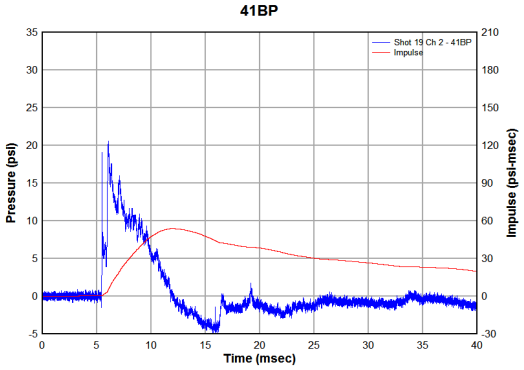

(b) Shot 19, ch2-41bp

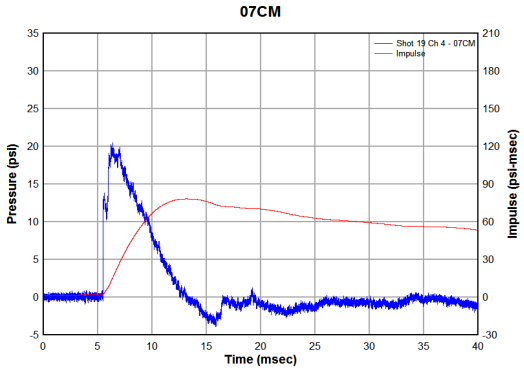

(c) Shot 19, ch4-07cm

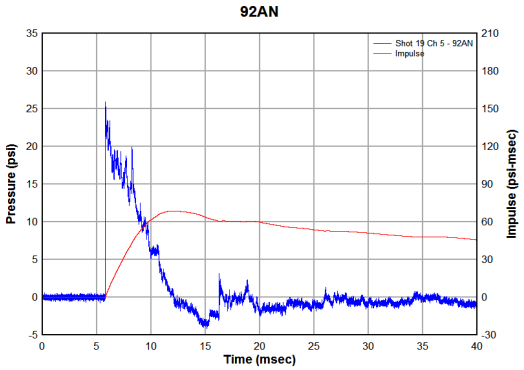

(d) Shot 19, ch5-92an

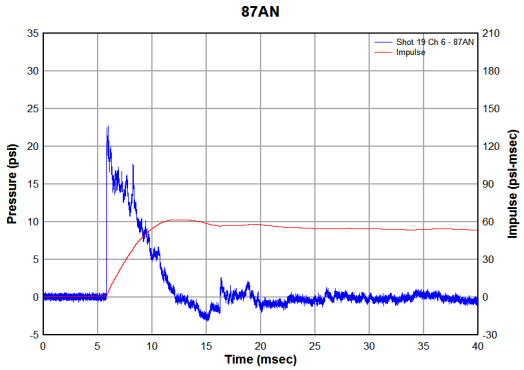

(e) Shot 19, ch6-87an

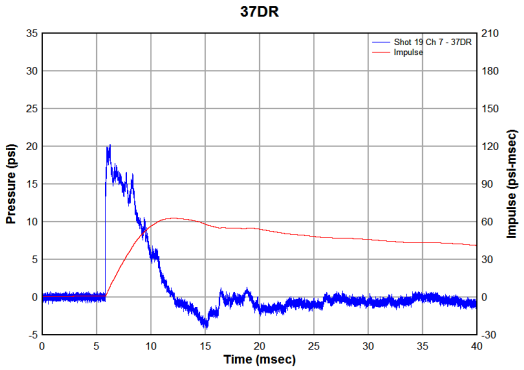

(f) Shot 19, ch7-37dr

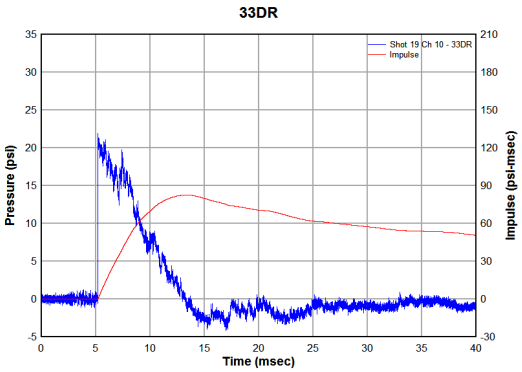

(a) Shot 19, ch10-33dr

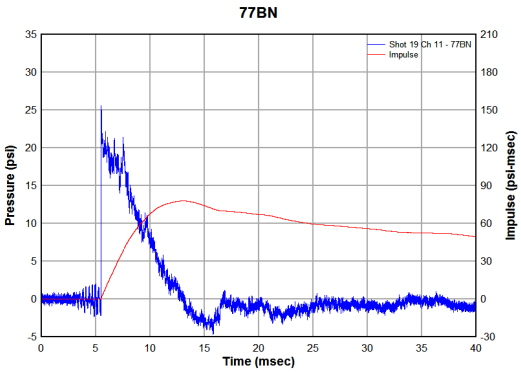

(b) Shot 19, ch11-77bn

SHOT 20 - 1/2-INCH PEAKED PLATE - 0.025-INCH DIAPHRAGM

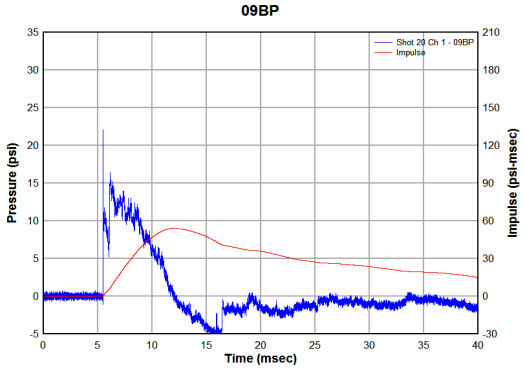

(a) Shot 20, ch1-09bp

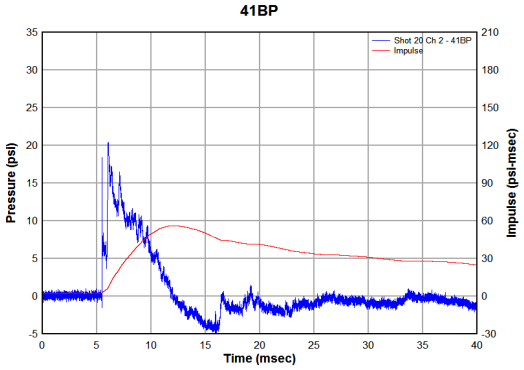

(b) Shot 20, ch2-41bp

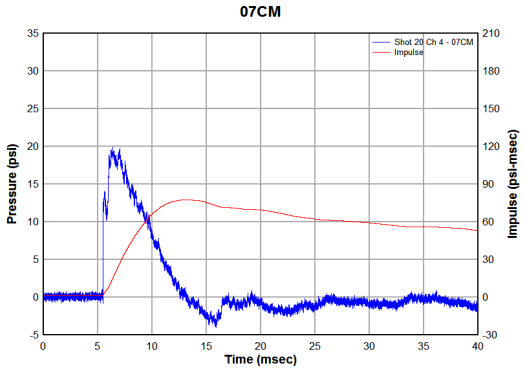

(c) Shot 20, ch4-07cm

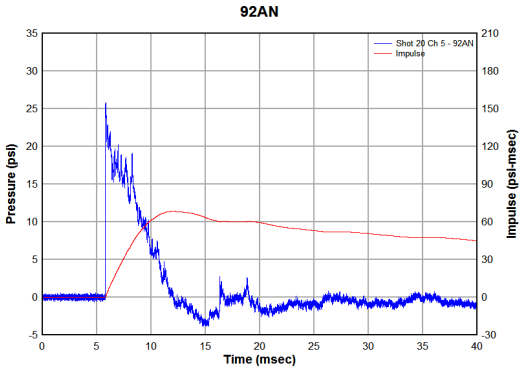

(d) Shot 20, ch5-92an

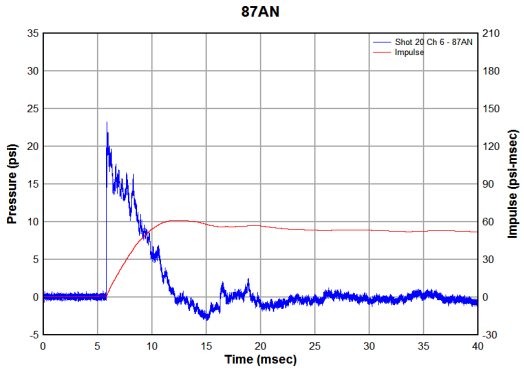

(e) Shot 20, ch6-87an

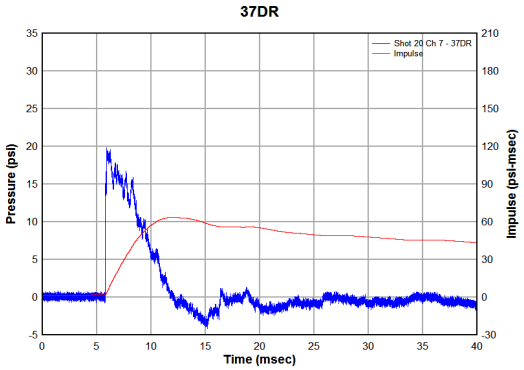

(f) Shot 20, ch7-37dr

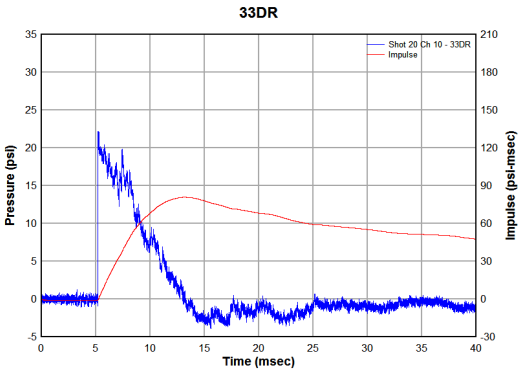

(a) Shot 20, ch10-33dr

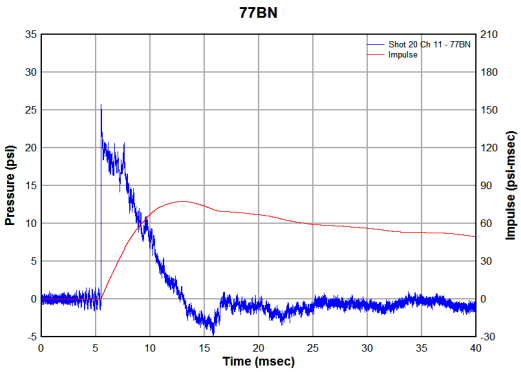

(b) Shot 20, ch11-77bn

SHOT 21 - 1/2-INCH PEAKED PLATE - 0.025-INCH DIAPHRAGM

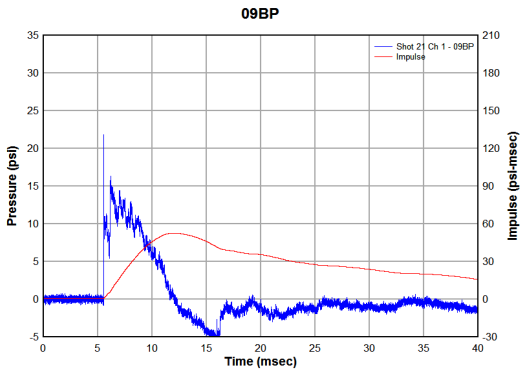

(a) Shot 21, ch1-09bp

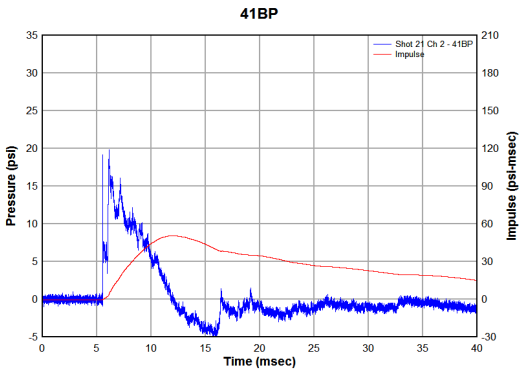

(b) Shot 21, ch2-41bp

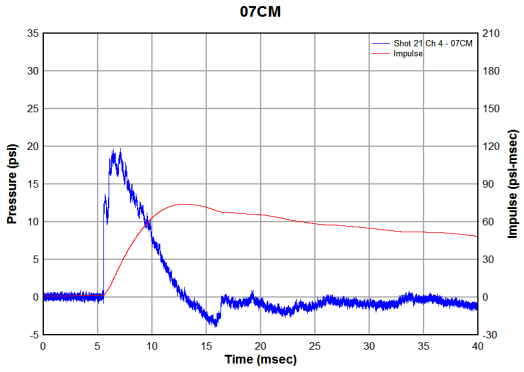

(c) Shot 21, ch4-07cm

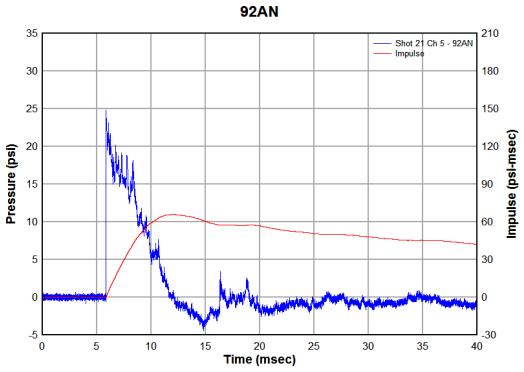

(d) Shot 21, ch5-92an

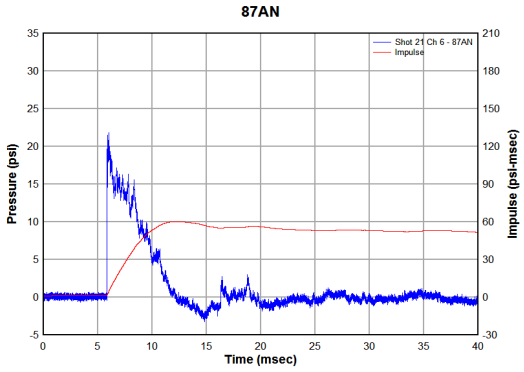

(e) Shot 21, ch6-87an

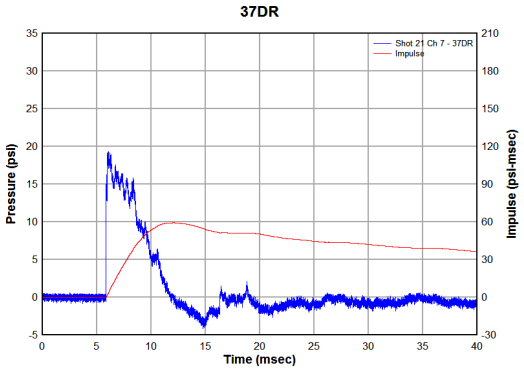

(f) Shot 21, ch7-37dr

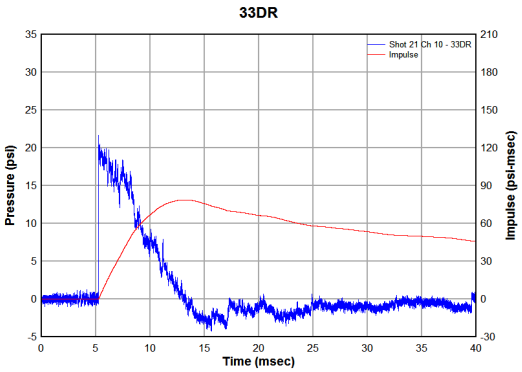

(a) Shot 21, ch10-33dr

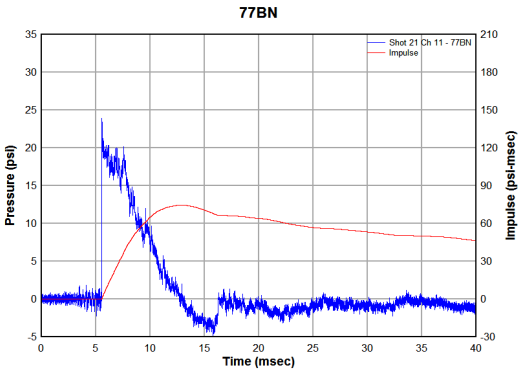

(b) Shot 21, ch11-77bn

SHOT 22 - FLAT, NO WING - 0.032" DIAPHRAGM

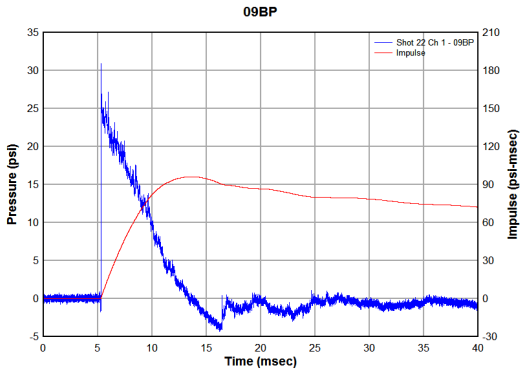

(a) Shot 22, ch1-09bp

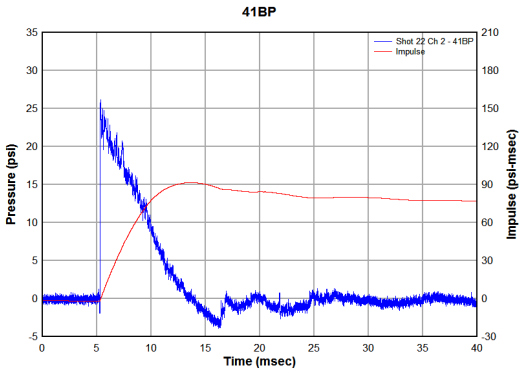

(b) Shot 22, ch2-41bp

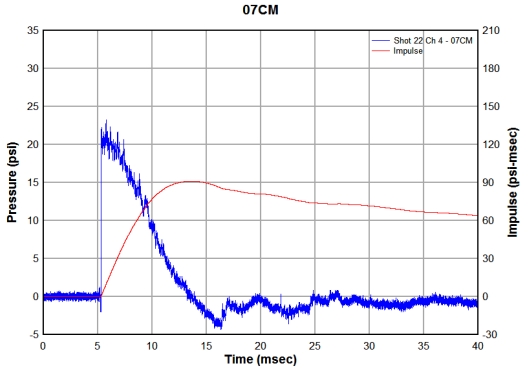

(c) Shot 22, ch4-07cm

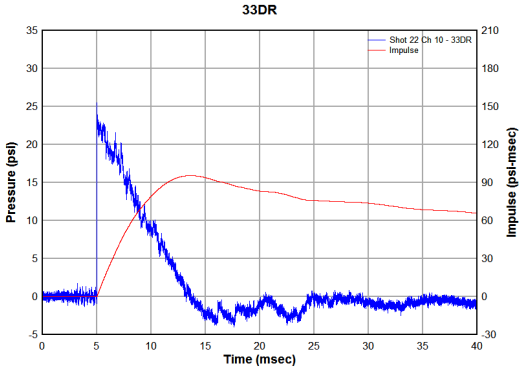

(d) Shot 22, ch10-33dr

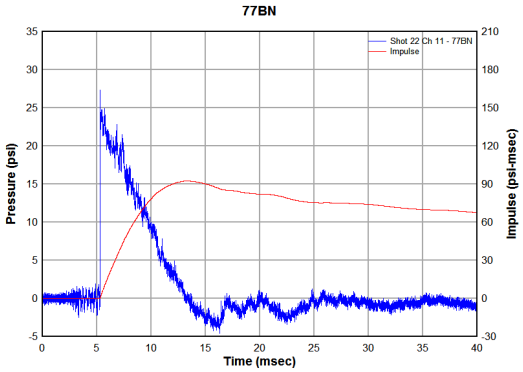

(e) Shot 22, ch11-77bn

SHOT 23 - FLAT, NO WING - 0.032" DIAPHRAGM

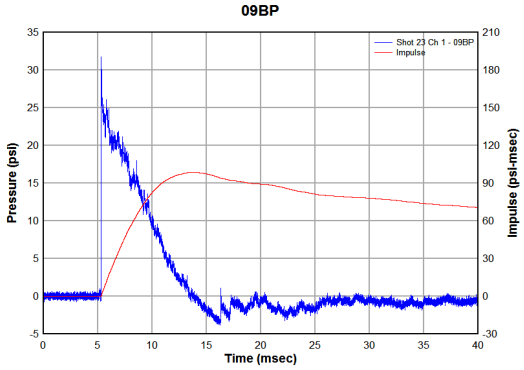

(a) Shot 23, ch1-09bp

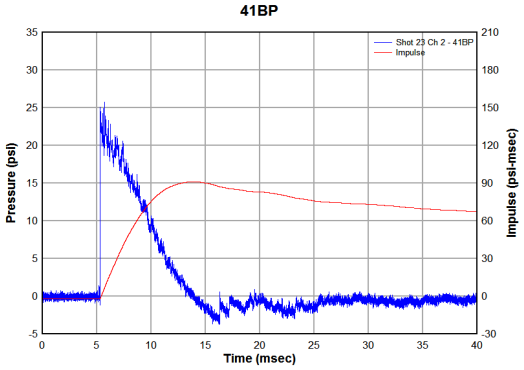

(b) Shot 23, ch2-41bp

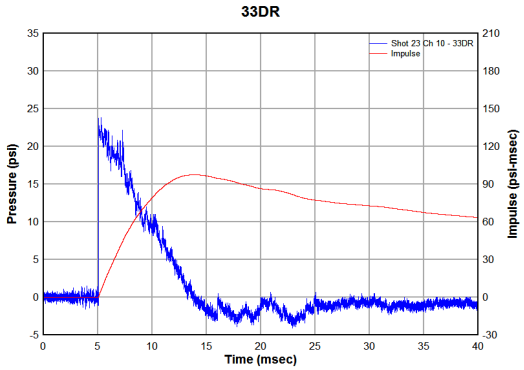

(c) Shot 23, ch10-33dr

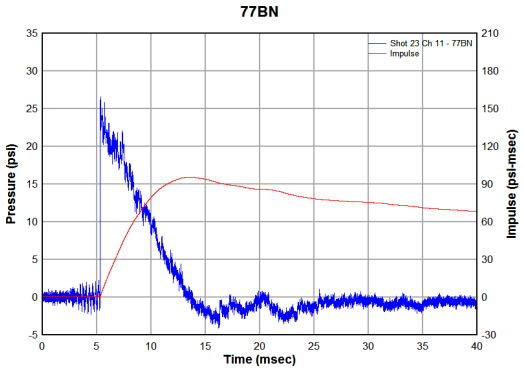

(d) Shot 23, ch11-77bn

SHOT 24 - 1/4-INCH WAVY PLATE - 0.032-INCH DIAPHRAGM

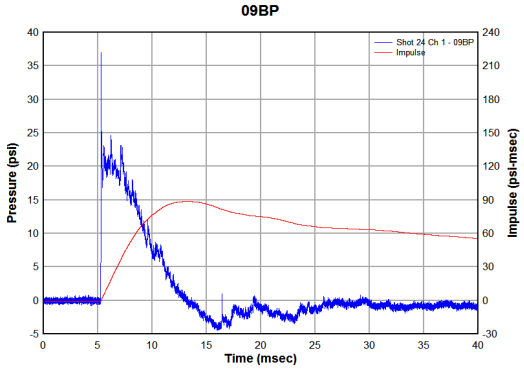

(a) Shot 24, ch1-09bp

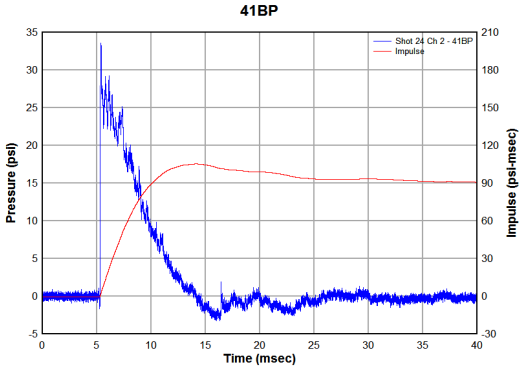

(b) Shot 24, ch2-41bp

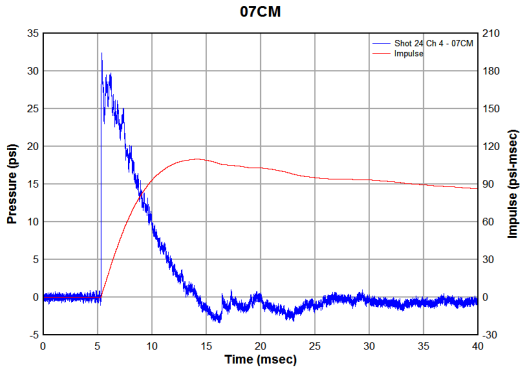

(c) Shot 24, ch4-07cm

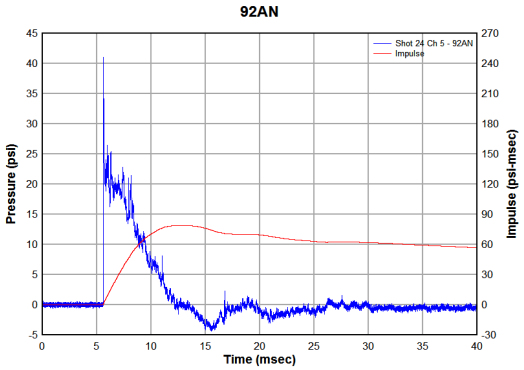

(d) Shot 24, ch5-92an

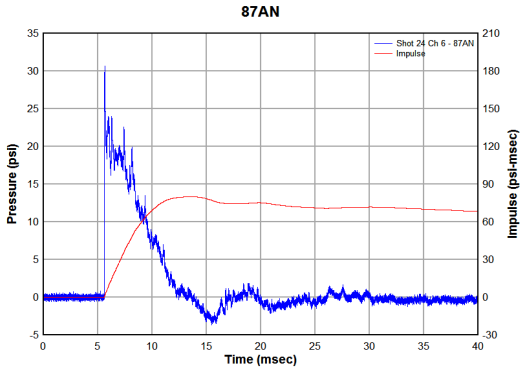

(e) Shot 24, ch6-87an

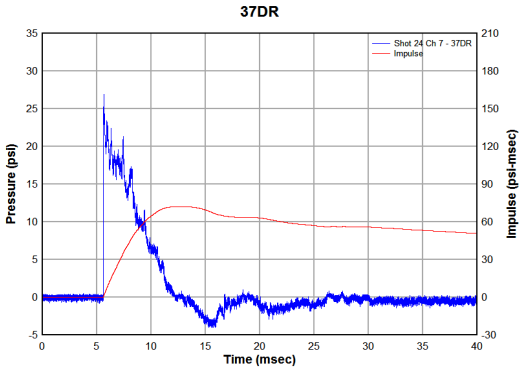

(f) Shot 24, ch7-37dr

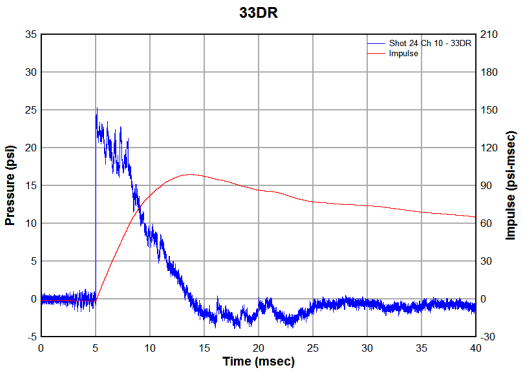

(a) Shot 24, ch10-33dr

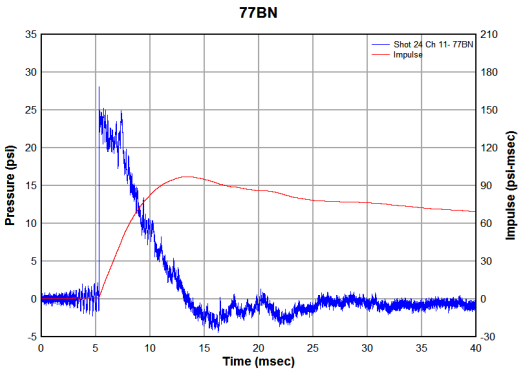

(b) Shot 24, ch11-77bn

SHOT 25 - 1/4-INCH WAVY PLATE - 0.032-INCH DIAPHRAGM

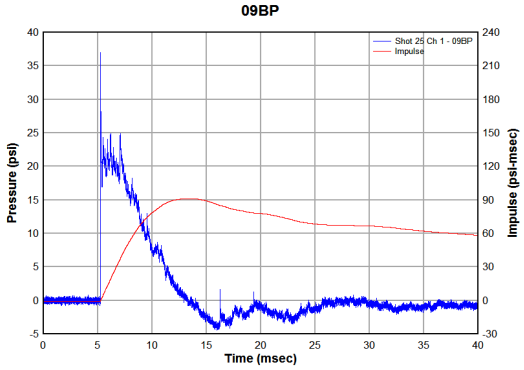

(a) Shot 25, ch1-09bp

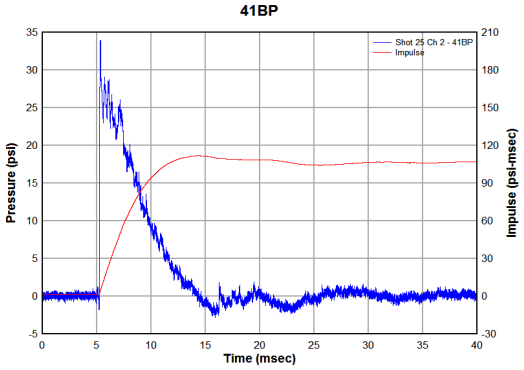

(b) Shot 25, ch2-41bp

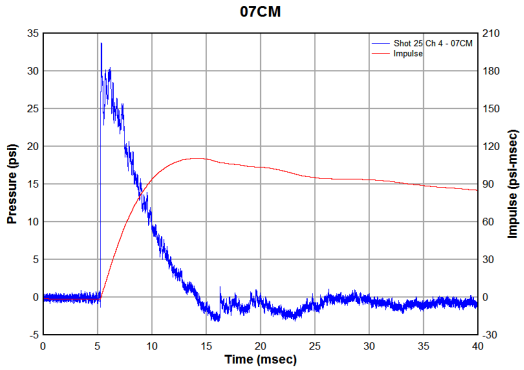

(c) Shot 25, ch4-07cm

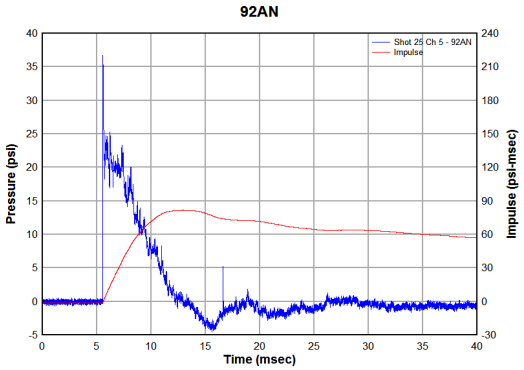

(d) Shot 25, ch5-92an

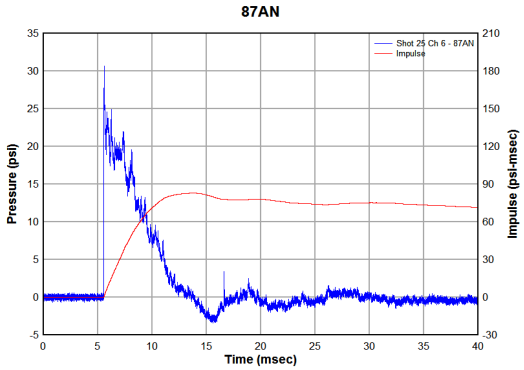

(e) Shot 25, ch6-87an

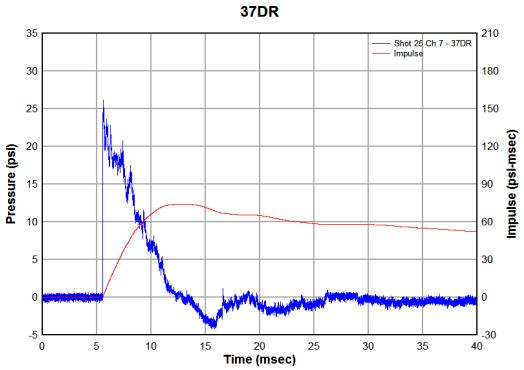

(f) Shot 25, ch7-37dr

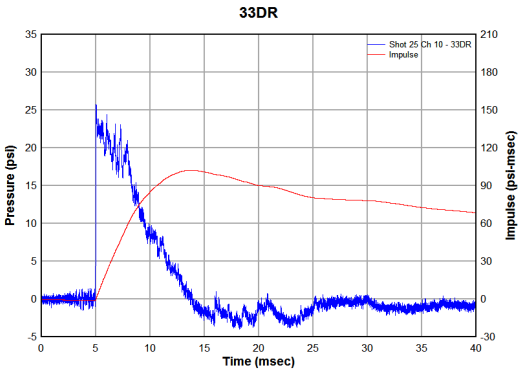

(a) Shot 25, ch10-33dr

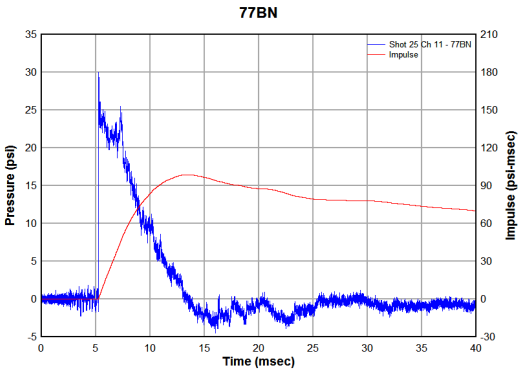

(b) Shot 25, ch11-77bn

SHOT 26 - 1/4-INCH WAVY PLATE - 0.032-INCH DIAPHRAGM

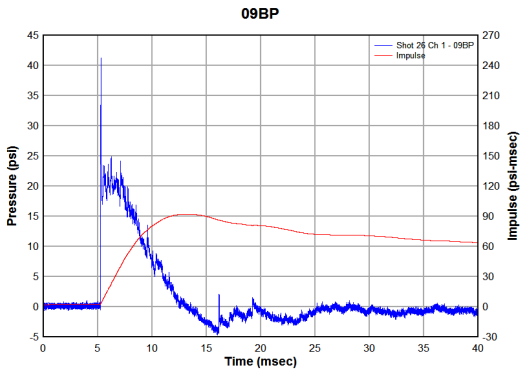

(a) Shot 26, ch1-09bp

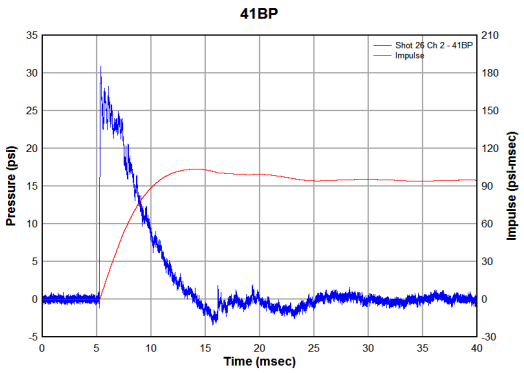

(b) Shot 26, ch2-41bp

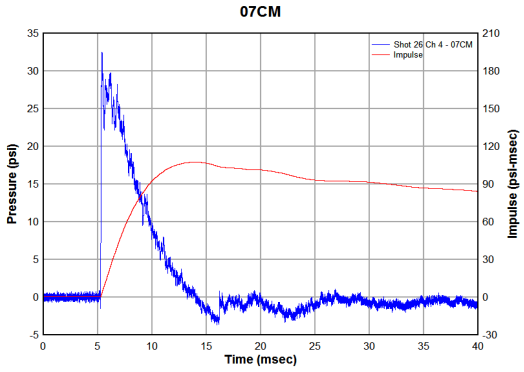

(c) Shot 26, ch4-07cm

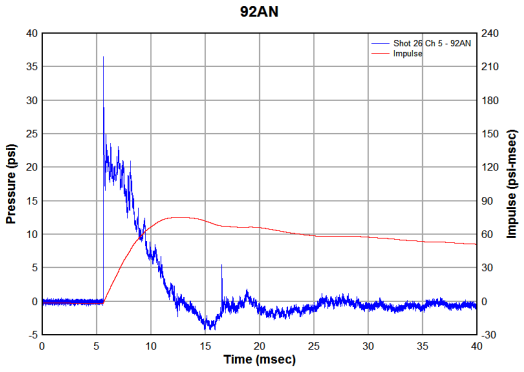

(d) Shot 26, ch5-92an

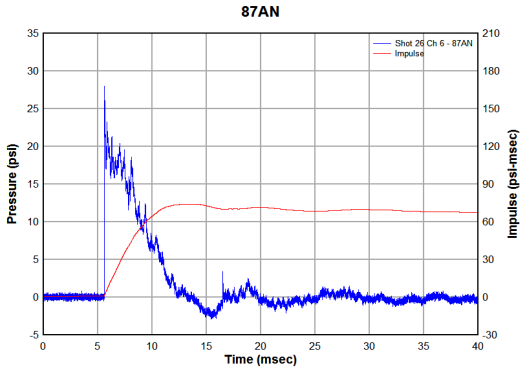

(e) Shot 26, ch6-87an

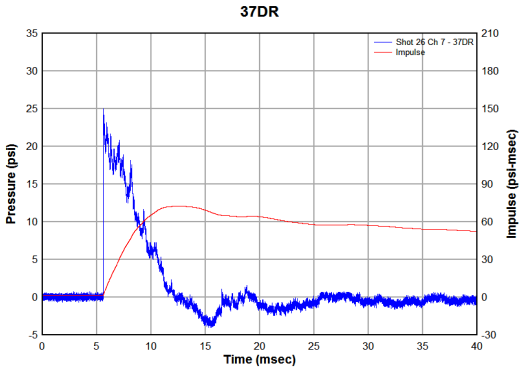

(f) Shot 26, ch7-37dr

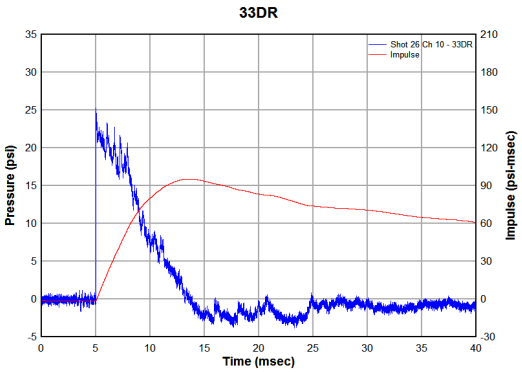

(a) Shot 26, ch10-33dr

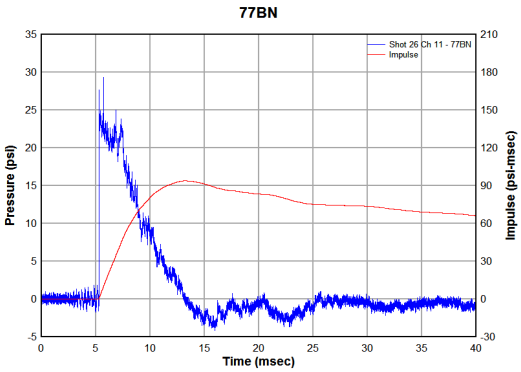

(b) Shot 26, ch11-77bn

SHOT 27 - 1/4-INCH WAVY PLATE - 0.032-INCH DIAPHRAGM

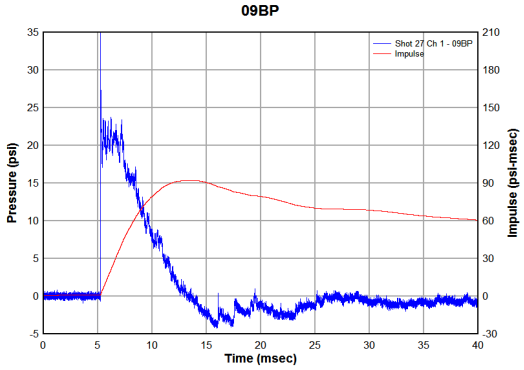

(a) Shot 27, ch1-09bp

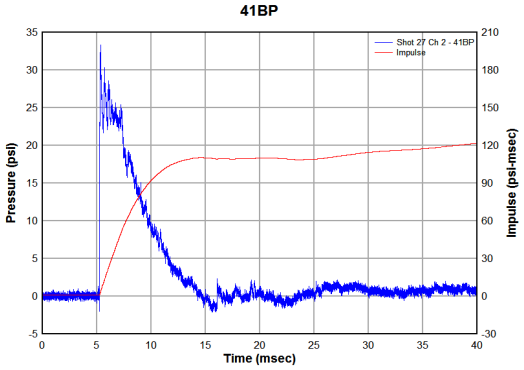

(b) Shot 27, ch2-41bp

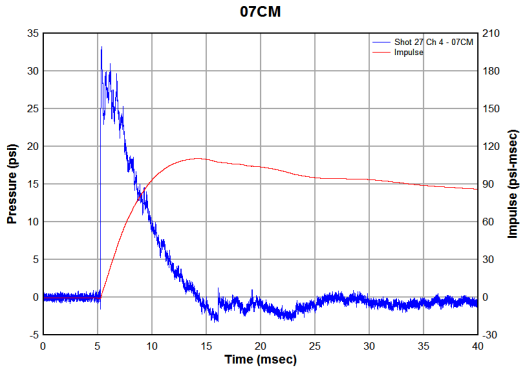

(c) Shot 27, ch4-07cm

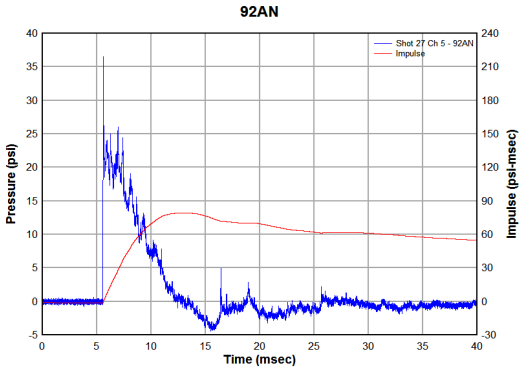

(d) Shot 27, ch5-92an

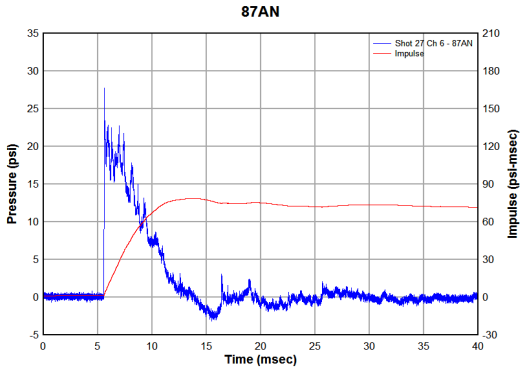

(e) Shot 27, ch6-87an

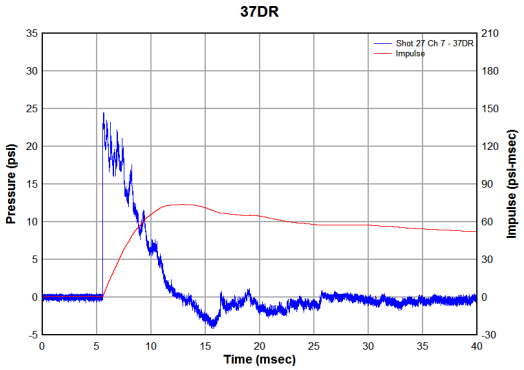

(f) Shot 27, ch7-37dr

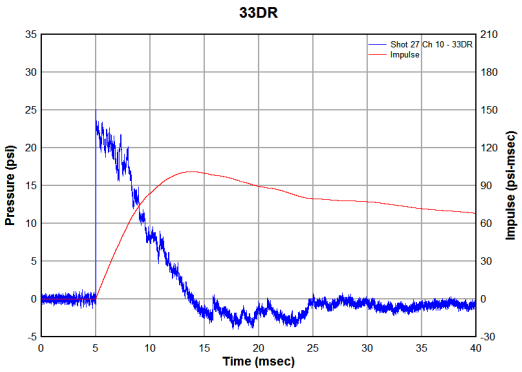

(a) Shot 27, ch10-33dr

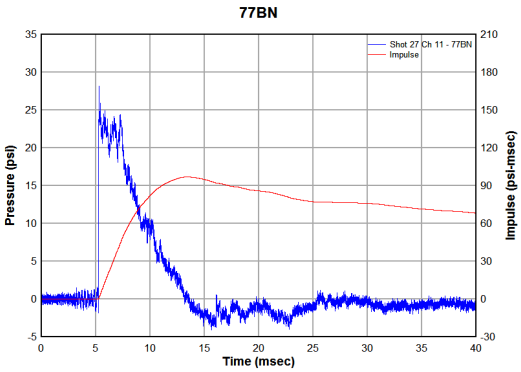

(b) Shot 27, ch11-77bn

SHOT 28 - 1/4-INCH WAVY PLATE - 0.025-INCH DIAPHRAGM

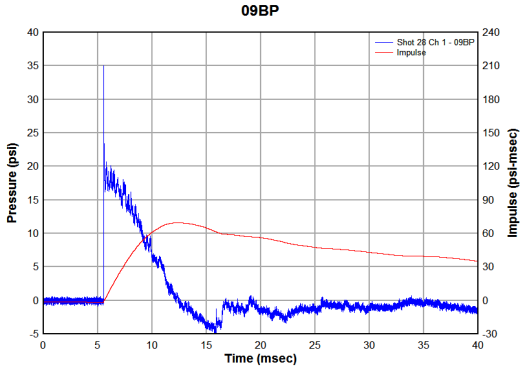

(a) Shot 28, ch1-09bp

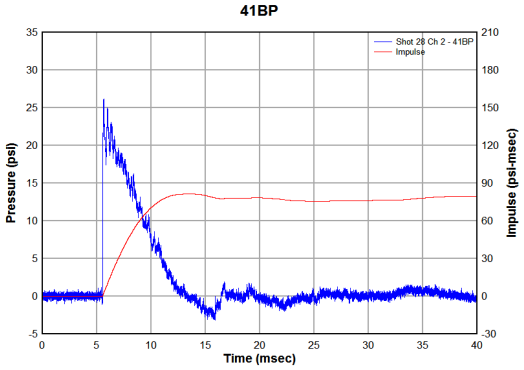

(b) Shot 28, ch2-41bp

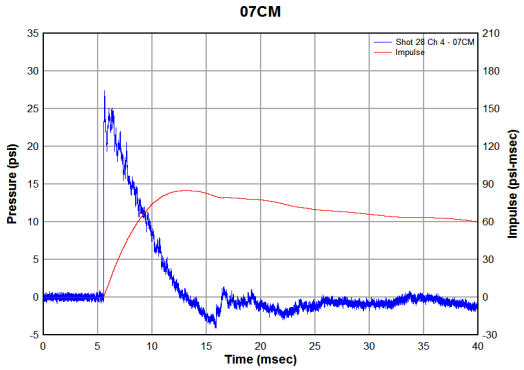

(c) Shot 28, ch4-07cm

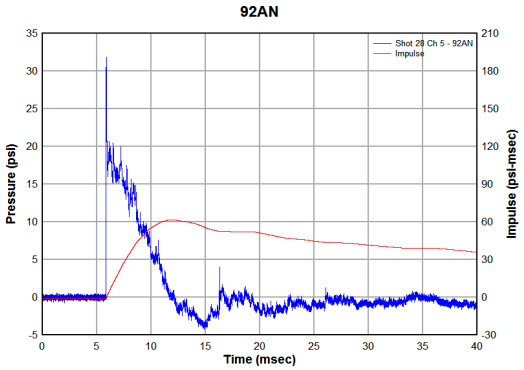

(d) Shot 28, ch5-92an

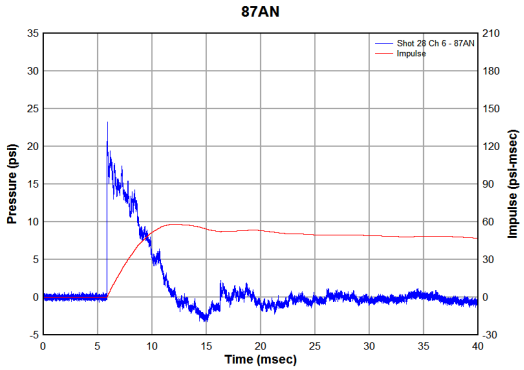

(e) Shot 28, ch6-87an

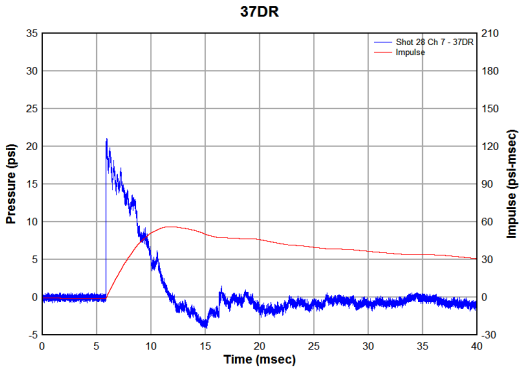

(f) Shot 28, ch7-37dr

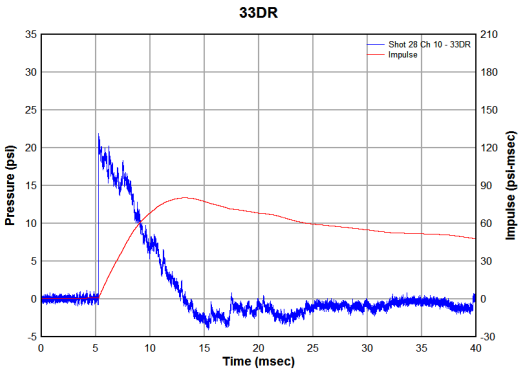

(a) Shot 28, ch10-33dr

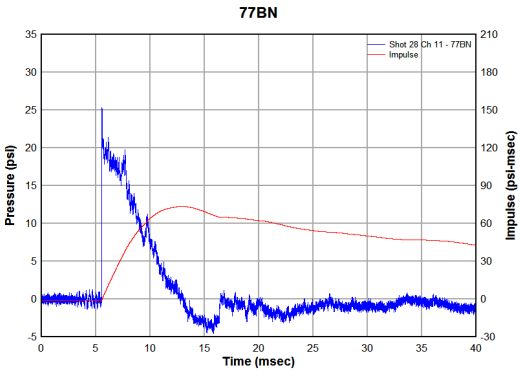

(b) Shot 28, ch11-77bn

SHOT 29 - 1/4-INCH WAVY PLATE - 0.025-INCH DIAPHRAGM

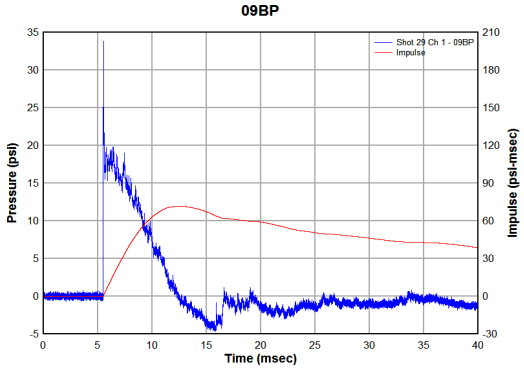

(a) Shot 29, ch1-09bp

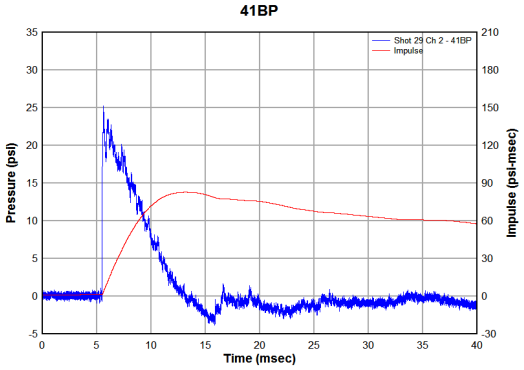

(b) Shot 29, ch2-41bp

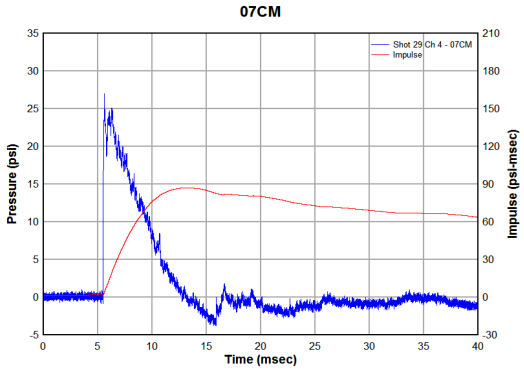

(c) Shot 29, ch4-07cm

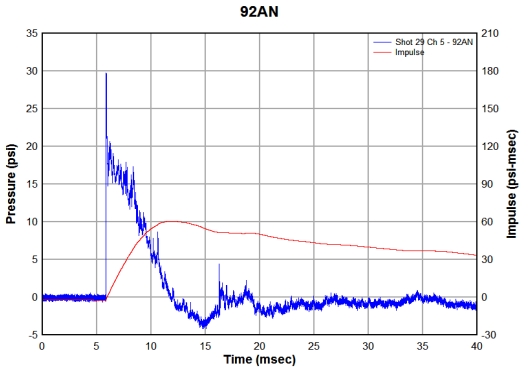

(d) Shot 29, ch5-92an

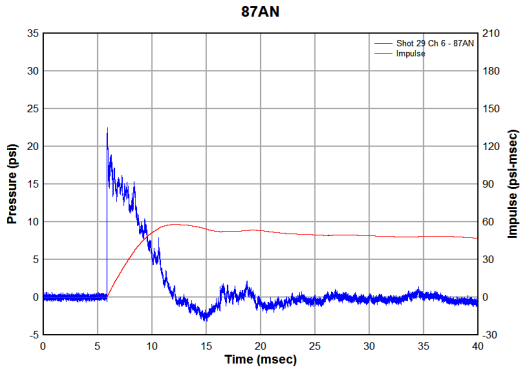

(e) Shot 29, ch6-87an

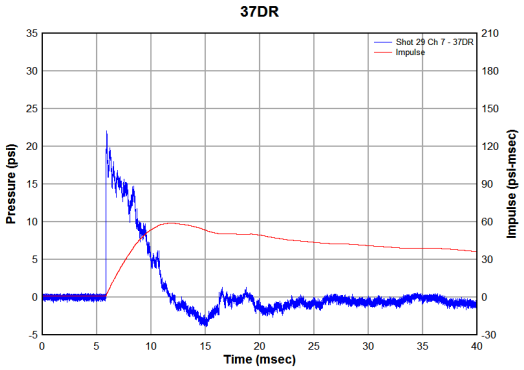

(f) Shot 29, ch7-37dr

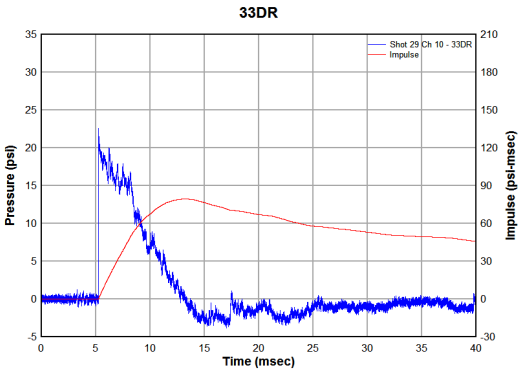

(a) Shot 29, ch10-33dr

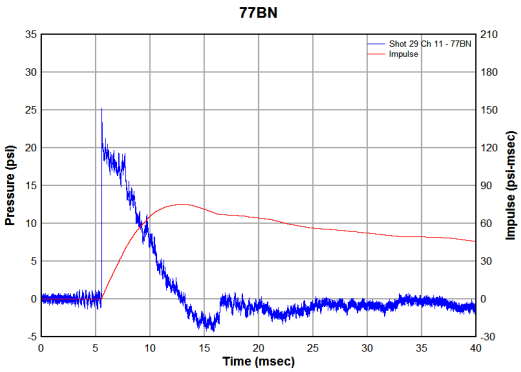

(b) Shot 29, ch11-77bn

SHOT 30 - 1/4-INCH WAVY PLATE - 0.025-INCH DIAPHRAGM

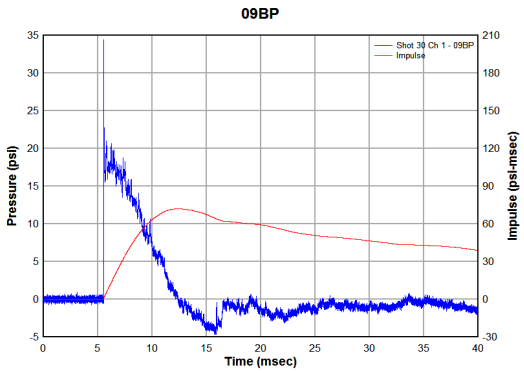

(a) Shot 30, ch1-09bp

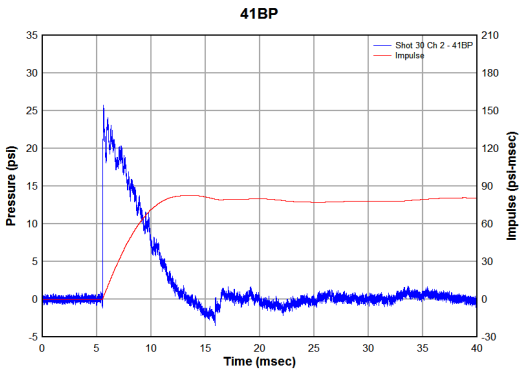

(b) Shot 30, ch2-41bp

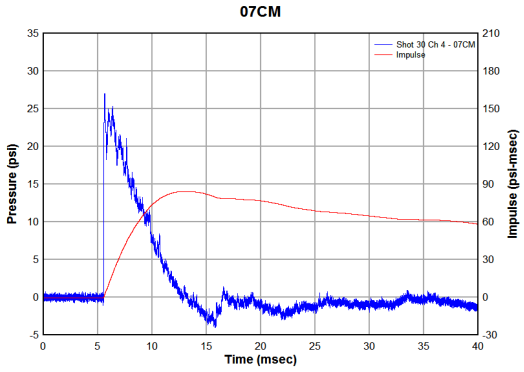

(c) Shot 30, ch4-07cm

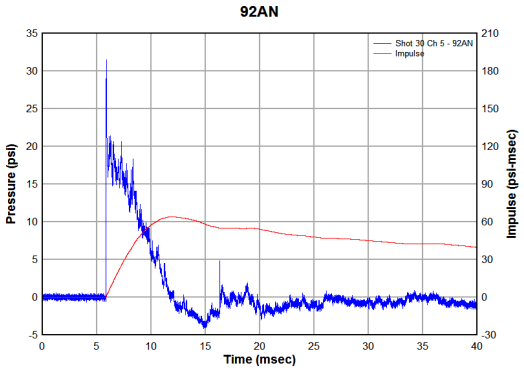

(d) Shot 30, ch5-92an

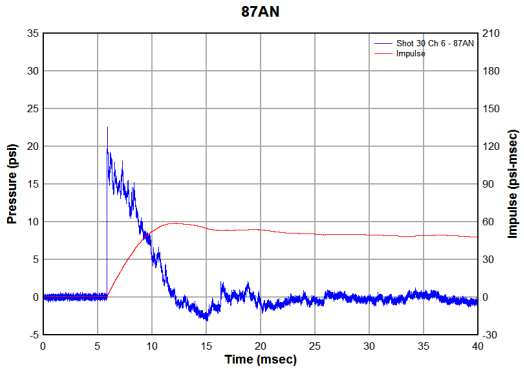

(e) Shot 30, ch6-87an

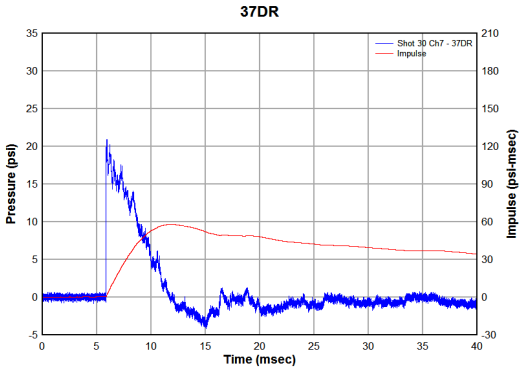

(f) Shot 30, ch7-37dr

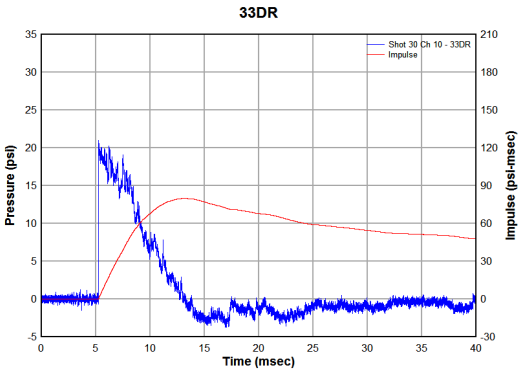

(a) Shot 30, ch10-33dr

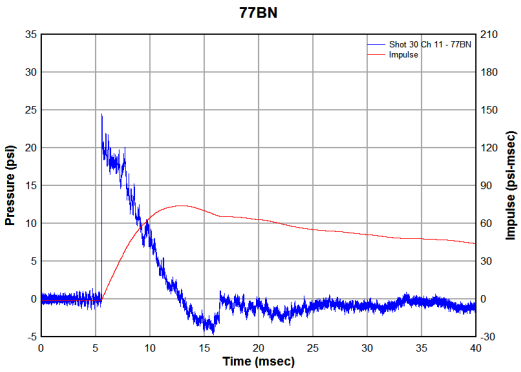

(b) Shot 30, ch11-77bn

SHOT 31 - 1/4-INCH WAVY PLATE - 0.025-INCH DIAPHRAGM

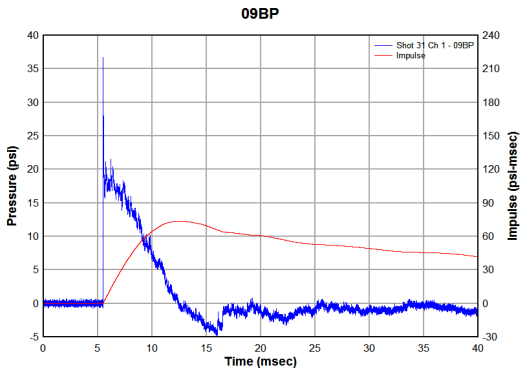

(a) Shot 31, ch1-09bp

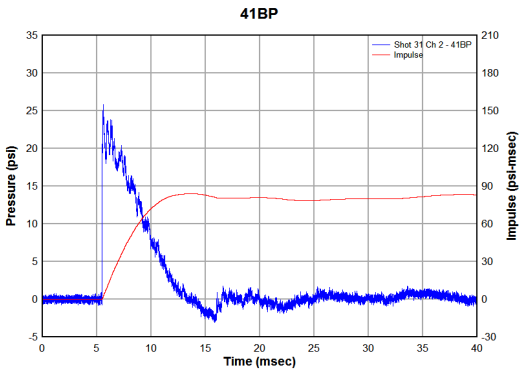

(b) Shot 31, ch2-41bp

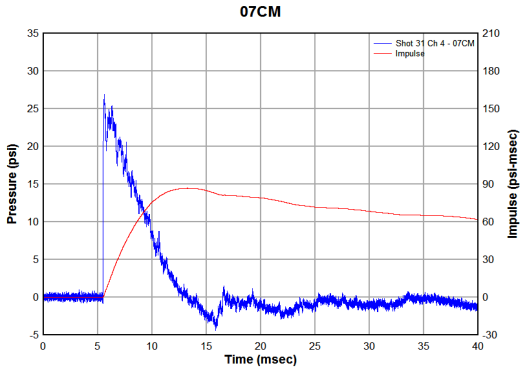

(c) Shot 31, ch4-07cm

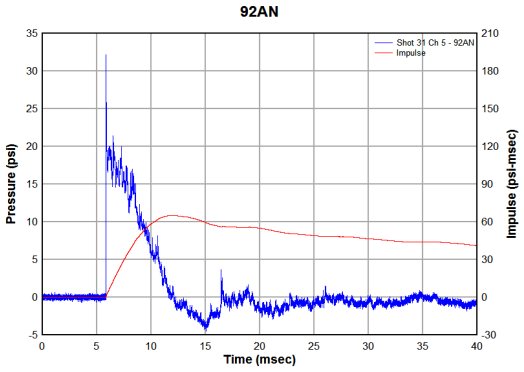

(d) Shot 31, ch5-92an

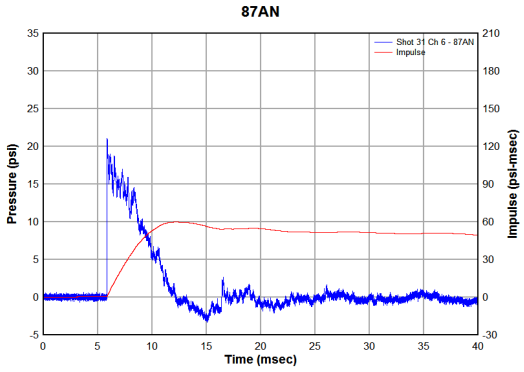

(e) Shot 31, ch6-87an

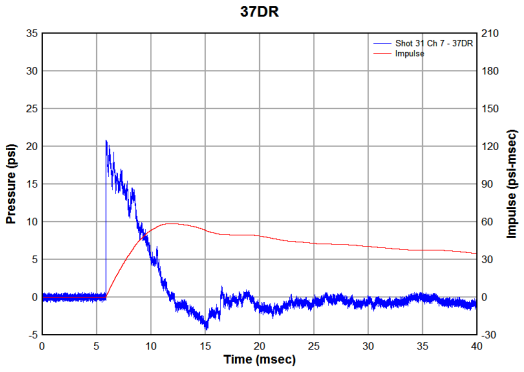

(f) Shot 31, ch7-37dr

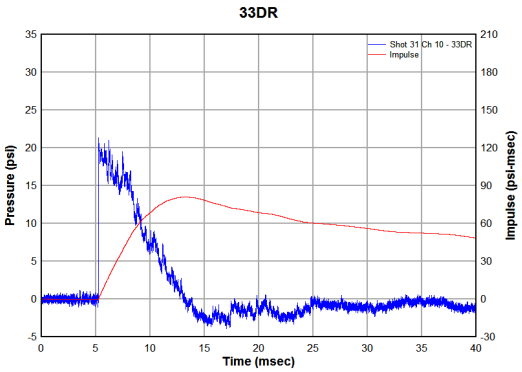

(a) Shot 31, ch10-33dr

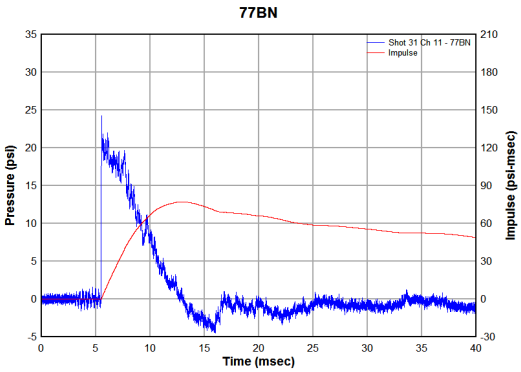

(b) Shot 31, ch11-77bn

SHOT 32 - FLAT PLATE, PRLI - 0.032-INCH DIAPHRAGM

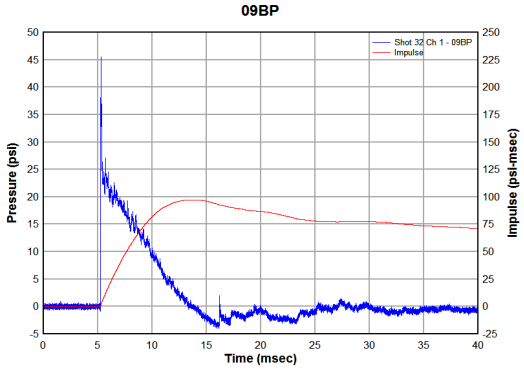

(a) Shot 32, ch1-09bp

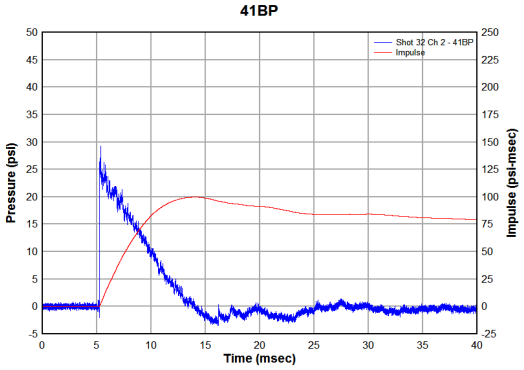

(b) Shot 32, ch2-41bp

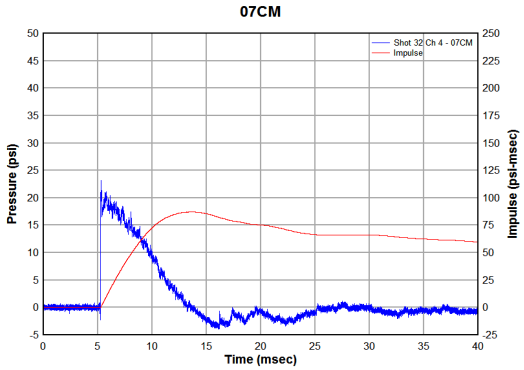

(c) Shot 32, ch4-07cm

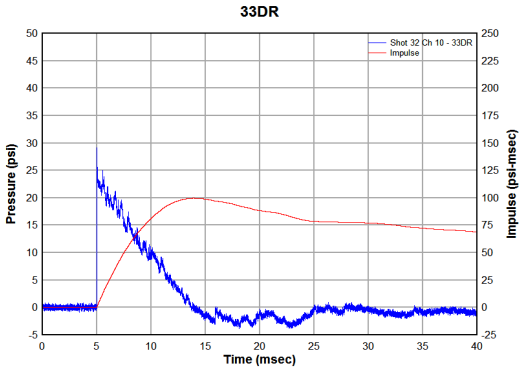

(d) Shot 32, ch10-33dr

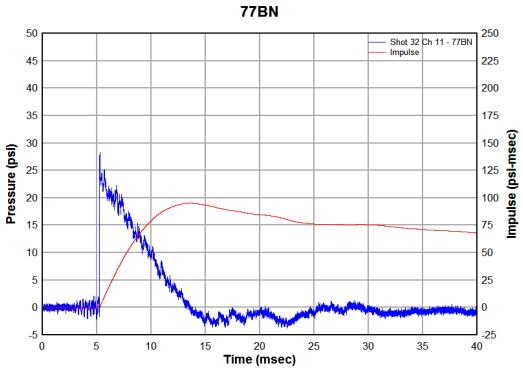

(e) Shot 32, ch11-77bn

SHOT 33 - FLAT PLATE, PRLI - 0.032-INCH DIAPHRAGM

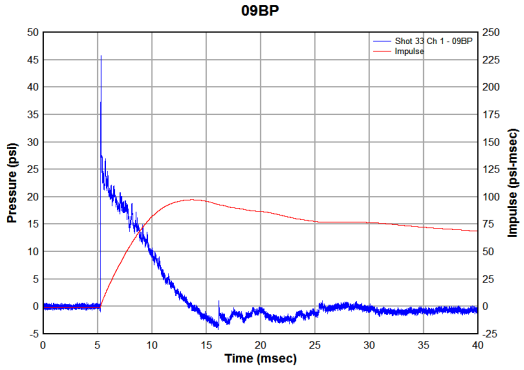

(a) Shot 33, ch1-09bp

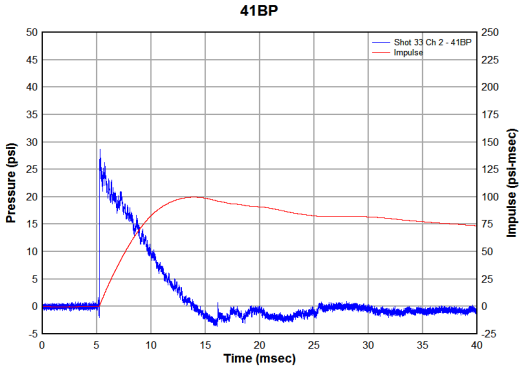

(b) Shot 33, ch2-41bp

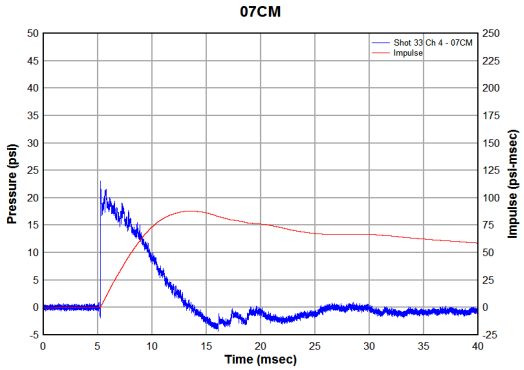

(c) Shot 33, ch4-07cm

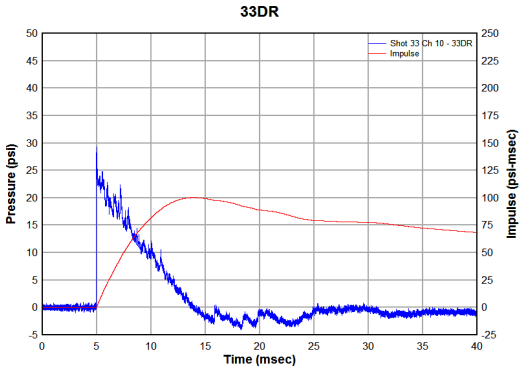

(d) Shot 33, ch10-33dr

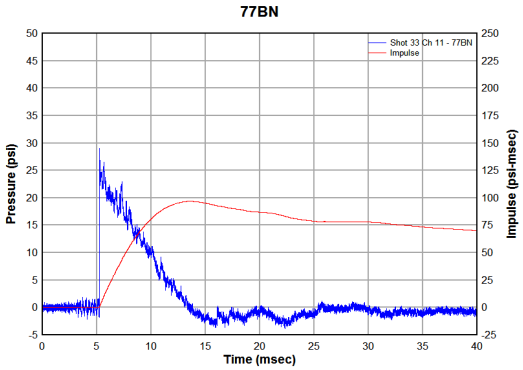

(e) Shot 33, ch11-77bn

SHOT 34 - FLAT PLATE, PRLI - 0.032-INCH DIAPHRAGM

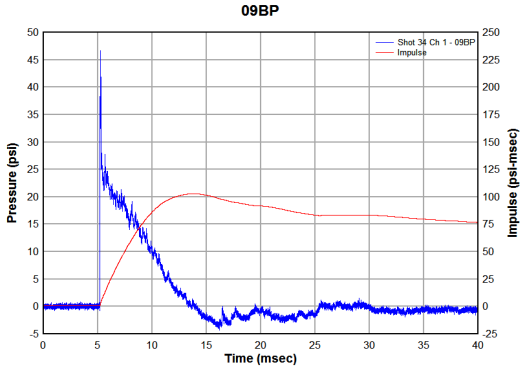

(a) Shot 34, ch1-09bp

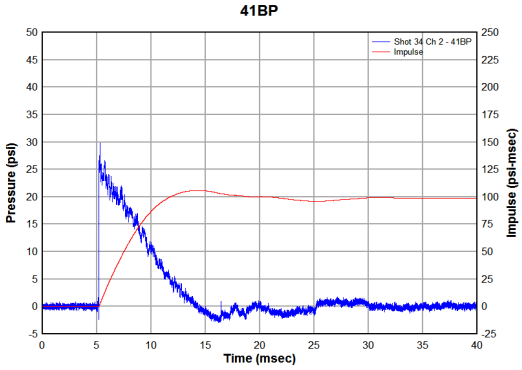

(b) Shot 34, ch2-41bp

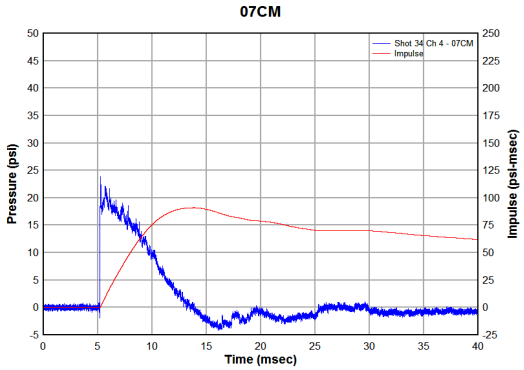

(c) Shot 34, ch4-07cm

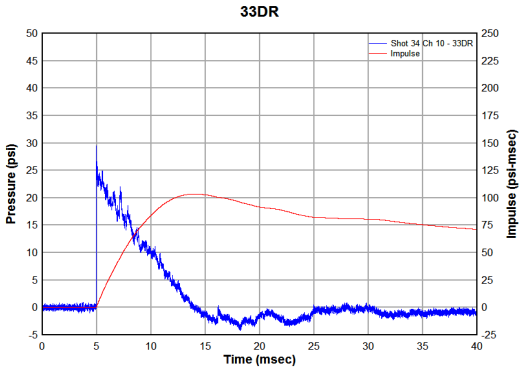

(d) Shot 34, ch10-33dr

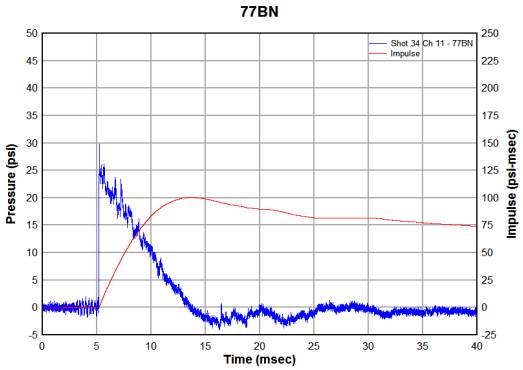

(e) Shot 34, ch11-77bn

SHOT 35 - FLAT PLATE, PRLI - 0.032-INCH DIAPHRAGM

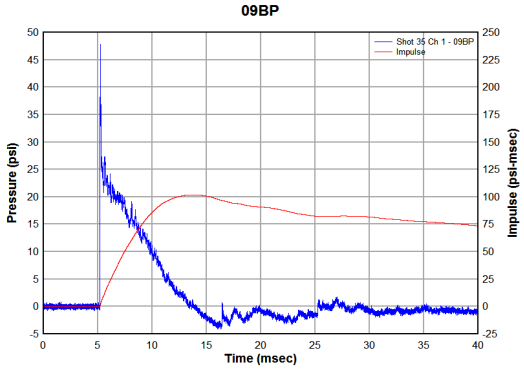

(a) Shot 35, ch1-09bp

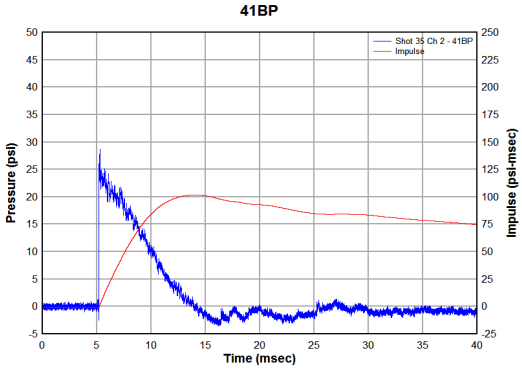

(b) Shot 35, ch2-41bp

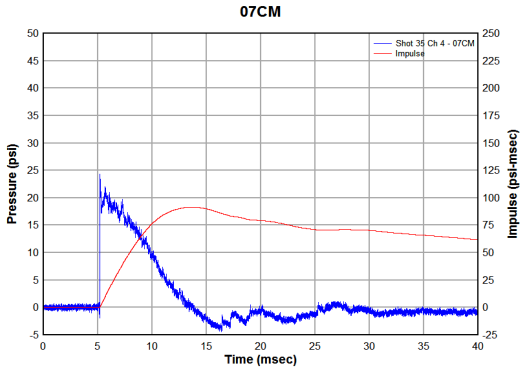

(c) Shot 35, ch4-07cm

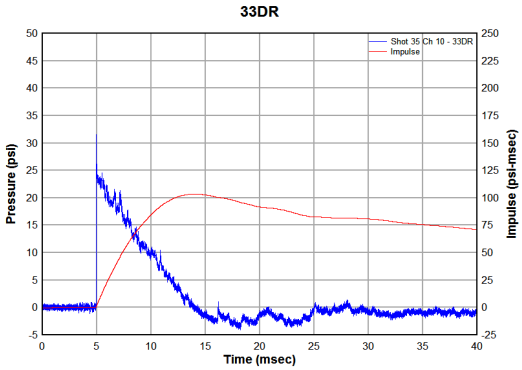

(d) Shot 35, ch10-33dr

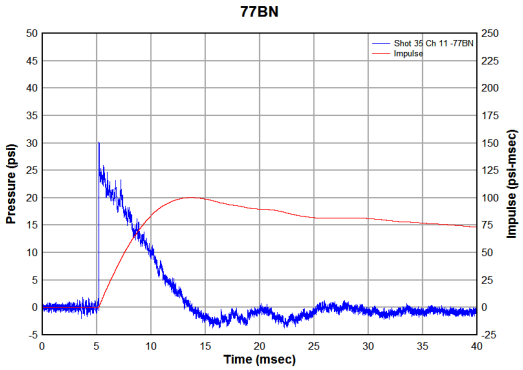

(e) Shot 35, ch11-77bn

SHOT 36 - FLAT PLATE, PRLI - 0.025-INCH DIAPHRAGM

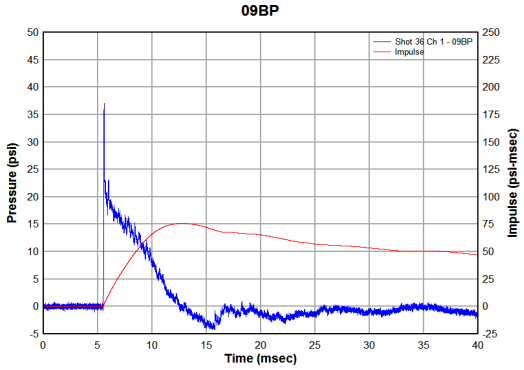

(a) Shot 36, ch1-09bp

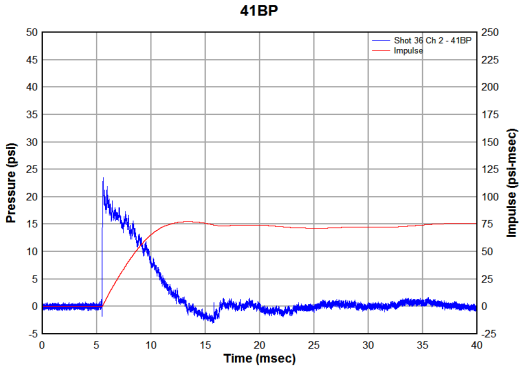

(b) Shot 36, ch2-41bp

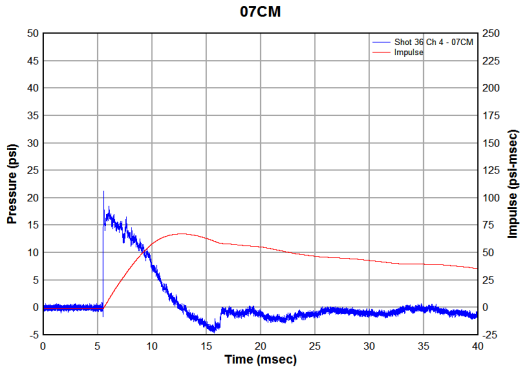

(c) Shot 36, ch4-07cm

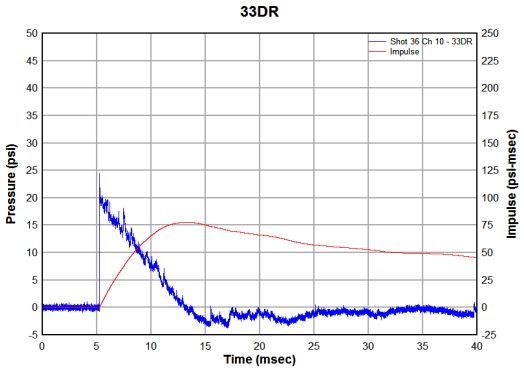

(d) Shot 36, ch10-33dr

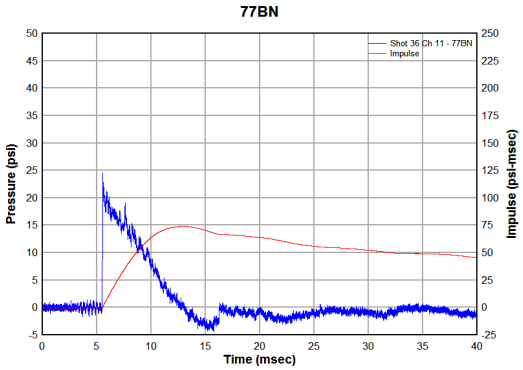

(e) Shot 36, ch11-77bn

SHOT 37 - FLAT PLATE, PRLI - 0.025-INCH DIAPHRAGM

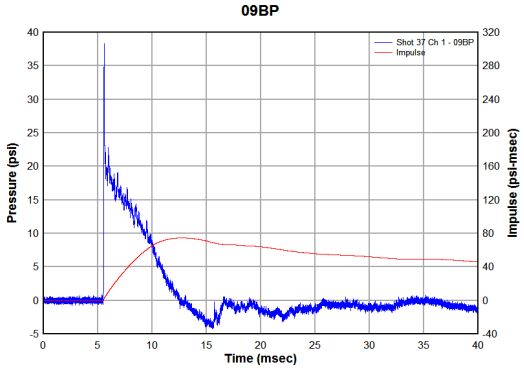

(a) Shot 37, ch1-09bp

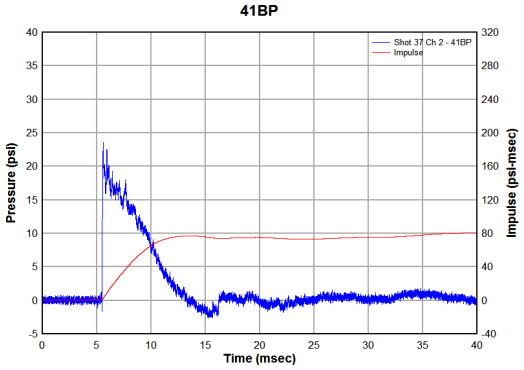

(b) Shot 37, ch2-41bp

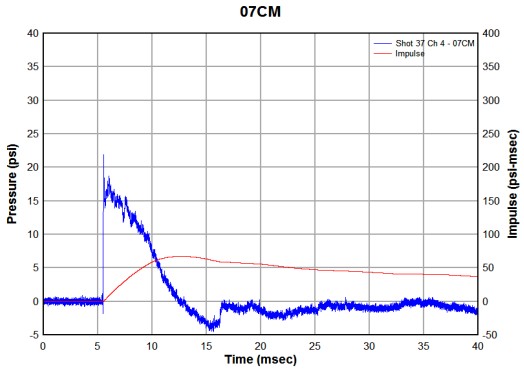

(c) Shot 37, ch4-07cm

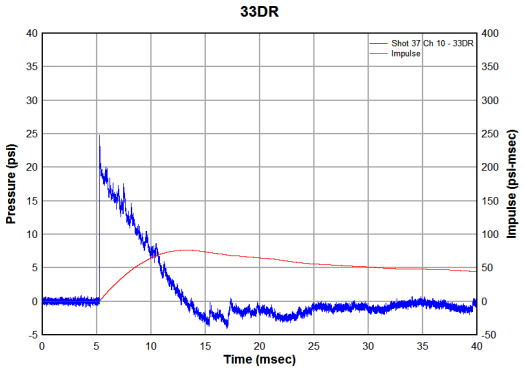

(d) Shot 37, ch10-33dr

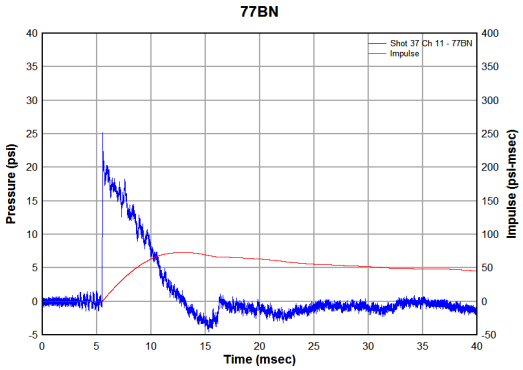

(e) Shot 37, ch11-77bn

SHOT 38 - FLAT PLATE, PRLI - 0.025-INCH DIAPHRAGM

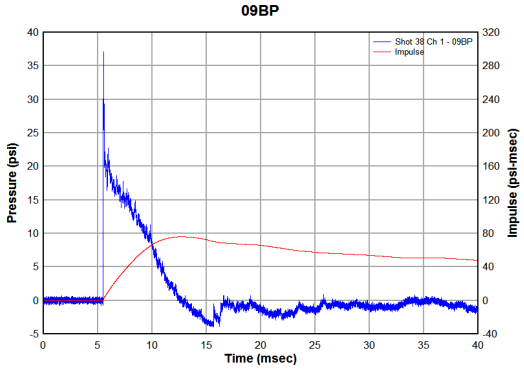

(a) Shot 38, ch1-09bp

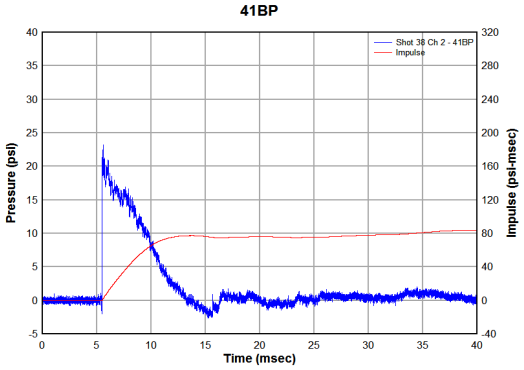

(b) Shot 38, ch2-41bp

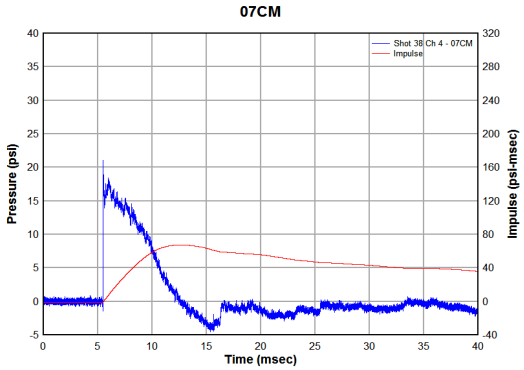

(c) Shot 38, ch4-07cm

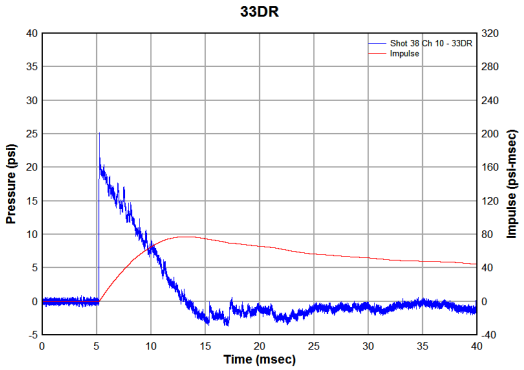

(d) Shot 38, ch10-33dr

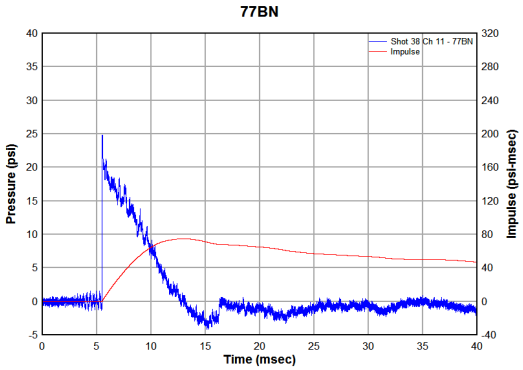

(e) Shot 38, ch11-77bn

SHOT 39 - FLAT PLATE, PRLI - 0.025-INCH DIAPHRAGM

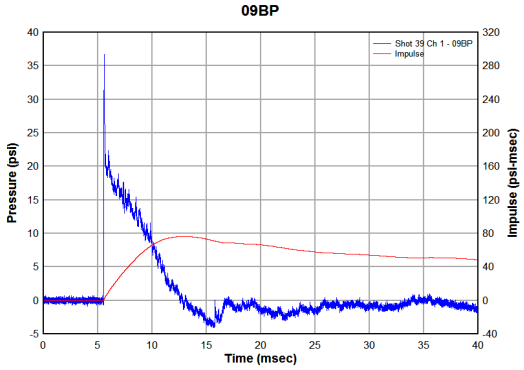

(a) Shot 39, ch1-09bp

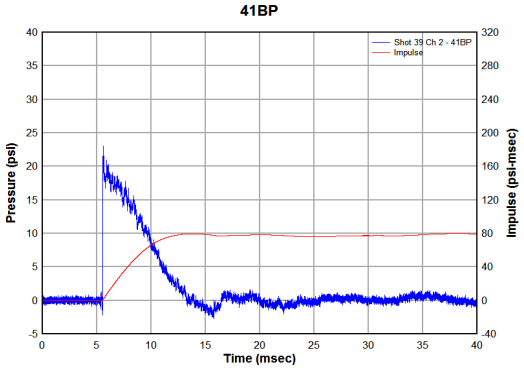

(b) Shot 39, ch2-41bp

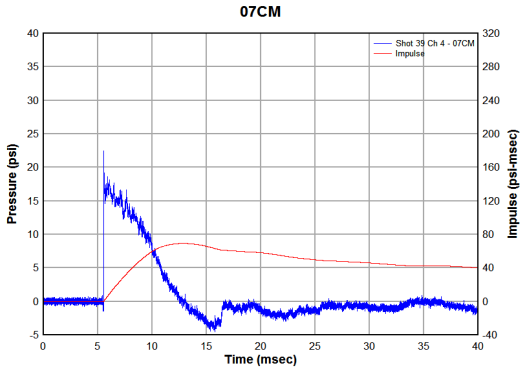

(c) Shot 39, ch4-07cm

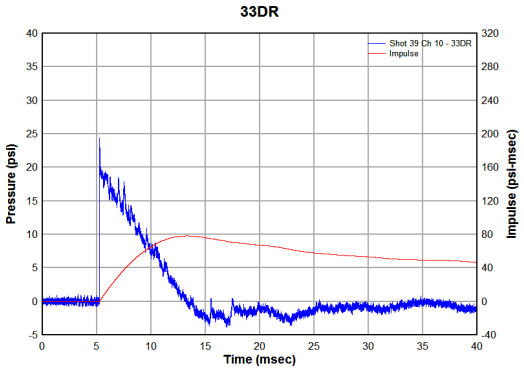

(d) Shot 39, ch10-33dr

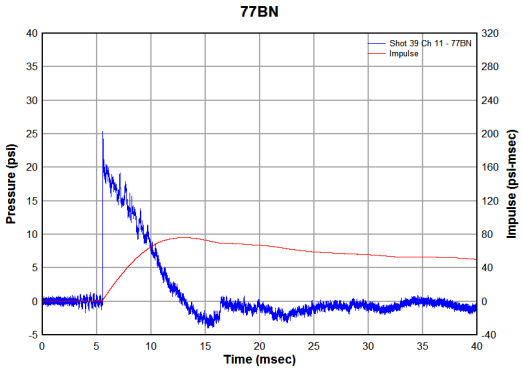

(e) Shot 39, ch11-77bn

SHOT 46 - 1-INCH PEAKED PLATE - 0.032-INCH DIAPHRAGM

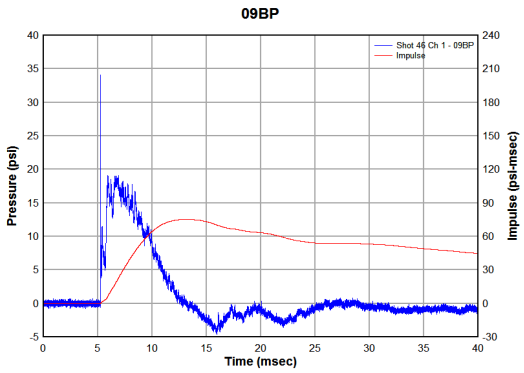

(a) Shot 46, ch1-09bp

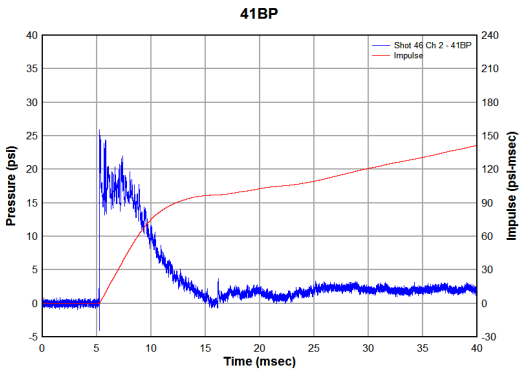

(b) Shot 46, ch2-41bp

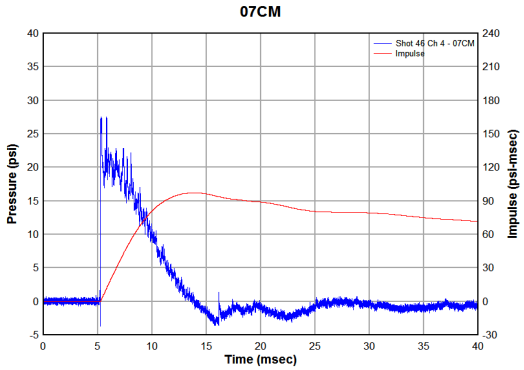

(c) Shot 46, ch4-07cm

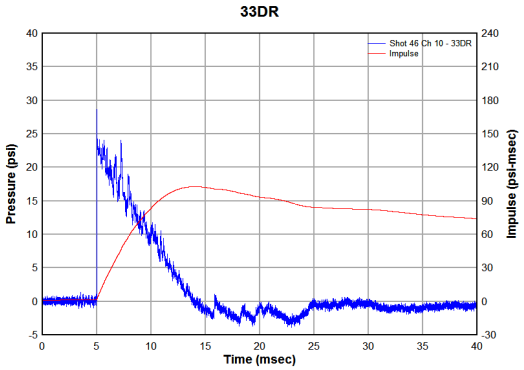

(d) Shot 46, ch10-33dr

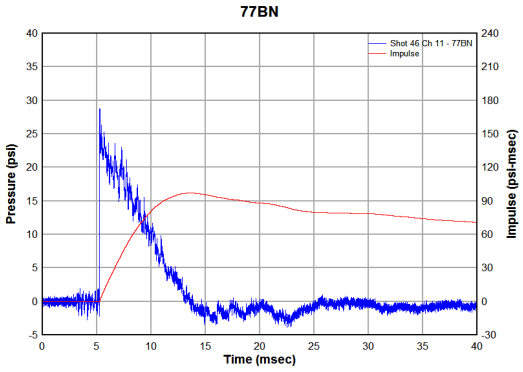

(e) Shot 46, ch11-77bn

SHOT 47 - 1-INCH PEAKED PLATE - 0.032-INCH DIAPHRAGM

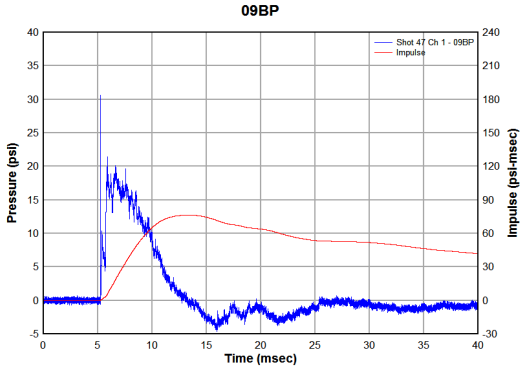

(a) Shot 47, ch1-09bp

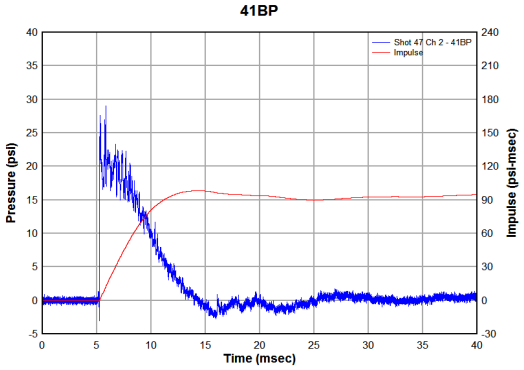

(b) Shot 47, ch2-41bp

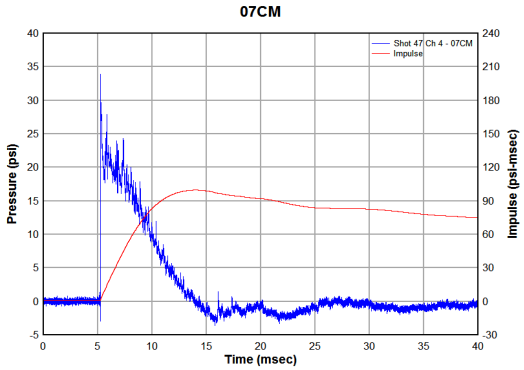

(c) Shot 47, ch4-07cm

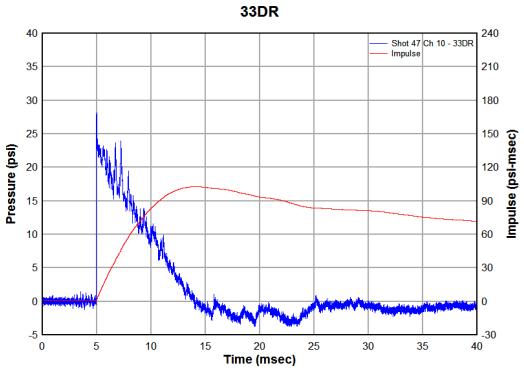

(d) Shot 47, ch10-33dr

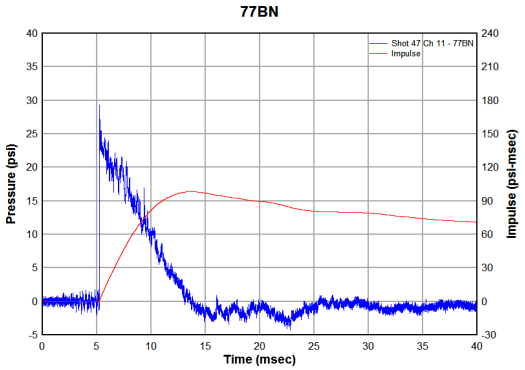

(e) Shot 47, ch11-77bn

SHOT 48 - 1-INCH PEAKED PLATE - 0.032-INCH DIAPHRAGM

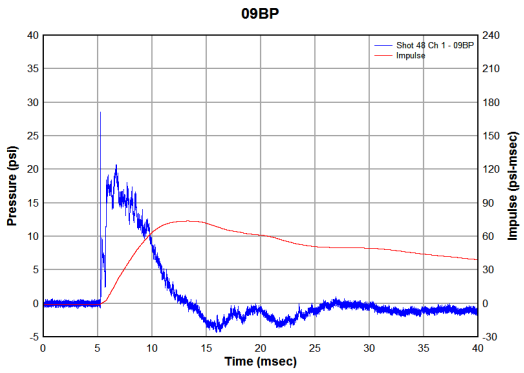

(a) Shot 48, ch1-09bp

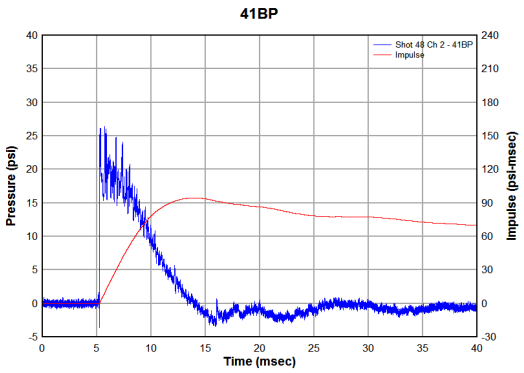

(b) Shot 48, ch2-41bp

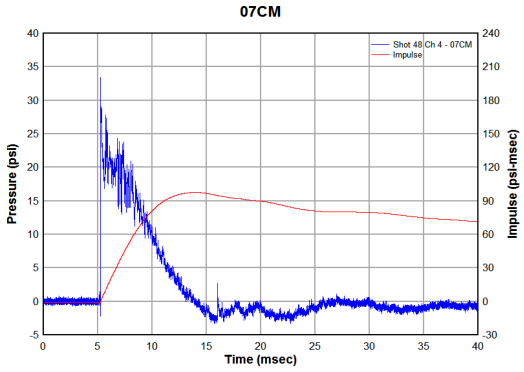

(c) Shot 48, ch4-07cm

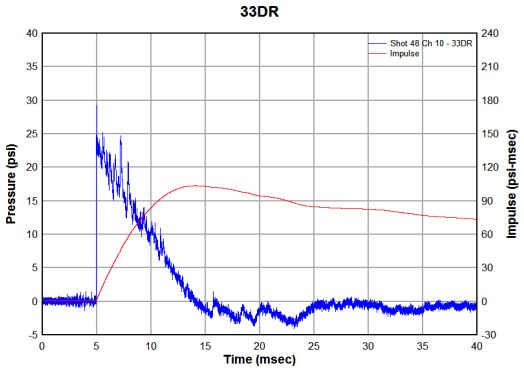

(d) Shot 48, ch10-33dr

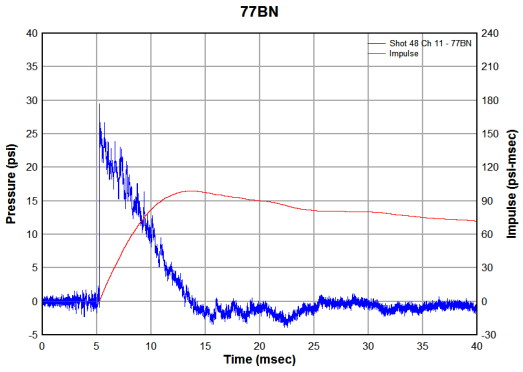

(e) Shot 48, ch11-77bn

SHOT 49 - 1-INCH PEAKED PLATE - 0.025-INCH DIAPHRAGM

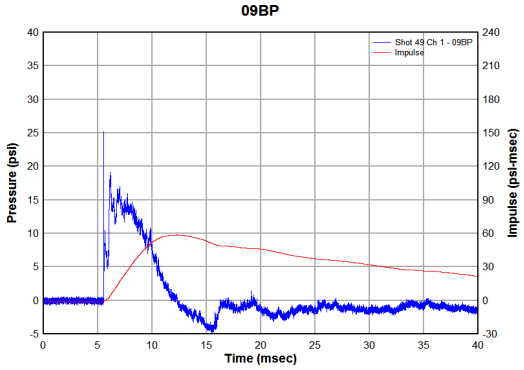

(a) Shot 49, ch1-09bp

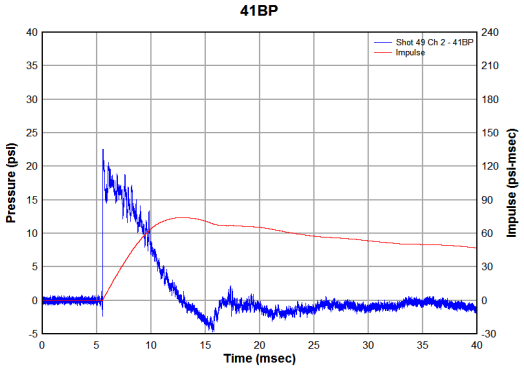

(b) Shot 49, ch2-41bp

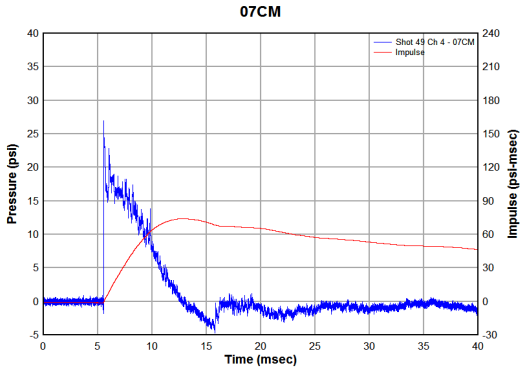

(c) Shot 49, ch4-07cm

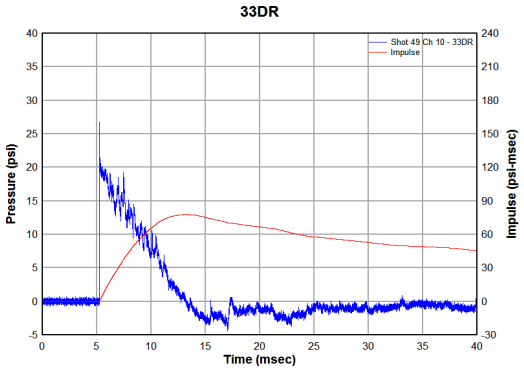

(d) Shot 49, ch10-33dr

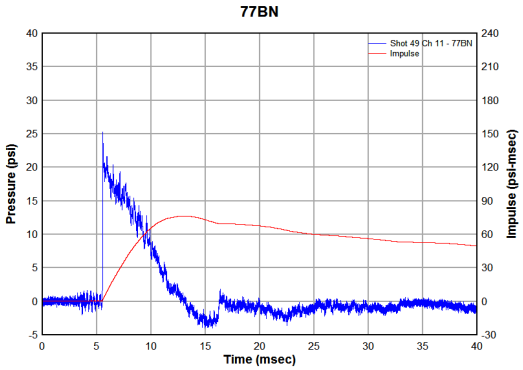

(e) Shot 49, ch11-77bn

SHOT 50 - 1-INCH PEAKED PLATE - 0.025-INCH DIAPHRAGM

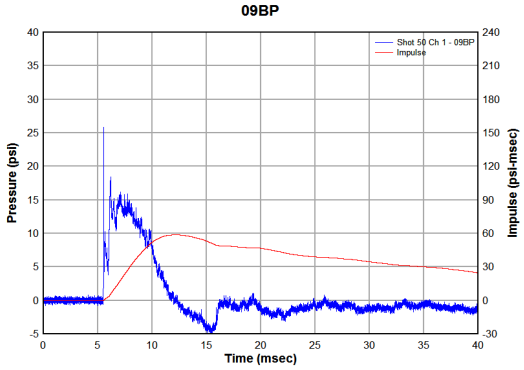

(a) Shot 50, ch1-09bp

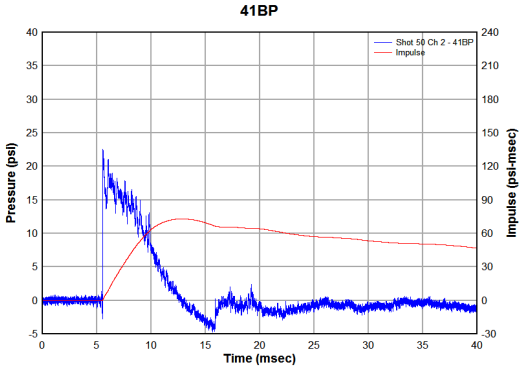

(b) Shot 50, ch2-41bp

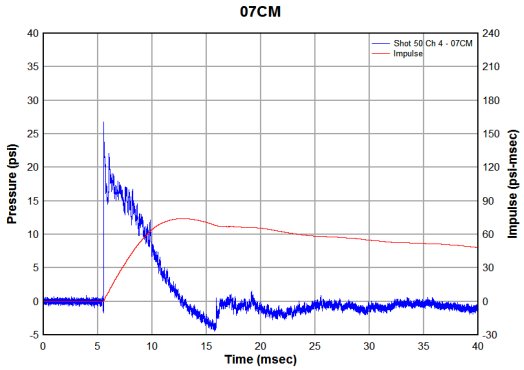

(c) Shot 50, ch4-07cm

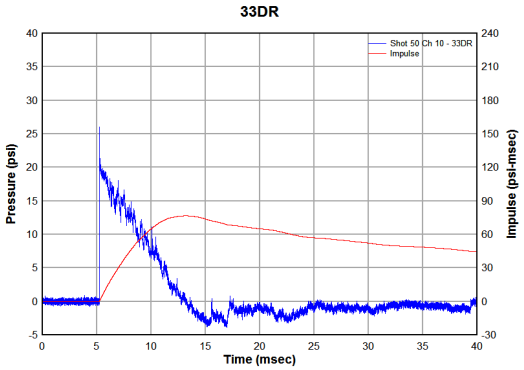

(d) Shot 50, ch10-33dr

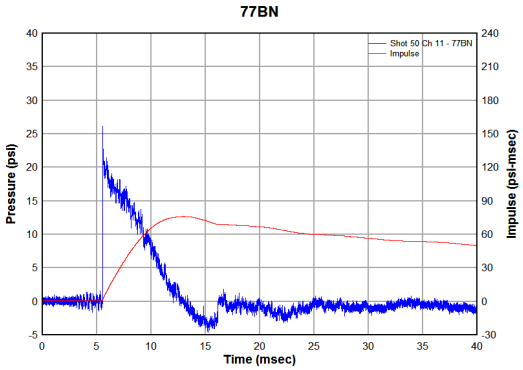

(e) Shot 50, ch11-77bn

SHOT 51 - 1-INCH PEAKED PLATE - 0.032-INCH DIAPHRAGM

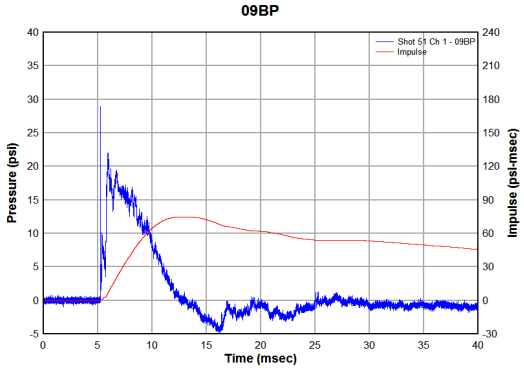

(a) Shot 51, ch1-09bp

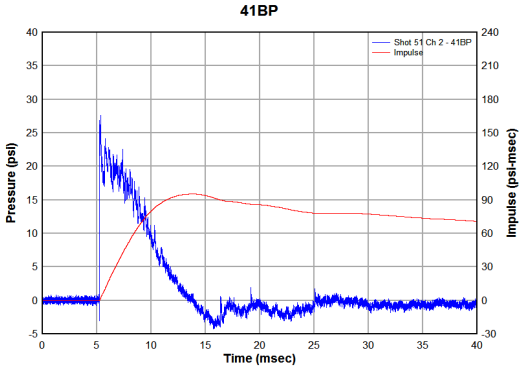

(b) Shot 51, ch2-41bp

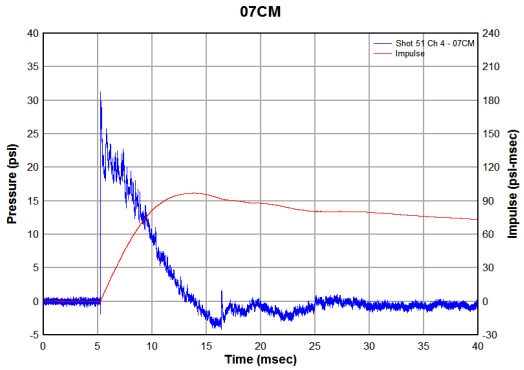

(c) Shot 51, ch4-07cm

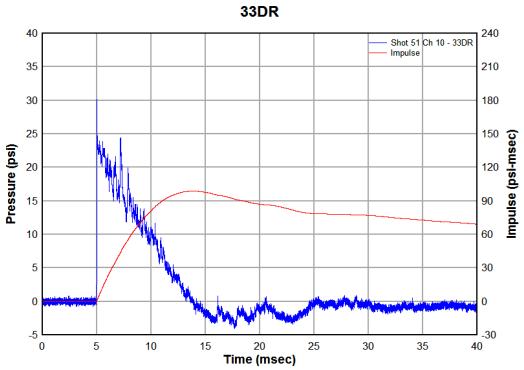

(d) Shot 51, ch10-33dr

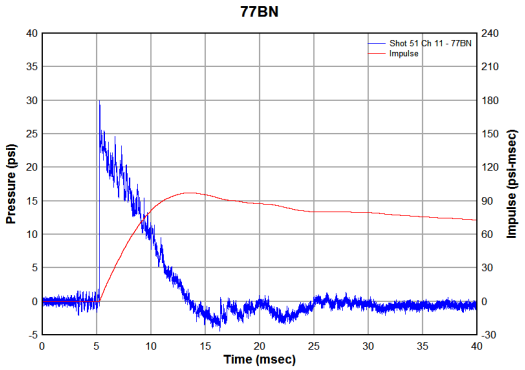

(e) Shot 51, ch11-77bn

SHOT 52 - 1-INCH PEAKED PLATE - 0.032-INCH DIAPHRAGM

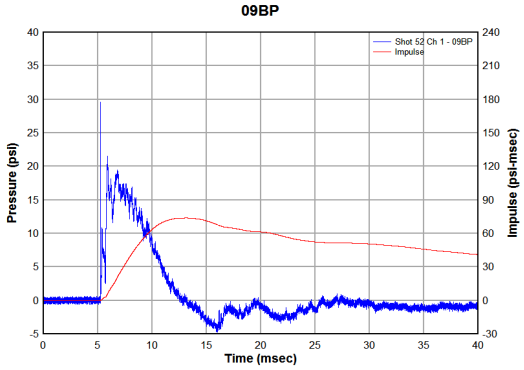

(a) Shot 52, ch1-09bp

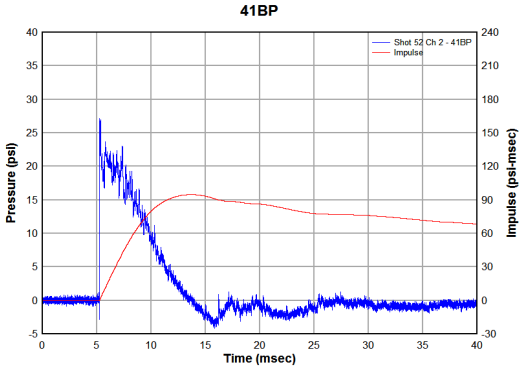

(b) Shot 52, ch2-41bp

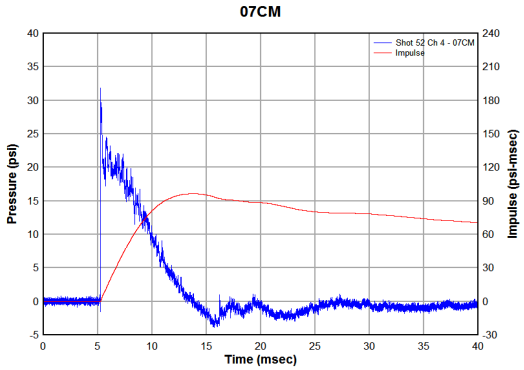

(c) Shot 52, ch4-07cm

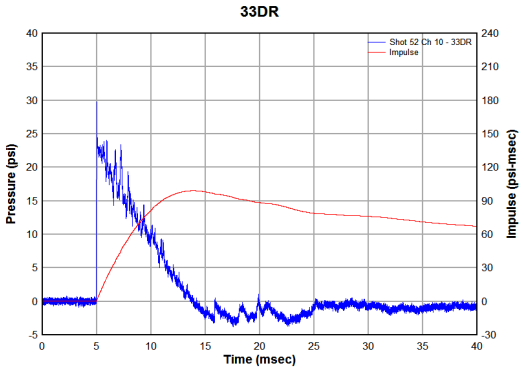

(d) Shot 52, ch10-33dr

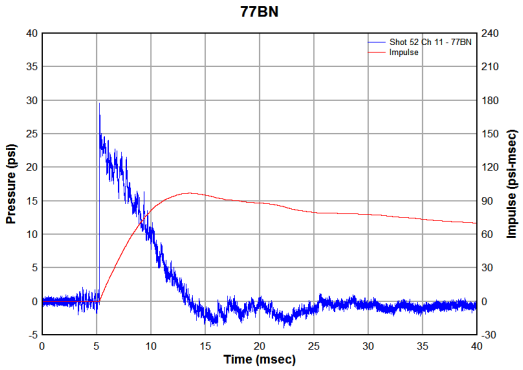

(e) Shot 52, ch11-77bn

SHOT 53 - FLAT PLATE - 0.025-INCH DIAPHRAGM

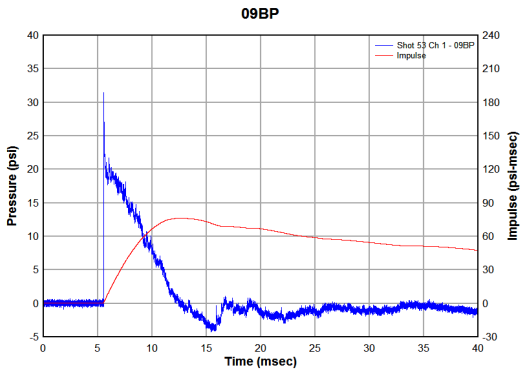

(a) Shot 53, ch1-09bp

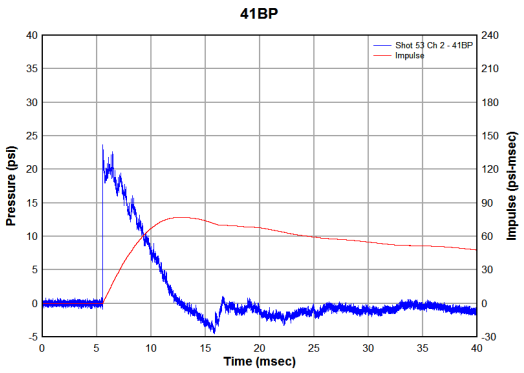

(b) Shot 53, ch2-41bp

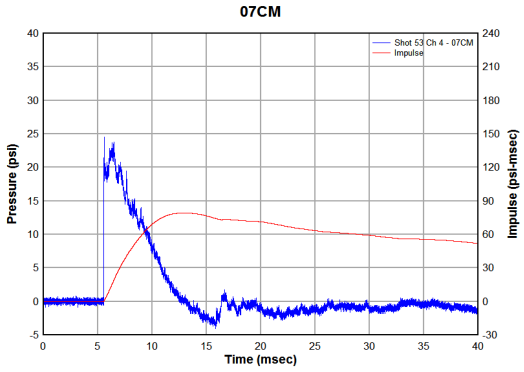

(c) Shot 53, ch4-07cm

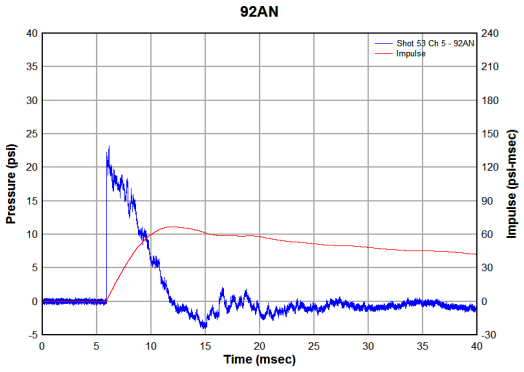

(d) Shot 53, ch5-92an

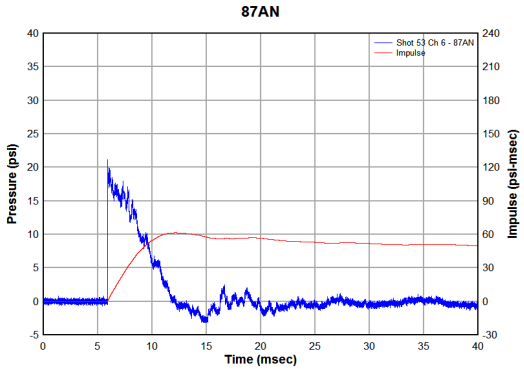

(e) Shot 53, ch6-87an

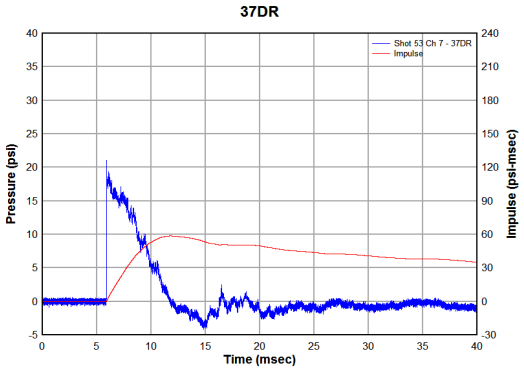

(f) Shot 53, ch7-37dr

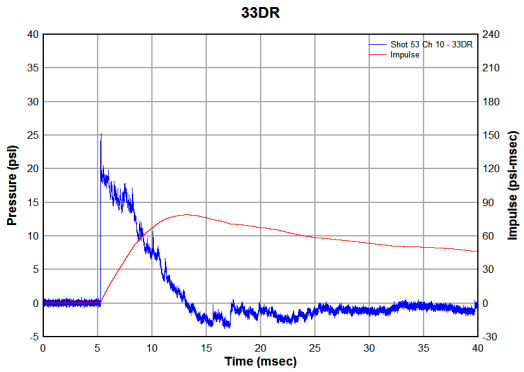

(a) Shot 53, ch10-33dr

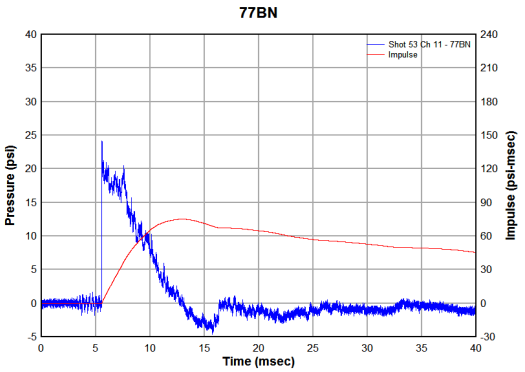

(b) Shot 53, ch11-77bn

SHOT 54 - FLAT PLATE - 0.025-INCH DIAPHRAGM

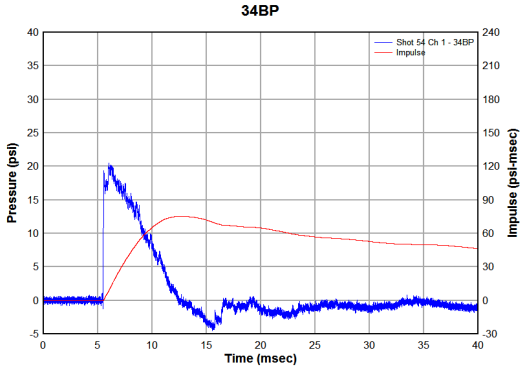

(a) Shot 54, ch1-34bp

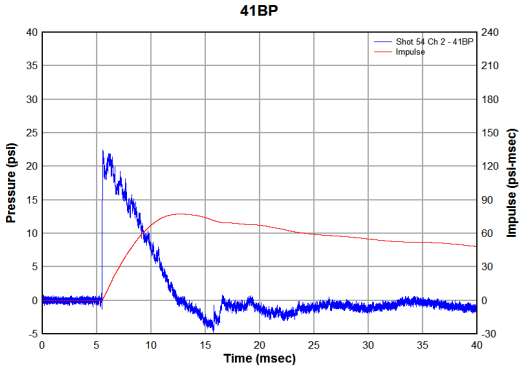

(b) Shot 54, ch2-41bp

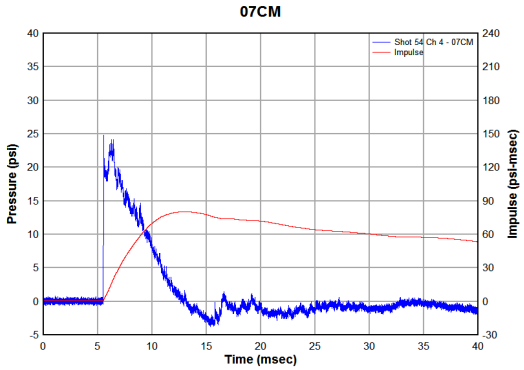

(c) Shot 54, ch4-07cm

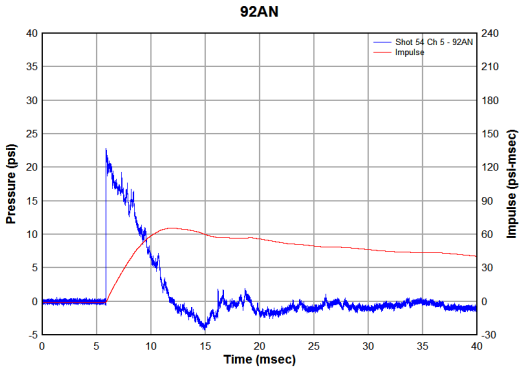

(d) Shot 54, ch5-92an

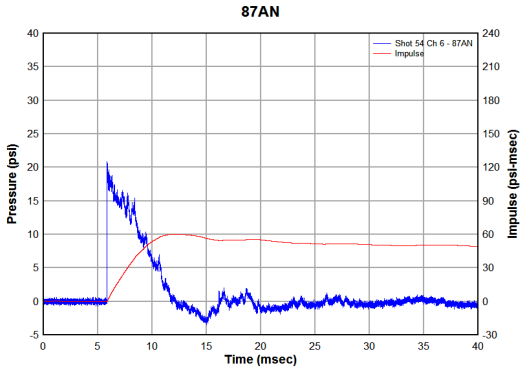

(e) Shot 54, ch6-87an

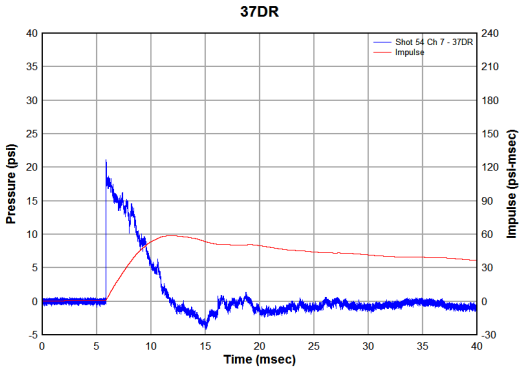

(f) Shot 54, ch7-37dr

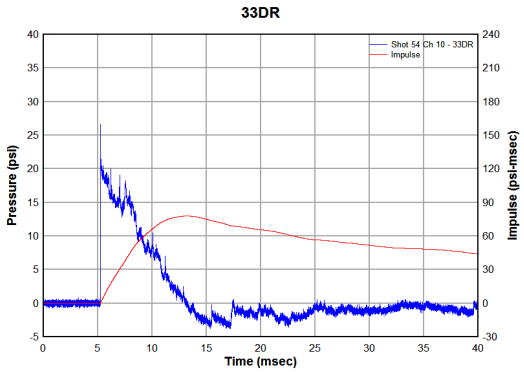

(a) Shot 54, ch10-33dr

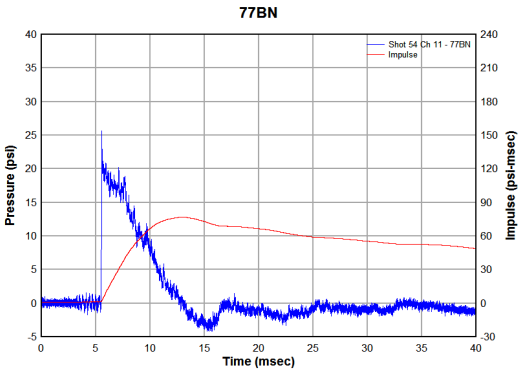

(b) Shot 54, ch11-77bn

SHOT 55 - FLAT PLATE - 0.025-INCH DIAPHRAGM

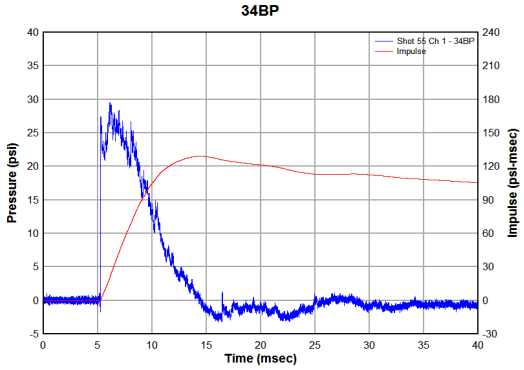

(a) Shot 55, ch1-34bp

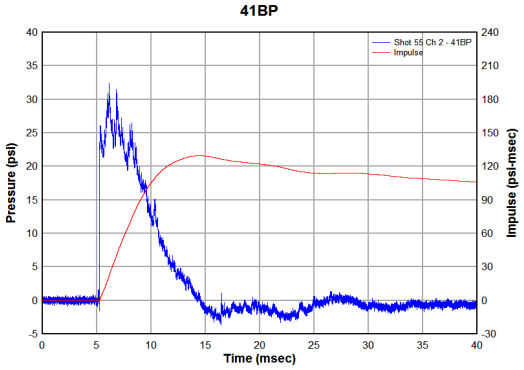

(b) Shot 55, ch2-41bp

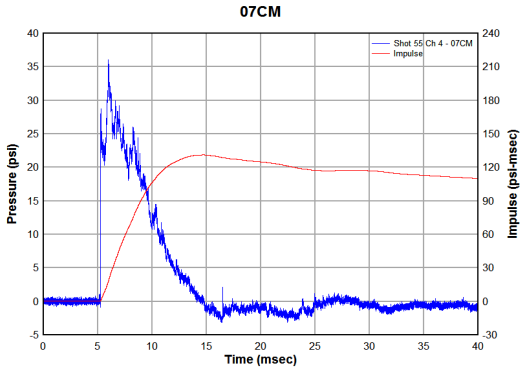

(c) Shot 55, ch4-07cm

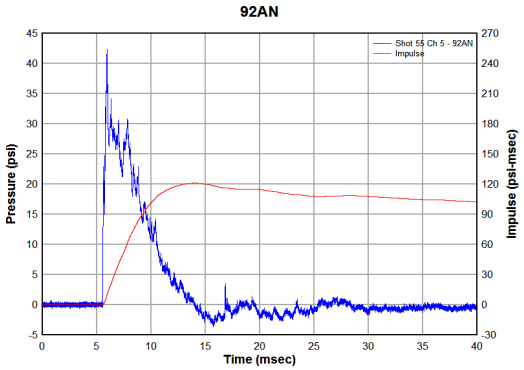

(d) Shot 55, ch5-92an

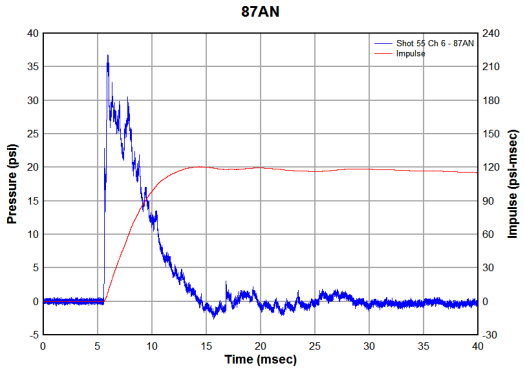

(e) Shot 55, ch6-87an

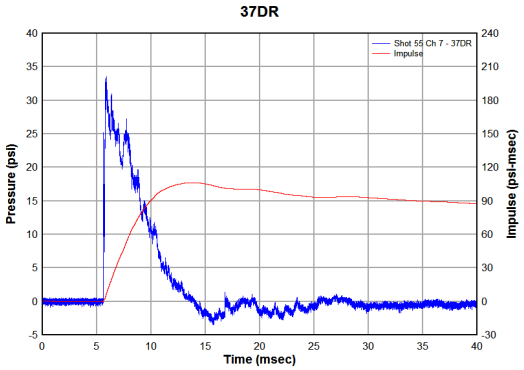

(f) Shot 55, ch7-37dr

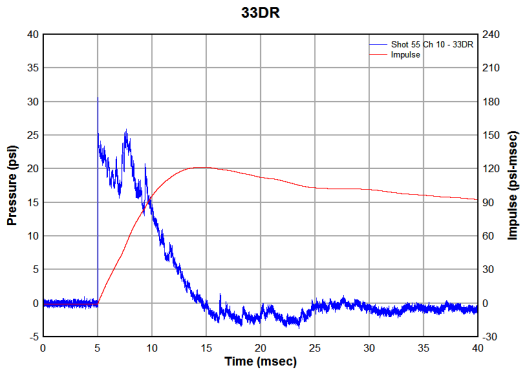

(a) Shot 55, ch10-33dr

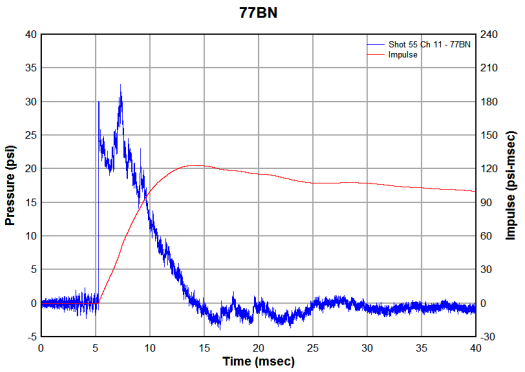

(b) Shot 55, ch11-77bn

APPENDIX B

FILM STRIPS

SHOT 5 - FLAT PLATE, 0.032-INCH DIAPHRAGM

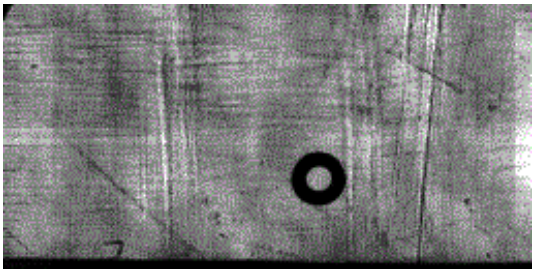

(a) Shot 5, Frame 412

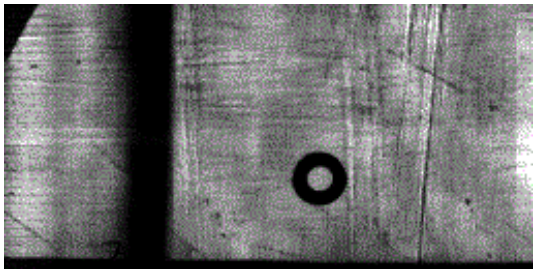

(b) Shot 5, Frame 415

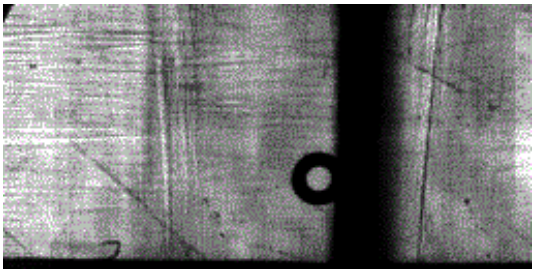

(c) Shot 5, Frame 417

SHOT 10 - 1/2-INCH WAVY PLATE, 0.025-INCH DIAPHRAGM

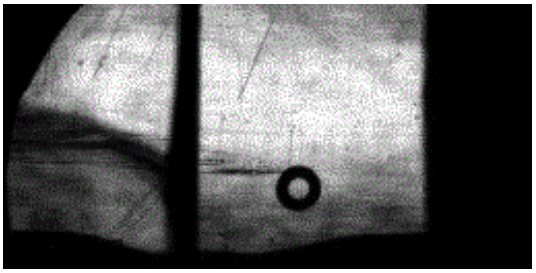

(a) Shot 10, Frame -619

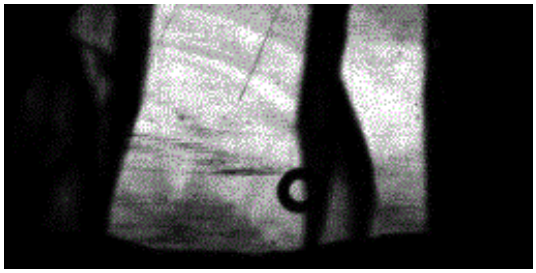

(b) Shot 10, Frame -617

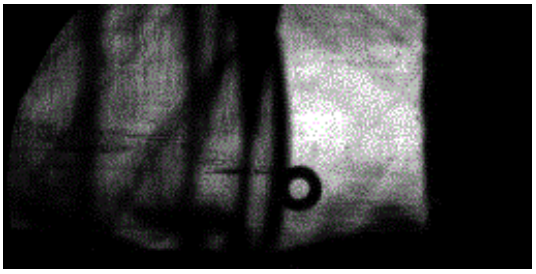

(c) Shot 10, Frame -615

SHOT 13 - 1/2-INCH WAVY PLATE, 0.025-INCH DIAPHRAGM - TALL VIEW

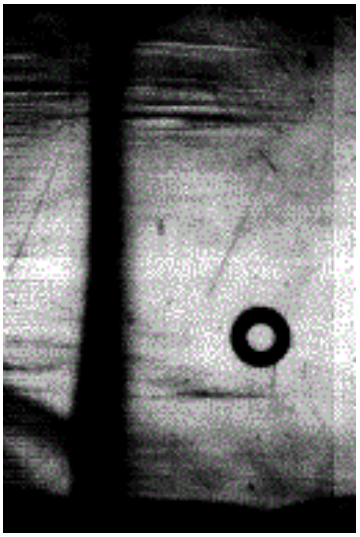

(a) Shot 13, Frame 376

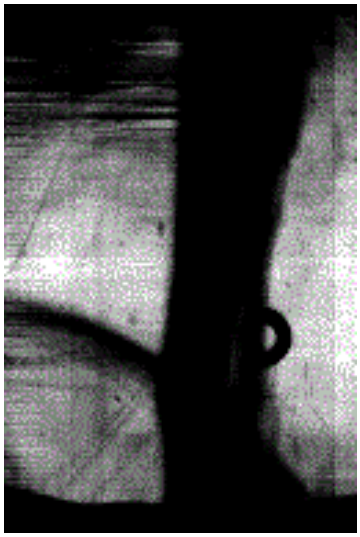

(b) Shot 13, Frame 377

(c) Shot 13, Frame 380

SHOT 17 - 1/2-INCH PEAKED PLATE, 0.032-INCH DIAPHRAGM

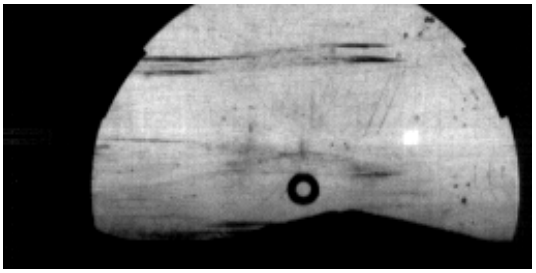

(a) Shot 17, Frame 328

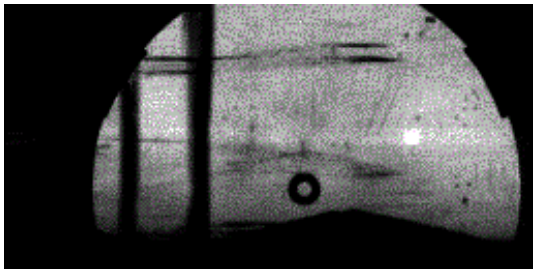

(b) Shot 17, Frame 331

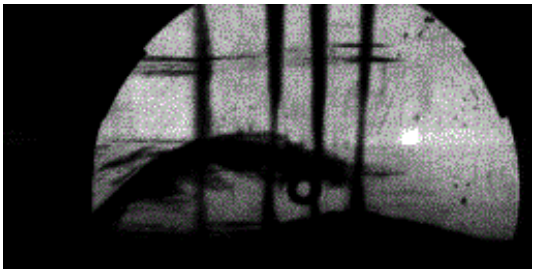

(c) Shot 17, Frame 334

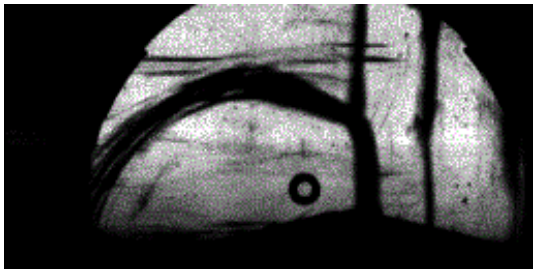

(d) Shot 17, Frame 336

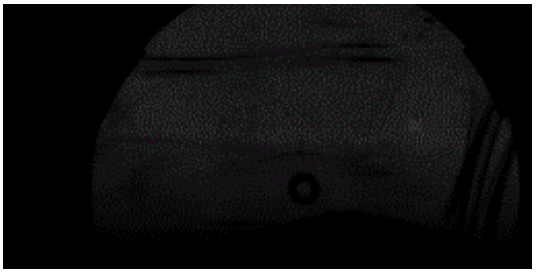

(e) Shot 17, Frame 357

(f) Shot 17, Frame 372

SHOT 21 - 1/2-INCH PEAKED PLATE, 0.025-INCH DIAPHRAGM

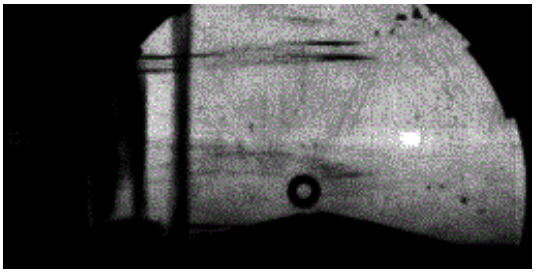

(a) Shot 21, Frame 351

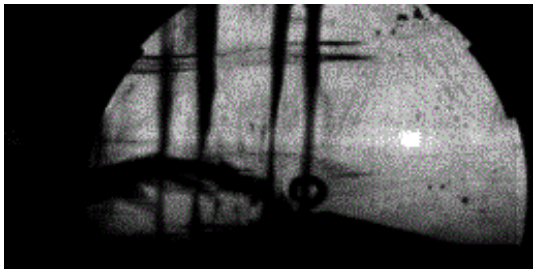

(b) Shot 21, Frame 353

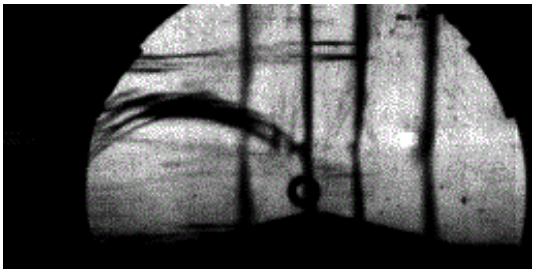

(c) Shot 21, Frame 355

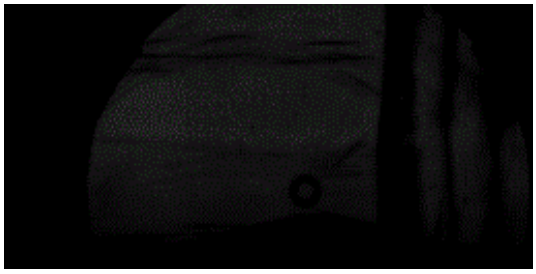

(d) Shot 21, Frame 357

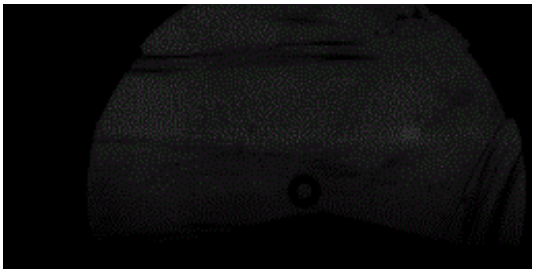

(e) Shot 21, Frame 371

(f) Shot 21, Frame 385

SHOT 34 - PROTRUDING, RECESSED, AND LOCAL IMPERFECTIONS, 0.032-INCH DIAPHRAGM

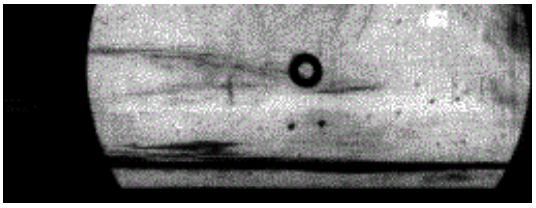

(a) Shot 34, Frame 397

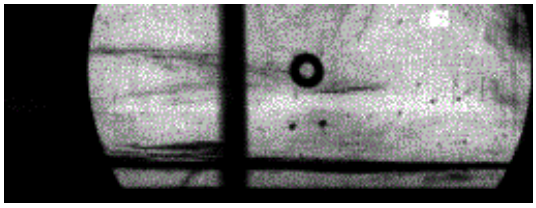

(b) Shot 34, Frame 406

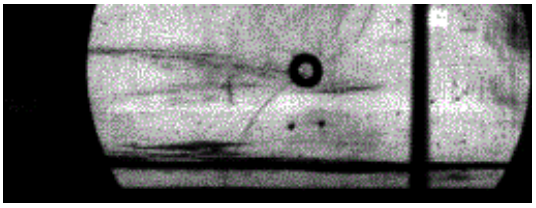

(c) Shot 34, Frame 409

SHOT 50 - 1-INCH PEAKED PLATE, 0.025-INCH DIAPHRAGM

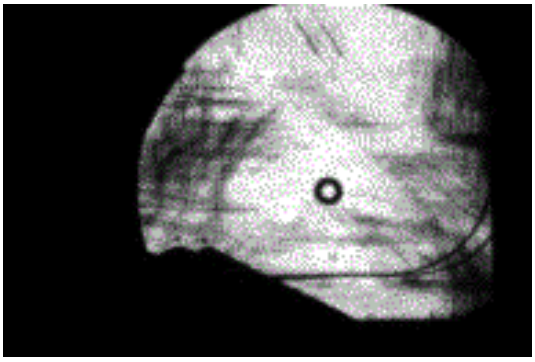

(a) Shot 50, Frame 412

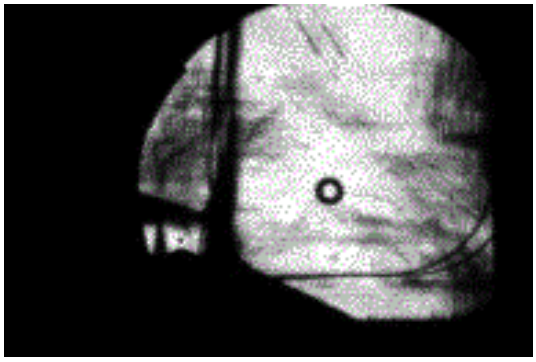

(b) Shot 50, Frame 415

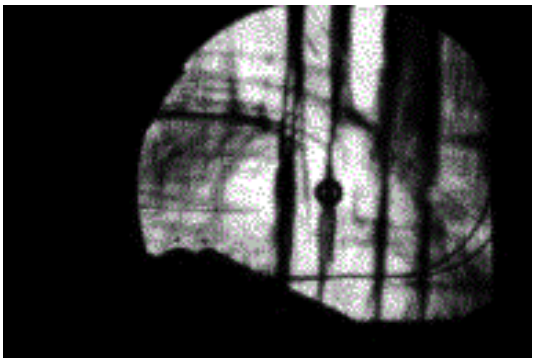

(c) Shot 50, Frame 419

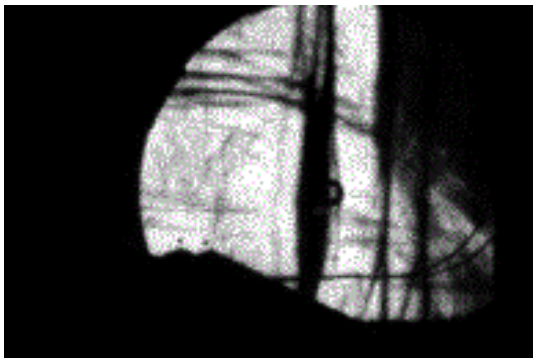

(d) Shot 50, Frame 420

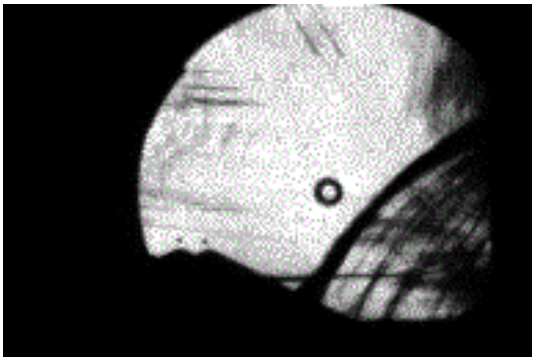

(e) Shot 50, Frame 433

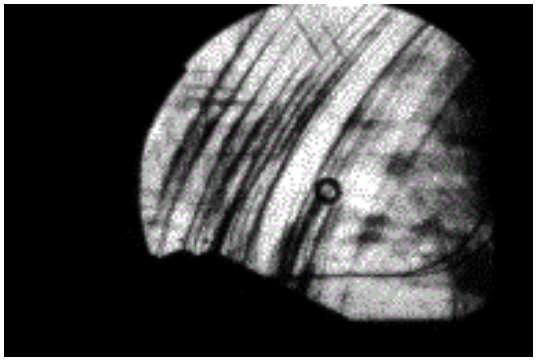

(f) Shot 50, Frame 444

SHOT 51 - 1-INCH PEAKED PLATE, 0.032-INCH DIAPHRAGM

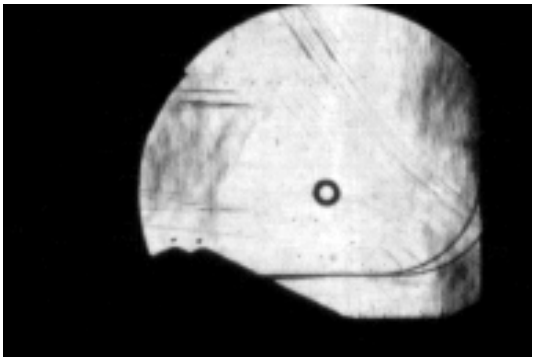

(a) Shot 51, Frame 391

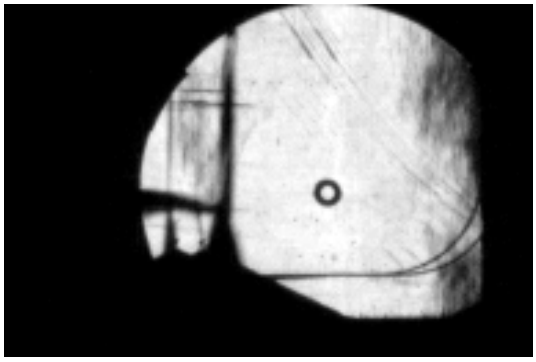

(b) Shot 51, Frame 395

(c) Shot 51, Frame 398

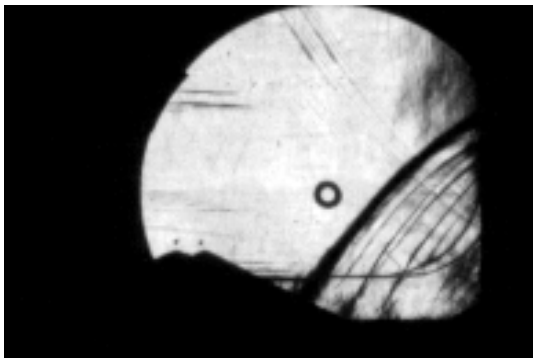

(d) Shot 51, Frame 413

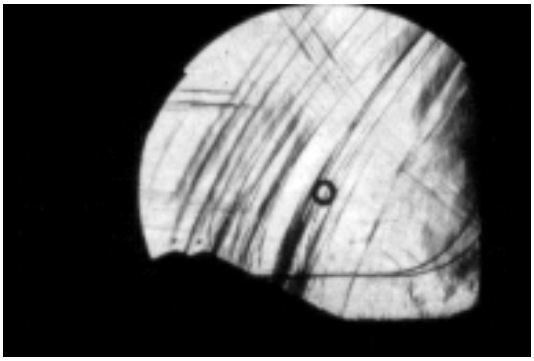

(e) Shot 51, Frame 424

SHOT 54 - FLAT PLATE, 0.025-INCH DIAPHRAGM

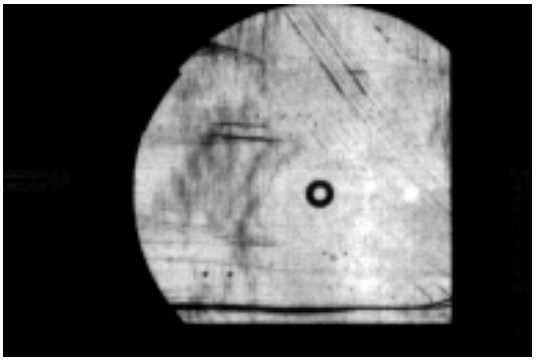

(a) Shot 54, Frame 410

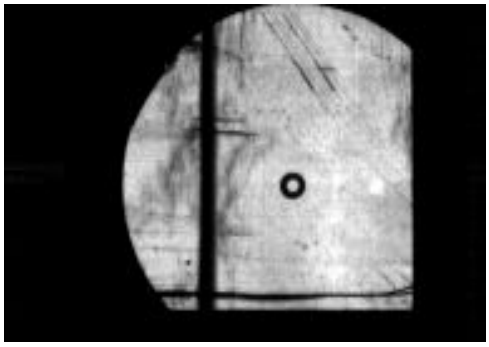

(b) Shot 54, Frame 413

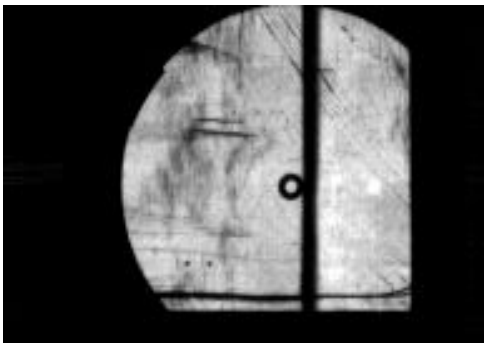

(c) Shot 54, Frame 417

BIBLIOGRAPHY

[1] Needham, Charles E. *Blast Waves*. Heidelberg: Springer, 2010. Print.

[2] Anderson, John David, *Modern Compressible Flow: With Historical Perspective*. Boston, MA: McGraw-Hill, 2003. Print.

[3] Kinney, Gilbert F., and Kenneth J. Graham. *Explosive Shocks in Air*. 2nd ed. New York: Springer-Verlag, 1985. Print.

[4] *A Guide for the Dynamic Calibration of Pressure Transducers*. Rep. no. ISA-37.16.01. Research Triangle Park: ISA, 2002.

[5] Schlichting, Hermann, and J. Kestin. *Boundary-Layer Theory*. 4th ed. New York: McGraw-Hill, 1979. Print.

[6] American National Standards Institute. Surface Texture (Surface Roughness, Waviness, and Lay). ANSI/ASME B46.1-1985.

[7] Skjeltorp, A. T. *Airblast Propagation through Tunnels and the Effects of Wall Roughness.* Rep. no. ADA020817. N.p.: Norwegian Defence Construction Service, 1975. Print.

[8] Skjeltorp, A. T., T. Hegdahl, and A. Jenssen. *Blast Propagation in Tunnel Systems.* Rep. no. ADA027067. N.p.: Norwegian Defence Construction Service, 1975. Print.

[9] "General Piezoelectric Theory." *General Piezoelectric Theory.* PCB Piezotronics, n.d. Web. 22 Mar. 2015.

[10] Cooper, Paul W. *Explosives Engineering.* New York, NY: VCH, 1996. Print.

[11] Hanson, Ronald K., Jay Jeffries, and David Davidson. *Introduction to the Aerosol Shock Tube*. N.p.: n.p., n.d. PDF.

[12] Kleinschmit, Nicholas N. *A Shock Tube Technique for Blast Wave Simulation and Studies of Flow Structure Interactions in Shock Tube Blast Experiments.* Thesis. University of Nebraska, 2011. Lincoln: U of Nebraska, 2011. Print.

[13] Silver, P.L. *Evaluation of Air Blast Measurement Techniques* 75th Shock and Vibration Proceedings, Virginia Beach, VA, October 17-22, 2004.

[14] Walter, Patrick L. *Measuring Static Overpressures in Air Blast Environments.* Tech. no. TN-27. Depew, NY: PCB Group, 2010. Print.

[15] Settles, G. S. *Schlieren and Shadowgraph Techniques: Visualizing Phenomena in Transparent Media: With 208 Figures and 48 Color Plates.* Berlin: Springer, 2006. Print.

[16] Hanson, Ronald K. *Introduction to the Aerosol Shock Tube.* Working paper. N.p.: n.p., n.d. Print.

[17] Damazo, J., J. Ziegler, J. Karnesky, and J. E. Shepard. *Investigating Shock WaveâĂŤBoundary Layer Interaction Caused By Reflecting Detonations.* Proc. of Eighth International Symposium on Hazards, Prevention and Mitigation of Industrial Explosions, Yokohama, Japan. N.p.: n.p., 2010. Web.

[18] Glass, I. I., and Jean Pascal Sislian. *Nonstationary Flows and Shock Waves.* Oxford: Clarendon, 1994. Print.

[19] "CTH Shock Physics." *Sandia National Laboratories: CTH Shock Physics: Home.* N.p., n.d. Web. 20 Sept. 2014.

VITA

Laurin Ashley Bookout was born on January 8, 1987, and lived in central Missouri for most of her life before enrolling in the University of Missouri-Rolla in 2005. She completed a Bachelor of Science, Cum Laude, in Civil Engineering at UMR in 2009, a Master of Science in Explosives Engineering at Missouri S&T (formerly UMR) in 2011, and a PhD in Explosives Engineering at Missouri S&T in 2015.

Laurin worked as a Graduate Research Assistant while attending Missouri S&T for her MS degree, where she obtained experience on a wide variety of projects in a short period of time. Laurin accepted a job after completion of her MS degree. She then pursued her PhD while working full time researching explosive effects and applications.